DEVELOPMENT OF MECHANISTIC TOOLS FOR UNDERSTANDING ORGANIC REACTIONS: FROM MANUAL TO AUTOMATED SAMPLING

by

Diana Yu

B.S., University of California, Los Angeles, 2012

A THESIS SUBMITTED IN PARTIAL FULFILLMENT OF

THE REQUIREMENTS FOR THE DEGREE OF

DOCTOR OF PHILOSOPHY

in

THE FACULTY OF GRADUATE AND POSTDOCTORAL STUDIES

(Chemistry)

THE UNIVERSITY OF BRITISH COLUMBIA

(Vancouver)

March 2017

Abstract

Kinetic studies were conducted on three unrelated reaction types using traditional and modified reaction monitoring tools. The Aza-Piancatelli rearrangement was studied through ReactIR and HPLC-MS to obtain a better understanding of why the substrate scope was limited. It was found that the Lewis acid catalyzed reaction is often zero-order, dependent on the lanthanide metal used. Off-cycle binding of the nucleophile to the Lewis acid was proposed to help explain the zero-order profile. Differences between Lewis and Brønsted acid catalysts were found through subsequent experiments assessing catalyst deactivation and the chemoselectivity of the products in the Aza-Piancatelli rearrangement. An automated sampling system was created for hands-free reaction monitoring and offline analysis by HPLC-MS to provide detailed information about more complicated reactions.

The automated sampling system was modified for the study of microwave assisted reactions. This application allowed for more information to be derived from the field of poorly-understood microwave chemistry than allowed by previous technology. Comparisons were made between microwave-assisted and conventionally heated reactions, using a Claisen rearrangement as a model reaction. As expected, it was found that the Claisen rearrangement of allylphenyl ethers displayed similar kinetics between the two heating modes. The technology was also used briefly to search for the existence of non-thermal effects. It was shown that the sampling apparatus could be useful for collecting data observed from microwave-specific effects.

Mechanistic studies were also conducted on the Kinugasa reaction to obtain a better understanding of why the reaction generally behaves poorly in regards to the formation of β-lactam product. To study the reaction, samples for HPLC-MS analysis were taken manually, then by a liquid handler, and then through direct-injection to the HPLC. It was found that its side-

product formation was directly coupled to the desired product formation, suggesting that both the product and imine side-product stem from a common intermediate. Another little-known side-product was isolated, suggesting the common intermediate could be intercepted by select nucleophiles to form an amide. This finding will direct future attempts to find conditions to favor either β-lactam or amide formation.

Preface

Half of Chapter 2 has been published in two separate papers in collaboration with members of the Read de Alaniz laboratory at the University of California, Santa Barbara. For the first paper published in 2013, I conducted the bulk of the kinetic experiments and wrote the first draft. My undergraduate assistant, Van Thai, assisted me in setting up experiments and synthesizing starting material. Members of the Read de Alaniz lab characterized the compounds and edited the manuscript, along with Dr. Hein. For the second paper published in 2015, Ryan Chung did the bulk of the kinetic studies and wrote the manuscript. I finished the kinetic studies, made calibration curves, and isolated an intermediate. With members of the Read de Alaniz lab and Dr. Hein, we all edited the manuscript. All of the work was done at the University of California, Merced before the Hein Lab moved to UBC.

Papers relating to Chapter 2:

Yu, D.; Thai, V.T.; Palmer, L.I.; Veits, G.K.; Cook, J.E.; Read de Alaniz, J.; Hein, J.E. *J. Org. Chem.* **2013**, *78*, 12784.

Chung, R.; Yu, D.; Thai, V.T.; Jones, A. F.; Veits, G.K.; Read de Alaniz, J.; Hein, J.E. *ACS Catal.* **2015**, *5*, 4579–4585.

The latter half of Chapter 2 is not published, and the experimental work was split between Van Thai and me.

Chapter 3 has not been published. I did the bulk of the experimental work. I was assisted by undergraduates Van Thai and Esma Al-Autman. Undergraduate Henry Situ was responsible for the development of the direct injection system into the HPLC, which was used for one reaction.

Chapter 4 has not been published. In collaboration with Drs. Greg Dudley and Al Stiegman from the University of West Virginia and Florida State University, respectively, Dr. Hein and I decided on the types of experiments to perform. The kinetic experiments were conducted by me. I was assisted by undergraduates Alyssa F. Jones, Carl A. Posadas, and Esma Al-Autman in synthesizing starting materials. I have written the first drafts of the manuscript.

Table of Contents

List of Tables

List of Figures

List of Abbreviations

©	copyright
1D	1-dimensional
2D	2-dimensional
Å	Angstrom, 10^{-10} meters
Ac	acetyl
aq	aqueous
Ar	aryl
BINOL	1,1′-bi-2-naphthol
bipy	bypyridine
Bn	benzyl
Boc	*tert*-butoxycarbonyl
Bu	butyl
Bz	benzoyl
cat	catalyst or catalytic
cm	centimeters
^{13}C-NMR	carbon nuclear magnetic resonance
CuAAC	copper(I)-catalyzed alkyne-azide cycloaddition
Cy	cyclo-
$CyNMe_2$	*N*,*N*-Dimethylcyclohexylamine
d	doublet (NMR spectroscopy)
DBU	1,8-diazabicycloundec-7-ene
DCM	dichloromethane

de	diastereomeric excess
DIPA	diisopropylamine
DIPEA	diisopropylethylamine
DMAP	4-dimethylaminopyridine
DMF	*N*,*N*-dimethylformamide
dppe	1,2-Bis(diphenylphosphino)ethane
ee	enantiomeric excess
EI	electron ionization
equiv	equivalents
ELSD	evaporative light scattering detector
EI	electron ionization
ESI-MS	electrospray ioniziation - mass spectrometry
Et	ethyl
EtOAc	ethyl acetate
EtOH	ethanol
FBRM	focused beam reflectance measurement
FID	flame ionization detector
FTIR	fourier transform infrared spectroscopy
g	gram
GC	gas chromatography
GHz	gigahertz
h	hour
HMBC	heteronuclear multiple bond coherence

^{1}H-NMR	proton nuclear magnetic resonance
HPLC	high performance liquid chromatography
hr	hour
HSQC	heteronuclear single quantum coherence
Hz	hertz
iPr	isopropyl
IPAc	isopropyl acetate
IR	infrared
ITC	isothermal calorimetry
J	coupling constant (NMR spectroscopy)
KIE	kinetic isotope effect
L	liter
L.A.	Lewis acid
LC	liquid chromatography
LFER	linear free energy relationships
Ln	lanthanide
M	concentration (moles/liter)
m	meta
M	metal
MAOS	microwave assisted organic synthesis
Me	methyl
MeCN	acetonitrile
$MeNO_2$	nitromethane

MeOH	methanol
mg	milligram
min	minute
mL	milliliter
mM	concentration (millimoles/liter)
mol	mole
MS	mass spectrometry
MTBE	methyl-*tert*-butyl ether
n/a	not available
n/d	not determined
NaBARF	sodium tetrakis[3,5-bis(trifluoromethyl)phenyl]borate
$NaHCO_3$	sodium bicarbonate
NBO	natural bond orbital
NMR	nuclear magnetic resonance
Nuc	nucleophile
o	ortho
º	degree
OMe	methoxy
OPr	propoxy
OTf	triflate, trifluoromethanesulfonate
p	para
PAT	process analytical technology
pdt	product

PEEK	polyether ether ketone
pet ether	petroleum ether
PG	protecting group
Ph	phenyl
pm	picometer
PPh_3	triphenylphosphine
PTFE	polytetrafluoroethylene
q	quartet (NMR spectroscopy)
R	organic group
RPKA	reaction progress kinetic analysis
RRF	relative response factors
rt	room temperature
s	second, or singlet (NMR spectroscopy)
t	triplet (NMR spectroscopy)
TBTA	tris(*tert*-butyltriazolyl)amine
t-Bu	*tert*-butyl
TCPTA	tris(cyclopentyltriazolyl)amine
TEA	triethylamine
TFA	trifluoroacetic acid
THF	tetrahydrofuran
TLC	thin layer chromatography
TMS	trimethylsilyl
Tol	toluene

UV	ultraviolet
W	watts
xs	excess
β	beta
δ	chemical shift in ppm
μ	mu, micro (10^{-6})
μL	microliter
ρ	rho
σ	sigma

Acknowledgements

I thank the University of California, Merced and the University of British Columbia for supporting this work and for providing travel grants, teaching appointments, and fellowships.

Great thanks to my two committees from both universities, who have given me insight, perspective, and help beyond the views of my lab.

I thank my collaborators (Drs. Javier Read de Alaniz, Richmond Sarpong, Dean Tantillo, Uttam Tambar, Greg Dudley, Al Stiegman, and their respective students) for allowing me to work on their chemistry, and for their patience and support.

I would like to thank my friends, family, and fellow grad students for their emotional support, time spent listening to me, and feeding me when I was hangry. In particular, I am indebted to Richard Hargrove, Loan Nguyen, Erika Escobar, Luke Reed, and NMR guru Dave Russell.

I thank Dr. Alfred Bacher for inspiring me to pursue a degree in organic chemistry and chatting with me even when he was not obligated to. Without him, I am unsure of where my academic path would have lead.

I would like to thank numerous previous and current members of the Hein Lab for putting up with my shenanigans and sudden outbursts, picking items from the top shelves beyond my reach, giving me advice, conducting experiments alongside me, and providing unconditional support. In particular, I thank Matt Berry, Ivy Price, Ryan Chung, Céline Rougeot, Aagam Patel, Blessing Cao, Henry Situ, Van Thai, and Alyssa Jones. Without their help, I would have surely become quite depressed.

Last but certainly not least, I am indebted to my advisor, Dr. Jason Hein, for taking me on as a student. Thank you for being kind throughout my extreme mood swings and for so quickly

understanding my frantic babbling, which no other scientist could even start to comprehend; for supporting me every time I wanted to change my career path, realistically or not; for allowing me so much freedom in choosing and conducting experiments, even if they were for black projects; for allowing me to decline a project if I felt it was not in my best interest; for your patience as I got tangled in tubing and raged over drivers that inappropriately updated; and of course, for allowing Matt, Céline, and I to follow you to UBC.

Dedication

This thesis is dedicated to my parents, Jun Liang Yu and Jin Yan Li, for their endless support and hard work.

"What I am looking for is a kind of spark:

An indication of deeply seated curiosity. I can train people to do lab work. But curiosity is a personality attribute that no amount of training can put in place. It is a form of enthusiasm mixed with fundamental persistence that originates in the brain stem and only leaves one's consciousness during sleep.

Science could be described as a way of being:

To be a scientist is to be one who constantly seeks understanding at its most fundamental level. It is a compulsion that drives one to continue to improve. Better insights. Better experiments. New techniques. And a willingness to keep hammering at a problem until something chips loose."

Th' Gaussling at gaussling.wordpress.com
Interview notes from the field, April 23, 2012

Chapter 1: Introduction

Mechanistic studies in organic chemistry encompass a broad and nonspecific set of experiments that are done with the goal of further understanding a reaction of interest. In the simplest sense, a chemist may predict the effects of changing a reaction parameter or using a new additive based on his or her current proposal of the reaction mechanism. Changing variables and assessing the outcomes is common in the process of developing or optimizing reactions. However, more in-depth mechanistic studies are sometimes desired. For example, finding the rate-determining or enantioselectivity-determining steps can be nontrivial. Tuning electronic properties on a ligand in a catalytic system and quantifying the effects requires confidence in measurements of rate and yield. Depending on the reaction, traditional mechanistic studies such as measuring initial rates or kinetic isotope effect calculations can be tedious. Due to a great variety of reaction types, not all mechanistic studies or analytical methods will provide useful information about every class of reaction. In addition, traditional methods of discerning mechanisms can be unamenable to reactions that do not already work well due to complicated speciation. There is a need for increased access to tools that enable more complicated mechanistic studies, as well as experimental methodologies that reduce the number of experiments necessary to derive pertinent information.

One of the central themes of this dissertation is studying organic reactions in great detail. Mechanistic studies can be applied to widely-known reactions to those that are poorly understood and/or hardly working. After a catalytic system and rate-determining steps are proposed, conditions can be found to disrupt the catalyst or coax it into cooperating. The philosophy to continually question the validity of a catalytic system is prevalent.

Alongside conducting mechanistic studies, an auxiliary goal is to develop or alter tools to facilitate kinetic studies and obtain more detailed information. As a consequence of being limited to the blind spots of the instruments we have at any given time, it has been necessary to modify and couple tools together to increase the use of automation and the quality of data obtained. These tools should not be so convoluted such that other researchers cannot easily use them, and their parts should be commercially available. Also, similar experimental set-ups should allow for multiple types of chemical processes to be run, enabling easy reconfiguration for any user, instead of having a set-up that is only useful for one reaction type.

The work contained in this dissertation centers on primarily organic, homogenous reactions. Although our lab has some means of monitoring heterogeneous reactions, work concerning heterogeneous reactions has been mostly omitted. The specific reactions between the various projects have no relation to each other; however, the re-tasking of similar tools used to study them is common.

1.1 Current in situ and ex situ analytical technology for the monitoring of homogenous reactions

The first step to conducting a mechanistic study is finding an appropriate analytical tool to monitor the progress of the reaction of interest. There are several factors that need to be considered. For example, do the reaction conditions require mild or extreme heating? Is the reaction particularly air or moisture-sensitive? What sort of functional groups are present in the substrate(s) or product(s)? Which compounds are UV active? Is the substrate very expensive or exhaustive to make, potentially limiting how many experiments can be done? Are any solids or gases produced in the reaction, and how would they potentially interfere with the results from the

analytical method? Would a nonreactive additive be necessary to be used as an internal standard, or can an inert compound already in the reaction function as an internal standard for kinetics? Is the analytical technique suitable for a reaction run without an internal standard? The following sections include a brief background on different spectroscopic techniques other groups have used to track organic reactions, as well as ways in which they have modified standard set-ups to accommodate more difficult conditions.

1.1.1 Nuclear magnetic resonance (NMR) spectroscopy

Using NMR spectroscopy to monitor reactions in real time is a standard and widely-used technique, especially for ^{1}H, ^{31}P, and ^{19}F nuclei. As most organic chemists have access to a spectrometer, NMR spectroscopy may be the one of the easiest reaction monitoring tools for homogenous reactions, as data collection is automated. The set-up may require few changes from a benchtop reaction, aside from exchanging the reaction flask and stirbar for the NMR tube. It is also convenient in that the NMR experiment can be set up without need for further attention. Higher quality and precision of data is correlated with longer delay times due to the relaxation time of nuclei. Unfortunately, this can also be a disadvantage, requiring longer acquisition times on what is often a shared instrument. The data analysis – which requires converting peak area into concentration – should also require no calibration curves, possibly even without an internal standard, if delay times are calculated.[1] Solvent suppression techniques have also allowed NMR to be run on reactions without the use of expensive deuterated solvents.[2] Peaks of interest may also overlap or drift in chemical shift with changes in pH. Fortunately, some NMR processing programs allow deconvolution of peaks in arrays, such as MestreNova's global peak deconvolution function.

For relatively fast organic reactions (100 ms to a few minutes), the time between mixing the reactants and positioning the tube into the spectrophotometer is a detriment for good data acquisition, combined with infrequent acquisitions. To allow acquisition of of kinetic data on relatively rapid reactions, stopped-flow NMR experiments using custom-made probes allow for two streams of reactants to be rapidly injected and mixed in the NMR detection region. The delay can then be varied to allow a fresh stream of reactants to mix for varying amounts of time to see different timepoints. This method can reveal information about short-lived intermediates and provide a level of detail that would be completely missed on a longer time scale. This technique has proven useful by a few research groups, such as the Lloyd-Jones group.[3] However, many research groups do not have access to such tools and would find it cumbersome and costly to obtain them for only a few experiments.

For reactions that require high temperatures (>120 °C) or require an intake of gas, NMR monitoring can be a poor choice of instrument. Experiments run at high temperature can cause boiling of the reaction solvent in the NMR tube, which may cause shimming problems or create a mess at the NMR probe if there is a leak. The standard NMR tubes are also not well-equipped for continuous gas intake at the standard spectrometer. The Landis group has also created a set-up for high pressure NMR for gas-liquid systems. A sapphire NMR tube with a titanium tube holder (for pressures up to 68 atm) serves as the reactor. The reactor is connected to a gas delivery system, a pressurized injection system, a circulator, and a wash system.[4] While this system is impressive, most organic or inorganic chemists would not put together such an elaborate system without the need to use it several times.

A reason for concern in using a standard NMR set-up as a reaction monitoring tool is the lack of stirring, since the use of a magnetic stirbar is impossible inside the spectrometer. Kinetic

studies were done by Foley et al. at Pfizer to compare reactions in static NMR tubes (run as a standard NMR experiment), online NMR (where samples are automatically withdrawn from a mixed vessel and fed in-line to the NMR with a custom set-up), and in a NMR tube that was manually shaken at specific intervals for periodic inversion (P.I., Figure 1.1).[5]

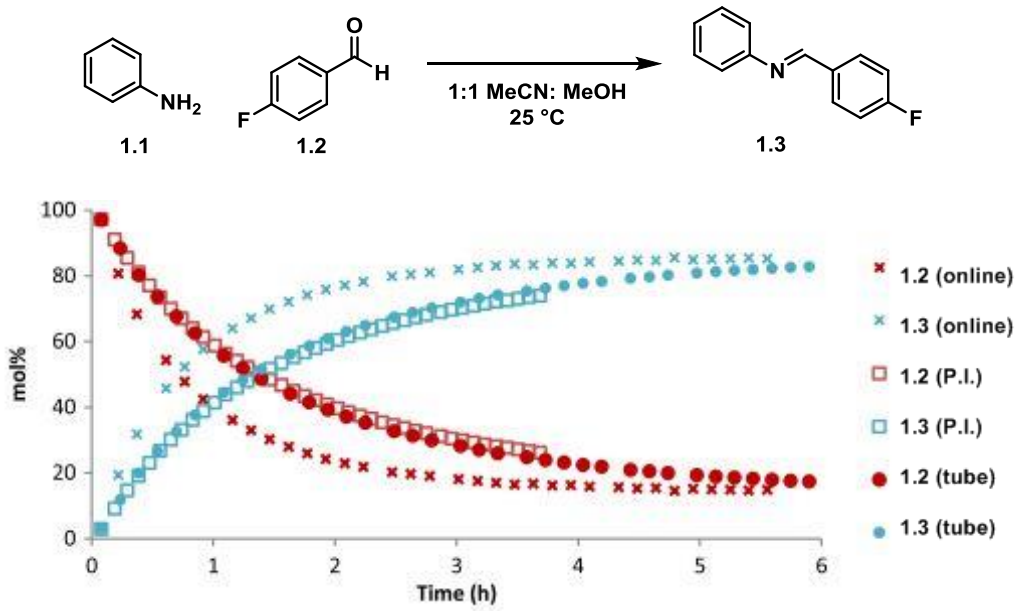

Figure 1.1: Model imine reaction monitored three different ways in the NMR spectrometer[5]

For a model homogeneous reaction, periodic inversion every 6-7 minutes is still not sufficient to mimic the online NMR experiment that has real stirring. The diffusion limited processes in the static NMR tube can change the kinetic analysis, and therefore have a large effect on what conclusions may be drawn from comparing static NMR experiments. Although static NMR experiments may be comparable to each other, the kinetic information we derive from them may not transfer well to larger, stirred reactions that are more synthetically relevant.

Unfortunately, at present, most people do not have the resources to use online NMR or stopped flow NMR techniques.

Benchtop NMRs with less powerful field strengths (60, 80, 90 MHz) are commercially available and have been used for monitoring reactions in flow.[6] This relatively inexpensive set-up can lessen the burden of booking large amounts of instrument time. It would also potentially allow for stirred reactions to be monitored by NMR. Unfortunately, the resolution of peaks is still not high, which can prohibit studying reactions more complex than a hydrolysis or condensation.

1.1.2 Heat-flow calorimetry

A less commonly used but high throughput reaction monitoring technique is heat-flow calorimetry. Commercially available calorimeters (such as those from Omnical) have multiple slots in which reaction vials can be placed. The heat coming in or out of the reactor is recorded throughout the reaction at a high data rate (3 Hz). Calorimetry is a useful technique if the heat produced from the reaction directly corresponds to the catalytic activity, or is directly proportional to the rate of product formation.[7] Hence, this involves an integral method of extracting reaction rate and then converting it to concentration (Figure 1.2). The heat ideally corresponds to the rate of product formation. The integral can be taken from the heat profile to mathematically derive the conversion of starting material to product. This assumes 100% (or near) conversion of starting material to product, and an endpoint sample should be taken for confirmation with analysis by another analytical method.

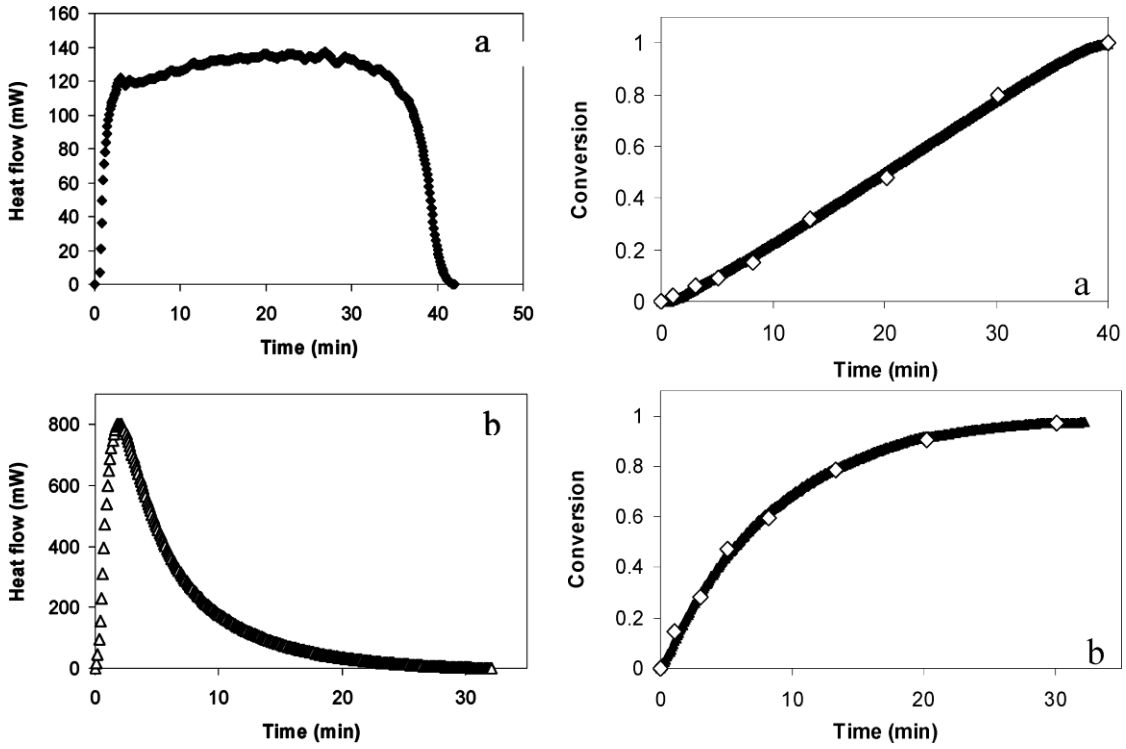

Figure 1.2: Data processing of heat output (rate) from calorimetry into conversion of starting material; a) zero order reaction, b) first order reaction

Advantages to this technique include the ability to run several reactions simultaneously, allowing more reproducible experiments and less wasted material by using stock solutions. Instead of determining order in a substrate by running experiments individually, a set of experiments can be done on two substrates simultaneously.[8] Catalyst deactivation can quickly be determined, as parallel runs can be conducted to assess catalyst robustness. Calorimetry is also useful for fast kinetic screens between different catalysts.[9] Because of the high resolution of data collected, subtle differences are more distinguishable. Microcalorimetry can also be used, with detection limits nearing 1 nW. Although microcalorimetry units are more frequently used in biochemical laboratories, they also have a place in physical organic studies.[10]

Unfortunately, if the heat evolved does not directly correspond to product formation, the calorimetry results must be interpreted carefully with extra steps in the mathematical analysis, or the results may not be useful at all.[7] While the rate-limiting step for product formation may be exothermic, if other processes are not directly coupled but produce significant amounts of heat, the overall heat generated may be too convoluted for worthwhile processing. Another reaction monitoring technique (GC, HPLC, NMR) must be used to check at least a few single point samples to ascertain that the calorimetry data corresponds to product formation.

The majority of the projects in this thesis did not have reactions whose heat curves corresponded to product formation. Some reactions were isothermal (Aza-Piancatelli); others had exothermic side reactions that did not relate to desired product formation (Kinugasa) (Scheme 1.1). As a result, calorimetry was not used as a major analytical tool for these reactions.

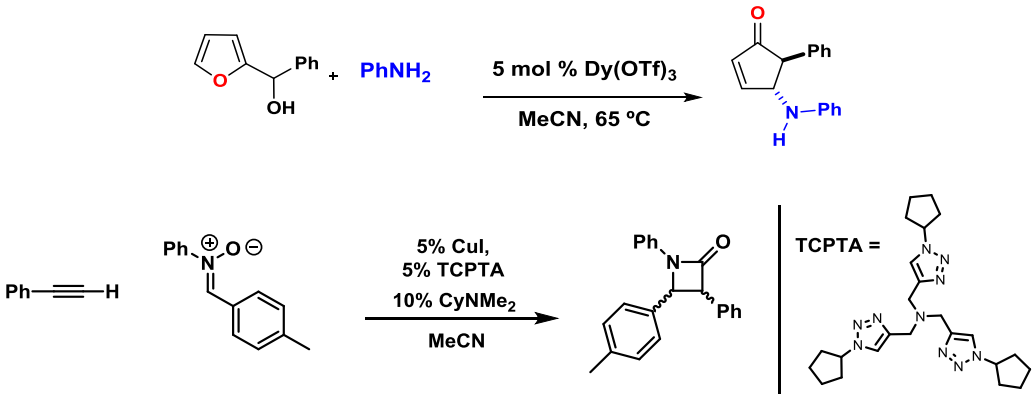

Scheme 1.1: The Aza-Piancatelli rearrangement (top) is isothermal. In the Kinugasa reaction (bottom), the product formation did not match calorimetry heat output.

1.1.3 Fourier transform infrared spectroscopy (FT-IR)

FT-IR can be used as a reaction monitoring tool that is noninvasive, fast, and requires no sampling. Peaks corresponding to characteristic stretching or bending frequencies in reactants, products, and intermediates can be shown with time. Sampling can be done by gas chromatography (GC) or LC to check that inverted product formation and substrate consumption trends overlay.[11] Commercial FTIR instruments have also become available for the purpose of reaction monitoring, such as the ReactIR. The standard ReactIR has an IR probe that is immersed into the reaction vessel. The probe contains a fiber optic cable fitted with a gold sealed diamond window. The ReactIR flow cell has also become available, requiring small amounts of fluid so that flow processes can be monitored instead of only immersing a probe in a batch reaction.[12] Aside from Mettler Toledo's ReactIR, some current FTIR spectrometers can be outfitted with a detector and flow cell for inline monitoring (Figure 1.3).[13,14]

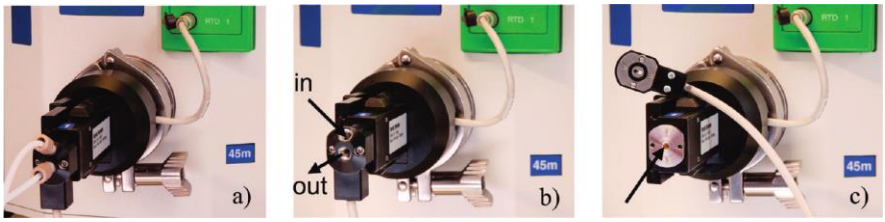

Figure 1.3: Flow cell for the ReactIR. a) flow cell with inlet/outlet fittings on; b) fittings taken off the flow cell; c) fittings head taken off[12]

A disadvantage of using FTIR is that certain probes have different "blindspot" windows where part of the spectra cannot be absorbed. The ReactIR diamond probe has a spectral window of 650-1950 cm^{-1} and 2250-2500 cm^{-1}, with a blind spot around 1950-2250 cm^{-1} with weak absorbance due to the diamond's C-C bond stretches (Figure 1.4).[13] The commercially available

flow cell widens the ranges to 650-1950 and 2250-4000 cm^{-1}. While the silicon probe does not have the same blind spot, it is less chemically resistant.[15]

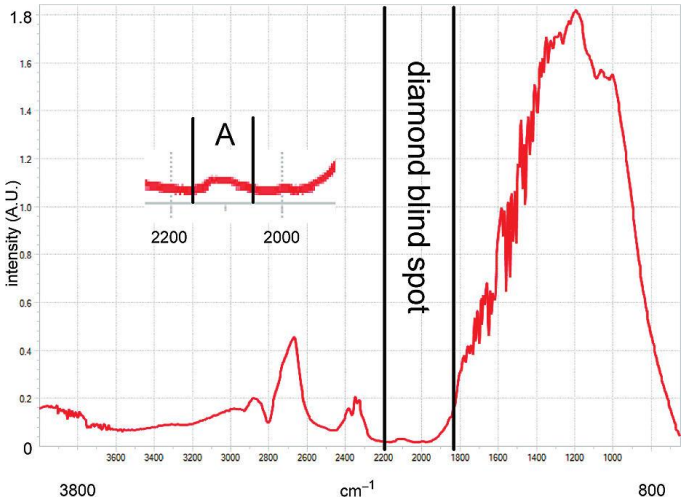

Figure 1.4: Window for a FTIR with diamond window[12]

In addition, reactions that are strongly corrosive or produce iodide can etch certain probes or destroy the gold seal inside the probe. The commercial ReactIR diamond probe is rated from pH range 1-14, but the silicon probe has a smaller range of 1-9.

Another disadvantage may be that a reaction does not have large or distinct IR-active peaks that track with the formation of product or disappearance of substrate(s). This is especially common with molecules without heteroatoms, or reactions that do not include bond forming or breaking with those heteroatoms. Overlapping peaks may also be a concern, but often enough mathematical processing and individually collected spectra of overlapping species can allow deconvolution. In particular, principle component analysis may be included in software packages to allow mathematical deconvolution.

Despite the above disadvantages, reaction monitoring by FTIR is still a common choice. Being relatively affordable and easy to maintain and transport, it is more likely for a research group to own or borrow a ReactIR than some other spectroscopic instruments for kinetic

experiments. The low barrier to using the instrument and processing the data, along with the in situ collection of data, makes FTIR a good choice for not only mechanistic studies but also for monitoring reactions done in batch from a process standpoint.[16,17,18]

1.1.4 Raman spectroscopy

Less popular than its complementary spectroscopic method FTIR, in situ Raman reaction monitoring has also been used. An example by Leadbeater uses in situ Raman in an open-flask microwave reactor.[19] Unfortunately, Raman spectra can require an extra processing step before analysis due to large variances in the fluorescent background between experiments.[20] However, Raman spectroscopy can be a useful tool for monitoring large-scale heterogeneous reactions with inorganic solids, where taking samples for HPLC can lead to uncertainty of whether the sample is representative of the whole reaction. Such was the case with an etherification reaction run with potassium carbonate, as shown by AstraZeneca. After calibration with HPLC, in situ Raman was enough to monitor the reaction on a 1500 L pilot scale.[20]

1.1.5 High performance liquid chromatography (HPLC)

HPLC is less commonly used as an in situ reaction monitoring technique. While it is often used to give an estimate of conversion by way of taking and diluting a few aliquots for analysis, it is not often used as an online/in-line monitoring technique for organic chemistry. HPLC (along with NMR) is one of the most commonly used techniques for offline analysis, although not necessarily for the construction of reaction progress curves. Rather, HPLC-MS is extremely widespread for inspecting reaction progress at a few time-points and in the use of searching for target masses in high throughput screening experiments. It is also often used to

validate another in situ technique (calorimetry, FTIR). For offline analysis, Amigo Chem is a commercially available reactor unit with a liquid handler for automated sampling, although researchers could potentially create their own unit. The samples are then suitable for offline analysis by HPLC or GC.

Most online HPLC applications have been in bioprocesses, or with permanently installed equipment for pilot plants.[21] A mobile, all-in-one sampling unit with direct injection to HPLC has been developed through a collaboration with Merck and Eksigent Technologies, Inc. in 2007 (Figure 1.5).[21] The unit was capable of collecting data on homogeneous samples, and used a frit with limited success for reactions that contained solids. The set-up was also able to monitor enantiomeric excess of the racemization of a drug with time, which instruments such as FTIR and calorimetry cannot track. Later, the set-up was used for sampling the exit stream for a reaction done in flow.[22] However, the need for a close collaboration to work on the instrumentation side to enable the online direct injection is prohibitive for many researchers.

Another online sampling system has been made before without direct collaboration with an instrumentation vendor. It utilized a push-pull capillary sampling system. Unfortunately, this system had significant delay times between sampling and online analysis, as well as potential for leaking into the reaction.[23] Progress in this endeavor seems to have slowed since, as direct-injection for HPLC-MS is largely limited to dedicated set-ups in process chemistry settings.

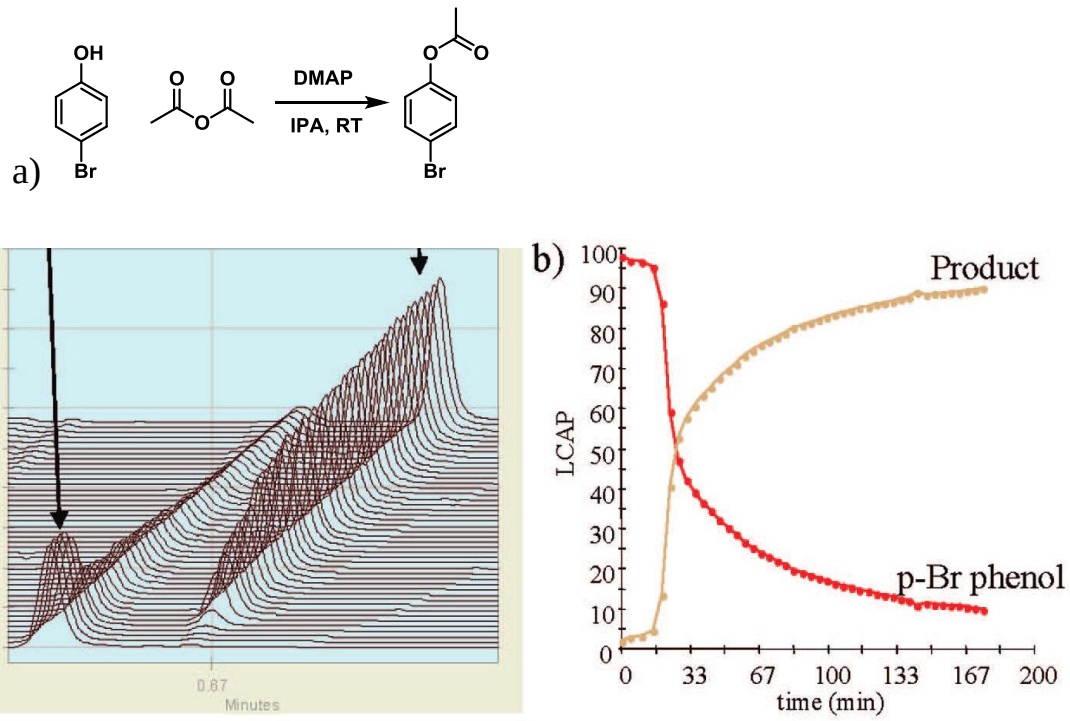

Figure 1.5: Reaction progress from the Merck/Eksigent direct-injection HPLC. a) the HPLC spectra stacked for display as a surface; b) The relative conversions correlating to the indicated peaks from the HPLC surface[21]

Unfortunately, compounds without UV-active chromophores are invisible by HPLC (unless coupled to an ELSD) and may be more suitable for analysis by GC. Many chemists lack an automated method of taking reaction samples for offline analysis, and manually taking samples can be very time-consuming and can lead to scattered data. Especially for gas chromatography, samples often need filtering to avoid inorganic build-up, leading to degradation of columns. However, for reactions using volatile compounds with no UV-active chromophore and paramagnetic metals, GC can be one of the last remaining options.[24]

A disadvantage to both HPLC and GC is that both require the user to take into account response factors of each compound of interest. This usually requires making calibration curves and ascertaining that the mass balance of the reaction makes sense. This can be tedious, as every new compound put into the reaction (and corresponding product(s)) requires an extra step to appropriately account for their concentrations.

In this thesis, HPLC was a vital tool, particularly for the creation of reaction progress tools. We hope to show that although it may be more labor intensive to analyze the HPLC data, the richness of data is worth the effort. It can be possible to take samples of slurries for analysis by HPLC followed by full dissolution in another solvent, although the representation of the reaction as a whole can be still be questionable. With the column technology rapidly improving, separation times decrease and the ability to separate more compounds increases. In addition, compounds that overlap by ^{1}H-NMR or FTIR can potentially be separated by HPLC.

1.1.6 Electrospray ionization – mass spectrometry (ESI-MS)

ESI-MS has been used without its HPLC counterpart as a reaction monitoring tool.[25,26,27] While it was first used as an in situ technique in 1994, it has seen little use until the past decade or so. Since it is a soft ionization technique, many compounds of interest can be observed without too much difficulty arising from fragmentation, as often observed with electron ionization (EI). For example, losses of ligands from an organometallic compound can be predicted easily, making identification of compounds relatively intuitive.

Advantages to the technique include its great sensitivity to charged ions, which can be made possible by the addition of an external aqueous acid source. Its need for only micromolar concentrations allow catalytic intermediates to be seen that would otherwise be baseline by other

spectroscopic methods (NMR, IR, HPLC). While nonpolar solvents may prove difficult (possibly due to lack of conductivity), ionic liquids can be added to the reaction solution that do not interfere with the chemistry.[28] However, a control reaction without the additive should be monitored by a different analytical tool to ascertain that the additive indeed has no effect on the reaction.

As a reaction monitoring tool, great success has been seen by the McIndoe group by pressurizing a reaction flask with an inert gas and slowly cannulating the reaction mixture through HPLC tubing into the mass spectrometer (Figure 1.6). Unfortunately, this technique requires reactions to be run at micromolar concentrations, which is generally not synthetically relevant. Catalyzed reactions that can be studied under this technique would need to be quite robust under ultra-dilute conditions, which does apply to many palladium catalyzed cross-coupling reactions.[28] FTIR has also been used in tandem to analyze reactions at higher concentrations, allowing FTIR detection of the major components while ESI-MS detects intermediates in lower concentrations.[29]

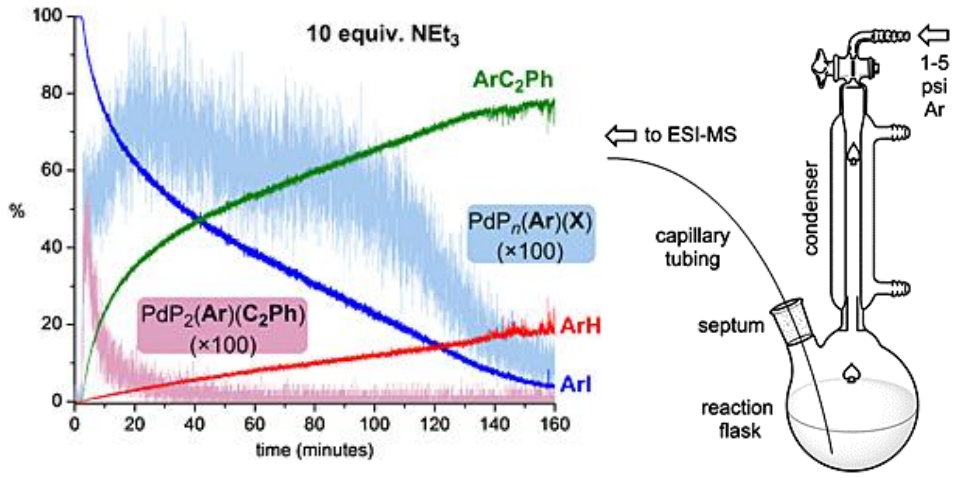

Figure 1.6: Right: Set-up for direct injection of a reaction to the ESI-MS for reaction monitoring. Left: percent conversion calculated from processed ESI-MS data[28]

An example of a process-scale reaction with online ESI-MS was demonstrated in 1999. The apparatus was able to take a sample, quench it, dilute it 3000-fold, and add a buffer for ionization and analysis. The data obtained at the time was noisy, but it showed detailed speciation of the compounds of interest in the reaction.[30]

1.1.7 Dual methods of reaction monitoring

The above mentioned tools are often used in industrial settings as part of Process Analytical Technology (PAT), which refers to the tools used for rapid analyses of processes. PAT is used to improve efficiency of modifying reactions in batch and studying the stability of potentially hazardous or transient intermediates and byproducts that may be produced. While most research groups might not use more than one analytical tool for mechanistic studies, pharmaceutical companies may have the resources to access several of them. Often, multiple spectroscopic tools can be used simultaneously to monitor a reaction, allowing one to either obtain more information than one tool could provide, or to more quickly decide which tool would be the most useful for the process at hand.

1.1.7.1 MS, FTIR, FBRM used together in a batch reactor

In a successful example, four techniques were used to monitor a heterogeneous batch reaction of a sulfonyl chloride reacting with aqueous ammonia to form the corresponding sulfonamide (Figure 1.7).[31] MS was used to assess the composition of gases in the headspace. FTIR was used to see the product formation in the liquid phase, followed by a drop in concentration when product precipitated out. Calorimetry was used to monitor the heat output

and watch for exotherms. Focused Beam Reflectance Measurement (FBRM) was used to analyze the solid phase, especially as crystallization occurred.

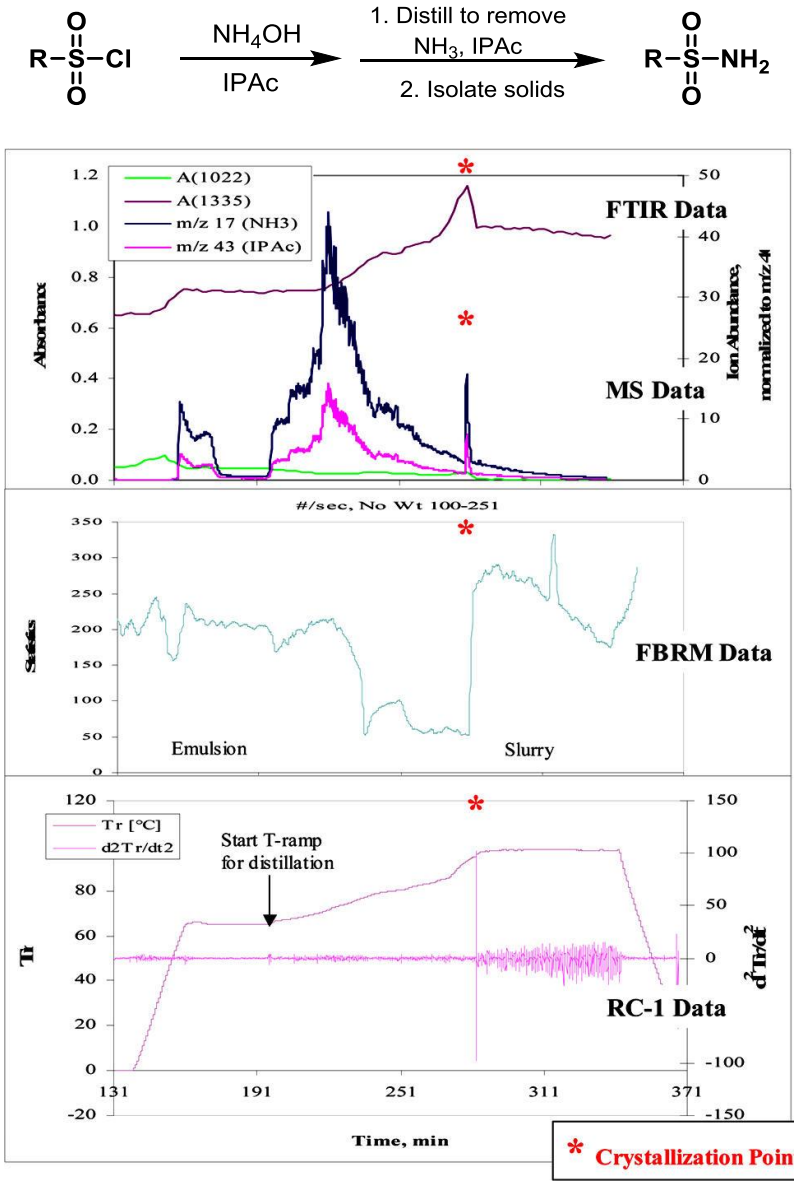

Figure 1.7: A batch reaction monitored by multiple methods: FTIR, MS, FBRM[31]

1.1.7.2 NMR and HPLC

Unfortunately, many analytical instruments use detectors that are not inherently quantitative, such as HPLC (UV detector) and GC (FID). Because even structurally similar compounds can have different relative response factors (RRF), samples of all the compounds of interest must be prepared or obtained to construct calibration curves against a standard to calculate RRF values. This can be tedious and time-consuming, especially compared to inherently quantitative techniques such as NMR. Coupling two such instruments together can account for the weaknesses in both. By creating a set-up that allows both in-line HPLC and in-line NMR through a flow cell, Foley and coworkers at Pfizer were able to calculate RRF values from one experiment by comparison to NMR, as well as monitor reactions by two orthogonal analytical methods.[32] The reaction is stirred in batch, allowing monitoring using synthetically relevant conditions. This set-up seems to work well for room-temperature, homogenous reactions.

NMR and FTIR have also been coupled together in use to monitor batch reactions. While in situ FTIR is widely accepted and used in PAT, online NMR is used less frequently, albeit it is becoming more prevalent.[33] Potentially, this may be because ReactIR is relatively easy to incorporate into a batch reactor set-up, whereas in-line NMR analysis can take a more dedicated set-up. In addition, taking samples for offline NMR analysis can be intrusive for unstable intermediates of interest. Online NMR would be much more informative if it can show sensitive species, unaltered by a quench. In contrast, FTIR is often unable to pick up all species in low concentrations, whereas NMR often can. NMR can also be used to identify and validate peaks observed by FTIR. Interestingly, in two recent examples of in-line NMR and FTIR, the progress reaction curves between the instruments are not compared, and experimental data fit poorly to

computationally optimized data.[34,33] While both projects could have been mainly characterized and monitored their reactions by NMR alone, the identification and validation of FTIR peaks by tandem NMR allows subsequent experiments to be monitored by ReactIR alone.

1.1.7.3 Comparison of reaction monitoring methods

A chart comparing disadvantages and advantages between the aforementioned reaction-tracking methods mentioned in this thesis has been constructed for convenience (Table 1.1). Unsurprisingly, NMR has a unique set of advantages that make it an extremely desirable tool for reaction monitoring; unfortunately, paramagnetic metals can make the process more difficult. In addition, there are several faster techniques listed.

	Fast Acquisition (1 Hz or more)	Automated data collection	Inherently Quantitative	Low concentrations detectable	Characterization data	Parallel reactions can be run
NMR		✓	✓	✓	✓	
HPLC				✓	✓ if MS attached	✓
GC				✓	✓ if split with EI	✓
ESI-MS	✓	✓		✓	✓	
FTIR	✓	✓				
Raman	✓	✓				
Calorimetry	✓	✓				✓

Table 1.1: Comparison of multiple reaction monitoring techniques

1.2 Methods of mechanistic analysis

Many reactions used in organic chemistry today have generalized mechanisms or catalytic cycles that include well-known elementary steps; however, reactions will often differ in their catalyst resting states, rate-limiting steps, and off-cycle processes. Most chemists focus on the productive on-cycle processes that afford them their desired product. Although robust

reaction are appreciated, equally interesting is how the catalyst spends its time off-cycle, as well as how the selectivity between desired products and potential side products may change with time (Scheme 1.2).

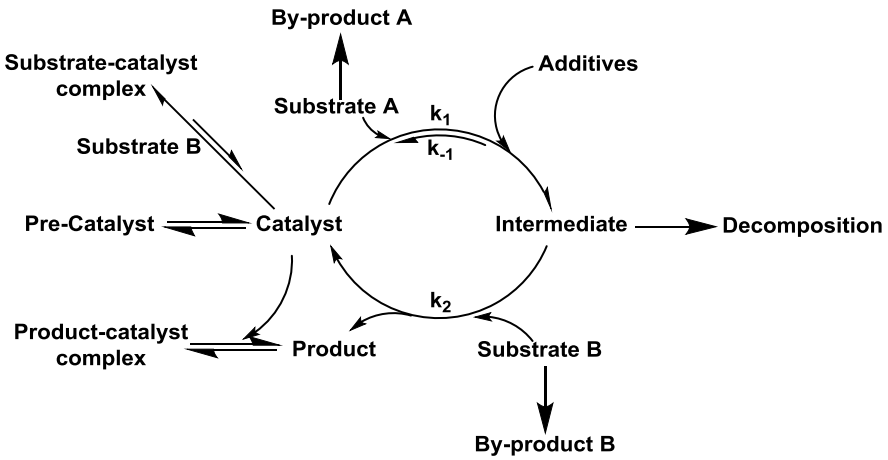

Scheme 1.2: A generalized catalytic cycle with several off-cycle processes

Some chemists screen catalysts with the mindset to find one that gives at least a trace of the desired product, and then further optimizes conditions with the same catalyst. Although many chemists will mix precatalyst and ligand pairings according to what they intuit would work for their reaction, identifying optimal conditions might only be possible by testing more possibilities and then working backwards. A more complete picture of the catalyst's resting state, as well as the reaction progress of the entire reaction, could help provide insight into how the reaction can be improved before disregarding potentially cheaper and more selective catalyst and ligand combinations. As the possibilities are nearly limitless, high throughput screening armed with some mechanistic insight could be much efficient than setting up numerous screens.

Rather than only studying by any single analytical technique or methodology, we were more interested in applying a plethora of tools to look at a reaction and then narrowing down to the most informative tools for the specific reaction. Often, simply looking at the kinetic

speciation throughout the entire reaction by a different analytical method allowed us to know something about the reaction that evaded those who originally developed the reaction.

Figure 1.8 shows examples of kinetic profiles of chemical species exhibiting different roles within a catalytic reaction. These profiles can help guide an initial guess of a molecule's role in a complicated web of reactions.[29]

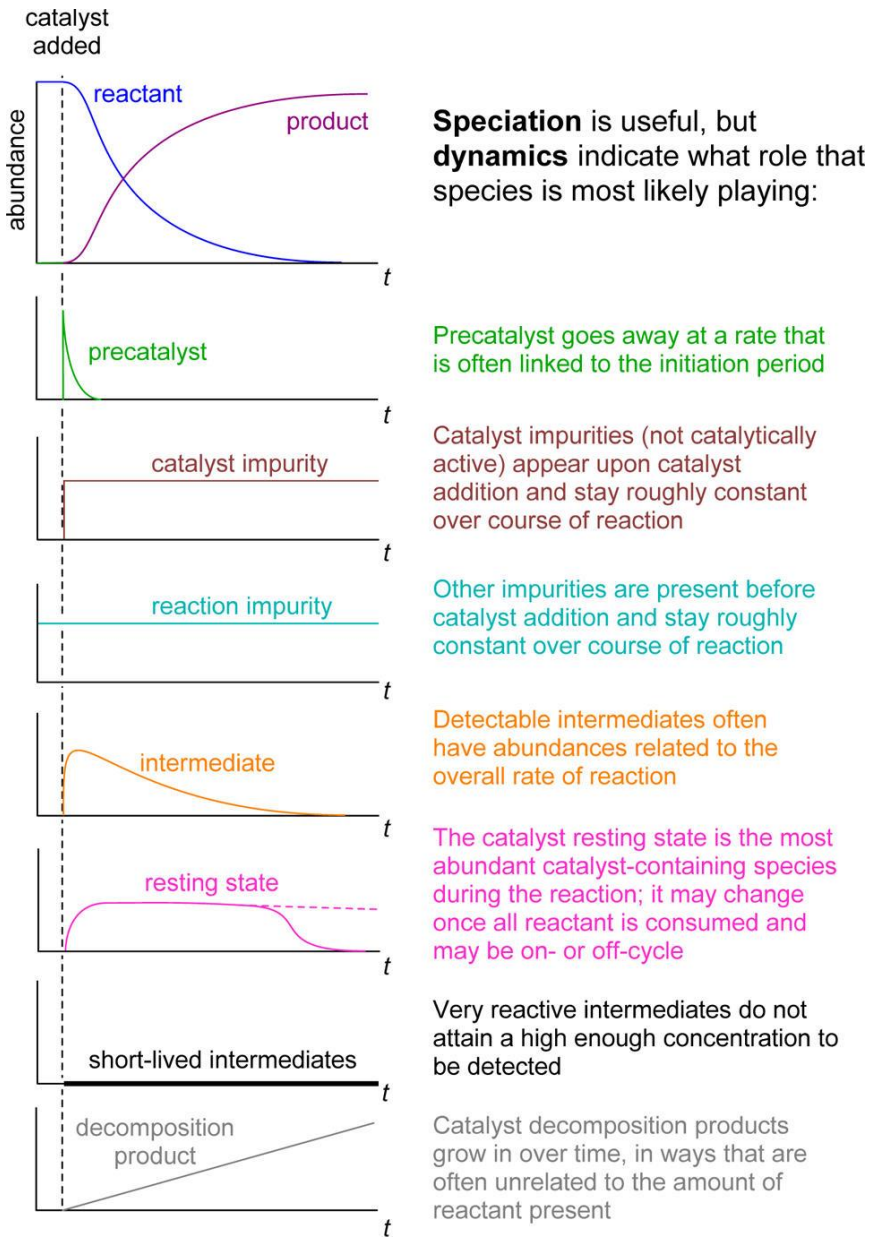

Figure 1.8: Examples of kinetic profiles of species with different roles in the reaction[29]

1.2.1 Michaelis-Menten kinetics

One of the simplest and widely-used models for catalytic reactions is the Michaelis-Menten model. Although it is described in terms of catalysis with enzymes, its principles are used in mechanistic organic chemistry. While its models may oversimplify catalytic cycles, it provided a preliminary methodology to model catalyzed reactions.

The model utilizes a simple catalytic system where the substrate (S) and catalyst (E for enzyme) form a substrate-catalyst complex (E:S). (Scheme 1.3) This complex undergoes a rate-limiting step to form a product-catalyst complex (E:P), which then releases the product. This model assumes that the rate-limiting step is the transformation from the substrate to the product (with rate (k_{cat})); the Michaelis-Menten will not work if the rate-limiting step refers to another step.

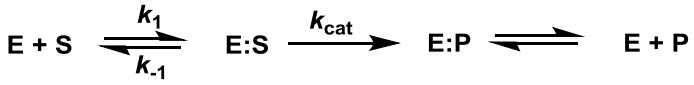

Scheme 1.3: Michaelis-Menten catalytic system

Because the rate-limiting step is from E:S to E:P, the rate law for product formation can be expressed as:

$$\frac{dP}{dt} = k_{cat}\,[E:S]$$

The steady state approximation can be used for [E:S]:

$$\frac{d[E:S]}{dt} = k_1([E]_0 - [E:S])[S] - k_{-1}[E:S] - k_{cat}[E:S] = 0$$

Solving for [E:S] and substituting into the equation for product formation provides the Michaelis-Menten equation:

$$\frac{dP}{dt} = \frac{k_{cat}[E]_0[S]}{[S] + K_M}$$

where

$$K_M = \frac{k_{cat} + k_{-1}}{k_1}$$

K_M is the Michaelis-Menten constant, and k_{cat} is the turnover number, both of which can be experimentally measured. The numerical value of K_M allows comparisons of the tightness of binding of a catalyst to a substrate. Evaluating K_M can necessitate measuring initial rates of reaction for varying concentrations of the substrate, which means looking at the kinetics of starting material consumption, usually with 10-15%. Unfortunately, this can cause important kinetic behavior to be missed beyond the initial behavior.

In Michaelis-Menten kinetics, the turnover number of the catalyst is the rate constant (k_{cat}) referring to the conversion of the substrate to the product with the active catalyst, per second. While this model refers to a single step with the k_{cat}, an overall rate constant can be observed for reactions that require multiple steps to convert the substrate to product. Also useful are the relative values of k_{-1} and k_{cat} because their ratio controls the extremes of the equation where the catalysis is relatively fast or slow.[35]

1.2.2 Reaction progress kinetic analysis

The Hein lab's approach to solving problems originated from Reaction Progress Kinetic Analysis (RPKA), coined by Prof. Donna Blackmond.[36,37] RPKA can suggest a few initial sets of experiments to determine reaction order in substrates and find any evidence of catalyst deactivation or product inhibition. RPKA can be thought of as an expanded view of Michaelis-Menten kinetics for more complicated systems. While the ideas and mathematics of RPKA are not new, RPKA encouraged a graphical approach that helped chemists design experiments more

efficiently and analyze their results with better understanding. Although the Hein lab does not always follow the suggested sequence of RPKA experiments, the ideas of graphical analysis and streamlined experiments (to gain the most information from fewer experiments) are utilized frequently.

RPKA encourages a standard set of experiments that should be done to minimize the number of experiments done while extracting the maximum amount of information. Instead of doing several repetitive experiments for less information, graphical manipulations of the timecourse data can reveal the same information in potentially less than half the number of experiments. Whereas classical kinetics may only give a glimpse at a small portion of the reaction, obtaining global kinetics can potentially show a broader and more detailed view of the catalytic lifecycle. Blackmond argues that global kinetic analysis can provide more information about the steady-state catalytic cycle, even if a catalytic species has already been identified.[37] Furthermore, as a reaction progresses, the relative concentrations of chemical species change, which can shift the role of certain intermediate catalytic species. As substrates are depleted and product is formed, it is possible for the mechanism to change, potentially causing different speciation of byproducts.

An example of a simplified catalytic system often used to model many coupling reactions is portrayed in Scheme 1.4. Substrate A binds to catalyst ("cat") to form intermediate I, to which substrate B adds to form intermediate II. The cross-coupling product C is formed and releases catalyst back into the cycle. Although isolating and characterizing catalytic intermediates is thought to prove a certain proposed mechanism correct, it is important to see the intermediate's role in the catalytic cycle. For example, if binding of the catalyst to A is the rate-limiting step, the intermediates I and II are likely to be transient and relatively low in concentration, making

isolation difficult. Conducting a few experiments to see the global kinetics could reveal this information early on so that efforts to isolate fleeting, unstable intermediates would not be in vain.

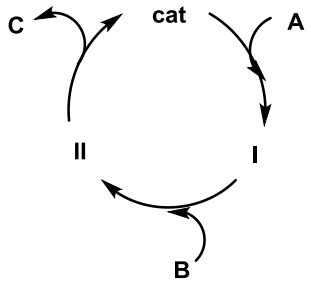

Scheme 1.4: Simple catalytic cycle

As with classical kinetics, one of the first set of experiments conducted should be to find the rate order in the substrates – in this case, A or B. Many catalyzed organic reactions exhibit a global first-order kinetic profile in product formation. However, this often means that the reaction is first-order in one substrate (A or B) and zero-order in the other (B or A). In classical kinetic experiments, usually one would run a set of experiments for both A and B, varying their concentrations individually and then use initial rates to determine order in either substrate. A keystone in RPKA is to use different "excess" experiments to find the same information. Excess ("xs") is defined as the difference between the initial concentrations of A and B, or $[xs] = [B]_0 - [A]_0 = [B] - [A]$. Assuming one mole of A is consumed for every mole of B, [xs] should stay constant throughout the reaction, allowing one concentration to be inferred from the other, therefore removing a degree of freedom from the rate equations. Just two different excess experiments are necessary to determine order in either substrate.

Excess experiments should have different but reasonable concentrations. As an example, an excess experiment can have $[A]_0 = 100$ mM, $[B]_0 = 140$ mM where [xs] = 40 mM. A separate

experiment could have $[A]_0$ = 70 mM, $[B]_0$ = 140 mM where [xs] = 70 mM. After reaction progress is collected from both experiments, the rate of product formation can be graphed against the concentration of the limiting substrate (A) for subsequent analysis. Alternatively, the analysis can still be done if concentration of product vs time data is collected without conversion to rate vs concentration of substrate (by taking the instantaneous rate). Another experiment may be necessary that varies the concentration of B, for example, $[A]_0$ = 100 mM, $[B]_0$ = 70 mM, where the $[A]_0$ was the same in one of the previous experiments. If a higher concentration in B increases the reaction rate for the same $[A]_0$, then there is a positive order in [B]. The inverse is true. In the first two experiments where $[A]_0$ was different but $[B]_0$ was the same, if the reaction rates did not change, there would be zero order in [A].

In contrast to different excess experiments, "same excess" experiments are done to see if catalytic activity changes over the course of the reaction – that is, is the catalyst deactivated at any point, or does product inhibit or accelerate the reaction? For example, an experiment can be done where $[A]_0$= 0.10 M, $[B]_0$ = 0.14 M, and another one where $[A]_0$ = 0.14 M and $[B]_0$ = 0.18 M, where for both [xs] = 0.04 M. Afterward, the progress curve of the first experiment (of lesser concentrations in both A and B) can be time-adjusted and overlaid with the second experiment (of higher concentration) at the time when [A] = 0.10 M. If the progress curves overlay after [A] = 0.10 M, then the catalyst activity does not change throughout the reaction. To see if the formation of product affects the kinetics, a third experiment can be done where product is added initially to the same conditions as the first or second experiment. Rate acceleration or deceleration due to product can be seen through overlay, or lack of. Effectively, these three experiments allow the reaction to start at different stages but with fresh catalyst, allowing the user to see if the catalyst becomes "old" through a deactivation or decomposition process.

Many reactions exhibit first order dependence in catalyst concentration, and excess experiments are not as useful unless this is true for the reaction in question. Deviance from typical first-order behavior under standard conditions can suggest unusual catalyst behavior through the formation of catalyst dimers (or higher order species) or aggregation, leading to less than first order in catalyst. Higher than first order in catalyst can be due to the need of having two catalyst molecules necessary for the rate-limiting step. There is also a new graphical method to determine order in catalyst by conducting only 2-3 experiments by normalizing the time axis with varying concentrations of total catalyst.[8]

Aside from comparing reactions through graphical overlay, it is important to simply look at the shape of the reaction progress curves. Deviation from first order behavior may indicate unusual catalytic behavior, indicated by inflection points (sudden changes in rate or product formation). Competition experiments between two electronically or sterically different substrates may also reveal hidden information about the catalyst. None of this information would be obtained from taking a single point analysis of the product(s) at the end of the reaction.

Unfortunately, RPKA methodology works best for relatively clean, catalyzed reactions that form one major product with about 90-100% conversion. RPKA's technique of graphical analysis falls short for complex reactions with many undesirable side products. RPKA experiments typically are not done until the conditions are found for which the reaction is well-behaved, usually following screens of solvents, additives, temperature, and catalysts.

1.2.3 Linear free energy relationships

Linear free energy relationships (LFER) are a method of parameterizing electronic or steric factors and relating them to relative free energies or relative rate constants. By varying a

specific group on a substrate and assessing the resulting rate of product formation, the effect of the group on the transition state of the rate-determining step or the mechanism of the reaction can be assessed quantitatively. Potentially, this can lead to predictions about other substrates that have not been studied.

Possibly the most popular LFER used for mechanistic studies in organic and organometallic chemistry is the Hammett plot. The Hammett equation is a commonly used empirical relationship that correlates substrate structure and reactivity. It is specifically for comparing reaction rates among substrates with varying substituents on an aryl ring. The Hammett equation is $\log (k/k_0) = \rho\sigma$, where k is the rate of a reaction and k_0 is the rate of reaction where the substituent X = H, σ is a tabulated constant for the substituent X, and ρ is the reaction constant calculated from the slope of the generated linear curve. The substitution constants σ are tabulated against a model reaction, the ionization of *m*- and *p*-substituted benzoic acids. Therefore, the equation is intended for *meta* and *para* substituted aryl rings.[38] Sigman et al. have also done some studies to help provide parameters to study *o*-substituted aryl rings, but with the inclusion of steric factors.[39] Substitution constant σ can be thought of as the extent to which a substituent changes the electron density at the reaction site, regardless of the reaction being studied. The reaction constant ρ that results from the relative differences between the rates is a reflection of how the reaction is affected by such changes in electronic factors.[40]

There have also been efforts to reduce σ into different components such that $\sigma = \sigma_F + \sigma_R$, where σ_F is a contributor from inductive/ field effects, and σ_R is from resonance effects. There are various methods of calculating and/or empirically finding values for the different contributors.[38]

Typically, Hammett Plots constructed from evaluating the rates of reactions will show a positive or negative linear relationship between log (k/k_0) and σ. With a positive ρ (or slope), electron-withdrawing substituents increase the reaction rate. A negative ρ means more electron-donating substituents accelerate the reaction. This is usually attributed to favoring increased/ decreased electron density at the transition state of the rate-determining step.

Uncommon nonlinear Hammett relationships have also been observed, usually indicated by a change in the opposite sign of the slope at X=H (for which $\sigma = 0$). A concave down shape is potentially a more common nonlinear Hammett relationship (Figure 1.9). This is generally attributed to the reaction having the same mechanism, but the rate-determining step shifts over to another step as the substituents tune the electronics. This is caused by relative changes in the energy barriers between the formerly rate-determining step and the new rate-determining step. Examples include the reaction of aromatic aldehydes with *n*-butylamine to form benzylidene *n*-butyl amines, following addition and elimination of water.[41] In contrast, a concave up shape is proposed to be caused by changing the mechanism or changing the structure of the rate-determining step as the substituents change from electron-donating to electron-withdrawing. Reactions with observed concave up Hammett relationships include certain reactions with alkyl and acyl halides with nucleophiles, for example, the reaction between *p*-substituted benzyl chlorides and thiosulfate.[42] Continuous Hammett relationships are also possible, where changes in mechanism occur more smoothly instead of having a sharp change.

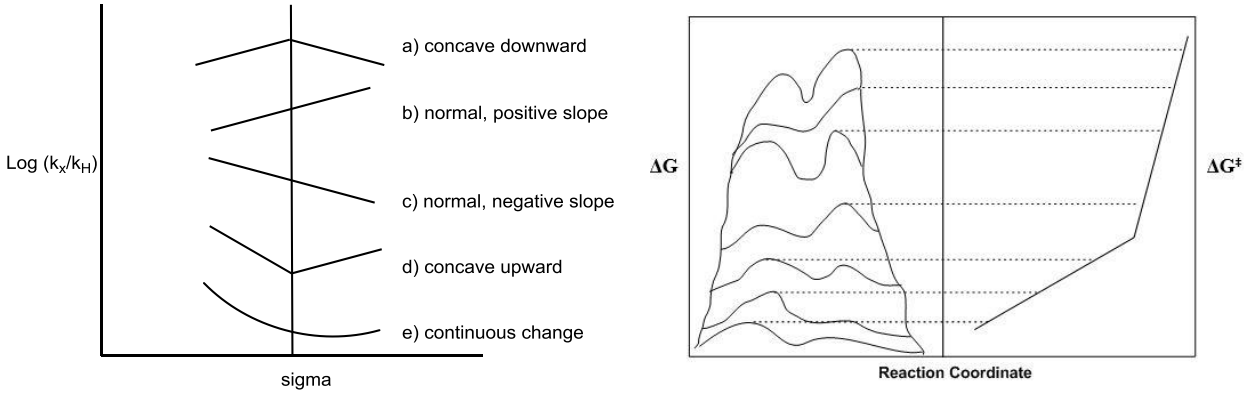

Figure 1.9: Left: types of nonlinear Hammett plots. Right: transition state diagram for a two-step reaction and its corresponding Hammett plot[40]

Most LFER analyses utilize only one steric or electronic parameter. Unfortunately, only choosing one parameter may not provide any sensible correlations. For example, the Taft/ Charton steric parameters were applied to a desymmetrization of bisphenols catalyzed by a peptide in the Miller group.[43] The resulting graph had no discernable trend. The Taft/ Charton parameters may not always be useful because they were derived from a specific mechanism (the acid-catalyzed hydrolysis of methyl esters), and therefore are not useful for all mechanistic studies on sterics.[44,43,45] As techniques for seeing reactions and studying mechanisms improve, the methods of analyses need to be altered to show meaningful relationships between structure and thermodynamics.

Recently, work has been done to combine multiple parameters, aside from the classic Hammett and Taft/ Charton steric parameters. The Sigman group focuses on analyzing substituents using both electronic and steric parameters, using both experimental data as training sets and forming predictive models through MATLAB, which is easily assessable by many researchers. To account for sterics, the Sterimol parameters are sometimes used because they

have three measurements to describe a substituent, and can be computationally derived for new substituents. In the above example, using the Sterimol parameters allowed a much better fit to a plausible trend. The Rovis group has also applied the Sterimol parameters, showing that the use of non-traditional parameters may be spreading.[46]

Aside from sterics, the chemical computational software Gaussian is used to minimize geometries of starting materials so that factors such as bond stretching frequencies, natural bond orbital (NBO) charges, and torsion angles can be used as parameters. Following a preliminary mechanistic analysis using more traditional mechanistic studies (KIE) to find the rate-determining step, parameters significant to transition state can be chosen. When screening for increased activity or enantioselectivity resulting from ligands, it is also suggested to sample the extremes of the steric and electronic factors to more quickly assess which factors are important.[44] Since the goal is to provide a better understanding of to what extent what factors affect the reaction, even "bad" results with poor yields or low enantioselectivities still provide useful information.

Despite the development of new techniques to analyze and parameterize kinetic information and high throughput screening processes to provide results, it is important to note that some mechanistic understanding must be obtained before attempting to perform more complicated analyses of the steric and electronic factors governing the mechanism. Just as in Sigman's group, there must be a solid handle on the reaction. A proposal for the rate-determining step must be supported, any side reactions should be known, and therefore at least some kinetic profiling is necessary. Much of this thesis will focus on the latter – being able to monitor non-ideal reactions reliably and collect reaction rates with high fidelity is essential to having believable data.

1.3 Overview of chapters

Due to the collaborative nature of conducting mechanistic studies for others and an interest in exploring different types of chemistry, the following chapters will consist largely of unrelated projects. While each project concerns a separate reaction of interest, the driving force for each project is to provide more insight into the reaction's mechanistic features. As a consequence, most or all projects involve adapting tools to enable seeing and analyzing the reaction in ways that were previously unavailable or underutilized. Due to the constantly changing resources available to our lab, some chapters show an evolution in analytical tools, although comparisons between reactions are done with an identical instrumental set-up.

Chapter 2 focuses on the Aza-Piancatelli Rearrangement, which was initially studied using ReactIR. As the chemical speciation became more complicated when different substrates were used, an automated sampling tool was developed to analyze the reaction by HPLC-MS in tandem with ReactIR. Stemming from this project, a few studies were done to compare lanthanide triflates (as a Lewis Acid) and Brønsted acid catalysis in this rearrangement.

Chapter 3 describes our progress on looking at the mechanism of the Kinugasa reaction, monitored by HPLC-MS. A preview of a new method of direct-injection HPLC is also given with this reaction as an example.

In Chapter 4 examines the modification the automated sampling apparatus from Chapter 2 to allow monitoring inside microwave reactors. The thermal aryl Claisen rearrangement was used as a model reaction, and the existence of non-thermal effects is sought for. Direct comparisons between microwave and conventional heating are also made.

Chapter 2: Mechanistic Studies on the Aza-Piancatelli Rearrangement

2.1 Introduction to the Piancatelli and Aza-Piancatelli rearrangements

Discovered in 1976, the Piancatelli rearrangement refers to the acid-catalyzed formation of 4-hydroxycyclopentenones from 2-furylcarbinols (Scheme 2.1). The reaction was thought to go through a mechanism similar to a Nazarov cyclization.[47] The cyclopentenone products are useful as scaffolds for prostaglandins. However, the Piancatelli rearrangement was not well developed at the time – it required stoichiometric acid, ultra-dilute conditions, and was limited to water as a nucleophile. The 4,5-*trans*-cyclopentenone can also further rearrange to the 2,4-cyclopentenone.

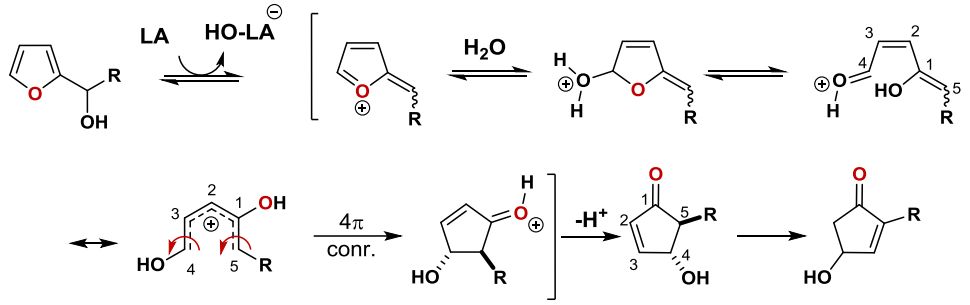

Scheme 2.1: The Piancatelli rearrangement, 1976

Henschke and coworkers modified the reaction by using $ZnCl_2$ as a catalyst, but unfortunately, these conditions were not selective for either isomer of the 4-hydroxycyclopentenone product. (Scheme 2.2).[48]

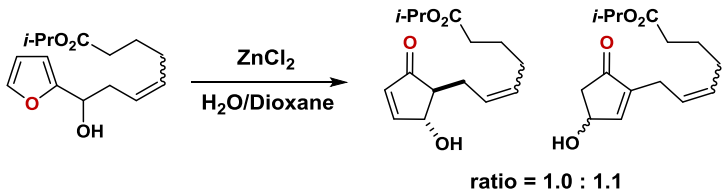

Scheme 2.2: Zinc-catalyzed Piancatelli rearrangement – Henschke, 2012

Reiser and coworkers also developed a non-catalytic, highly pressurized and heated Piancatelli rearrangement which selected for one cyclopentenone isomer, but with moderate diasteroselectivity (Scheme 2.3).[49]

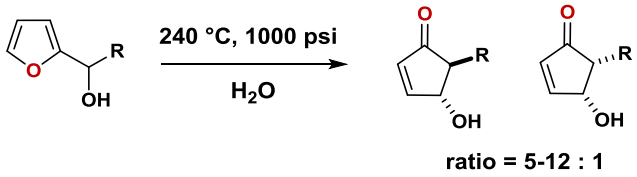

Scheme 2.3: Pressurized, heated Piancatelli rearrangement – Reiser, 2013

In a similar dysprosium-catalyzed electrocyclization, the Batey group formed 4,5-diaminocyclopent-2-enones from furfural and an amine, catalyzed by lanthanide triflates (Scheme 2.4). Their nucleophiles included primary and secondary amines.[50] Inspired, the Read de Alaniz group used lanthanide triflates to catalyze a rearrangement between 2-phenylfurylcarbinols and amines, calling the reaction the Aza-Piancatelli Rearrangement as a modification to the original rearrangement (Scheme 2.5).[51]

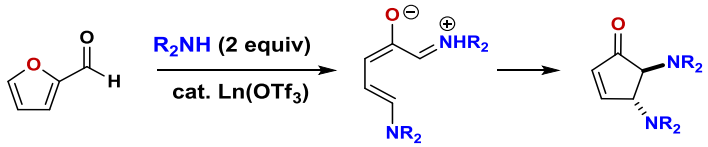

Scheme 2.4: Domino condensation/ring-opening/electrocyclization process to form 4,5-diaminocyclopent-2-enones – Batey, 2007

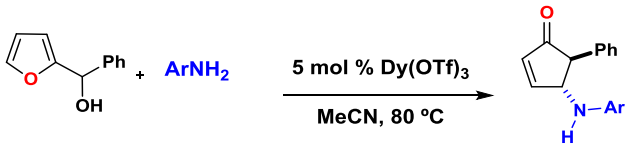

Scheme 2.5: Aza-Piancatelli rearrangement – Read de Alaniz, 2010

The Read group was successful in expanding the substrate scope of the Aza-Piancatelli rearrangement to aniline nucleophiles, catalyzed by lanthanide triflates under synthetically relevant conditions. Dysprosium (III) triflate was chosen as their lanthanide due to its low cost and lessened hygroscopic nature relative to other lanthanide salts. This Lewis acid catalyst was also observed to suppress the formation of Friedel-Crafts byproducts found when a Brønsted acid was used. The reaction was also utilized in an intramolecular rearrangement to form azaspirocycles with arylamines tethered to the furlycarbinol.[52] Although the furylcarbinol could be varied at the 2 position to include alkyl substituents, once again, the amine was limited to arylamines.

Similar to the Piancatelli rearrangement, it is assumed some basic transformations must occur in the mechanism of the Aza-Piancatelli rearrangement (Scheme 2.6). The phenylfurylcarbinol is activated by a Lewis or Brønsted acid, allowing water to be lost, and an oxocarbenium ion is formed. This oxocarbenium ion is captured by an amine nucleophile. The Aza-Piancatelli rearrangement is thought to go through a 4π conrotary electrocyclization, analogous to a Nazarov cyclization, leading to only the 4,5-*trans*-cyclopentenone diastereomer after deprotonation, unlike the previous catalytic and non-catalytic versions.

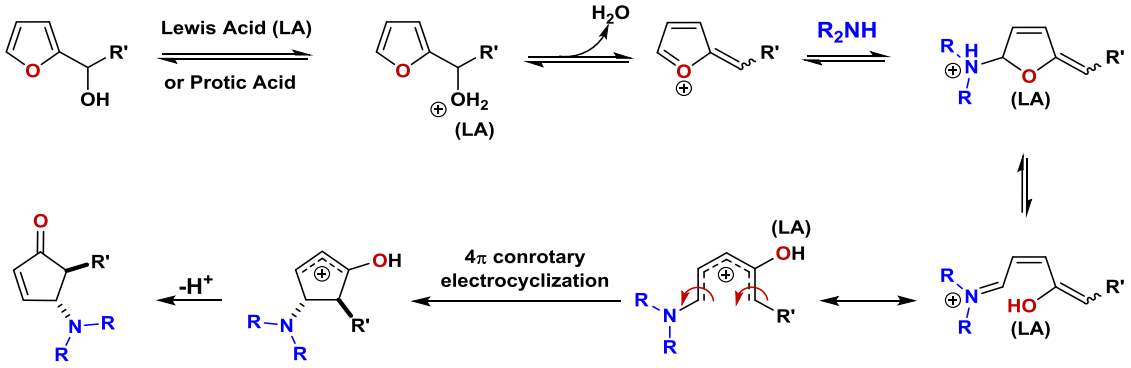

Scheme 2.6: Proposed general mechanism of the Aza-Piancatelli rearrangement

The collaboration with the Read de Alaniz group began to augment their initial mechanistic studies, which had given them little useful information. We were interested in understanding the reaction for a couple of reasons. The most apparent downside to the reaction was its apparent limited amine substrate scope. Among many amine nucleophiles that had been used, only anilines gave any conversion to the desired cyclopentenone product. The use of alkylamines gave no product – even using a simple switch from aniline to benzylamine as the nucleophile gave no conversion. The narrow range of chemoselectivity was intriguing, and a more thorough understanding of the catalytic activity was sought to aid expansion to a broader substrate scope.

In addition, various chiral ligands had also been previously screened by the Read de Alaniz group, but not even modest enantioselectivities were found. It was thought that a better idea of the catalyst's involvements in the later intermediates (before or during the electrocyclization step) could help us understand what type of ligand could allow an asymmetric transformation. However, improving the enantioselectivity by screening different ligands was not an important focus for this particular reaction in our studies.

As experiments were conducted, a key objective was to study the differences between Lewis and Brønsted acid catalysis. It has been argued that the lanthanide triflates are merely more easily handled form of triflic acid, and that the triflic acid (especially with trace water) was the true catalyst.[53] Mechanistic studies were done with this possibility in mind in case it would affect the observed kinetic behavior.

2.2 Initial mechanistic studies by ReactIR

ReactIR was initially used to observe reaction progress. The carbinol was monitored by the disappearance of the peak at 1013 cm^{-1}, most likely corresponding to the breaking of the C-O bond of the furylcarbinol. The cyclopentenone formation was monitored with the 1715 cm^{-1} peak, presumably corresponding to the C=O stretch of the ketone. It was immediately apparent that the reaction had an overall zero-order profile in both consumption of the furylcarbinol substrate and the formation of the product (Figure 2.1). Overlay was observed by inverting the product trend and comparing with the starting material trend. This ascertained that the mass balanced for conversion of the furylcarbinol starting material to the pentenone.

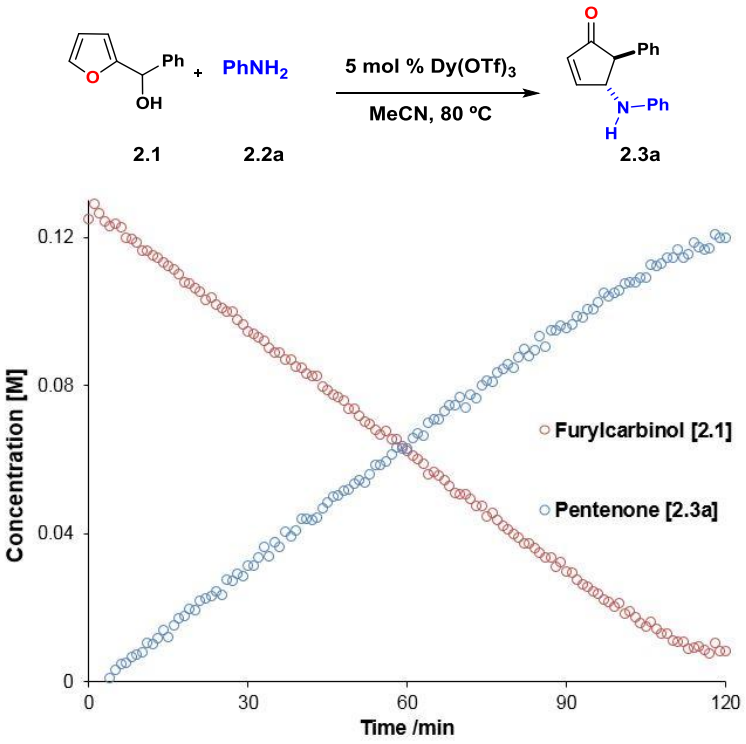

Figure 2.1: Initial kinetic studies by ReactIR showing zero-order profile

To check that this zero-order profile was not an artifact only seen by ReactIR, the reaction was run again with the IR probe, with aliquots taken for offline analysis by HPLC-MS

(Figure 2.2). The agreement between IR and HPLC-MS was agreeable, so further studies were done individually with ReactIR.

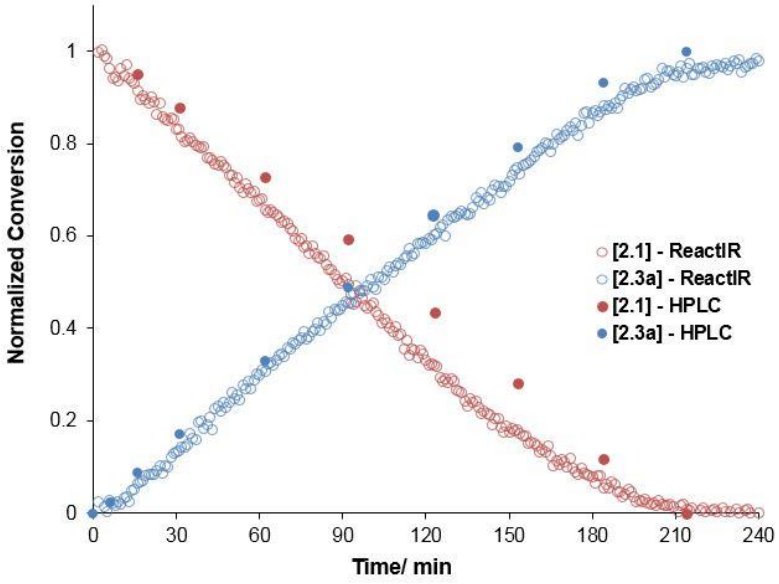

Figure 2.2: Validation of ReactIR trends by HPLC-MS

Since catalyzed reactions typically have an overall first-order profile, the zero-order reaction profile was intriguing. A reaction with true zero-order in product formation and substrate consumption would imply that varying the concentrations of the furylcarbinol or aniline nucleophile would not affect the reaction rates. Although the experiment was found to be positive order in $Dy(OTf)_3$, (see Experimental section) the order in both substrates was unclear.

With this information in hand, we decided to conduct classical RPKA methodology on the model reaction by conducting same excess experiments, typically done to assess catalyst deactivation, as introduced in Chapter 1. The following initial conditions were used in four separate reactions, with a constant catalyst concentration: **a**) $[\mathbf{2.1}]_0 = 0.12$ M, $[\mathbf{2.2a}]_0 = 0.14$ M, **b**) [furylcarbinol **2.1**]$_0$ = 0.10 M, [aniline **2.2a**]$_0$ = 0.12 M (xs= 0.02 M in aniline); and two with

the inverted concentrations with an excess of 0.02 M in the furylcarbinol (experiments **c**, **d**). It can be seen in Figure 2.3 that experiments with an excess of aniline (**a**, **b**) are slower than experiments with an excess of furylcarbinol (**c**, **d**). More importantly, experiments **a** and **b** with the same excess of aniline, even at different absolute concentrations, have very similar rates. Hence, the relative amounts of aniline and furylcarbinol control the rate when the concentration of dysprosium catalyst is kept constant. The reaction quickens with increased furylcarbinol and slows down with excess aniline. This observation is a departure from the traditional interpretations derived from RPKA due to the unusual effects in the aniline substrate.

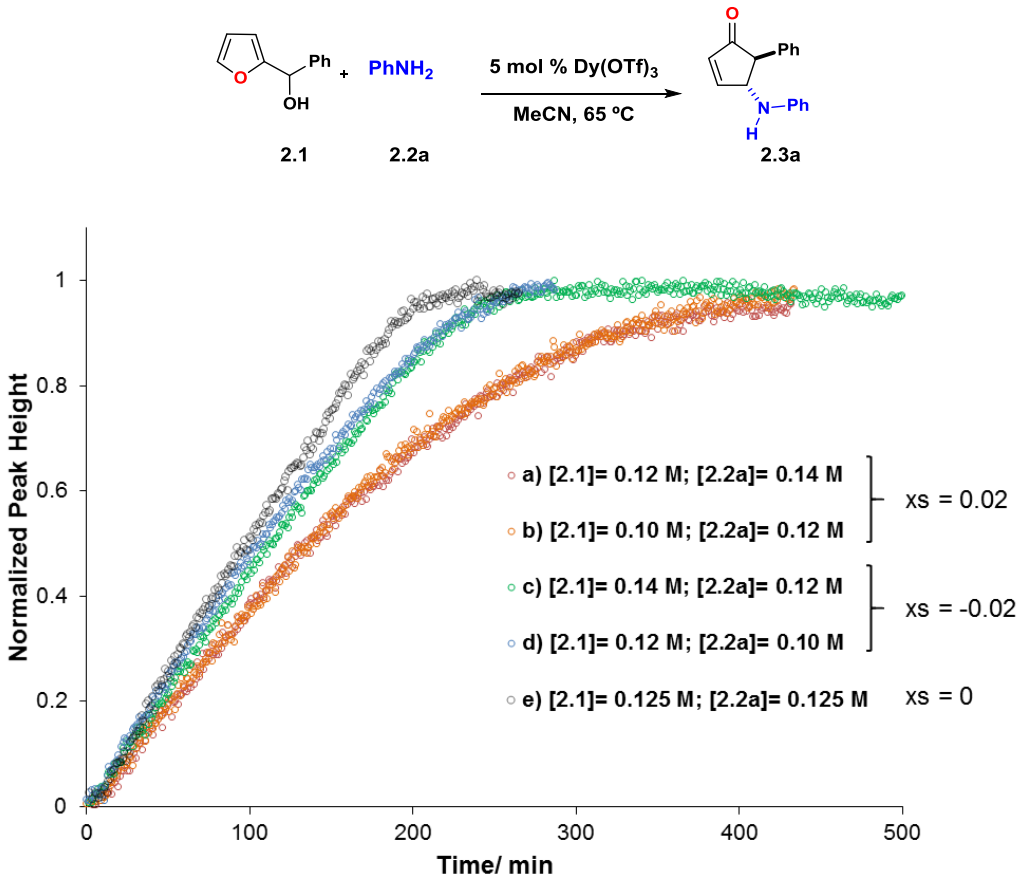

Figure 2.3: Experiments with same absolute initial excess concentrations of aniline or furylcarbinol, showing product formation by ReactIR

Instead of starting with both substrates with a small excess, additional experiments were done. Slow additions of each substrate were done in separate experiments. Slow addition of the aniline (starting with only furylcarbinol) immediately led to the decomposition of the furylcarbinol through the formation of Friedel-Crafts side products, as detected by HPLC-MS. The opposite procedure of adding furylcarbinol portionwise to a solution of aniline and the dysprosium catalyst did not cause the sudden formation of Friedel-Crafts side products; instead, the reaction rate was merely slow. Clearly, the amine had to be present in sufficient proportions to prevent the side reactions of the furylcarbinol that were catalyzed by dysprosium triflate.

Substrate control was most succinctly portrayed in two simple experiments. A reaction with an initial excess in furylcarbinol (0.12 M and 0.07 M in aniline) was allowed to run for 25 minutes. Then, the remaining aniline (0.05 M) was added at once to the solution. Immediately, the reaction rate dropped. The inverse was also done (0.05 M furylcarbinol added to a reaction with initially 0.07 M furylcarbinol and 0.12 M aniline), showing that the reaction speeds up (Figure 2.4). After delayed addition of either reagent, the reaction rates are nearly identical, even though the reactions started with different conditions. Clearly, although the reaction displays an apparent zero order, the relative concentrations of both substrates do affect the rate of catalysis.

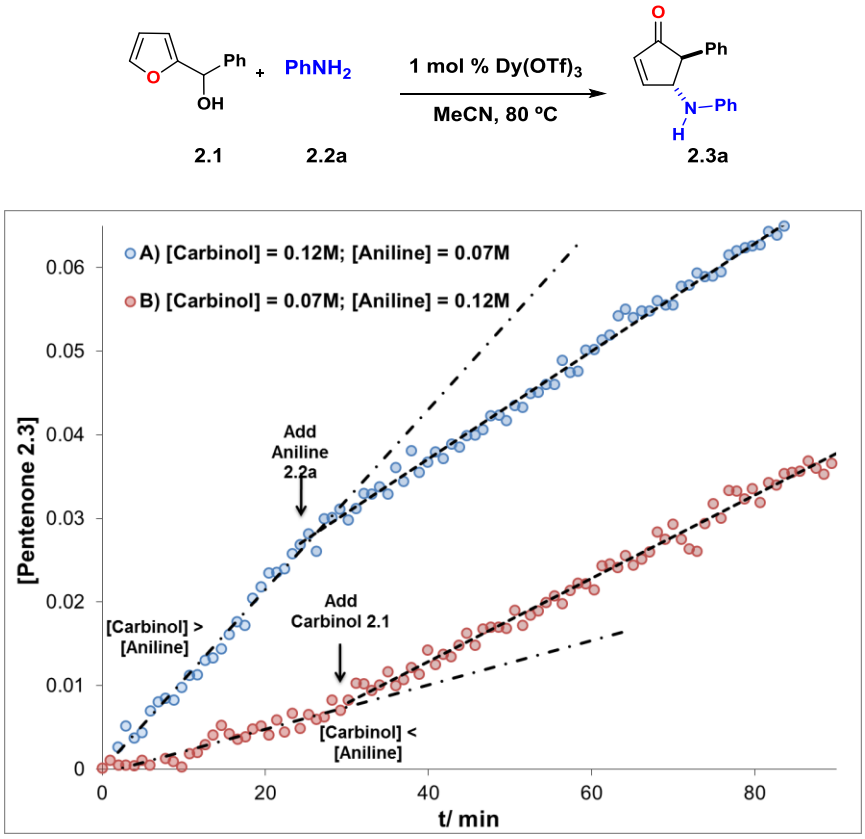

Figure 2.4: Late partial addition of substrate in two experiments – showing product formation

2.3 Linear free energy relationships and competition experiments

As with many traditional mechanistic studies, we decided to employ LFER with a Hammett plot to assess the effects of electronics on the reaction, as discussed in Chapter 1 (Figure 2.5). A Hammett plot was constructed for the Aza-Piancatelli rearrangement with varying the substituent at the *para* position on the aniline. ReactIR was once again used to monitor the consumption of furylcarbinol and formation of pentenone product. The relative rates of linear product formation were calculated and compared to the reaction with aniline (substituent X=H).

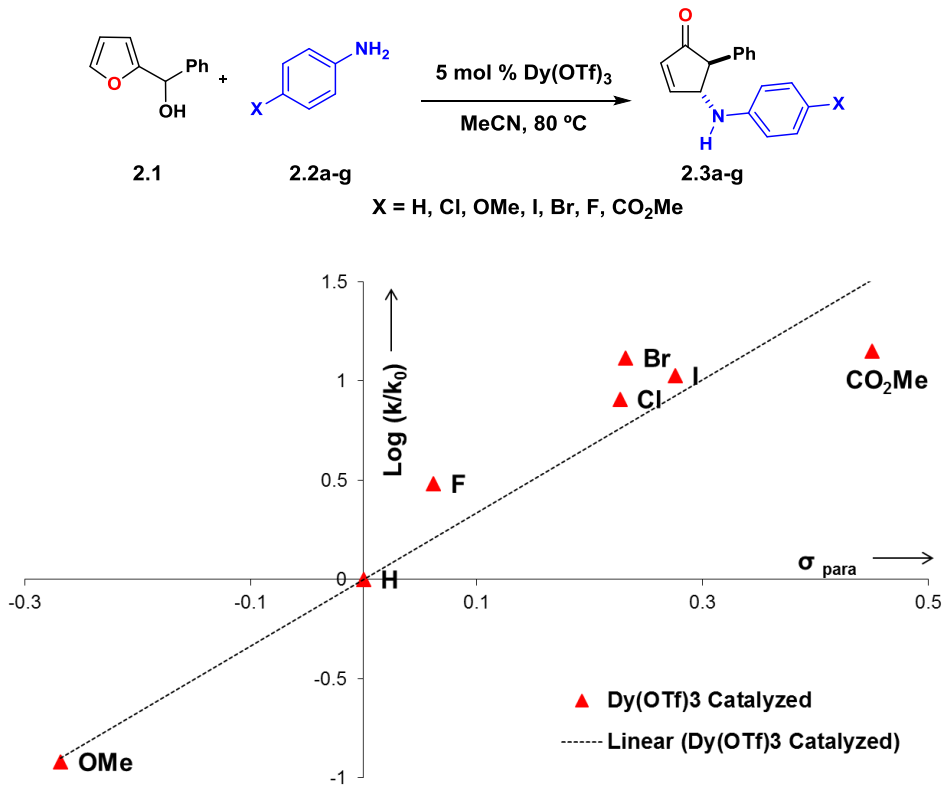

Figure 2.5: Hammett plot for dysprosium-catalyzed Aza-Piancatelli rearrangement, created by ReactIR

A positive ρ value was found, indicating that the rate increased for electron-withdrawing substituents on the aniline. As mentioned before, the positive ρ value would classically suggest that the transition state of the rate-determining step is aided by decreased electron density on the amine. However, another interpretation could be possible: electron-donating anilines bind to the dysprosium catalyst more tightly, more greatly limiting the amount of free catalyst able to participate on-cycle (Scheme 2.7). This is outside of the normal Hammett interpretation, which does not take metal catalyst binding into consideration, since the parameters are built upon the disassociation of substituted benzoic acids.

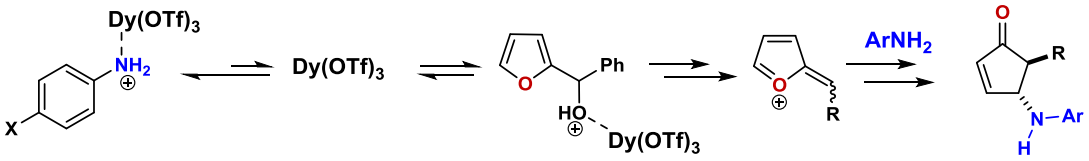

Scheme 2.7: Aniline substrate binding to dysprosium

With this knowledge in mind, a competition experiment was conducted between two anilines of different *para* substituents, 4-methoxyaniline (compound **2.2b**) and 4-chloroaniline (compound **2.2c**) (Figure 2.6). The experiments were monitored by manual sampling and analysis by HPLC-MS, as the two ketone products were not easily differentiated by ReactIR. Given the results of the Hammett plot, it was expected that formation of the methoxypentenone **2.3b** to be significantly slower than that of the chloropentenone **2.3c**. When the ratio of substrates was 2 furylcarbinol : 1 Cl aniline : 1 OMe aniline, the opposite result was found. The rate of formation of the chloride product **2.3c** was depressed, while the OMe product **2.3b** formed. When the OMe aniline was mostly consumed, the rate of Cl product formation suddenly increased.

In this experiment with 1 Cl-aniline : 1 OMe-aniline : 2 furylcarbinol, the contradictory result where the methoxypentenone product **2.3b** is formed in favor of the chloropentenone **2.3c** provides mechanistic insight (Figure 2.6). For the first 60 minutes of the reaction, the large excess of aniline (relative to catalyst) binds to the majority of the dysprosium catalyst. For whatever amount of oxocarbenium ion is generated from activation with dysprosium, the better nucleophile (methoxyaniline, due to the electron-donating X substituent) is more likely to intercept the oxocarbenium intermediate. Until most of the methoxyaniline has been consumed, the weaker nucleophile (4-chloroaniline) shows a lower rate of addition to form the

corresponding chloropentenone product **2.3c**. Later in the reaction, as the 4-methoxyaniline is nearly consumed and allows lessened binding of the dysprosium catalyst, the 4-chloroaniline is finally free to attack the oxocarbenium intermediate, causing a rate acceleration in chloropentenone formation.

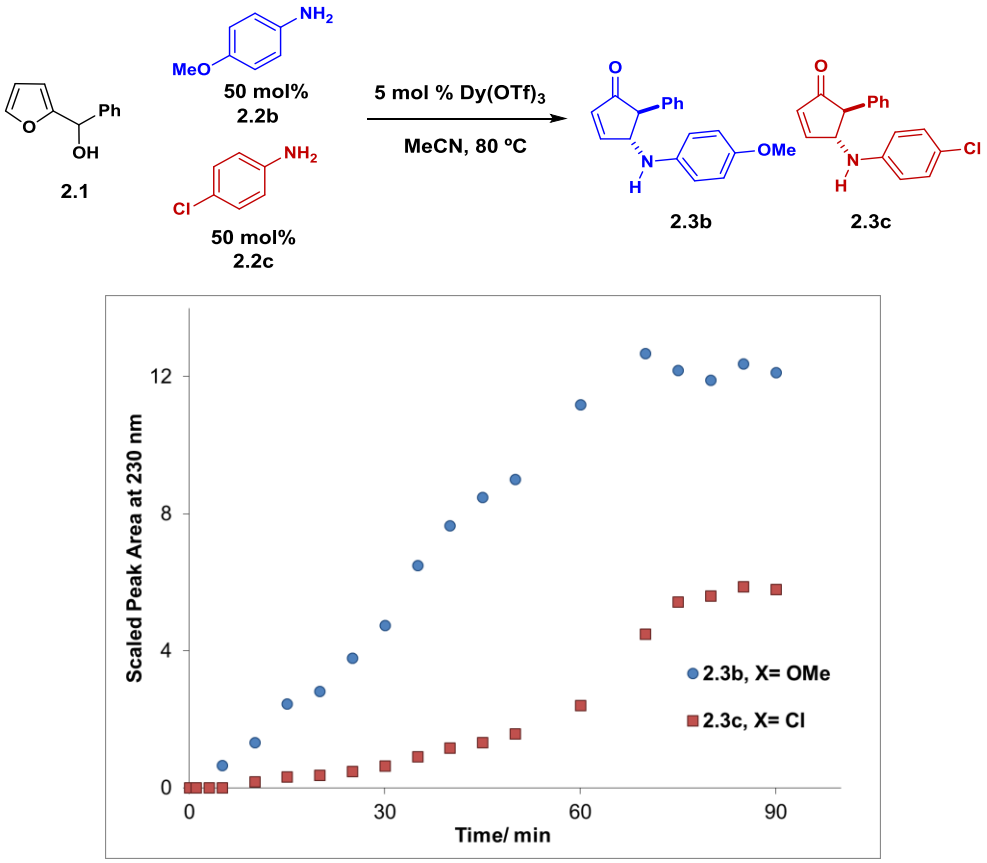

Figure 2.6: Competition experiment with 2 furylcarbinol : 1 Cl : 1 OMe, with pentenone formation monitored by HPLC-MS

The conversion to the chloropentenone is less than expected, most likely due to a less than expected amount of remaining furylcarbinol. This can be attributed to formation the of Friedel-Crafts products that have been observed with electron-donating anilines like anisidine and 2,6 dimethylaniline (Scheme 2.8).[51]

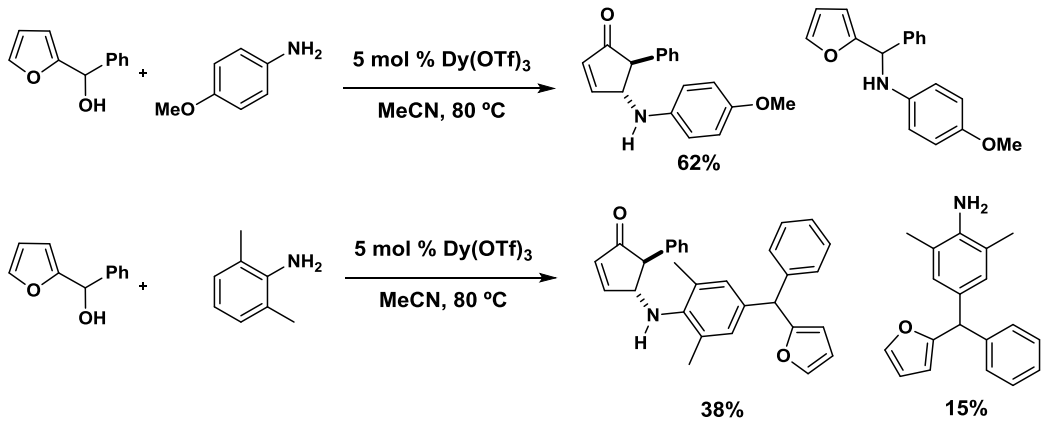

Scheme 2.8 Isolated yields of Friedel-Crafts side-products with electron-rich anilines

When the ratio of substrates was changed so that the amount of aniline was double the amount of furylcarbinol (1 Cl aniline : 1 OMe aniline : 1 furylcarbinol), the rate of formation of product **2.3b** is similar to the case in which chloroaniline is absent; hence, the rate of methoxypentenone **2.3b** formation has not changed significantly. The rate of methoxypentenone **2.3b** formation in the absence of another aniline is shown in Figure 2.7 in an experiment monitored by ReactIR. The ReactIR product formation trend of **2.3b** is overlaid with the HPLC data for the competition experiment with anilines **2.2b** and **2.3c**. Only the rate of chloropentenone product **2.3c** formation is depressed – formation of **2.3b** is not accelerated. As with the case with less total aniline, the selectivity for the methoxyaniline is much higher.

These results suggest that the rate and selectivity controlling steps are separate (Scheme 2.9). The relative amount of binding amine nucleophile to the Lewis acid dysprosium catalyst controls the rate, as shown by the Hammett Plot. However, if there is enough free catalyst to generate the oxocarbenium ion from the furylcarbinol, the best nucleophile available (e.g., an electron-donating amine) will proceed to product formation, therefore controlling selectivity.

This decoupled control of selectivity from rate is supported by the previous competition experiments.

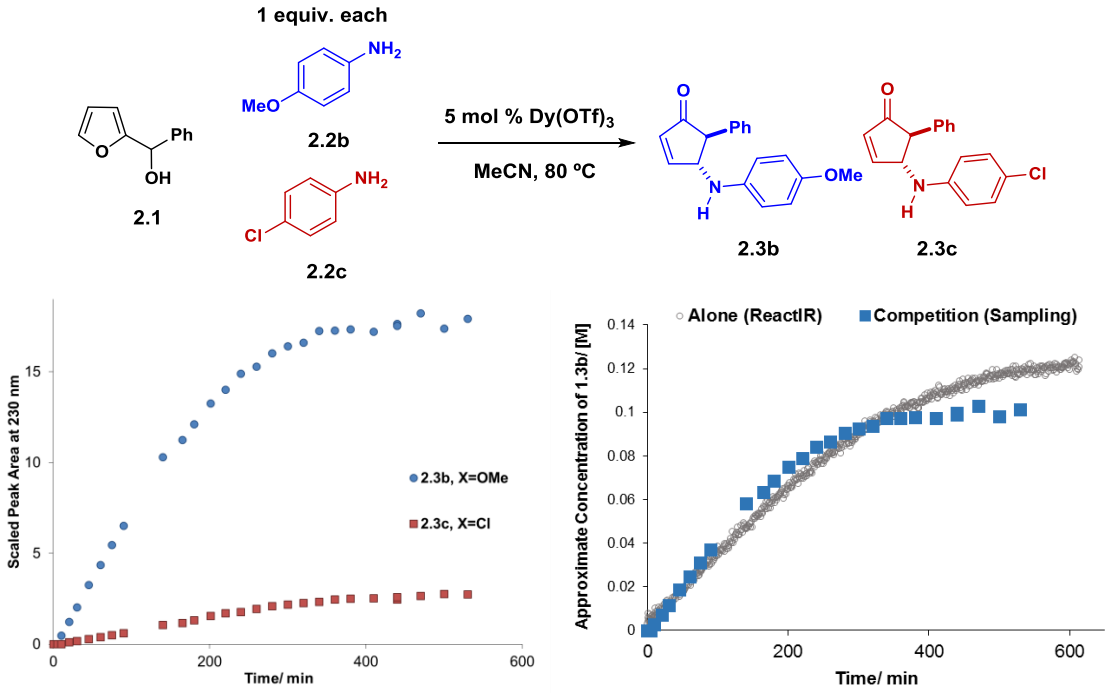

Figure 2.7: Competition experiment with 1 furylcarbinol : 1 Cl : 1 OMe. Left: HPLC data for conversion of the two pentenone products; Right: ReactIR vs HPLC data for the methoxypentenone formation in a noncompetitive reaction

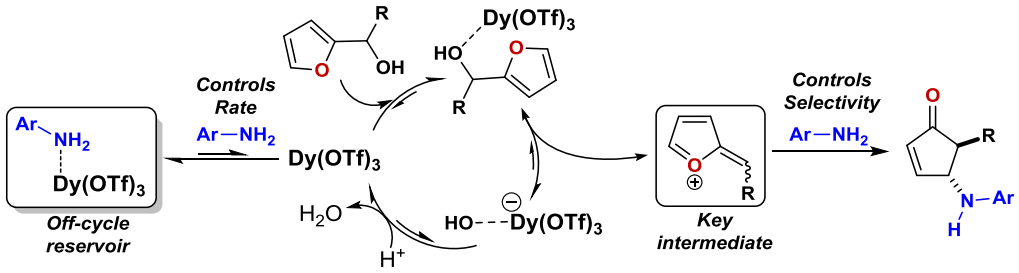

Scheme 2.9: Proposed catalytic cycle for the dysprosium-catalyzed Aza-Piancatelli rearrangement

A rate law for the proposed catalytic cycle was derived to ensure that it showed zero-order behavior in product formation under standard conditions. The catalytic cycle can be portrayed as in Scheme 2.10:

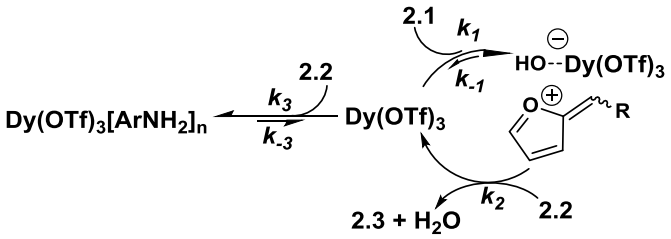

Scheme 2.10: Rate law schematic for the dysprosium-catalyzed Aza-Piancatelli rearrangement

Or drawn in general (Scheme 2.11):

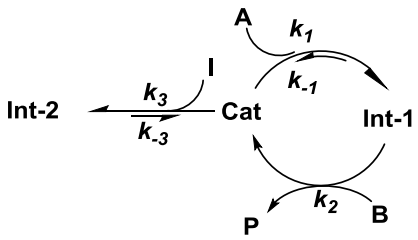

Scheme 2.11: Rate law schematic rewritten for a generalized catalytic cycle

A detailed derivation is in the experimental section of this chapter. The rate of product formation reduces down the following:

$$\frac{d[P]}{dt} = \frac{k_1 k_{-3} [A] [cat_{tot}]}{k_3 [B]}$$

2.4 Brønsted vs Lewis acid catalysis in the Aza-Piancatelli rearrangement

While dysprosium (III) triflate was assumed to act as a Lewis acid catalyst through the metal center, there was concern about whether the catalyst was merely a solid, weighable source to slowly release triflic acid to catalyze the reaction. This would mean that the reaction was truly catalyzed by a Brønsted acid. Instead of running experiments to compare with triflic acid as a more direct comparison to dysprosium (III) triflate, trifluoroacetic acid (TFA) was used due to its lower price and ease of handling. Trichloroacetic acid, a weighable solid, was not used more than once due to its tendency to decompose into carbon dioxide and chloroform under these conditions, particularly in acetonitrile.

2.4.1 Replication of dysprosium-catalyzed reactions with TFA

It was found that a Brønsted acid such as TFA caused a first-order overall profile in the Aza-Piancatelli rearrangement by ReactIR (Figure 2.8). For the reaction to finish in approximately the same amount of time, it required approximately five more equivalents of TFA than dysprosium (III) triflate.

The change from zero to first order by changing from a Lewis acid to a Brønsted acid catalyst – instead of merely a change of rate – was the first indication that that using a dysprosium catalyst did not give the same kinetic behavior as a Brønsted acid.

While switching from a Lewis acid to a Brønsted acid catalyst caused the shape of the kinetic profiles to change, many characteristics appeared to be similar. For example, the Hammett plot was redone with TFA and compared with the dysprosium-catalyzed plot (Figure 2.9). The relative rates were in good agreement, as seen by the similar ρ values of 3.30 and 3.36.

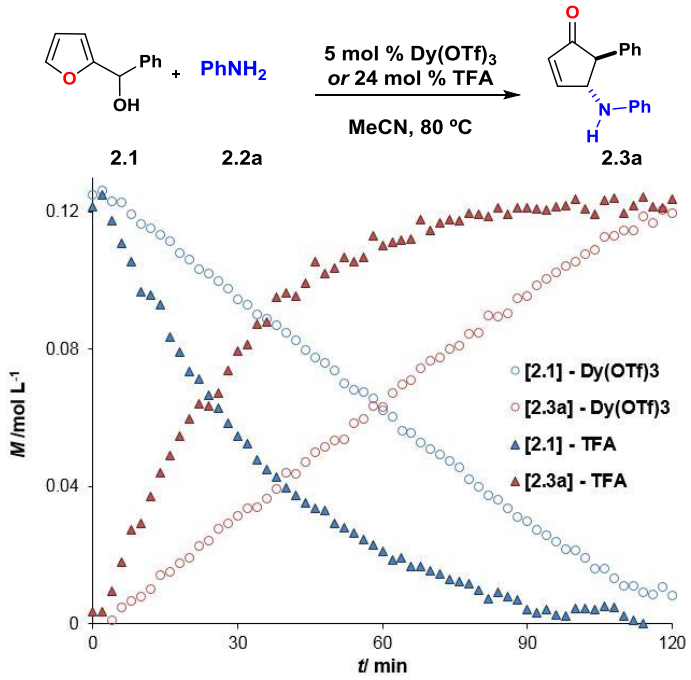

Figure 2.8: $Dy(OTf)_3$ vs. TFA-catalyzed rearrangement, monitored by ReactIR

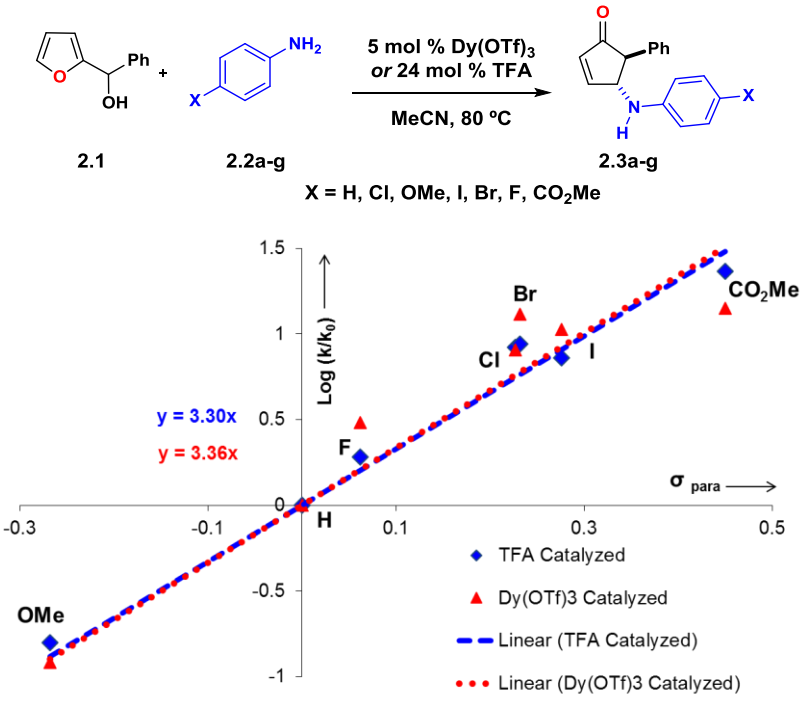

Figure 2.9: Hammett plot for dysprosium (III) triflate vs. TFA-catalyzed Aza-Piancatelli rearrangement

The competition experiments between 4-chloroaniline and 4-methoxyaniline were redone under TFA-catalyzed conditions to see if they yield similar results as the dysprosium-catalyzed conditions. As predicted, the competition experiment with TFA provided a similar qualitative result as with $Dy(OTf)_3$, although with less of a dramatic increase in rate of the chloropentenone product **2.3c** (Figure 2.10).

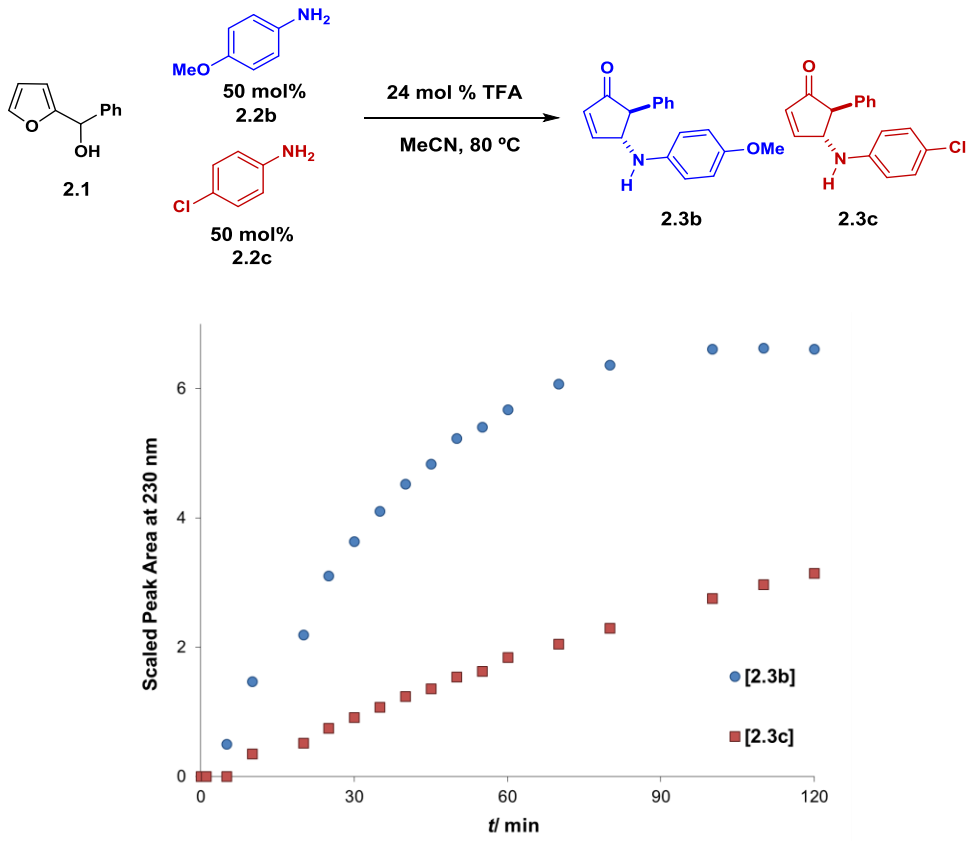

Figure 2.10: TFA-catalyzed competition experiment with 2 furylcarbinol : 1 OMe : 1 Cl, showing product formation by HPLC-MS

To rationalize why the kinetic profile changes from zero to first order when switching from a Lewis acid (dysprosium) to a Brønsted acid (TFA), we can suggest a shift in the rate-determining step and relative rate constants (Scheme 2.13). For the reaction catalyzed by

Brønsted acid, the rate-controlling step is the generation of the oxocarbenium intermediate. This is supported by a positive order in furylcarbinol, as supported by the experiment that showed faster rate for a late addition of furylcarbinol (Figure 2.4). The ionization reaction of TFA and aniline is nearly immediate, allowing the rate-determining step to depend on the formation of the oxocarbenium ion. In contrast, the dysprosium catalyst is sequestered by the aniline substrate, and the release of free dysprosium from the off-cycle binding to aniline creates a significant backward rate. Balanced by the forward rate of oxocarbenium formation, the high rate of off-cycle binding of dysprosium shifts the overall profile to appear zero-order. Effectively, the rate for both systems is governed by the ability to generate oxocarbenium ion; the dysprosium-catalyzed case is merely slowed down by the large off-cycle binding to aniline.

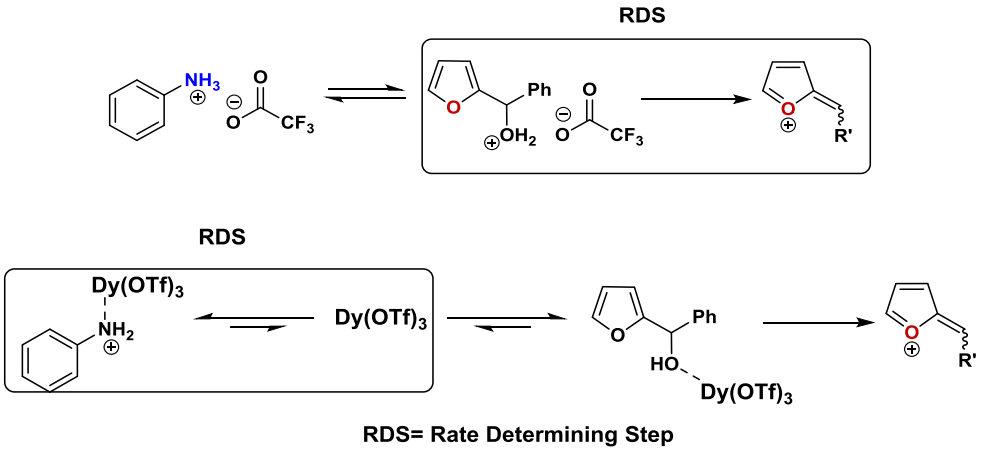

Scheme 2.12: Change in rate-determining step between Brønsted acid and Lewis acid-catalyzed reactions

Our collaborators in the Read de Alaniz group previously found that the addition of an inorganic base (potassium carbonate) shut down Brønsted acid catalysis with triflic acid, but not with dysprosium triflate. Similar experiments were conducted to reaffirm this observation

Scheme 2.13). If an equivalent of potassium carbonate is added to a reaction catalyzed by 60% TFA, the reaction stops forming the desired product. If an equivalent of potassium carbonate is added to a reaction with 5% dysprosium triflate, which were standard reaction conditions, the reaction still proceeds, albeit more slowly. Even though a very large amount of the Brønsted acid catalyst had been added, it was not enough to keep the reaction going with the addition of excess base. The Lewis acid catalyst, however, is still active. This observation supports the conclusion that the dysprosium triflate catalyst is not just a source of Brønsted acid. While ionization of TFA with extraneous base is sufficient to halt the reaction, this problem is not present when $Dy(OTf)_3$ is used.

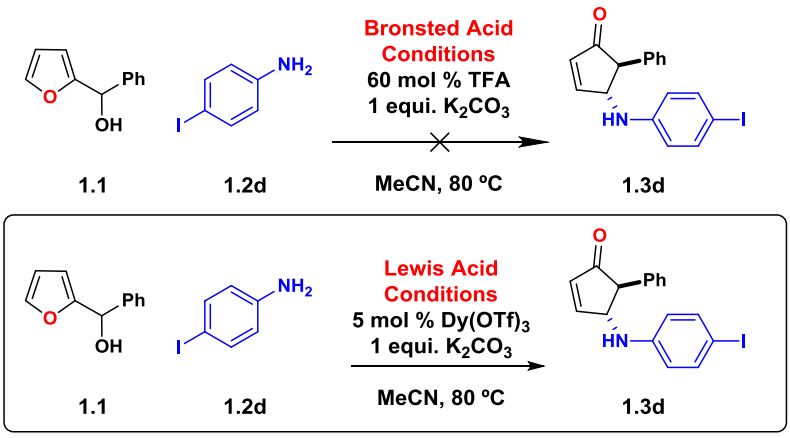

Scheme 2.13: Lewis vs Brønsted acid shut down by addition of base

With many discussions with the Read de Alaniz group, it was found that combining the two catalyst modes could be effective for promoting formerly obstinate reactions. Dysprosium (III) triflate was used as the main catalyst, while TFA was added to provide more discrete graduations in reactivity when an increase in the catalytic loading of dysprosium (III) triflate caused the furylcarbinol to decompose too quickly. This combination has been used in a more robust and diastereoselective synthesis of 4-hydroxycyclopentenones. The $Dy(OTf)_3$-catalyzed

reaction was not driven to completion with 10% catalyst, but 30% catalyst caused decomposition (Table 2.1). Decomposition and low conversions were also observed with 5-20% TFA. However, the combination of 10% $Dy(OTf)_3$ and 5% TFA allowed a much cleaner 90% yield. The mild Lewis acid source of dysprosium and a small amount of Brønsted acid to give a slight boost without adding too much dysprosium allowed for more efficient catalysis.[54]

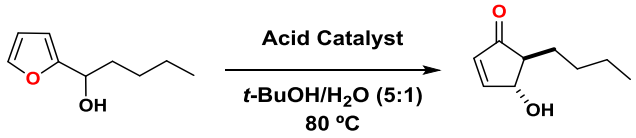

Entry	Acid	equiv	Time (h)	Yield (%)
1	$Dy(OTf)_3$	0.10	72	60
2	$Dy(OTf)_3$	0.30	--	Decomp.
3	TFA	0.05	96	Decomp.
4	TFA	0.20	18	24
5	$Dy(OTf)_3$ + TFA	0.10+0.05	16	90

Table 2.1: Dual Brønsted/Lewis catalyst optimization of a Piancatelli rearrangement[54]

2.4.2 Order in TFA in the Aza-Piancatelli rearrangement

While the reaction had been found to be first order in $Dy(OTf)_3$, the order in TFA was more complicated. A set of experiments utilizing the model reaction was run with varying initial concentrations of TFA (3.1-25.0 mM). When the relative rates of furylcarbinol consumption (found by taking the slope of the natural logarithm of the first-order profile by ReactIR) were related to the concentration of TFA added, it appeared that the relative rate increased exponentially as a function of TFA (Figure 2.11). Traditionally, this would imply that the reaction has a second-order dependence in TFA catalyst.

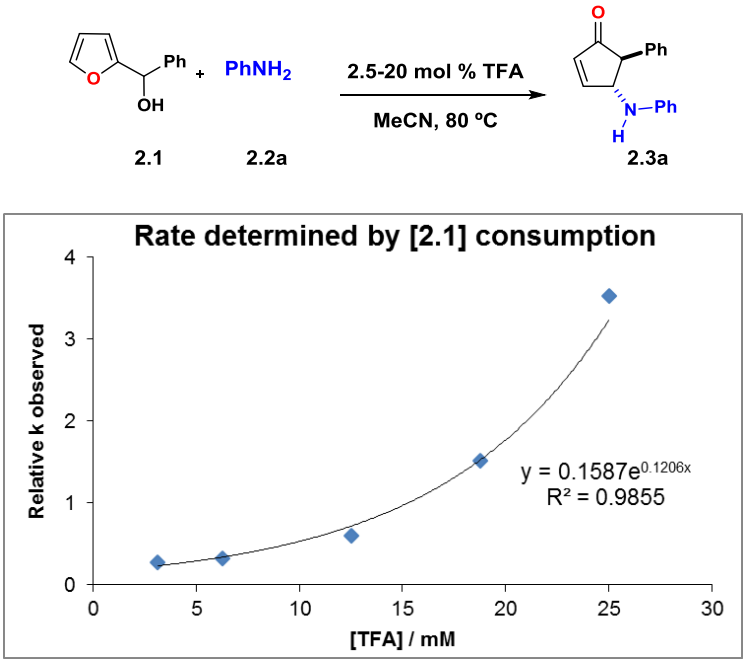

Figure 2.11: Relative rate of furylcarbinol consumption with varying TFA catalyst

Upon inspection of the end reaction solutions by HPLC-MS, it was found that Friedel-Crafts side products had formed. Similar data treatment with the cyclopentenone product curves found a scattered relationship between the relative rate and the concentration of TFA (Figure 2.12). It appears that increasing the concentration of TFA also increased the formation of Friedel-Crafts byproducts, and in all cases, there was unconsumed furylcarbinol long after the reaction trends stopped changing by ReactIR. Hence, the conclusion based on Figure 2.11 that the reaction is second-order in TFA would be inaccurate. Rather, TFA causes a change in selectivity between desired and side products, as well as changes conversion of the starting materials. In contrast, $Dy(OTf)_3$ allows higher conversions with lower catalyst loadings with little decomposition of the starting material. This study also showed that a simple set of experiments designed to study order in catalyst can provide less straightforward results than expected. Often a reaction will show positive order in catalyst, reflected by faster consumption of

starting material. However, as reflected in these results, the conversion to desired product and selectivity of side-products should also be considered in evaluating the positive order in catalyst.

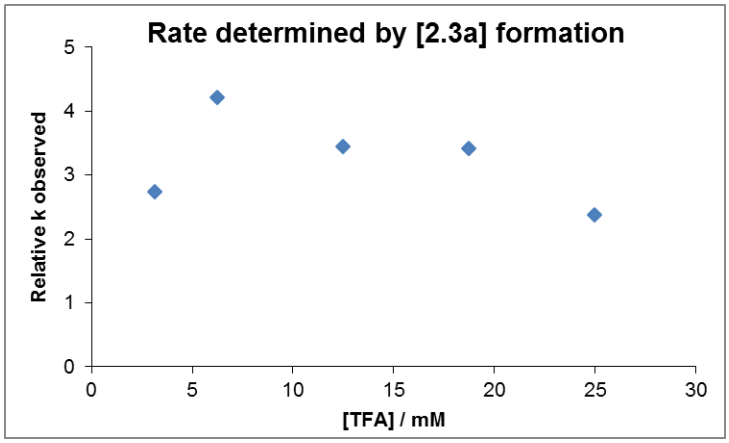

Figure 2.12: Relative rate of cyclopentenone 2.3a formation with varying TFA catalyst

2.5 A kinetic study of lanthanide triflates in the Aza-Piancatelli rearrangement

It was questioned whether there were any differences between dysprosium triflate and the other lanthanide triflates. While studies had been conducted with dysprosium because it is relatively inexpensive and less prone to absorbing water, there lacked a rigorous comparison of dysprosium to other lanthanide triflates. Commercially available lanthanide triflates were screened under the same conditions, and the product formation was compared between each catalyst by ReactIR (Figure 2.13). Although not lanthanides, scandium and ytterium triflates were also screened, as some prefer them due to their high acidity.[55]

Although with varying rates, most lanthanides still showed a zero-order profile for the Aza-Piancatelli rearrangement. Some lanthanides leaned more toward first-order behavior. It is easier to see such differences when the product conversion is graphed against normalized time, therefore graphing fractional conversion (Figure 2.14). Lanthanum triflate, in particular, causes

the reaction to look more first order than zero. This can be explained by larger forward rate toward forming the oxocarbenium ion than the backward rate of off-cycle binding of the metal catalyst to aniline. Additionally, it is possible that rates could be affected by how hygroscopic the catalysts are, potentially affecting the amount of free triflic acid in solution. There were no experiments done to compare catalysts dried in a vacuum oven versus catalysts taken out of new bottles (for which all these experiments used).

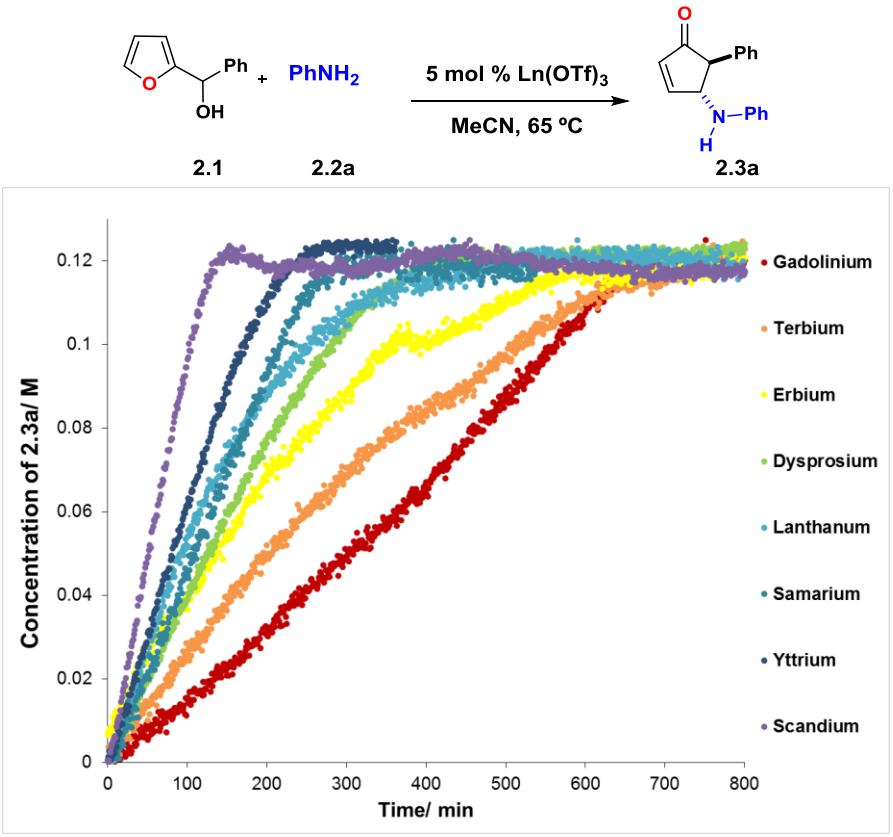

Figure 2.13: Comparison of rates of product formation for different metal triflates for the Aza-Piancatelli rearrangement by ReactIR

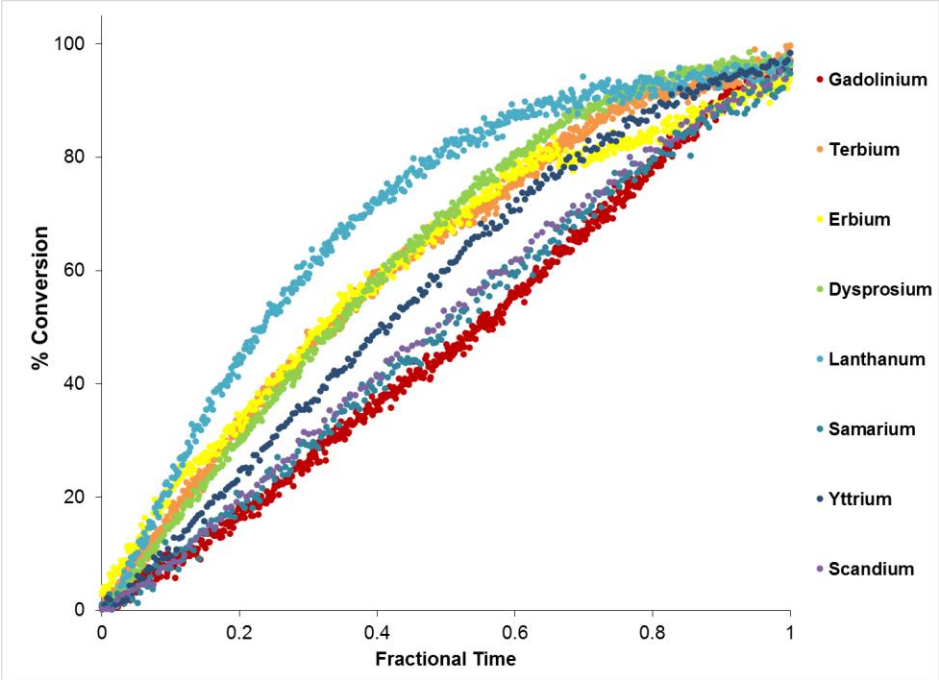

Figure 2.14: Normalized conversion for the kinetic screen of lanthanide triflates

The relative rates were then graphed against various parameters in an attempt to find a correlation. It had been proposed that there would be a relationship between the relative rates and the propensity of amine substrate binding to the metal center. It was hypothesized that increased amine binding to the metal would correlate to slower reaction rates. A previous study determined the number of bound ligands to a metal center using isothermal calorimetry (ITC).[56] Sudden drops in heat flow occurred after the equivalencies of ligand bound were exceeded. A few experiments with our Omnical calorimeter for reaction monitoring showed that it was not sensitive enough for small changes to be observed, as with ITC. With no direct measurement of the number of bound ligands, we sought to use other parameters that have been previously tabulated.

It had been hypothesized that graphing against electronegativity would show a clear relationship, since electronegativity may relate to the metal's ability to bind to ligands – i.e., a

more electropositive metal center might for more binding to amines. However, graphing against electronegativity showed an unclear correlation (Figure 2.15). When the relative rates were compared to the effective radii of the M^{+3} metal center, the trend of the lanthanides were inverted relative to the appearance to the electronegativity graph. The radii took into account the lanthanide contraction, where radii for the lanthanides decreases more than expected with increasing atomic number due to poor shielding from the nucleus. This was unsurprising – the smaller radii generally related to increased electronegativity. However, the nonlinear trend suggested that ligand exchange with the amine nucleophile was not necessarily slower with increasing or decreasing radii.

Eventually, the parameter that most seemed to show the most rational trend was atomic number. With increasing atomic number, the relative rate of reaction generally decreased, although the correlation is not consistent with terbium or gadolinium. This may mean that as atomic number increases, the effective charge is also higher for the charged lanthanide ion (and less offset by electrons). This may cause the amine nucleophile to be bound more tightly, therefore slowing down the reaction. Strangely, for atomic numbers larger than that of lanthanum, the trend for the lanthanides is inverted compared to the trend for effective radii.

Two sources of hydration energy were also used as parameters.[57,58] The correlation was unclear and at least superficially appeared unrelated to the other parameters. There was also little correlation when the pKa was used as a parameter (not shown).[59]

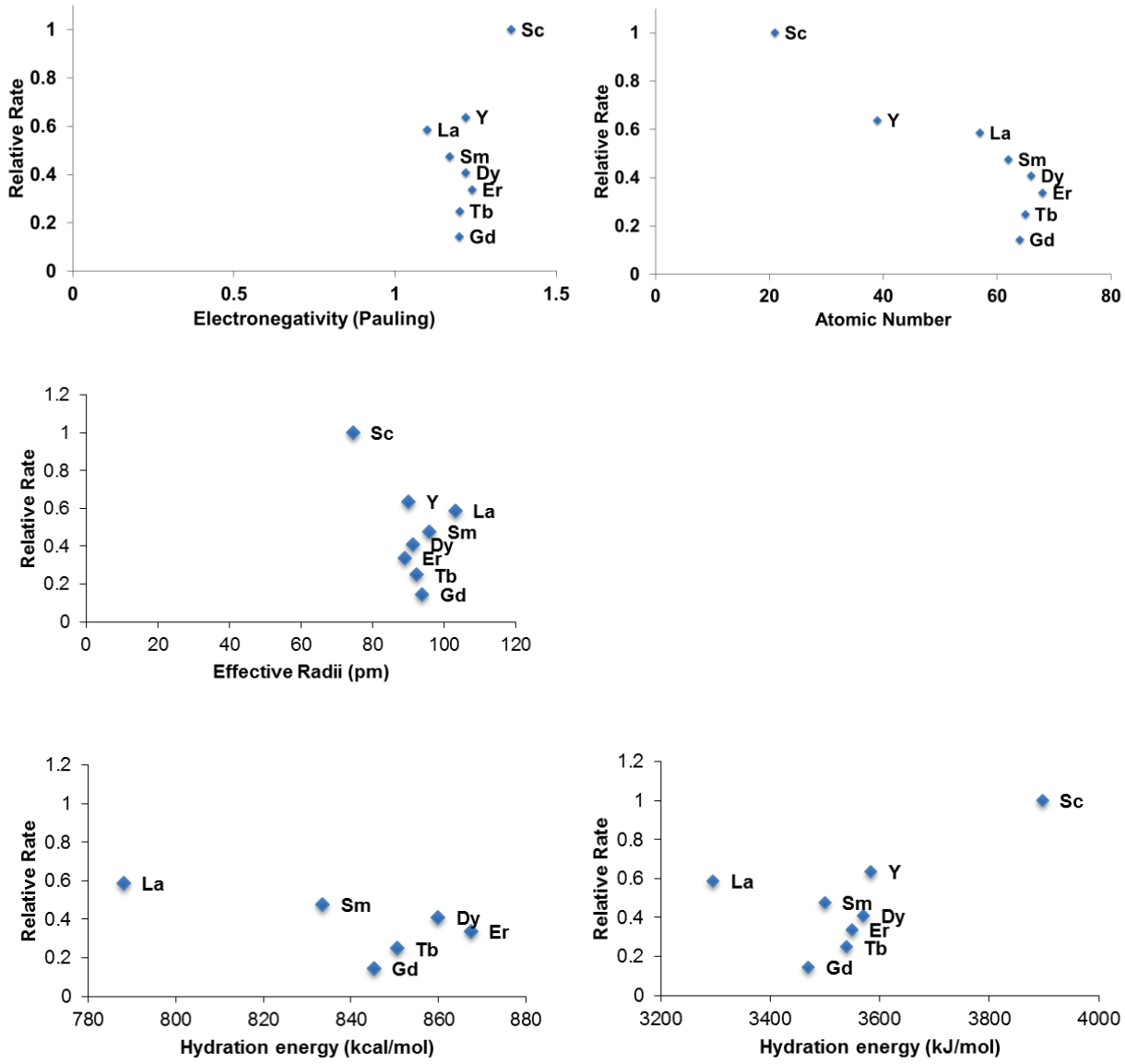

Electronegativity values[60]

Figure 2.15: Parameterization of results from lanthanide triflate kinetic screen

The products from these reactions were not isolated to evaluate for yield. Endpoints taken for analysis by HPLC-MS did not show any significant formation or rearrangement from the 4,5 isomer to the 3,5 isomer, which had been observed to occur with the cyclopentenone product

2.3a if concentrated with acid (Scheme 2.14). While these Lewis acid catalysts did not seem to be different from each other in terms of their synthetic utility for the aniline substrate in the Aza-Piancatelli rearrangement, work with unrelated reactions classes has shown a greater difference between the different metal salts.[61,62]

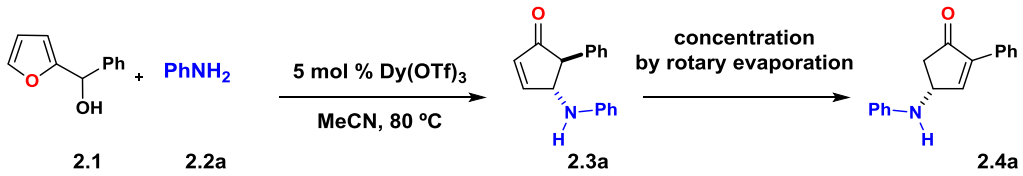

Scheme 2.14: Rearrangement to another cyclopentenone isomer

2.6 Kinetic studies with an automated sampling apparatus

2.6.1 Expansion of a limited substrate scope

As mentioned before, the substrate scope for the Aza-Piancatelli rearrangement was previously limited to anilines, and many other amines showed no conversion. After mechanistic studies had been conducted, the scarcity of suitable classes of amines was attributed to the off-cycle binding with the dysprosium catalyst. The right pairing of basic nucleophile and dysprosium catalyst may be necessary to allow the rearrangement to proceed. Anilines, with a pKa of 4.6 in their protonated form, may happen to be in the range of tolerable substrates that bind to the Lewis acid catalyst, but not so tightly such that catalysis is inhibited. However, some binding of the catalyst is necessary to prevent all of the furylcarbinol from converting to the oxocarbenium ion all at once, leading to Friedel-Crafts products. Amines that are too basic (such as alkylamines) bind too tightly to allow oxocarbenium formation at all (Scheme 2.15). In contrast, slightly acidic amines like sulfonamides without another amine cause decomposition of the furylcarbinol, as observed by the Read de Alaniz group.[63]

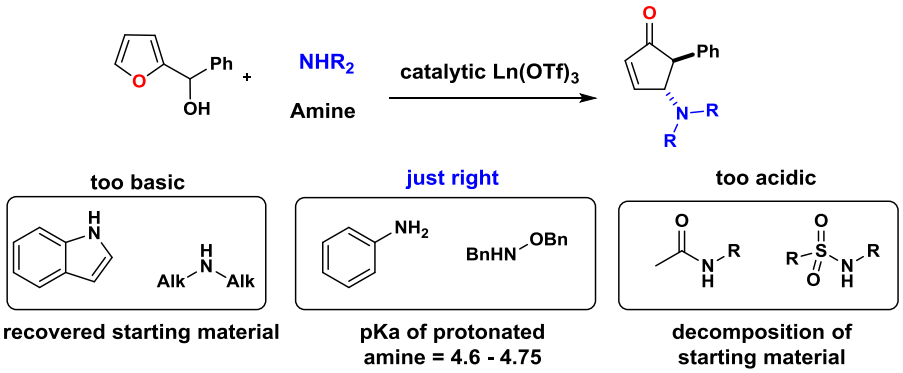

Scheme 2.15: Initially limited nucleophile scope

Among the suitable substrates, *N*,*O*-dibenzylamine was later found to allow high yields.[64] When protonated, its pKa is around 4.75, close to that of anilines.[65] Protecting the amine allowed for more products to be accessible, even if deprotection may be necessary at a subsequent synthetic step. With time, it was found that intramolecular rearrangements could also occur with tethered alcohols (instead of amines) to form spirocyclic ethers, going through a spiroketal enol ether intermediate.[66]

2.6.2 Development of automated sampling for HPLC-MS in tandem with ReactIR

It was decided to look at the reaction with the new *N*,*O*-dibenzylamine nucleophile **2.5** with manual sampling and analysis by HPLC-MS as the reaction was monitored in situ with ReactIR (Figure 2.16, Figure 2.17). As the reaction was run with a ReactIR probe inserted inside the vial, samples were withdrawn manually with a syringe and long needle through a needle vent in the vial's septa. With the withdrawal of most samples, a sudden dip or rise in the ReactIR profiles is observed. This can be attributed to a sudden decrease in pressure in the heated the reaction by pulling a sample, causing slight changes in temperature that affect the peak height.

Hence, by manually sampling out of the reaction, pressure and temperature changes occurred, and the IR surface was disrupted. Likewise, it would probably have been even more disruptive to unscrew the cap of the heated reaction, take a sample, and recap the vial, which many researchers might do to initially conduct kinetic studies.

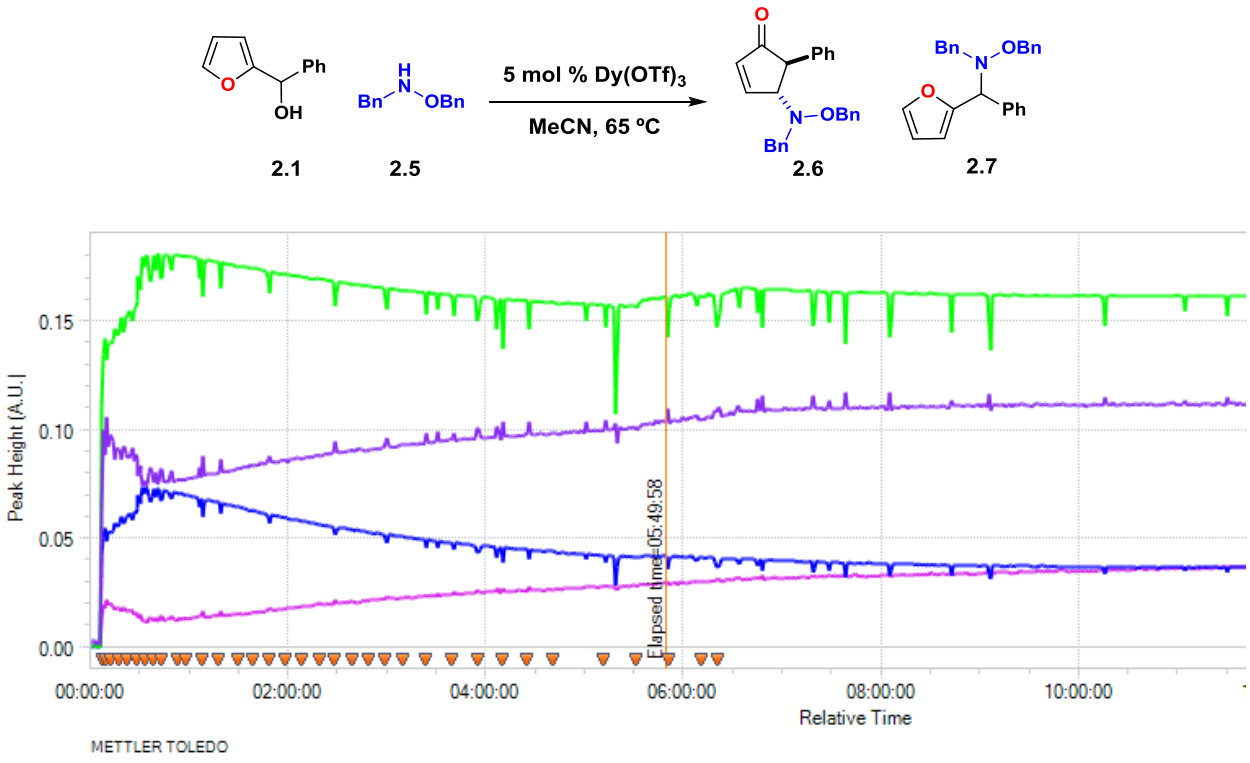

Figure 2.16: ReactIR profiles show disruptions when a sampled is manually pulled from the reaction

As for the HPLC-MS data, we saw that a new compound seemed to build up and then disappear as the desired pentenone product **2.6** was formed. This supposed intermediate ionized by ESI-MS to be the mass of the oxocarbenium ion, but was more nonpolar than the product, as inferred from HPLC. It was hypothesized that this intermediate **2.7** came from the nucleophile attacking the oxocarbenium ion at the 5' position of the furylcarbinol, forming an exo-substituted

product. Ionization by ESI-MS caused this C-N bond to cleave, causing the compound to ionize as the mass of only the oxocarbenium ion. This compound was later isolated and characterized.

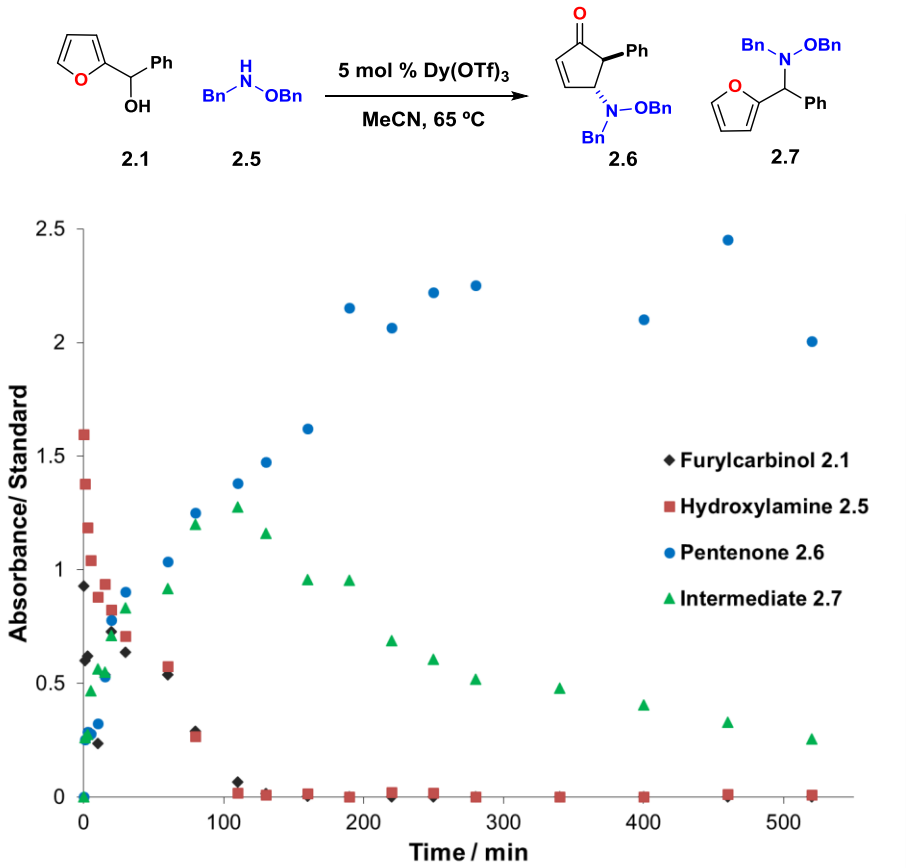

Figure 2.17: Manual sampling and HPLC-MS monitoring of the reaction with *N,O*-dibenzylamine

With the increasing number of chemical species, especially some in lower concentrations, a need developed for an analytical tool that could see more information that ReactIR was blind to, or that it could not reliably pick up on. Although manual sampling with HPLC was useful and could show more information about species in low concentrations, manual sampling at elevated temperatures and long reaction times often called for tedious experiments that yielded scattered

data. The experiment in Figure 2.17 is an example of how the data obtained from manual sampling can result in poorly-formed trends. The fidelity of samples taken can vary widely depending on the reaction temperature, method of taking the aliquot, analytical method, and stability of the compounds. For this experiment, it was clear that the reaction needed a more reliable method of monitoring.

It was sought to make a tool that could allow for information-rich experiments with less tedium, higher reproducibility, and better quality data. After several variations, one of the first reliable prototypes utilized a liquid handling robot, rheodyne, and programmable syringe pump to create an automated system to withdraw samples from the reaction vessel at prefixed times, allowing reactions to be run without constant maintenance (Figure 2.18). Samples were withdrawn by a programmable syringe pump from the reaction vial through the PEEK tubing connected to a Gilson 815 rheodyne valve. The timing was configured such that the withdrawal of the syringe pump triggered the actuation of the rheodyne, which is coupled to a Gilson 215 automated liquid handling robot. Triggering of the liquid handler by the rheodyne allows for dilution with methanol of the reaction aliquot into waiting LC vials. Offline analysis was conducted of these LC vials after completion of the sampling period. As an option, a ReactIR (or potentially some other probe) could be inserted to validate the trends detected by HPLC, or to see global kinetics.

It has been asked before why we did not test our apparatus with a more simple system that is already mechanistically well understood and established. Monitoring by ReactIR and HPLC-MS are both already well established; offline analysis by HPLC is nothing new and does not need to be revalidated on a chemical system that will offer no complexity or new information.

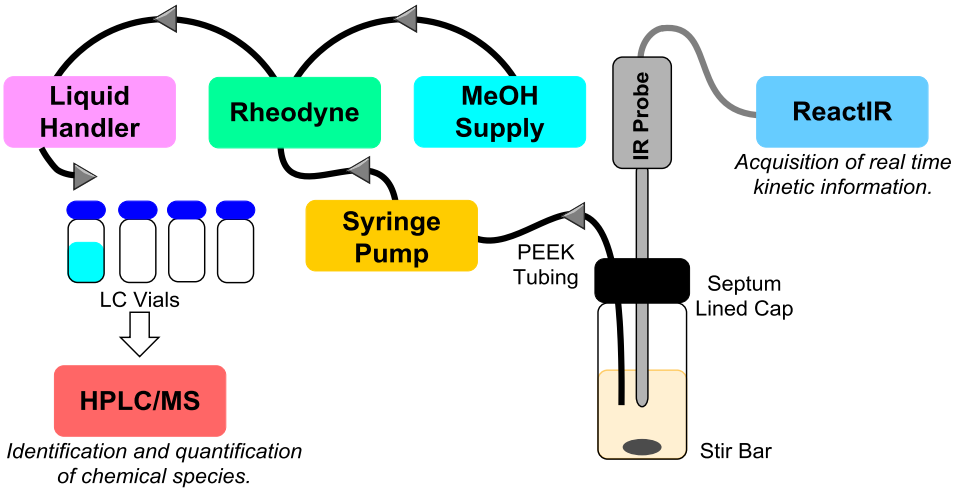

Figure 2.18: Automated sampling apparatus with tandem ReactIR

The Aza-Piancatelli rearrangement using substrate **2.5** was monitored using the ReactIR in tandem with the automated sampling system for HPLC-MS (Figure 2.19). The trends for furylcarbinol consumption and pentenone formation have very good agreement. Whereas the peak for the intermediate species **2.7** is more subtle by ReactIR and may be difficult to extract, it is easily visible by HPLC-MS. Combining these two methods helped to cross-validate ReactIR and HPLC-MS data, meanwhile providing an intermediate trend that was more difficult to deconvolute by ReactIR. It is also now easier to see that as the intermediate **2.7** decays, the cyclopentenone product **2.6** is formed, and that formation of **2.7** is most likely reversible (i.e., **2.7** is not decomposing into a side product that is unobservable by HPLC-MS).

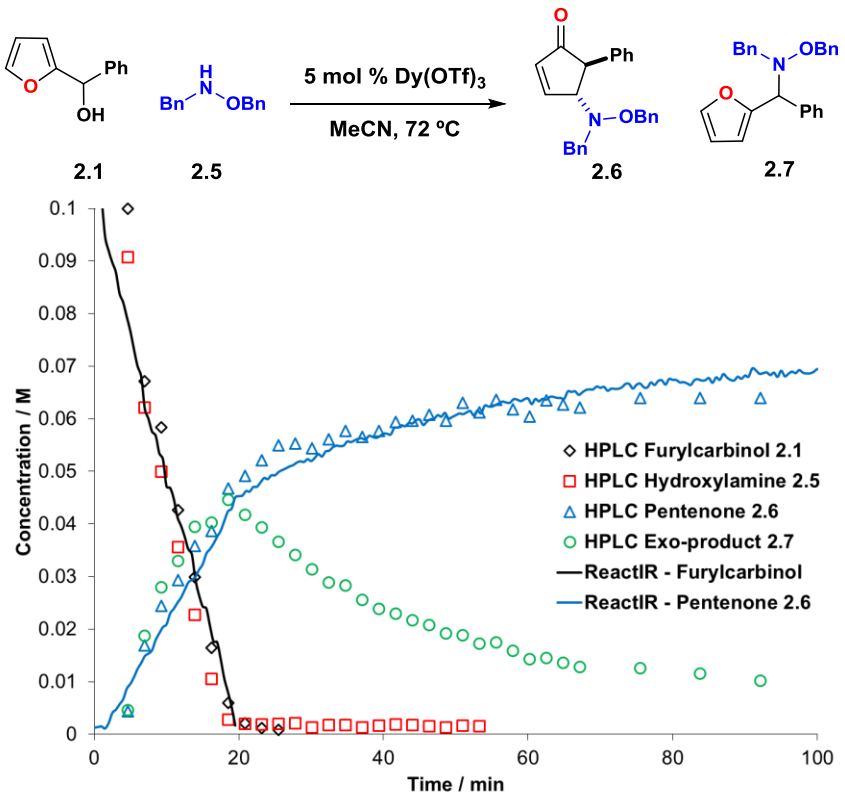

Figure 2.19: Automated HPLC-MS and ReactIR monitoring of the reaction with *N,O*-dibenzylamine

The intermediate **2.7** was isolated, purified, and heated with 5% $Dy(OTf)_3$ to ascertain that it would rearrange to form the cyclopentenone product **2.6**. Indeed, it proceeded to the desired product (Figure 2.20). The rate of cyclopentenone product formation was similar to starting with the furylcarbinol and hydroxylamine **2.5**, albeit slightly slower. Since starting from furylcarbinol **2.1** and nucleophile **2.5** does not allow a full 0.10 M of intermediate **2.7** to be formed, it would not be a one-to-one comparison to the experiment starting with 0.10 M of intermediate **2.7**. This experiment merely confirms that that formation of **2.7** is reversible, therefore reforming oxocarbenium intermediate **2.8** that can further go on to rearrange to **2.6** (Scheme 2.16).

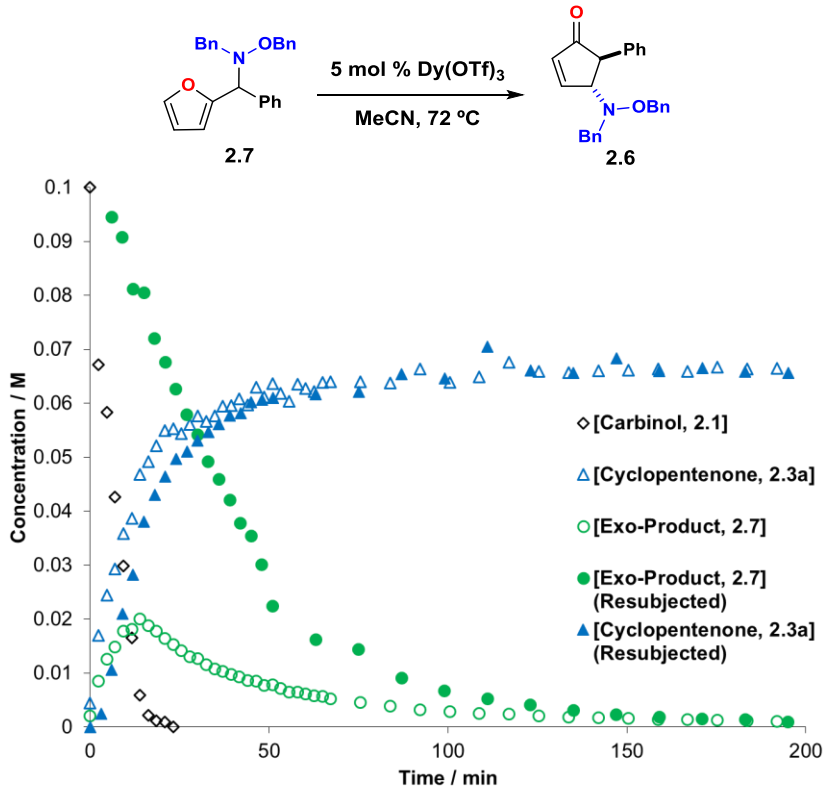

Figure 2.20: Resubjection of isolated intermediate into the Aza-Piancatelli rearrangement, monitored with automated sampling with analysis by HPLC-MS

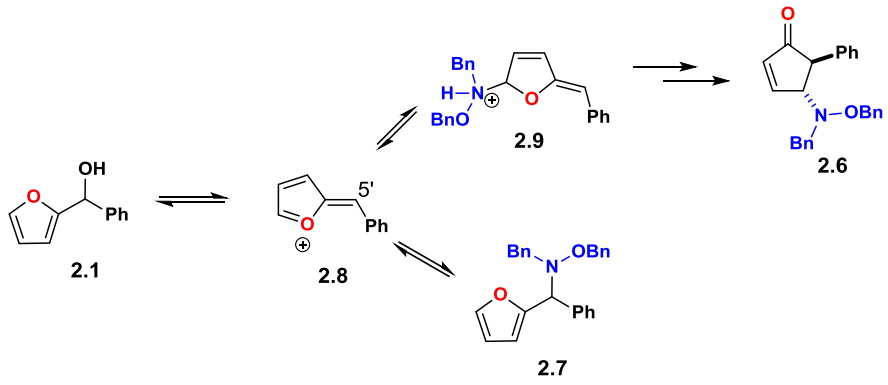

Scheme 2.16: Competitive pathway for the oxocarbenium intermediate

A competition experiment between the classical aniline nucleophile **2.2a** and the hydroxylamine nucleophile **2.5** was conducted (Figure 2.21). The resulting experiment can be

divided up into three different regimes of behavior. Between 0 and 30 minutes, the aniline cyclopentenone **2.3a** is still formed with a zero-order profile, and much more quickly than the hydroxylamine product. This may indicate a preference for the aniline nucleophile, which appears to be more nucleophilic than hydroxylamine **2.5**. The rates of formation of the intermediate **2.7** and hydroxylamine cyclopentenone product **2.6** are similar. Between 30 and 50 minutes, fast and subtle rate changes are detected cleanly. As the aniline concentration decreases after 50 minutes, the hydroxylamine intermediate **2.7** and cyclopentenone product **2.6** formation increases in rate. This is likely because there is less aniline that binds off-cycle to the dysprosium catalyst.

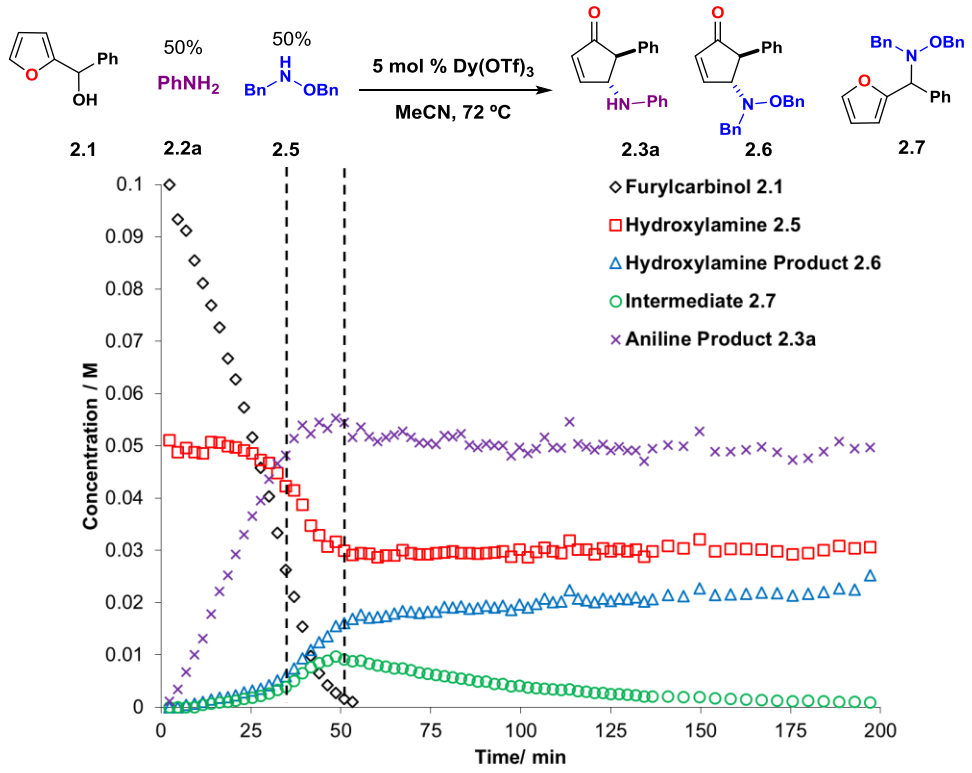

Figure 2.21: Automated monitoring of competition experiment with two nucleophiles, with subsequent analysis by HPLC-MS

This competition experiment is an example of why HPLC can be an excellent choice of a reaction monitoring tool. The reasons why other instruments would be problematic are many for this particular reaction: the potential for overlapping carbonyl stretches in ReactIR; the ability to confidently deconvolute the concentrations of the exo-product **2.7** and the two cyclopentenone products; the low volatility of the products that would require long method times by GC, as well as filtering individual samples to remove the dysprosium catalyst; and the paramagnetic catalyst would make shimming and locking more difficult for NMR. While the addition of automated sampling was not absolutely essential, it is unlikely that manual sampling would have allowed to the subtle changes in rate to be seen. The data would likely be rather scattered. This would make mechanistic interpretations less believable, and kinetic modeling (such as with the program COPASI) would also be more difficult.

2.6.3 Competition experiments with other substrates with automated sampling

It was attempted to look at more poorly behaving chemical reactions with the automated sampling system with analysis by HPLC-MS. Substrates such as unprotected hydroxylamines were known to be troublesome with the Read de Alaniz group, as there never seemed to be any desirable product formation. This experiment gave more information that a few TLCs taken after 30 minutes or a few hours. Using *N*-phenylhydroxylamine **2.10**, the desired product **2.11** forms quickly but decomposes into another compound after about 70 minutes (Figure 2.22). The side-products were not isolated; however, it appears that a compound with the same mass as the pentenone product made from the aniline nucleophile is formed. It may be that the hydroxylamine was reduced to the aniline and then reacted. Alternatively, the hydroxylamine pentenone product may have formed, then the N-O bond may have been reduced, even though

dysprosium is not known for use in N-O bond reductions. A byproduct with m/z = 422 $(M+H)^+$ molecule **2.12**, is also rapidly formed but does also decomposes. Its mass is consistent with a Friedel-Crafts product with the furylcarbinol and the pentenone product formed with phenylhydroxylamine. A byproduct that appears with a mass with m/z = 264 $(M+H)^+$, two less than the substrate – as though two protons had been removed – is also prevalent.

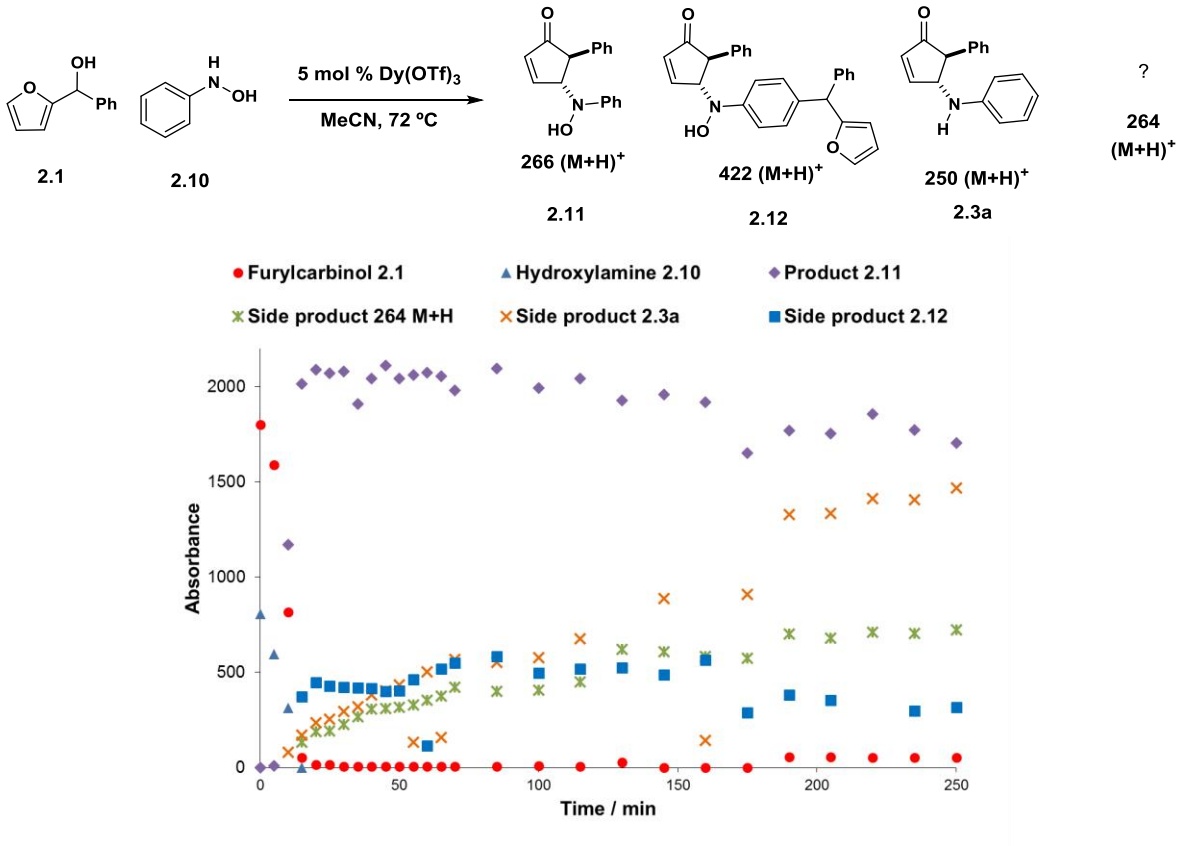

Figure 2.22: Kinetics of a reaction with *N*-Phenylhydroxylamine as a nucleophile in the Aza-Piancatelli rearrangement, monitored by automated sampling for HPLC-MS

Although the reaction was not optimized, creating a detailed kinetic profile by HPLC was informative. It did seem that the desired product **2.11** was quickly formed, but several competing side reactions also occurred. Not only did these undesirable reactions dominate, but the desired

product **2.11** itself was not stable under these conditions. In this case, it was not that the substrates could not form product under the conditions, but that the product was unstable in the reaction conditions, leading to low yields.

A competition experiment between *N*-phenylhydroxylamine **2.10** and 4-bromoaniline **2.2e** were conducted to assess if the addition of a less problematic nucleophile would lessen the byproducts from the phenylhydroxylamine (Figure 2.23). Presumably, electrophilic intermediates could be intercepted by the aniline nucleophile. When 4-bromoaniline **2.2e** was added, both pentenone products **1.11** and **1.3e** are formed with lessened decomposition of product **2.11**. The relative changes in rate between the two nucleophiles seems to be small.

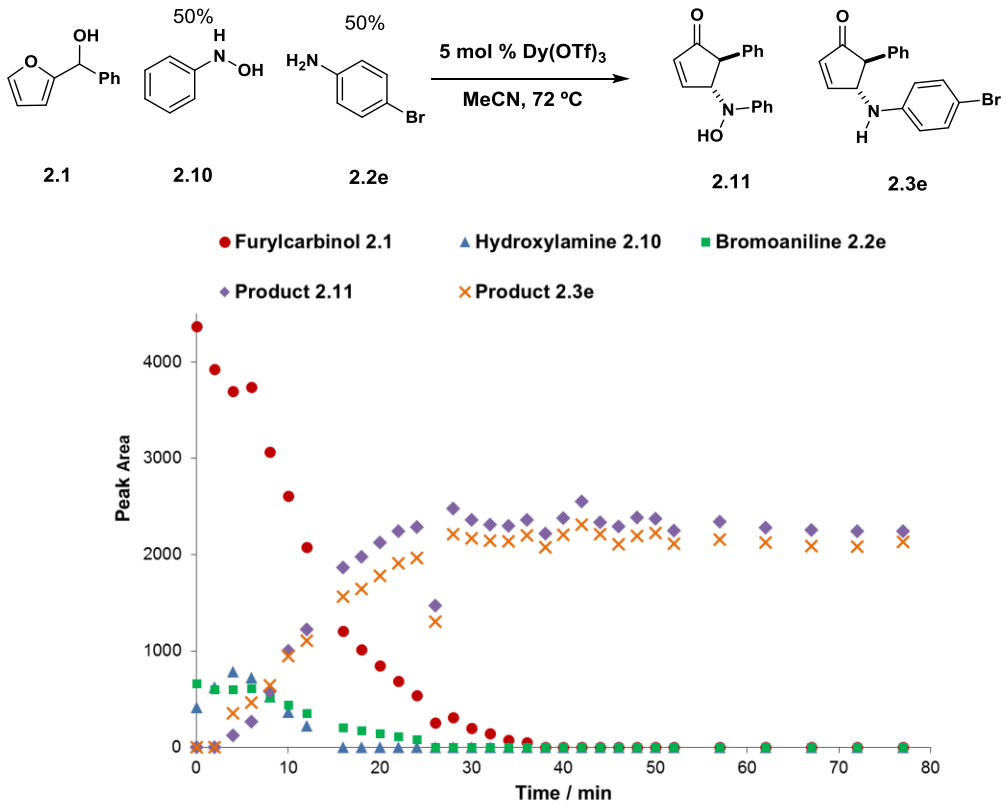

Figure 2.23: Competition experiment between *N*-phenylhydroxylamine and 4-bromoaniline, monitored by automated sampling for HPLC-MS

Since concentrations were not calculated for these systems, it is important not to try to glean too much emphasis on relative rates from these experiments. However, when another nucleophile is added, since the hydroxylamine product **2.11** seems to decompose less and there are less side-products, despite having another nucleophile substrate present. It is possible that the aniline nucleophile "distracts" the catalyst from being overly active, allowing smoother conversion to the phenylhydroxylamine product instead of decomposition of the furylcarbinol. It was not attempted to see if lowering the catalyst loading to 1% dysprosium triflate or adding catalytic amounts of a Brønsted acid with 1% dysprosium triflate to a noncompetitive reaction for the phenylhydroxylamine **2.10** would decrease the formation of side products that were seen in the former experiment.

2.7 NaBARF as a cocatalyst for the Aza-Piancatelli Rearrangement

The Read de Alaniz group later found that the addition of sodium tetrakis[3,5-bis(trifluoromethyl)phenyl]borate, **2.14** (herein referred to as NaBARF) as a co-catalyst allowed the reaction to proceed at room temperature in various toluene, no longer requiring moderate temperatures (50-80 °C). Although presumably acting as a weakly non-coordinating anion with $Dy(OTf)_3$, the structure of the new catalyst complex in solution and how it greatly reduced the activation energy barrier was poorly understood. For example, the BARF anion could potentially swap out a triflate ion.[67] The addition of NaBARF to various reactions has been known to increase yields, and is proposed to form a cationic metal complex with a relatively diffuse counterion.[68] On the basis of analysis of crystal structures, BARF has been proposed to be in the class of the most weakly coordinating anions to transition metals due to the abundance of fluorine atoms; this relation may also transfer to lanthanide ions.[69]

The room temperature reaction with added NaBARF was studied briefly by ReactIR (Figure 2.24). The kinetics still best fit a zero-order profile in substrate consumption and product formation. However, there are other dynamic peaks belonging to unidentified compounds forming and decaying throughout and long after the desired reaction has consumed the furylcarbinol (e.g., at 1038, 1488, and 1283 cm^{-1}). This may be related to the low solubility of the dysprosium- NaBARF mixture in toluene, which remains poorly dissolved throughout most of the reaction. The kinetic profiles of the unidentified compounds have unusual shapes, not linear, as might be expected from slow dissolution of solids. HPLC-MS in both positive and negative modes did not show anything informative about the BARF anion other than it was present.

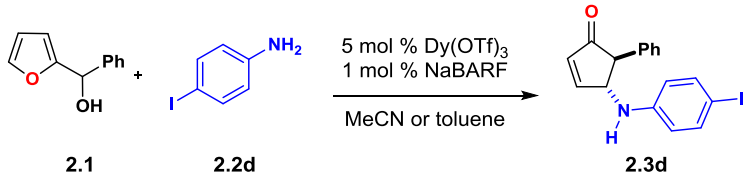

2.1 2.2d 2.3d

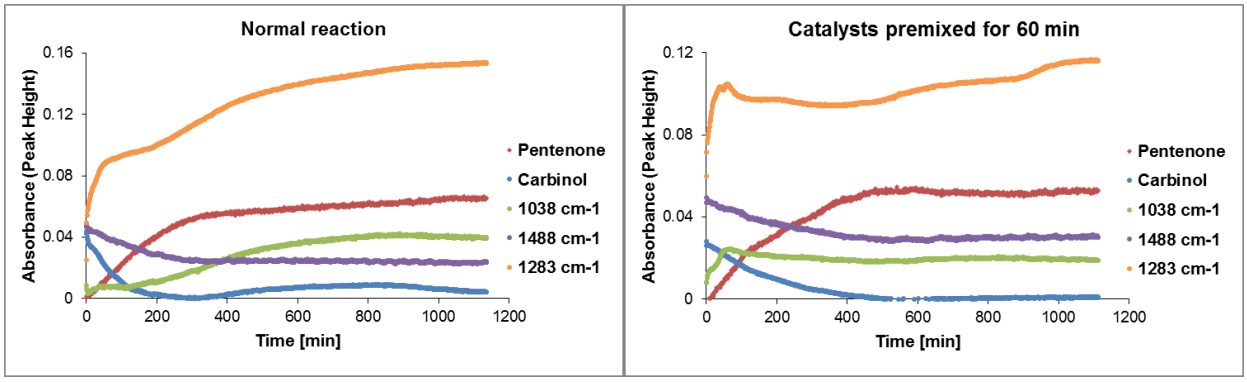

Figure 2.24: Pre-stirred vs not mixtures of NaBARF and $Dy(OTf)_3$ for the Aza-Piancatellli reaction – monitored by ReactIR

Although the kinetic profiles did not strongly suggest a catalyst induction period, it was wondered whether precomplexation of the dysprosium catalyst and NaBARF changed the

reaction. Stirring the $Dy(OTf)_3$–NaBARF mixture in toluene for one hour before the addition of the furylcarbinol and aniline actually halved the reaction rate instead of speeding the reaction up. It is unclear whether the hour stirring only decreased particle size and increased solubility, or if different complexes are formed with time. It is possible that the decreased solubility of whatever complex(es) formed actually increased reaction rate. Unfortunately, attempts to look at mixtures of reaction's components by ^{19}F NMR and ^{11}B were thwarted due to dysprosium's paramagnetic nucleus.

Since the Aza-Piancatelli rearrangement was previously routinely done in acetonitrile, we wanted to compare the reaction rates between acetonitrile and the new solvent, toluene, to understand why the solvent had been switched by the Read de Alaniz group. $Dy(OTf)_3$ is soluble in acetonitrile, and the small mass of NaBARF appeared more soluble in acetonitrile than toluene. However, even though the combination of NaBARF and $Dy(OTf)_3$ did not dissolve well in toluene, the reaction was much faster in toluene than in acetonitrile at room temperature, which is consistent with the previous result of *faster* rate with *less* dissolution (Figure 2.25). Potentially, different catalyst-NaBARF complexes may form in the two solvents, altering reactivity of the metal center.

The reactions were monitored by HPLC-MS to attempt to see any more detailed chemical speciation that would be otherwise indiscernible from the background of ReactIR. More importantly, it appears that an intermediate, presumed to be an analogue to the exocyclic product **2.13**, where iodoaniline attacks the oxocarbenium ion at the exo position instead, is detected when NaBARF is used. In acetonitrile, this intermediate is relatively long-lived. This intermediate is analogous to the one isolated when *N*,*O*-benzylhydroxylamine **2.5** was used as a nucleophile to form **2.7**. The aniline analogue has not been isolated, although it has been briefly

seen with certain substrates.[63] Although it was also not isolated in our laboratory, its fragmentation pattern by ESI-MS and relative polarity, similar to that of intermediate **2.7**, make compound **2.13** the most likely candidate.

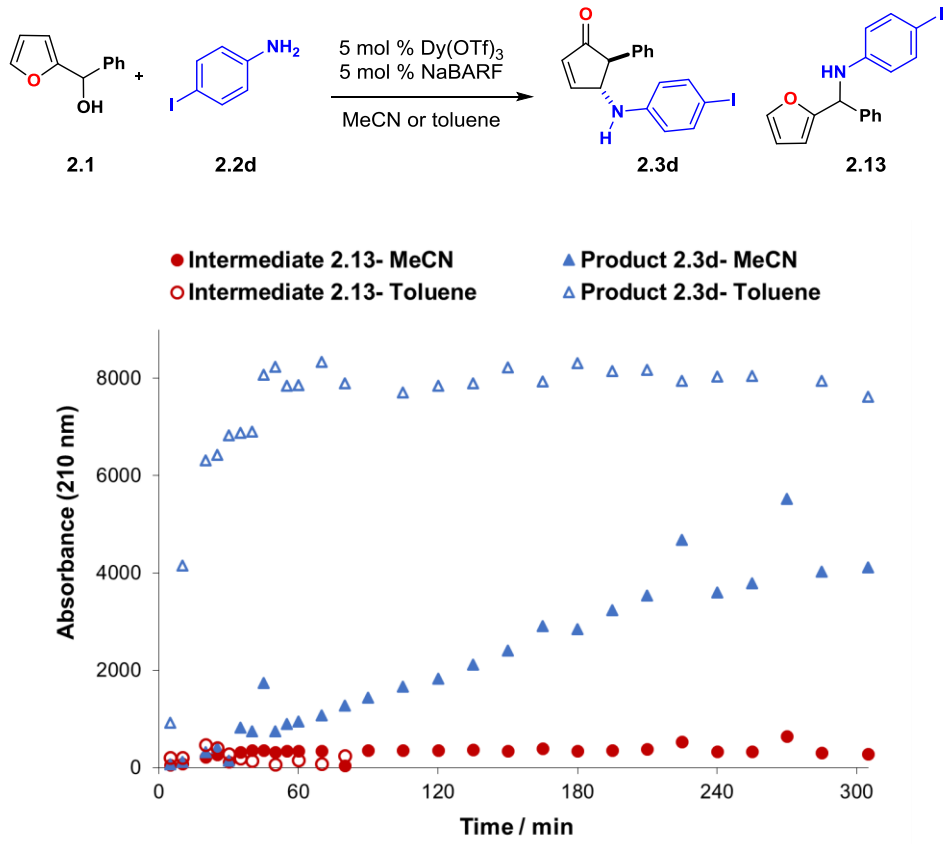

Figure 2.25: The NaBARF-Dy(OTf)$_3$ catalyzed Aza-Piancatelli rearrangement in two solvents, monitored by HPLC-MS

It is apparent that the addition of NaBARF seems to stabilize the intermediate enough for it to be long-lived enough or in high enough concentrations to be detected. Potentially, the BARF anion pairs with the oxocarbenium ion to provide increased stability, extending the lifetime and concentration of this electrophilic intermediate. Perhaps with the less polar solvent toluene, this complex is more reactive if a nucleophile is in the solvent sphere. It has been previously

suggested for another reaction type that the BARF anion can stabilize a transient β-silyl carbocation intermediate.[68] This would increase the possibility of reversible rearrangement to oxocarbenium intermediate **2.8** to **2.13**.

2.8 Conclusions

It was found that the Aza-Piancatelli rearrangement behaves differently when catalyzed by a Lewis acid versus a Brønsted acid. While a Brønsted acid catalyst in the reaction can be effectively shut down by the addition of excess inorganic base, a Lewis acid can still catalyze the reaction. In addition, the use of too little Brønsted acid does not always allow full conversion to the cyclopentenone product, whereas adding too much can cause the formation of Friedel-Crafts products. $Dy(OTf)_3$ did not cause the formation of the same side-products when a small (2-5%) catalytic amount was added.

As we found by ReactIR, some Lewis acids, such as $Dy(OTf)_3$, can cause the reaction profile to appear zero-order overall. This is attributed to the off-cycle binding of the amine nucleophile to the metal catalyst, shifting the rate-limiting step toward release of the active catalyst. The mechanistic experiments conducted helped the Read de Alaniz group provide rationale for such claims about the reactivity of amines the reaction. This knowledge was used to help titrate the amount of Brønsted acid used in combination with $Dy(OTf)_3$ to catalyze a reaction that was sensitive to too much $Dy(OTf)_3$ but would not proceed with only TFA.[54]

Competition experiments were shown to be a useful tool in showing changes in chemoselectivity that would otherwise be missed. While more nucleophilic anilines slowed the reaction down, if they were used in a competition experiment with a less nucleophilic aniline, the

pentenone product with the more nucleophilic aniline was formed more quickly and in higher concentration. This helped show that the selectivity- and rate-determining steps were decoupled.

Knowing that some amine nucleophiles were too basic and inhibited Lewis acid catalysis, collaborators found a few more types of suitable nucleophiles in the small pKa range, including protected *N,O*-hydroxylamines. Motivated to study how combinations of nucleophiles would change the reaction as it progressed, an automated sampling system was used to monitor more complicated reactions. This apparatus allowed programmable sampling from a hot solvent and data with well-defined trends. The apparatus was easily modified and transferrable to different reaction types and vessels, as seen in Chapter 4.

The automated sampling system was used in tandem with ReactIR. Automated sampling and off-line analysis by HPLC-MS does not provide results in real time. A separate analytical method need to be made for differing mixtures of compound. Furthermore, at least a couple samples must be run and analyzed to provide any information, several minutes after the reaction has moved past the time the samples were taken. Coupling sample-taking with off-line HPLC-MS with ReactIR allows reaction progress to be seen in real time. This allows the user to quickly decide if a new reagent should be added to the reaction to see its effects. Meanwhile, HPLC-MS gives more detailed information about speciation past the broad view that ReactIR provides.

2.9 Experimental

2.9.1 General remarks.

Furan-2-yl(phenyl)methanol was prepared according to literature precedent of a similar transformation by reacting furfural with phenylmagnesium bromide.[70] Dysprosium (III)

trifluoromethanesulfonate ($Dy(OTf)_3$) was used as received from Strem Chemicals, Inc. Sodium tetrakis[3,5-bis(trifluoromethyl)phenyl]borate (NaBARF) was synthesized by a previously published procedure.[71] *N*-phenylhydroxylamine was made by a previously published procedure.[72] All other materials were obtained from conventional suppliers and used as received. Flash chromatography was carried out using Sorbtech silica gel 60A (230x400 mesh) or Fisher Chemical silica gel 60 Å (230 x 400 mesh). Thin-layer chromatography (TLC) was performed on Sorbtech precoated silica gel plates and was visualized by irradiation with UV light or staining with potassium permanganate solution.

In situ FT-IR monitoring was conducted with a Mettler-Toledo ReactIR 10 and ReactIR 15 equipped with a DiComp (Diamond) ATR probe connected via an AgX (silver halide) 6 mm x 1.5 m fiber. Kinetic studies with automated sampling were conducted with a ReactIR ic15. Sampling was carried out over 2000-800 cm^{-1} at 4 wavenumber resolution with 1x gain. Reaction temperatures were controlled using an internal temperature modulator.

2-Methoxynaphthalene was used as an internal standard in some experiments as specified, and had no effect on the reaction, as confirmed by monitoring reactions via ReactIR and HPLC-MS both with and in the absence of the standard.

^1H NMR spectra were recorded on an NMR spectrometer (at 400, 500 or 600 MHz) and are reported relative to deuterated solvent signals. Data for ^1H NMR spectra are reported as follows: chemical shift (δ ppm), multiplicity, coupling constant (Hz) and integration. ^{13}C NMR spectra were recorded on Varian Spectrometers (125 MHz). Data for ^{13}C NMR spectra are reported as follows: shift (δ ppm), multiplicity and coupling constant (Hz). IR spectra were recorded on by ATR-FT-IR and are reported in terms of frequency of absorption (cm^{-1}).

The LC samples were analyzed by HPLC/MS conducted on an Agilent 1260 Infinity apparatus under the one of the following conditions:

(1) Agilent ZORBAX Eclipse XDB C18, 3.5 μm, 3.0 x 100 mm column.

Solvent A= Water, 0.05% TFA; Solvent B= Acetonitrile, 0.05% TFA. Initial conditions: B=38%; 20 min, 100% B. Flow rate = 0.400 mL/min.

(2) Agilent ZORBAX Eclipse XDB C18, 3.5 μm, 3.0 x 100 mm column.

Solvent A= Water, 0.05% TFA; Solvent B= Acetonitrile, 0.05% TFA. Initial conditions: 10% B. 6.5 min, 45% B; 18 min, 65% B; 20 min, 100% B. Flow rate 0.400 mL/min. Column: Agilent Eclipse XDB C18, 3.5 μm, 3.0 x 75 mm.

(3) Poroshell 120 SB-C18, 3.0 x 100 mm, 2.7 μm column; Temperature = 25 ºC;

Solvent A = water, 0.05 % formic acid; Solvent B = acetonitrile, 0.05 % formic acid; Flow Rate = 0.425 mL/min; Starting Conditions = 70 % A, 30 % B; 0.1–4.8 min, 30 % B; 4.9–8.9 min = 85 % B; 9–10 min, B = 100 %.

(4) Poroshell 120 EC-C8, 2.1 x 50 mm, 2.7 μm column; Temperature = 25 ºC;

Solvent A = water, 0.05 % formic acid; Solvent B = acetonitrile, 0.05 % formic acid; Flow Rate = 0.650 mL/min; Starting Conditions = 80 % A, 20 % B; 0.1–2.8 min, 30 % B; 2.9–6 min, 85 % B; 6.01–6.50 min, 100% B.

(5) Poroshell 120 EC-C8, 2.1 x 50 mm, 2.7 μm column; Temperature = 25 ºC;

Solvent A = water, 0.05 % TFA; Solvent B = acetonitrile, 0.05 % TFA; Flow Rate = 0.650 mL/min; Starting Conditions = 80 % A, 20 % B; 0.1 min 30 % B; 1.1 min, 55 % B; 4.5 min, 60% B; 5.7 min, 70% B; 7.0 min, 80% B; 8.0-9.0 min, 100% B.

2.9.2 Reaction monitoring by ReactIR

The peaks at 1013 and 1719 cm^{-1} were used for reaction monitoring by FTIR (ReactIR ic10 and ic15). An example of the spectral surface can be seen in Figure 2.26.

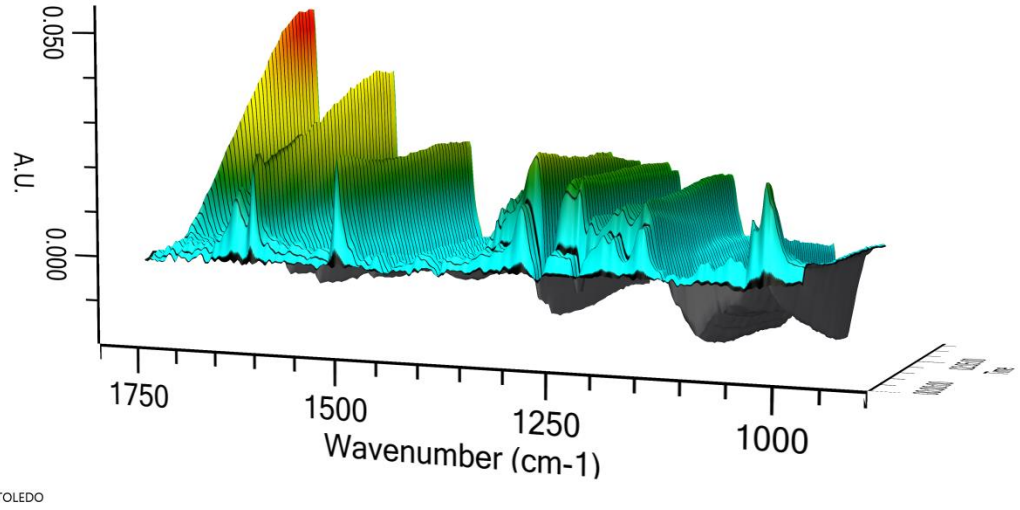

Figure 2.26: Sample FTIR spectra of $Dy(OTf)_3$ – catalyzed zero-order reaction

2.9.2.1 Validation of FTIR for reaction analysis

Validation of FTIR as a suitable technique for in situ reaction analysis was performed through reaction sampling and HPLC-MS analysis of reaction conversion and product formation as a function of time. The reaction was sampled by withdrawal of approximately 5 microliter aliquots of the reaction solution and diluted with methanol at room temperature. Samples were analyzed by HPLC-MS immediately. HPLC-MS analysis was conducted HPLC method #1.

Analysis of the reaction conversion time course by FTIR and sampling methods were in agreement.

2.9.2.2 General procedure for kinetic experiments

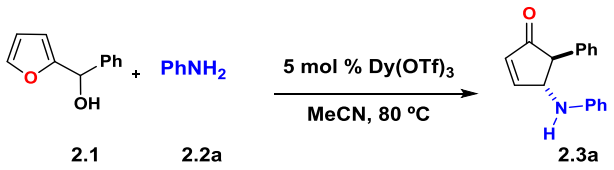

2.1 2.2a 2.3a

To a 10 mL vial with PTFE-silicon septum and open screw-cap was added 2 mL of acetonitrile. The vial was placed in a pre-heated oil-bath at 80 °C and allowed to equilibrate. After taking a background scan in hot solvent, furan-2-yl(phenyl)methanol **2.1** (44.0 mg, 0.250 mmol, 0.125 M) and aniline **2.2a** (23.0 mg, 0.250 mmol, 0.125 M) were added to the pre-equilibrated acetonitrile. After a stable FTIR signal was observed, $Dy(OTf)_3$ (7.6 mg, 0.013 mmol, 5 mol %) catalyst was added. Reaction progress was monitored by FTIR using two peaks: 1013 cm^{-1} for the consumption of furylcarbinol **2.1**, and 1715 cm^{-1} for the appearance of cyclopentenone **2.3a**.

Experiments conducted with different lanthanide triflates used the corresponding amount of solid catalyst.

2.9.2.3 Experiments with same absolute excess

As an internal standard, 20 μL of a 0.58 M stock solution of 2-methoxynaphthalene was used in each reaction. On the ReactIR, a background scan was taken in 65 °C acetonitrile and 2-methoxynaphthalene. Stock solutions of furylcarbinol **2.1** and aniline **2.2a** were injected, followed by subsequent addition of solid $Dy(OTf)_3$. All experiments in same excess used the same concentration of $Dy(OTf)_3$ (6.25 mM) and a total reaction volume of 2 mL. The following table summarizes the molarities and excesses of furylcarbinol **2.1** to aniline **2.2a**.

Experiment	$[2.1]_0$ / M	$[2.2a]_0$ / M	[2.2a]-[2.1] / M
Same excess [2.1]	0.12	0.10	- 0.02
Same excess [2.1]	0.14	0.12	- 0.02
Same excess [2.2a]	0.10	0.12	0.02
Same excess [2.2a]	0.12	0.14	0.02

Table 2.2: Concentrations for same absolute excess experiments

2.9.2.4 Order in $Dy(OTf)_3$ catalyst

Stock solutions of **2.1** and **2.2a** in acetonitrile were prepared and used within two days. Reactions were 0.125 M in **2.1** and **2.2a** and were run at 65 °C. Concentrations of $Dy(OTf)_3$ were as follows: 2, 4, 6.25, 8, 10, and 12 mM. To a pre-heated vial of acetonitrile, the stock solutions of furylcarbinol **2.1** and aniline **2.2a** were added. When a steady signal was reached on the FTIR, the appropriate amount of $Dy(OTf)_3$ was added as a solid. The slope of the rate of up to 70% conversion of **2.2a** in each reaction was used in finding the order in $Dy(OTf)_3$. The positive and linear fit implies that the Piancatelli reaction is first order in $Dy(OTf)_3$. *Note*: these are not absolute rate (k) constants, but relative k values.

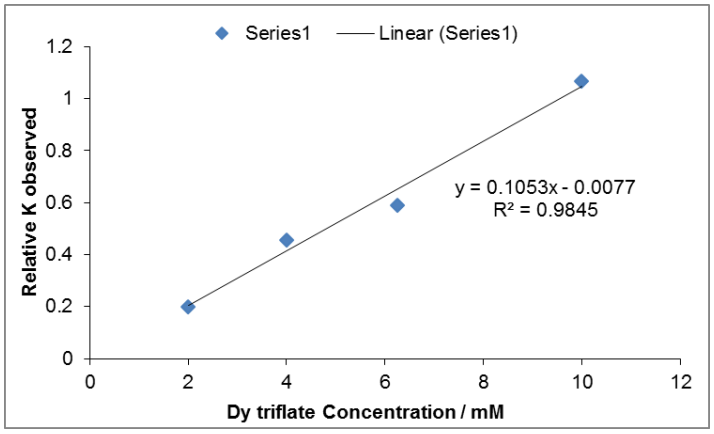

Figure 2.27: Relative rate as a function of $Dy(OTf)_3$ catalyst, determined by ReactIR

2.9.2.5 Order in trifluoroacetic acid catalyst

Stock solutions of **2.1**, **2.2a**, and trifluoroacetic acid (TFA) in acetonitrile were prepared and used within two days. Reactions were 0.125 M in **2.1** and **2.2a** and were run at 65 °C. Concentrations of TFA were as follows: 3.125, 6.25, 12.5, 18.75, 25, and 30 mM. To a pre-heated vial of acetonitrile, the stock solutions of furylcarbinol **2.1** and aniline **2.2a** were added. When a steady signal was reached on the FTIR, an appropriate portion of the TFA stock solution was injected. Graphs were included in the main chapter.

2.9.3 Linear free energy relationships and competition experiments

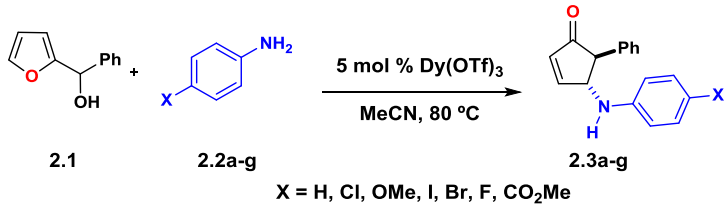

A stock solution of **2.1** in acetonitrile was prepared and used within two days. Reactions were 0.125 M in **2.1** and the substituted aniline **2.2a-g** and were run at 80 °C on a 2 mL scale. To a pre-heated vial of acetonitrile, the stock solutions of furylcarbinol **2.1** and the substituted aniline **2.2a-g** were added. When a steady signal was reached on the FTIR, $Dy(OTf)_3$ (7.6 mg, 0.013 mmol, 5 mol % relative to furylcarbinol) was added as a solid. For the TFA-catalyzed experiments, 0.02 mL of a 0.3 M TFA stock solution was used to provide a 2 mL reaction solution that was 30 mM in TFA (24 mol % relative to furylcarbinol **2.1**). The slopes of initial rate of formation of **2.3a-g** in individual reactions were used in graphing the Hammett Plots.

2.9.3.1 Competition experiments

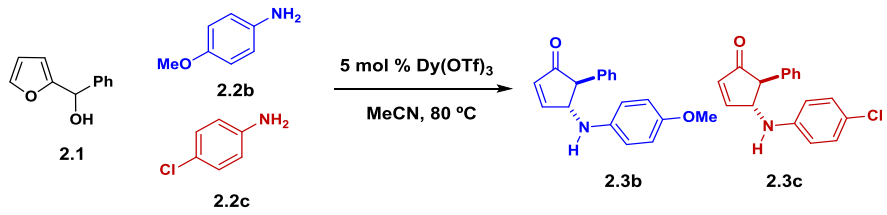

Competition experiments were conducted at 80 °C with 4-chloroaniline **2.2c** and 4-methoxyaniline **2.2b** to make cyclopentenones **2.3c** and **2.3b**, respectively. As a standard, 0.1 mL of a 0.101 M stock solution of 2-methoxynaphthalene for every 1 mL reaction solution was used. A 3 mL solution of acetonitrile and 2-methoxynaphthalene was preheated to 80 °C. Furylcarbinol **2.1** was added by dissolution from a tared syringe, followed by solid aniline **2.2c** or **2.2b**. A sample was taken at this point for analysis of initial conditions. Either $Dy(OTf)_3$ (5 mol % relative to furylcarbinol **2.1**) or TFA (24 mol % relative to furylcarbinol **2.1**) was added. The reactions were sampled by taking approximately 5 µL aliquots and dilution with approximately 1 mL of methanol and immediately analyzed by HPLC-MS.

Experiment	Catalyst	$[2.1]_0$ /M	$[2.2b]_0$ / M	$[2.2c]_0$ / M	Catalyst / M
Figure 2.6	$Dy(OTf)_3$	0.125	0.0625	0.0625	0.0063
Figure 2.10	TFA	0.125	0.0625	0.0625	0.030
Figure 2.7	$Dy(OTf)_3$	0.125	0.125	0.125	0.0063

Table 2.3: Concentrations used for substituted aniline competition experiments

A calibration curve was created between the two cyclopentenone products **2.3c** and **2.3b** and the standard, 2-methoxynaphthalene, to determine the selectivity for either product over time. Each cyclopentenone was synthesized by the standard procedure[2] and purified by flash column chromatography (1:6 to 1:4 EtOAc:hexanes). Relative UV absorptivities at 230 nm with 8 µL injections were analyzed by HPLC-MS for the following calibration curves:

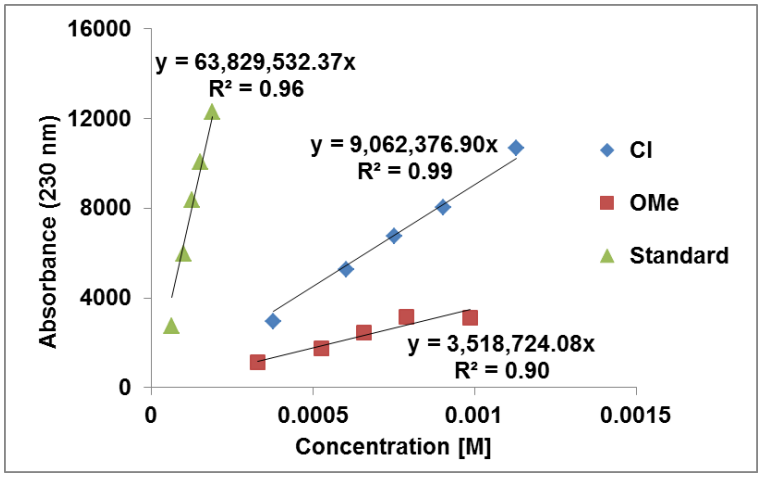

Figure 2.28: Calibration curves for compounds 2.3b, 2.3c

The HPLC conditions used were #2.

2.9.4 Derivation of a steady state rate law

The proposed mechanism based on the competitive inhibition model follows the scheme:

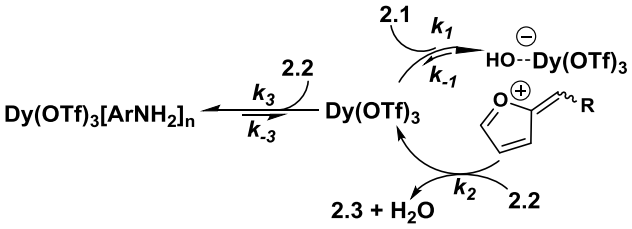

Or drawn in general:

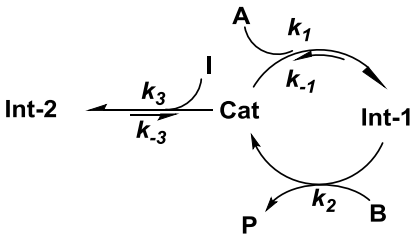

Assumptions:

Mass balance for the catalyst is given by

1) $[cat_{tot}] = [cat_0] = [cat] + [Int1] + [Int2]$

By using steady state approximations,

2a) $\frac{d[cat]}{dt} \approx 0 \approx -k_1[cat][A] + k_{-1}[Int1] + k_2[B][Int1] - k_3[I][cat] + k_{-3}[Int2]$

2b) $\frac{d[Int1]}{dt} \approx 0 \approx k_1[cat][A] - k_{-1}[Int1] - k_2[Int1][B]$

2c) $\frac{d[Int2]}{dt} \approx 0 \approx k_3[cat][I] - k_{-3}[Int2]$

Rate of product formation:

$\frac{d[P]}{dt} = k_2[Int1][B]$

Define [cat] in terms of [Int1] by using 2b):

$k_1[cat][A] = k_{-1}[Int1] + k_2[Int1][B]$

$[cat] = \frac{k_{-1}[Int1] + k_2[Int1][B]}{k_1[A]} = \frac{(k_{-1} + k_2[B])[Int1]}{k_1[A]}$

Substitute [cat] into 2c)

$0 = k_3[I]\left(\frac{(k_{-1} + k_2[B])[Int1]}{k_1[A]}\right) - k_{-3}[Int2]$

$[Int2] = \frac{k_3(k_{-1} + k_2[B])[Int1][I]}{k_{-3}k_1[A]}$

Substitute [Int2] into $[cat_{tot}]$:

$[cat_{tot}] = \frac{(k_{-1} + k_2[B])[Int1]}{k_1[A]} + [Int1] + \frac{k_3[Int1][I](k_{-1} + k_2[B])}{k_{-3}k_1[A]}$

$[cat_{tot}] = [Int1]\left(\frac{(k_{-1} + k_2[B])}{k_1[A]}\right) + [Int1] + [Int1]\left(\frac{k_3[I](k_{-1} + k_2[B])}{k_{-3}k_1[A]}\right)$

$$[cat_{tot}] = [Int1]\frac{k_{-3}(k_{-1} + k_2[B]) + k_{-3}k_1[A] + k_3[I](k_{-1} + k_2[B])}{k_{-3}k_1[A]}$$

$$[Int1] = \frac{[cat_{tot}]k_{-3}k_1[A]}{k_{-3}(k_{-1} + k_2[B]) + k_{-3}k_1[A] + k_3[I](k_{-1} + k_2[B])}$$

Therefore, rate of product formation is:

$$\frac{d[B]}{dt} = k_2[B][Int1] = \frac{k_1k_2k_{-3}[A][B][cat_{tot}]}{k_{-3}(k_{-1} + k_2[B]) + k_{-3}k_1[A] + k_3[I](k_{-1} + k_2[B])}$$

If I = B,

$$\frac{d[P]}{dt} = \frac{k_1k_2k_{-3}[A][B][cat_{tot}]}{k_{-3}(k_{-1} + k_2[B] + k_1[A]) + k_3(k_{-1}[B] + k_2[B]^2)}$$

If we assume the terms k_3 and k_2 are the most important (largest magnitude) this reduces to:

$$\frac{d[P]}{dt} = \frac{k_1k_{-3}[A][cat_{tot}]}{k_3[B]}$$

2.9.5 Experiments with automated sampling for analysis by HPLC-MS

All kinetic experiments were conducted with automated sampling with a custom-built apparatus. From the reaction vial, 15 μL samples were automatically taken by a programmable syringe pump at defined time points. Samples were rerouted with a Gilson 918 Injection Valve Actuator to a Gilson 215 Liquid Handler, which allowed for the dilution of the samples with 1 mL of methanol directly into LC vials.

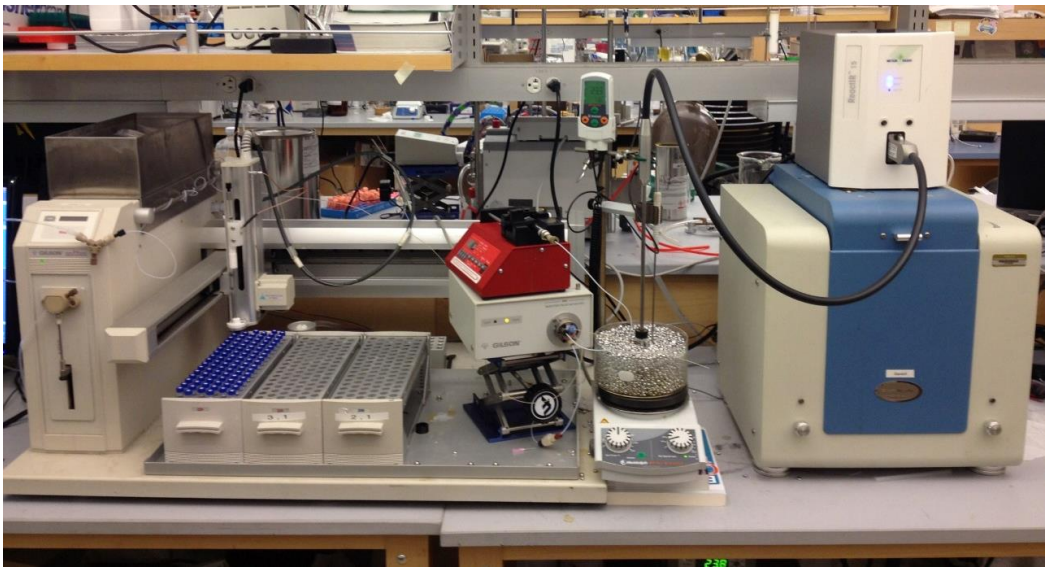

Figure 2.29 Set up for tandem reaction progress monitoring with ReactIR, syringe pump, and liquid handler

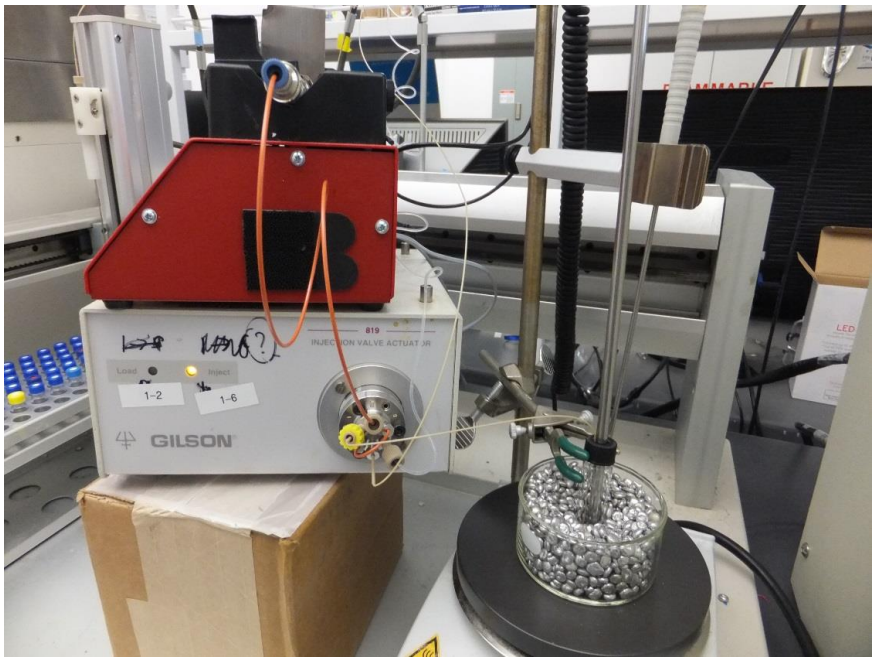

Figure 2.30: Reactor set-up showing the ReactIR probe for in situ IR analysis and Rheodyne/syringe pump for liquid sampling

2.9.5.1 Reaction monitoring of Aza-Piancatelli with *N,O*-dibenzylhydroxylamine nucleophile

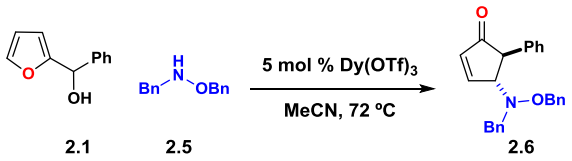

2.1 2.5 2.6

To a 10 mL glass vial equipped with PTFE-silicon septum, open-top screw cap, and magnetic stir bar was added 4.5 mL of acetonitrile, furan-2-yl(phenyl)methanol (87.0 mg, 0.5 mmol) and *N,O*-dibenzylhydroxylamine (106.0 mg, 0.50 mmol). The vial was placed in a pre-heated bath of aluminum beads at 72 °C and allowed to reach thermal equilibrium. The in situ FT-IR instrument was blanked in hot solvent (72 °C) contained in a separate vial. The probe was then immediately fitted onto the reaction vial. After a stable FT-IR signal was observed, $Dy(OTf)_3$ (15.0 mg, 0.025 mmol, 5 mol % catalyst) dissolved in 0.5 mL of acetonitrile was injected via syringe. For HPLC/MS analysis, sampling of the reaction began immediately after injection of the catalyst. The samples were collected every 5 minutes until 65 minutes and then every 8 minutes. LC samples were analyzed with HPLC method #3.

2.9.5.2 Reaction monitoring of conversion of intermediate 2.7 to *trans*-cyclopentenone 2.6

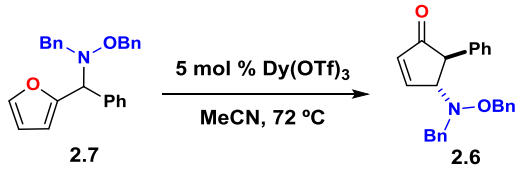

2.7 2.6

To a 4 mL glass vial equipped with PTFE-silicon septum, open-top screw cap, and magnetic stir bar was added 2 mL of acetonitrile and *N,O*-dibenzyl-N-(furan-2-yl(phenyl)methyl)hydroxylamine (74.26 mg, 0.201 mmol). The vial was placed in a pre-heated

bath of aluminum beads at 70 ºC and allowed to reach thermal equilibrium. $Dy(OTf)_3$ (6.23 mg, 0.0102 mmol, 5.1 mol % catalyst) was then added. For HPLC/MS analysis, sampling of the reaction began before addition of the catalyst. The first 20 samples were collected every 3 min while the remaining 25 samples were collected every 12 min. LC samples were analyzed with HPLC method #3.

2.9.5.3 Competition experiment between aniline 2.2a and *N,O*-dibenzylhydroxylamine 2.5

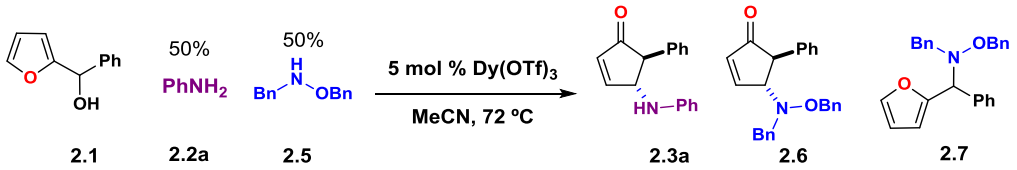

To a 10 mL glass vial equipped with PTFE-silicon septum, open-top screw cap, and magnetic stir bar was added 4.5 mL of acetonitrile, furan-2-yl(phenyl)methanol (87.0 mg, 0.5 mmol), *N,O*-dibenzylhydroxylamine (53.0 mg, 0.25 mmol), and aniline (23.0 mg, 0.25 mmol). The vial was placed in a pre-heated bath of aluminum beads at 72 ºC and allowed to reach thermal equilibrium. The in situ FT-IR instrument was blanked in hot solvent (72 ºC) contained in a separate vial. The probe was then immediately fitted onto the reaction vial. After a stable FT-IR signal was observed, $Dy(OTf)_3$ (15.0 mg, 0.025 mmol, 5 mol % catalyst) dissolved in 0.5 mL of acetonitrile was injected via syringe. For HPLC/MS analysis, sampling of the reaction began immediately after injection of the catalyst. The first 60 samples were collected every 2 min while the remaining 36 samples were collected every 4 min. LC samples were analyzed with HPLC method #4.

2.9.5.4 Calibration curves

To find relative absorptivity constants of all observable reactants, products, and intermediates (except aniline), stock solutions of each compound were made. Varying volumes of each stock solution were placed into LC vials, and the subsequent mixtures were analyzed by HPLC-MS under HPLC method #4. Integrations were taken at 210 nm. Concentrations were calculated for mixtures of all compounds in LC vials for the same injection volume as detailed previously.

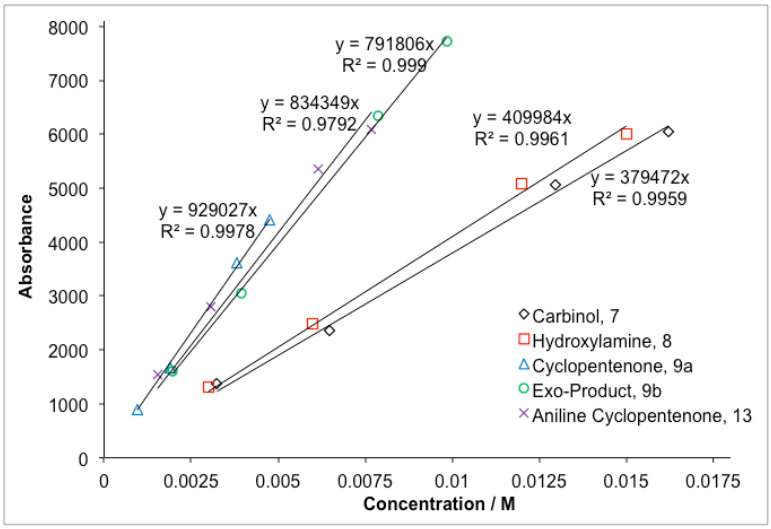

Figure 2.31: Calibration curves for competition experiment with aniline and *N,O*-dibenzylhydroxylamine

2.9.5.5 Reaction progress with *N*-phenylhydroxylamine as a nucleophile

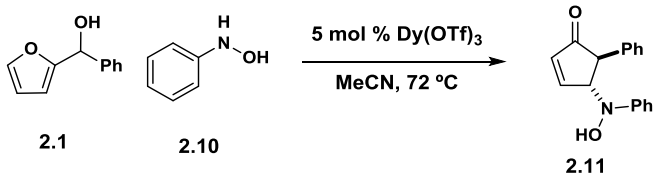

2.1 2.10 2.11

To a 8 mL glass vial equipped with PTFE-silicon septum, open-top screw cap, and magnetic stir bar was added 3 mL of acetonitrile, furan-2-yl(phenyl)methanol (52.0 mg, 0.3 mmol) and *N*-phenylhydroxylamine (32.0 mg, 0.3 mmol). The vial was placed in a pre-heated bath of aluminum beads at 72 ºC and allowed to reach thermal equilibrium. For HPLC/MS analysis, sampling of the reaction began immediately before injection of the catalyst. The $Dy(OTf)_3$ (9.2 mg, 0.015 mmol, 5 mol % catalyst) was added as a solid. Samples were collected every 5 minutes for 70 minutes, and then every 15 minutes until 250 minutes. LC samples were analyzed with HPLC method #5.

2.9.5.6 Reaction progress with *N*-phenylhydroxylamine competing with 4-bromoaniline

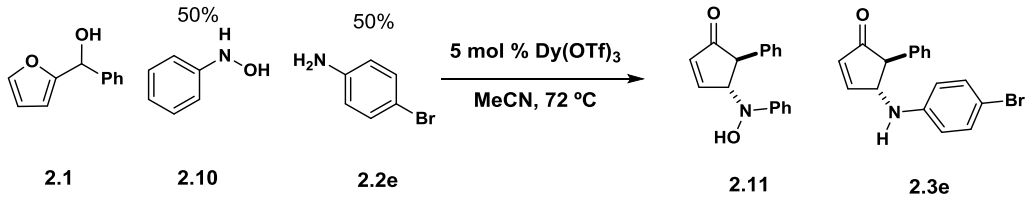

To a 8 mL glass vial equipped with PTFE-silicon septum, open-top screw cap, and magnetic stir bar was added 3 mL of acetonitrile, furan-2-yl(phenyl)methanol (52.0 mg, 0.3 mmol), *N*-phenylhydroxylamine (16.0 mg, 0.15 mmol), and 4-bromoaniline (26.0 mg, 0.15 mmol). The vial was placed in a pre-heated bath of aluminum beads at 72 ºC and allowed to reach thermal equilibrium. For HPLC/MS analysis, sampling of the reaction began immediately before injection of the catalyst. The $Dy(OTf)_3$ (9.2 mg, 0.015 mmol, 5 mol % catalyst) was added as a solid. Samples were collected every 2 minutes for 52 minutes, and then every 5 minutes until 117 minutes. LC samples were analyzed with HPLC method #5.

2.9.6 General procedure for experiments with NaBARF as an additive

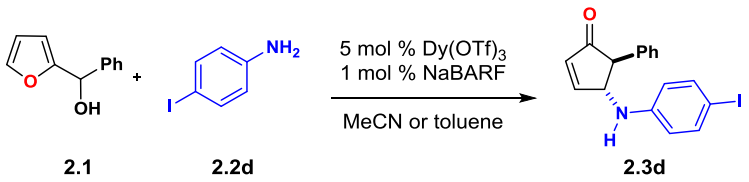

2.1 2.2d 2.3d

To an 8 mL vial with PTFE-silicon septum and open screw-cap was added 2 mL of toluene. After taking a background scan in solvent, furan-2-yl(phenyl)methanol **2.1** (35.0 mg, 0.20 mmol) and aniline **2.2d** (44.0 mg, 0.20 mmol) were added to the pre-equilibrated toluene. After a stable FTIR signal was observed, dysprosium (III) triflate (6.1 mg, 0.010 mmol, 5 mol %) catalyst and NaBARF (1.7 mg, 0.002 mmol, 1 mol %) was added in one portion. Reaction progress was monitored by FTIR using two peaks: 1013 cm^{-1} for the consumption of furylcarbinol **2.1**, and 1715 cm^{-1} for the appearance of cyclopentenone **2.3d**.

For experiments with varying mixing time of $Dy(OTf)_3$ and NaBARF, 0.5 mL of toluene was set aside previously, to which the solids were added and stirred for a set amount of time before addition to the reaction vial.

2.9.7 Syntheses of compounds

2.9.7.1 Synthesis of 4-(Benzyl(benzyloxy)amino)-5-phenylcyclopent-2-en-1-one

2.1 2.5 2.6

This compound was prepared in accordance with the published procedure.[64] Furan-2-yl(phenyl)methanol (38.2 mg, 0.220 mmol) and *N*,*O*-dibenzylhydroxylamine (2) (46.8 mg, 0.220 mmol) were treated with $Dy(OTf)_3$ (6.7 mg, 0.011 mmol) in $MeNO_2$ (2.2 mL). The resulting

reaction mixture was heated to 80 ºC for 30 min. The reaction was then quenched at 23 ºC with saturated aqueous $NaHCO_3$ (5 mL) and extracted with ethyl acetate (3 × 5 mL). The combined organic layers were dried over $MgSO_4$, filtered and then concentrated *in vacuo*. The residue was purified by flash column chromatography to afford cyclopentenone **3** (71.6 mg, 88%) as a light orange/yellow solid. **^{1}H NMR** (600 MHz, $CDCl_3$) δ 7.61 (s, 1H), 7.36 – 7.20 (m, 9H), 7.15 – 7.04 (m, 6H), 6.33 (dd, *J* = 5.8, 1.9 Hz, 1H), 4.43 (d, *J* = 11.9 Hz, 1H), 4.41 (d, *J* = 10.2 Hz, 1H), 4.24 (ddd, *J* = 2.3, 2.3, 2.3 Hz, 1H), 4.01 (d, *J* = 12.6 Hz, 1H), 3.93 (s, 1H), 3.80 (d, *J* = 12.6 Hz, 1H) ppm; **^{13}C NMR** (125 MHz, $CDCl_3$) δ 207.1, 162.4, 139.0, 136.7, 136.6, 134.9, 129.9, 129.2, 129.1, 128.5, 128.4, 128.3, 128.3, 127.7, 127.2, 76.9, 73.9, 61.3, 52.7 ppm; **IR** (thin film) 3063, 3031, 2919, 1709, 1595, 1454, 1265, 1029, 975 cm^{-1}; **MS** (ESI) *m/z* 392.1636 (392.1626 calcd for $C_{25}H_{23}NNaO_2^+$ $[MNa]^+$).

2.9.7.2 Isolation of *N*,*O*-dibenzyl-*N*-(furan-2-yl(phenyl)methyl)hydroxylamine

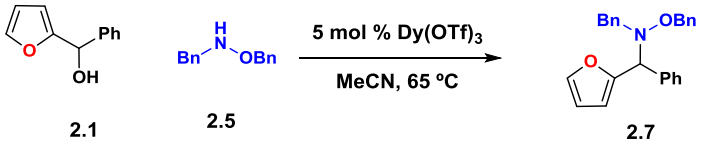

2.1 2.5 2.7

Two reactions were conducted and combined to yield the product. For the first reaction, a 16 mL glass vial equipped with PTFE-silicon septum, open top screw cap, and magnetic stir bar was charged with 10 mL acetonitrile, furan-2-yl(phenyl)methanol (0.174 g, 1 mmol) and *N*,*O*-dibenzylhydroxylamine (0.213 g, 1 mmol), and $Dy(OTf)_3$ (0.030 g, 0.05 mmol, 5% catalyst). For the second reaction, a 20 mL glass vial was charged with 15 mL acetonitrile, furan-2-yl(phenyl)methanol) (0.261 g, 1.5 mmol) and *N*,*O*-dibenzylhydroxylamine (0.320 g, 1.500 mmol), and $Dy(OTf)_3$ (0.027 g, 0.045 mmol, 3% catalyst). Both reactions were stirred and heated at 65 °C for two hours. The reactions were separately quenched at 23 ºC with saturated aqueous

$NaHCO_3$ and extracted with dichloromethane (4 x 10 mL). The combined organic layers were dried over Na_2SO_4 and concentrated *in vacuo*. The crude gel from both reactions was purified by flash column chromatography with a gradient starting with hexanes with increasing ethyl acetate. The intermediate *N*,*O*-dibenzyl-*N*-(furan-2-yl(phenyl)methyl)hydroxylamine is collected from fractions with compounds with high R_f values and concentrated to afford a clear gel, which upon freezing solidifies as a white solid (combined yield 0.319 g, 0.864 mmol, 34.6%). The compound remains solid at room temperature. **^{1}H NMR** (500 MHz, $CDCl_3$) δ 7.65 – 7.61 (m, 2H), 7.44 – 7.27 (m, 9H), 7.21 – 7.12 (m, 2H), 7.19 – 7.13 (m, 3H), 6.71 (d, *J* = 6.1 Hz, 2H), 6.39 – 6.35 (m, 2H), 4.95 (s, 1H), 3.97 (d, *J* = 9.3 Hz, 1H), 3.94 (d, *J* = 9.3 Hz, 1H), 3.84 (d, *J* = 13.0 Hz, 1H), 3.76 (d, *J* = 12.7 Hz, 1H) ppm; **^{13}C NMR** (125 MHz, $CDCl_3$) δ 153.8, 142.0, 139.3, 138.1, 136.6, 130.2, 129.4, 129.1, 128.5, 128.2, 128.2, 127.9, 127.4, 110.6, 109.1, 76.9, 69.8, 61.3 ppm; **HRMS** (ESI) *m/z* 392.1609 (392.1626 calcd for $C_{25}H_{23}NNaO_2$ $[MNa]^+$).

2.9.7.3 Synthesis of 4-(phenylamino)-5-phenylcyclopent-2-en-1-one and related compounds

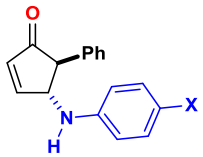

2.3a-g

Compounds **2.3a-g** was synthesized and characterized according to the procedures previously reported.[51, 73]

Chapter 3: Understanding Pathways for Side-Product Formation in the Kinugasa Reaction

3.1 Background of the Kinugasa reaction

β-Lactams are common scaffolds for antibiotics, notably penicillin derivatives, making them desirable synthetic targets. The first synthetic β-lactam was made through the [2+2] cycloaddition of a ketene and imine by Hermann Staudinger in 1907 (Scheme 3.1).[74] Other methods include enolate/imine condensation, carbonylation of an aziridine, and intramolecular alkylations (Scheme 3.2).[75] Only recently in 2016 has there been a palladium-catalyzed carbonylation of acyclic, aliphatic amines to yield β-lactams.[76]

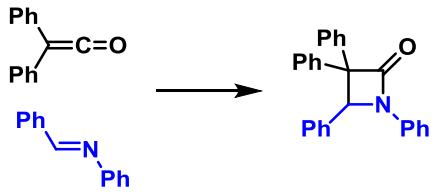

Scheme 3.1: First β-lactam synthesis by Staudinger, 1907

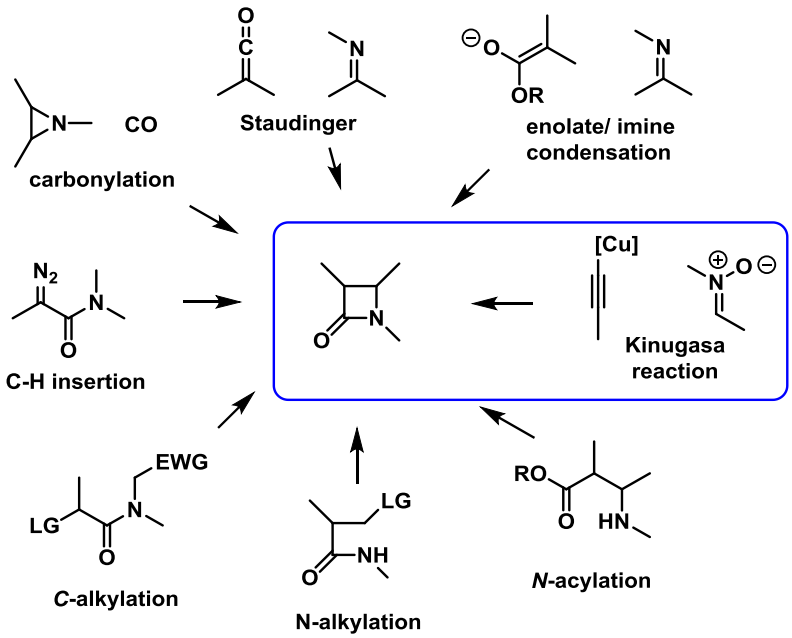

Scheme 3.2: Various synthetic routes to β-lactams[75]

The Kinugasa reaction is a 1,3 dipolar cycloaddition that couples together nitrones and terminal alkynes to yield β-lactams, catalyzed by copper salts. In some cases, the reaction requires substrates that take less preparation, and it can also incorporate asymmetric catalysis to control the enantioselectivity. The first report of the Kinugasa reaction in 1972 used copper(I) phenylacetylide directly with aryl nitrones to provide 51-60% yields of the *cis*-β-lactam (Scheme 3.3).[77] Since then, the reaction was found to be relatively tolerant of many functional groups (alcohols, halides, esters, etc). Although requiring easily available substrates, the Kinugasa method is far from the most well-known or heavily utilized method of synthesizing β-lactams due to predominantly poor to moderate yields.

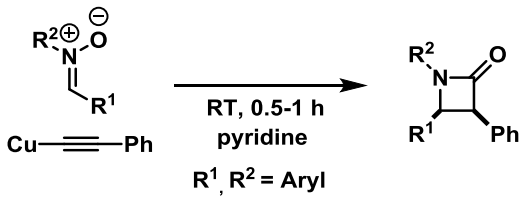

Scheme 3.3: The first Kinugasa reaction, 1972

This chapter concerns our work on the mechanistic study of the Kinugasa reaction, a relatively obscure method of synthesizing β-lactams. While some work was done in attempts to optimize the reaction, the overarching goal was to understand what factors positively and negatively affected the reaction, not increase yield. The Kinugasa reaction was of interest because of its differences from its cousin, the copper-catalyzed alkyne-azide cycloaddition (CuAAC). This copper-catalyzed 1,3 dipolar cycloaddition is also studied for its intriguing mechanistic features. While the CuAAC was a robust click reaction that was extensively developed for use as a coupling reaction that works in a multitude of conditions, the Kinugasa

reaction is not a commonly used reaction. Usually providing low to moderate yields for most substrates, the Kinugasa reaction has been called the "ugly duckling" of β-lactam chemistry.[75]

A proposed catalytic cycle in provided in Scheme 3.4, combining contributions from the Tang and Ding groups.[78,79] Like in the CuAAC, a copper catalyst activates the alkyne **3.1** for deprotonation by a base, forming copper acetylide **3.4**. At this point, a number of organocopper species can exist, sometimes forming less soluble aggregates for certain alkynes and in some solvents. Smaller aggregates of copper(I) acetylides can be more reactive.[80] The copper acetylide **3.4** can couple with the nitrone **3.2** in a 1,3 dipolar cycloaddition to form a copper-bound isoxazoline **3.5**, which must rearrange to eventually form the β-lactam **3.3**. The presence of intermediate isoxazoline is supported by an experiment with a nonterminal alkyne. The analogous stable intermediate isoxazoline was isolated when a non-terminal alkyne is used, as it formed the isoxazoline, not the β-lactam (Scheme 3.5).[81]

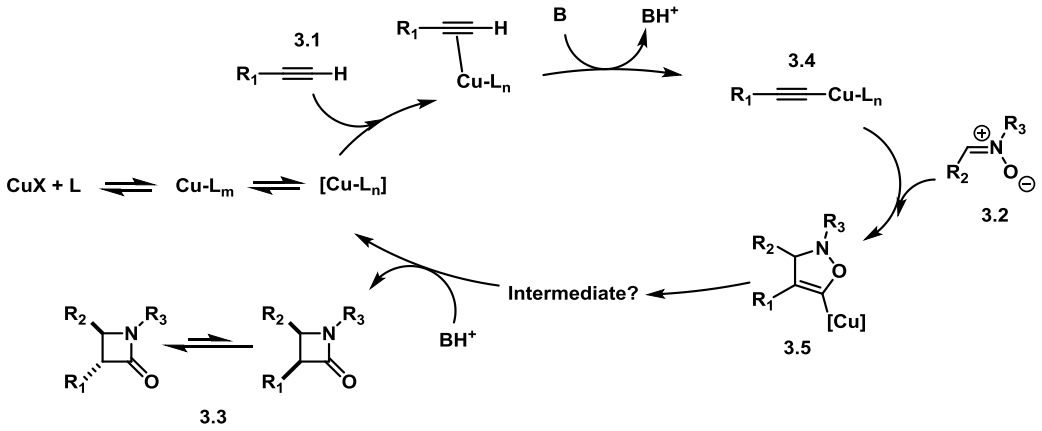

Scheme 3.4: Generalized mechanism for Kinugasa reaction

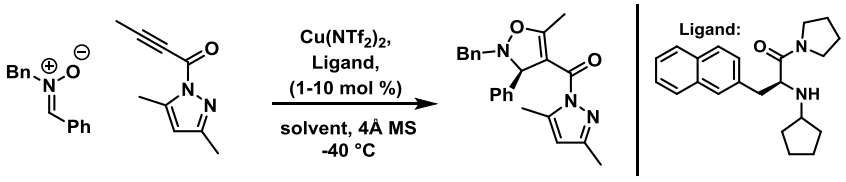

Scheme 3.5: Intercepted isoxazoline with a non-terminal alkyne

The intermediate(s) stemming from the copper-bound isoxazoline and the β-lactam or copper catalyst are released are still debatable. In one of the earliest accepted mechanisms, it was suggested by Ding and Irwin that a strained oxaziridinium intermediate **3.7a** is formed (Scheme 3.6, Path I).[78] As studies were conducted in our lab, we felt this pathway was unlikely, as it would be difficult to form intermediate **3.7a**. Alternatively, Tang et al. suggests that isoxazoline **3.5a** undergoes a retrocycloaddition. This would form **3.6a** which can break down to observed imine **3.9a** and the corresponding ketene (Scheme 3.6, Path II). The ketene and imine would then go through the Staudinger reaction to form the β-lactam **3.3a**, similarly to Scheme 3.1.[79] Protonation of the copper enolate **3.8a** leading to the β-lactam **3.3a** from the less sterically hindered side provides the *cis* isomer, which can isomerize to the *trans* isomer with certain amine base choices and increased reaction time.[82] Usually, the cis isomer is formed as the major or sole isomer.[78]

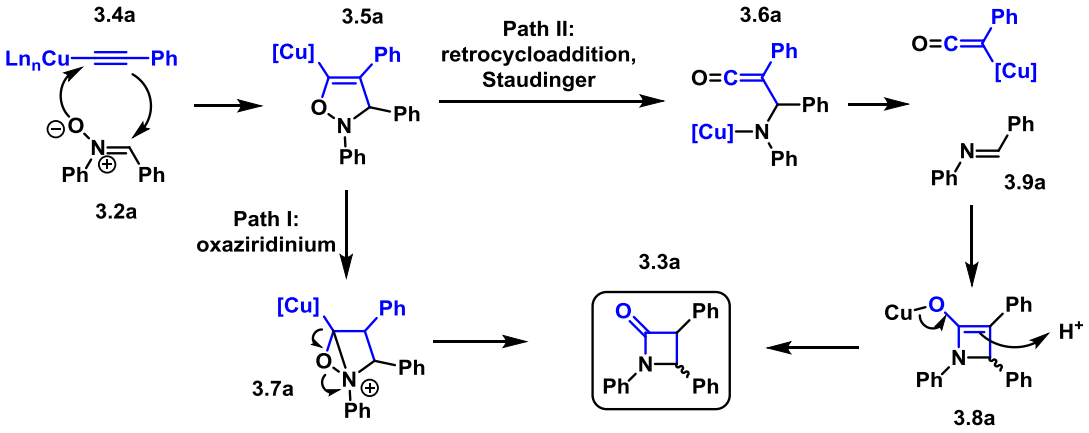

Scheme 3.6: Two formerly proposed pathways for the Kinugasa reaction[79]

The mediocre yields of β-lactam can at least be partially attributed to multiple side products (Scheme 3.7). Previously, other groups have observed deoxygenation of the nitrone substrate, resulting in the corresponding imine **3.9**. Indeed, deoxygenation from *N*-oxides,

including nitrones, have been observed by using stoichiometric copper, catalyzed by the addition of base.[83] From the hydrolysis of the imine, the corresponding aldehyde (and therefore potentially also the carboxylic acid) and amine can also be observed. A propargylic amine **3.11** can also form, resulting from the copper acetylide **3.4** coupling to the imine **3.9**.[84] For aryl alkynes, Glaser coupling can occur between two molecules of copper phenylacetylide to form the Glaser coupling product **3.10**.

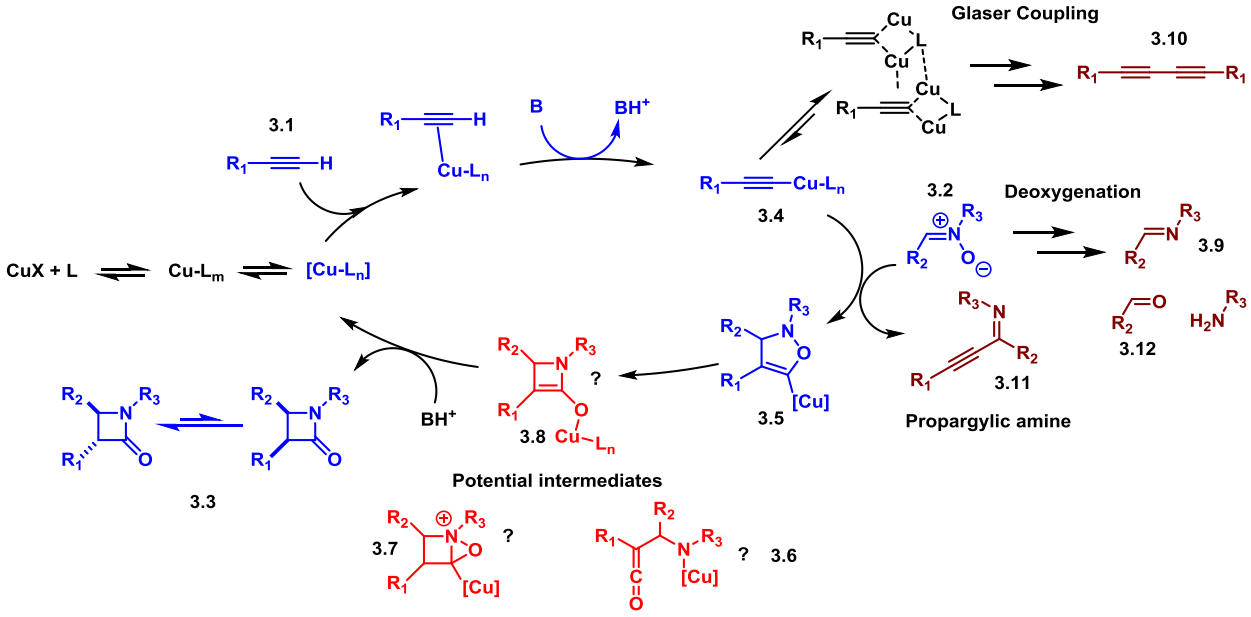

Scheme 3.7: Various side products from the Kinugasa reaction

Unfortunately, the majority of reports of the Kinugasa reaction provides a wide range of yields, rarely more than 85% for more than a few substrates. For example, one of the earlier screens of the Kinugasa reaction in 1995 by Miura et al. varied the electronics of the aryl groups on the nitrone. The lowest yield provided 21% β-lactam, 72% imine with R_1, R_2= Ph and R_3= 4-$MeOC_6H_4$, an electron-donating substituent (Table 3.1). The highest yield of β-lactam was 82%, with 11% imine, for R_3= 4-$(MeO_2C)C_6H_4$, an electron-withdrawing substituent. They note that

electron-withdrawing substituents on the nitrone increased the ratio of β-lactam to imine, as well as the reaction rate. They also noted that increased reaction temperature led to increased imine formation.[84] It is unclear whether the imine concentration increases through deoxygenation of the nitrone with time or if the electronics dictated the selectivity.

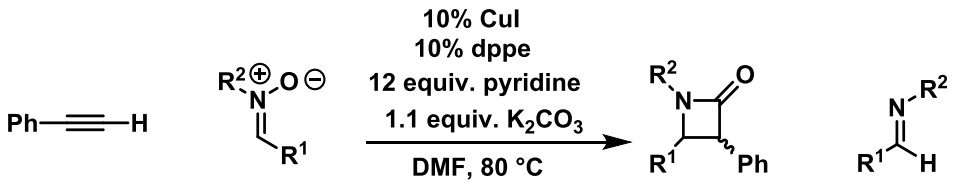

Entry	Nitrone R^1	R^2	Time (hr)	% Yield 3.3 (trans/cis)	% Yield 3.9
1	**Ph**	**4-(MeOOC)C_6H_4**	**2**	**82 (54:64)**	**11**
2	Ph	4-ClC_6H_4	2	73 (30:70)	25
3	Ph	Ph	3	65 (34:66)	26
4	Ph	4-MeC_6H_4	4	54 (35:65)	35
5	**Ph**	**4-MeOC_6H_4**	**5**	**21 (40:60)**	**72**
6	4-ClC_6H_4	Ph	3	69 (38:62)	27
7	4-MeC_6H_4	Ph	3	65 (34:66)	31
8	4-MeOC_6H_4	Ph	5	32 (55:45)	58

Table 3.1: Early development of the Kinugasa reaction[84]

Complementary to Miura's findings, Tang and coworkers found in 2003 that electron-withdrawing groups on the nitrone increased reactivity but decreased the enantioselectivity of the resulting β-lactams when a tris(oxazoline) $Cu(ClO_4)_2 \cdot 6H_2O$ catalyst/ligand combination was used under ambient conditions (Scheme 3.8). Formerly, the Kinugasa reaction had been conducted under an atmosphere of nitrogen, thought to decrease Glaser coupling. It was found that using a copper(II) salt, without any efforts to exclude air, still allowed for viable catalysis. Unfortunately, yields still remained around 36-70% for a variety of nitrones with different

substitutions on either two of its aryl rings, with an unique outlier of 98% for R_2 = *p*-$(EtO_2C)C_6H_4$.[85]

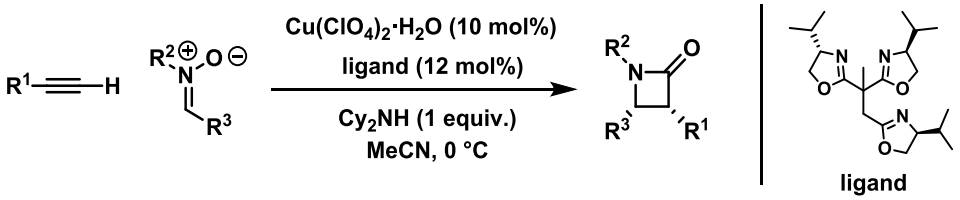

Scheme 3.8: Tang's asymmetric synthesis of β-lactams[85]

More recently, groups have used the Kinugasa reaction to form a scaffold for further functionalization to build monobactams and nocardicins.[86] Unfortunately, final conditions required two equivalents of copper(I) chloride to provide 48-66% yield at -30 to -35 °C, for deoxygenation of the nitrone occurred above those temperatures (unsurprisingly) (Scheme 3.9). Although the reaction is still useful for the initial formation of β-lactam scaffolds due to the ease of procuring or synthesizing the two starting materials, it is still evident that more studies need to be done to better understand what conditions are counterproductive. It is unclear whether or not catalytic conditions were attempted.

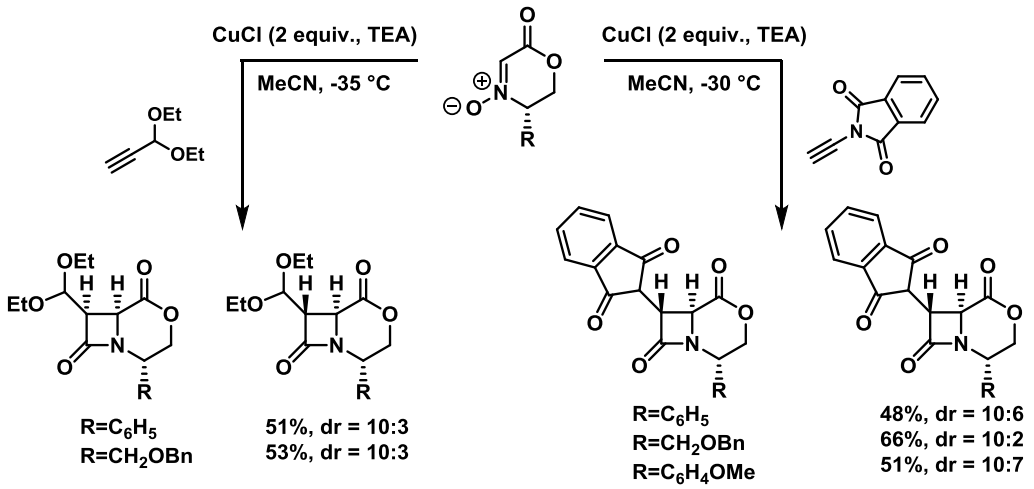

Scheme 3.9: Kinugasa reaction with superstoichiometric copper

Attempts to increase the selectivity of the reaction have been met with moderate success. A recent example in the synthesis of fluoroalkylated β-lactams shows mixed results: up to 26% ee, 42-99% de, and 51-93% combined yields of stereoisomers (Scheme 3.10). However, the scope showed little variation of the nitrone (possibly due to a small range of electronic tolerance for the nitrone) and a couple examples for the alkyne. Five ligands (including BINOL and pybox derivatives) are included in their best results, indicating that no one particular ligand gave good results across their substrate scope. In addition, stoichiometric copper (and catalytic ligand) are used, possibly suggesting either such a high copper loading appeared to be necessary to improve yield, or that catalytic copper was not attempted.[87]

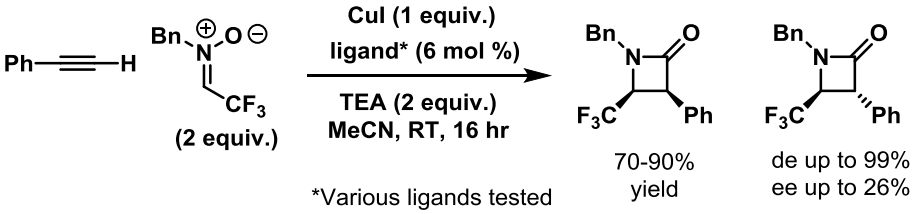

Scheme 3.10: Synthesis of asymmetric trifluoromethylated β-lactams, 2016

An example with more success at increasing enantioselectivity was from Fu and coworkers, which helped revive interest in the Kinugasa reaction (Scheme 3.11).[88,89] Small loadings of copper(I) chloride and a methyl-substituted bis(azaferrocene) ligand was used to drive the asymmetric reaction. Unlike the previous example with higher yields but poor enantioselectivity, this method allowed isolation of the β-lactam in 42-65% yield, 70-93% ee for the major *cis* isomer. Unfortunately, like Tang et al., they find that either yield or enantioselectivity must be compromised. Both the alkyne and nitrone's substituents were independently varied. Electron-donating groups on the *N*-aryl group of the nitrone were found to increase enantioselectivity – which unfortunately decreased yield, as discussed before.

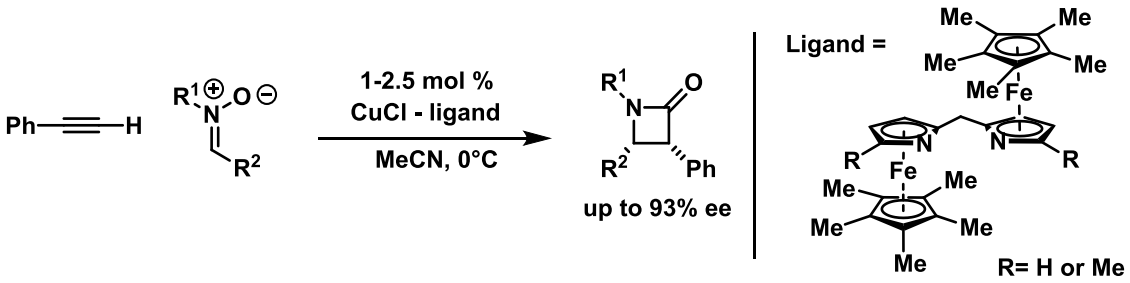

Scheme 3.11: Chiral ferrocenyl ligands for the asymmetric Kinugasa reaction

The main goal of this study was not to optimize conditions for the Kinugasa reaction. Rather, we were more interested in understanding why the reaction suffers from poor yields despite several groups' attempts to control it. The most important goal was to build understanding of the catalytic cycle. This would include finding out which factors controlled the selectivity between the target product and the side-products.

3.2 Initial experiments by heat-flow calorimetry and HPLC-MS: order in alkyne, nitrone, and base

Since the CuAAC had previously been reliably monitored by heat-flow calorimetry in our lab, it was thought that the same tool could be used to study the Kinugasa reaction. It was hoped that the heat evolved would correspond directly to β-lactam formation. Previous studies by a student in the group (Anh Vo) simultaneously ran two sets of experiments, one varying alkyne concentration, and the other varying nitrone concentration (Figure 3.1). It was apparent that increasing the nitrone concentration had a positive effect on the reaction rate, as more heat evolved with increasing nitrone concentration.

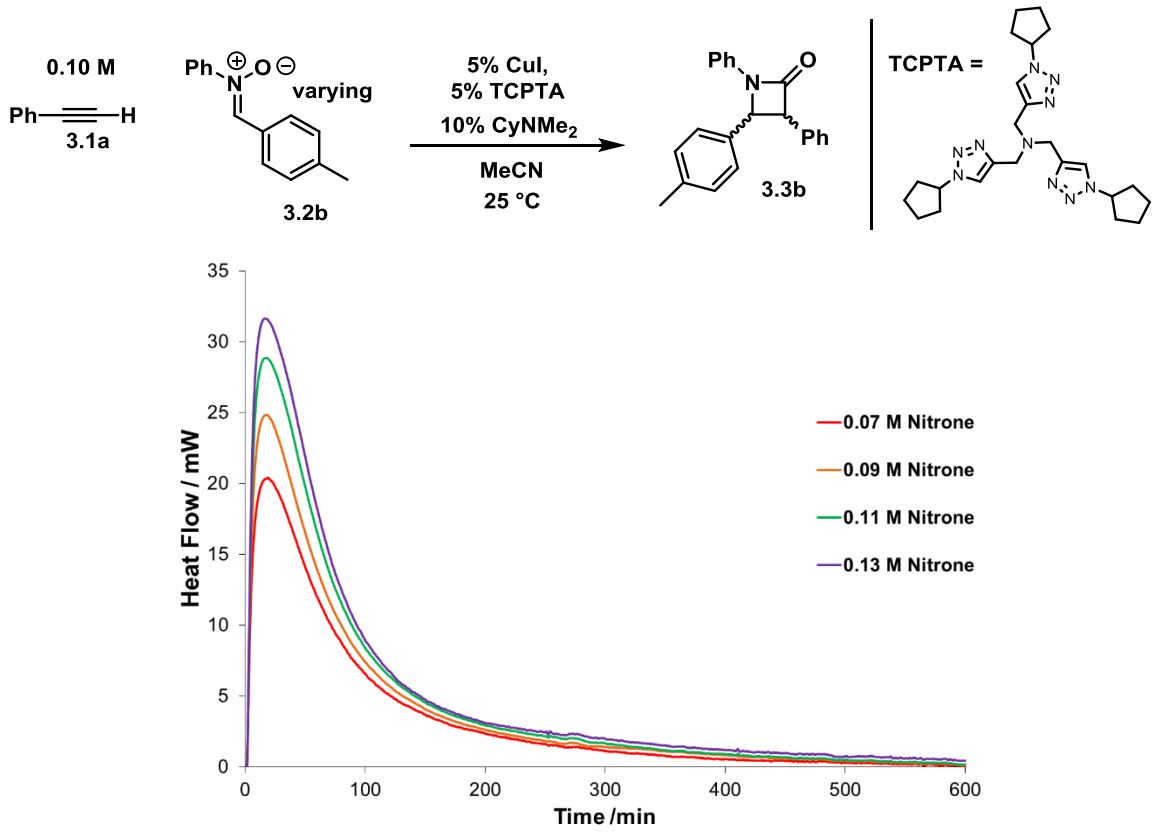

Figure 3.1: Varying nitrone concentration: monitoring by heat-flow calorimetry

The experiments were repeated with different conditions and analyzed by HPLC-MS to obtain more information on the chemical speciation. The reaction was monitored by HPLC-MS by either manually taking aliquots of reactions or with an automated liquid handler at predetermined times. The samples were diluted with a "quenching" solution already in vial, allowing for subsequent analysis by HPLC. The quenching solution contained bicinchoninic acid (BCA) for which two molecules can bind to one Cu^{+1} ion, based on the BCA assay for protein quantification by Smith.[90] Assuming the BCA binds quickly to the active copper(I) species, catalysis effectively stops in the LC vial, accompanied by an intense purple color. It was ascertained that sufficient BCA was previously dispensed into each LC vial to allow fast quenching, and that the contents of the LC vial did not change with time.

The data in Figure 3.2 shows the relative concentration of substrates or products with time across reactions with different initial concentrations of nitrone **3.2a**. As with calorimetry, automated sampling and analysis by HPLC-MS confirmed a positive order in nitrone in that rate of β-lactam formation increased with increasing nitrone concentration (Figure 3.2, graph a). Immediately, this may also cause calorimetry data to be questionable because the imine formation may also contribute to the overall heat profile. Unfortunately, not all of the reactions reach the same conversion to β-lactam (graph a). Imine formation is also higher for higher nitrone concentration (graph c). This can also can be thought of as higher with higher β-lactam formation. However, with increasing nitrone (and increasing rate), selectivity for lactam vs imine is slightly higher with time (graph e). Even though three out of the four reactions theoretically have enough alkyne, some alkyne is consumed in Glaser coupling (not shown; alkyne consumption is shown in graph b).

The complementary set of experiments monitored by heat-flow calorimetry where alkyne concentration was varied showed that all reactions had the same heat profile, which would indicate zero order in alkyne concentration (Figure 3.3). This suggested that the reaction rate only varied with the nitrone concentration, and that it was zero-order in alkyne.

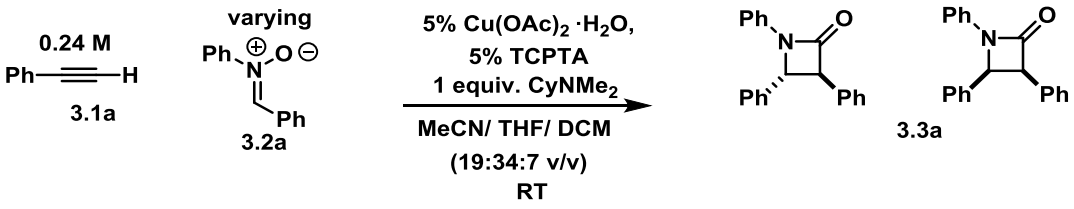

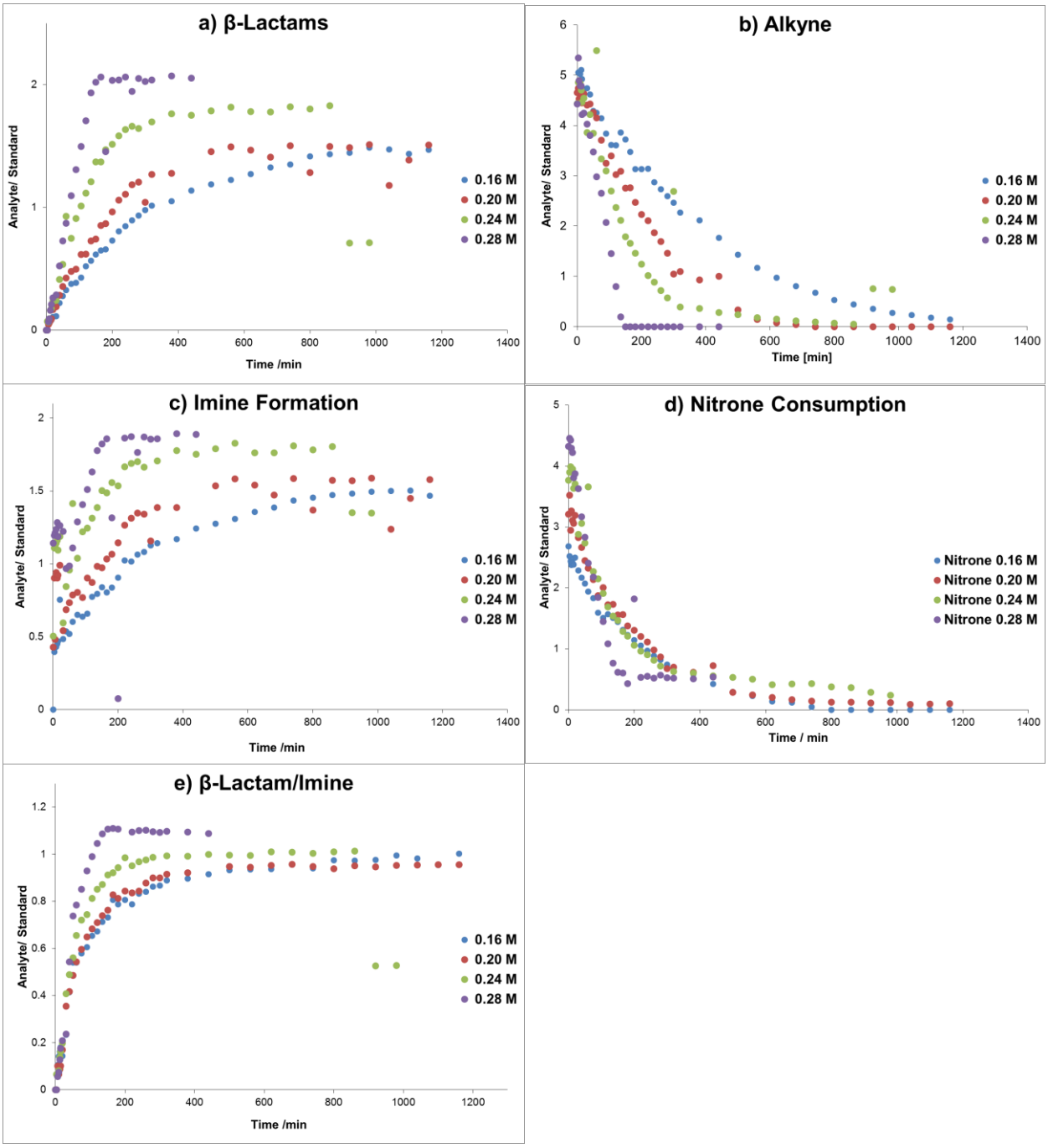

Figure 3.2: Experiments with varying nitrone concentration, monitored by HPLC-MS

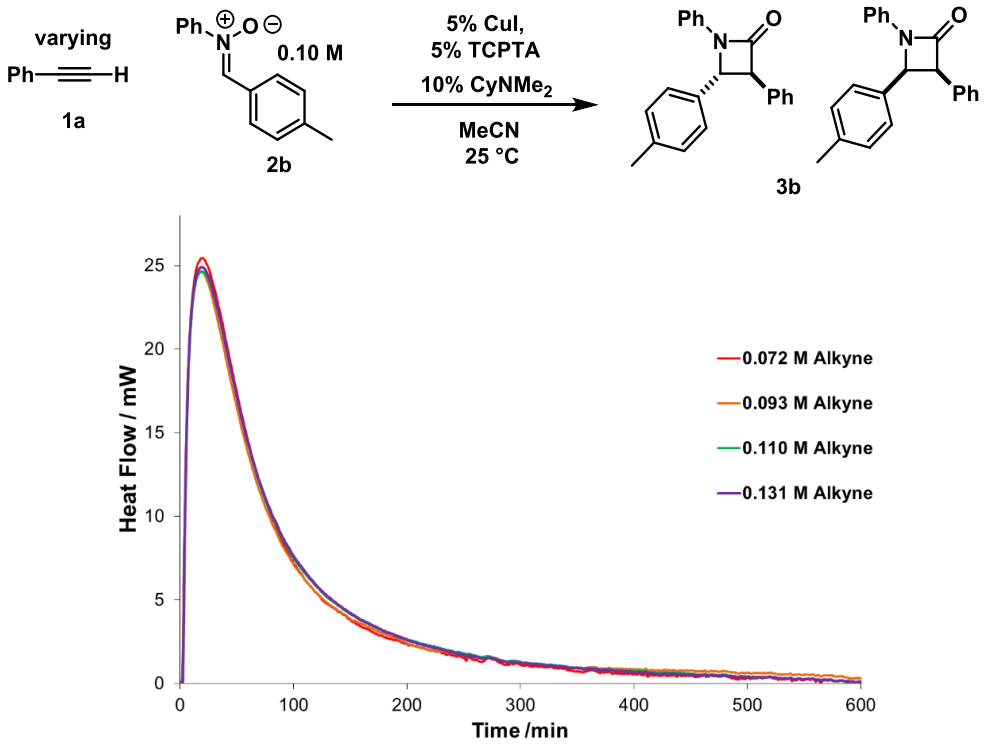

Figure 3.3: Varying alkyne concentration – monitoring by heat-flow calorimetry

When the set of experiments varying alkyne concentration were monitored by HPLC-MS, the results disagreed with those of heat-flow calorimetry (Figure 3.4). By manual sampling and offline analysis by HPLC-MS, it was seen that with increasing alkyne concentration, the rate and yield of β-lactam increased (graph a). The effect is not as dramatic as with varying nitrone concentration, but this may be due to smaller differences in concentrations between the two sets of experiments of order in nitrone vs order in alkyne. Although the same initial concentrations of nitrone **3.2a** are used, the imine **3.9a** formation is higher for increased initial alkyne concentration (graph d). This can also be thought of as imine formation is higher with increased β-lactam formation. However, the selectivity for β-lactam **3.3a** versus imine **3.9a** is higher for higher initial alkyne concentration (graph f). This was also seen in the previous experiments with varying initial concentration of nitrone.

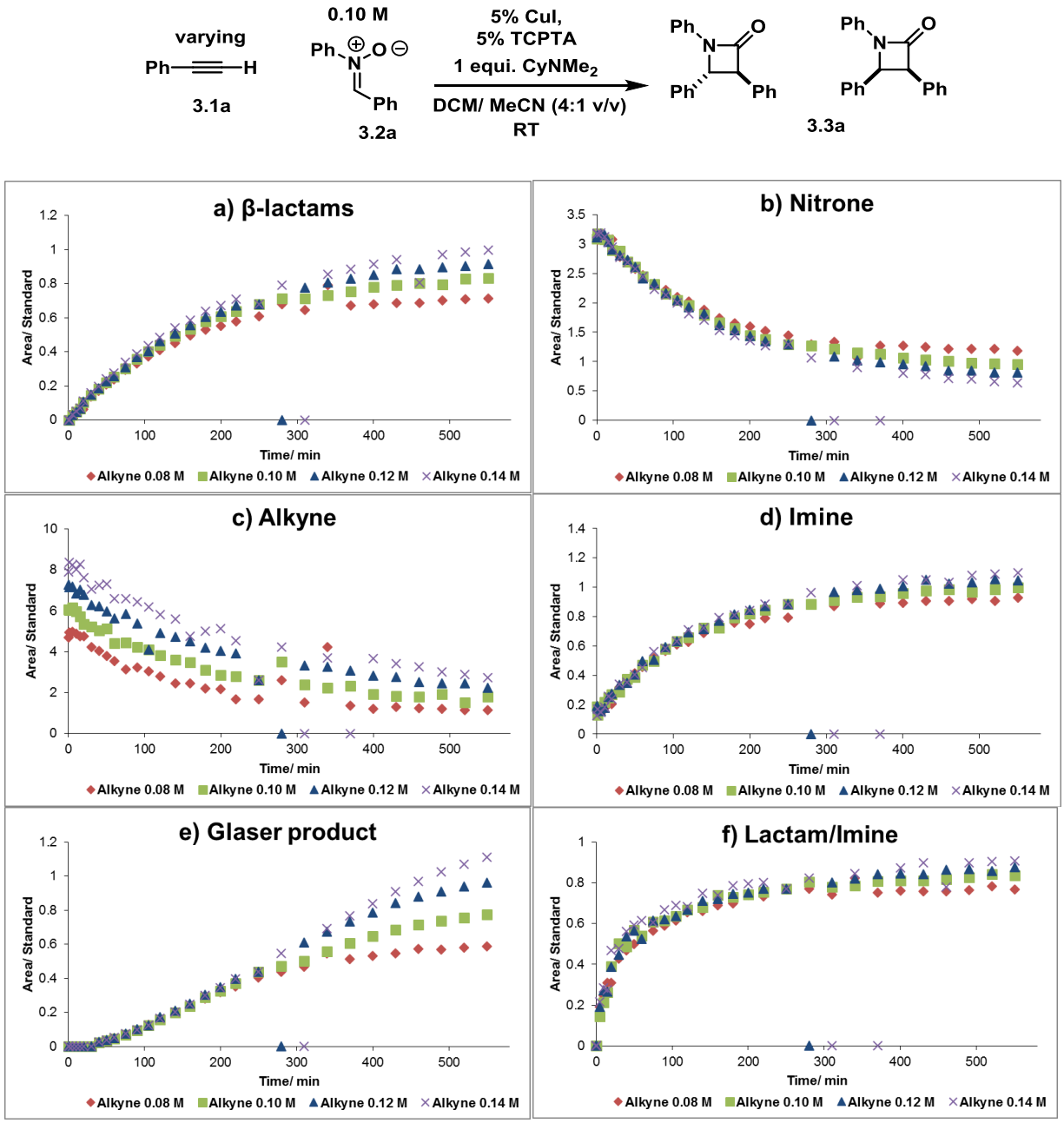

Figure 3.4: Varying alkyne concentration – monitoring by HPLC-MS

The discrepancy between the calorimetry experiments' result of zero-order in alkyne and the HPLC experiments' positive-order in alkyne can be explained. It is possible that the heat generated observed by calorimetry mainly corresponds to the reactions with the nitrone or Glaser coupling or copper phenylacetylide formation, or another process that does not involve forming

β-lactam. Notably, only the reaction progress of the Glaser coupling product (Figure 3.4, graph e) for the first 250 minutes appears to be extremely similar in the HPLC experiments, which may correspond to the nearly identical heat-flow traces in Figure 3.3). However, the two sets of reactions were done under different conditions, so they may not be a one-to-one comparison.

Copper phenylacetylide was often seen forming as a slurry of yellow precipitates. Since the formation of precipitates is exothermic, this is the most likely source of the observed heat. This would not directly explain why there is more heat generated for increased initial nitrone concentration (Figure 3.1), unless increased copper phenylacetylide formation is linked to higher nitrone concentrations. Potentially, deoxygenation of the nitrone could also explain the heat increase, catalyzed by copper.

A reaction was monitored by calorimetry and separately by sampling on the benchtop (Figure 3.5). At least for some copper catalysts, the shape of the heat curve is unusual, and it does not clearly correspond to any trends found by HPLC-MS. Perhaps calorimetry tracks β-lactam formation only if the reaction is completely homogenous at all times. This served as an example where calorimetry does not necessarily track only the heat-flow stemming from the formation of the desired product. While it may be questioned whether HPLC-MS or the quenching process somehow misconstrues the concentrations, higher conversions by HPLC-MS were backed by higher conversion by ^{1}H-NMR as well.

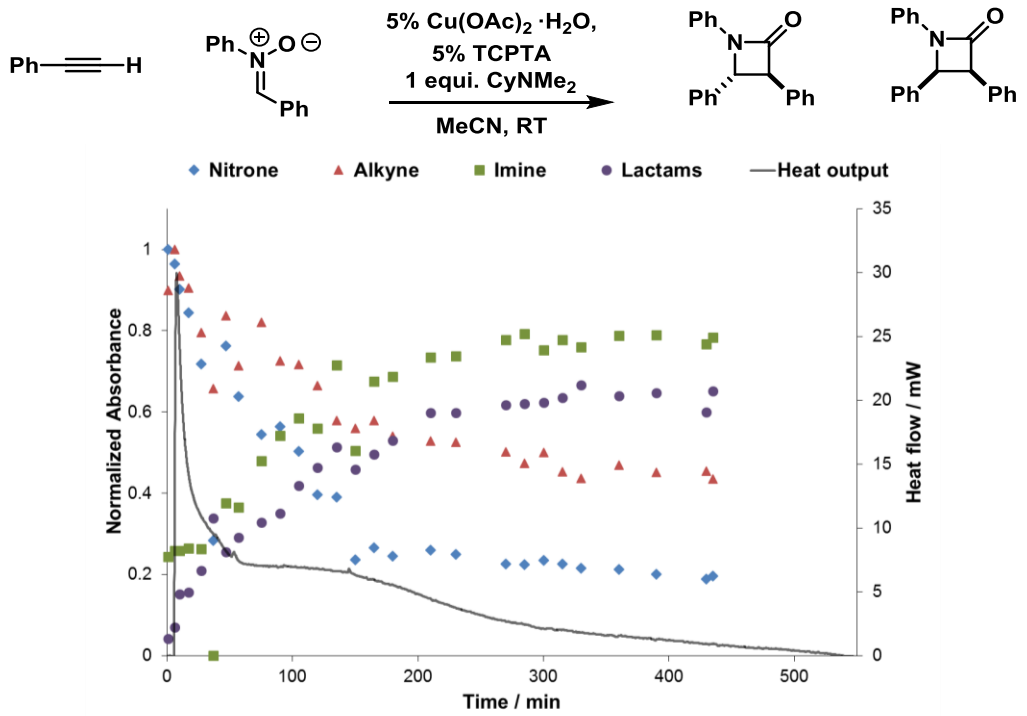

Figure 3.5: Heat-flow calorimetry overlaid with HPLC-MS

Further studies were solely conducted by manual sampling and analysis for HPLC-MS, with the exception of two sets of experiments, as will be discussed later. At the time, there was no robotic liquid handler available in the lab until most of the experiments had already been conducted. Although the analytical technique was more tedious, HPLC-MS appeared to be the most appropriate tool at the time because more information could be gleamed. Multiple experiments can be run simultaneously, unlike with some in situ techniques like ReactIR. Figure 3.6 shows a single experiment to allow comparison of the kinetic profiles of individual components. Aside from the β-lactam concentration increasing, the Glaser side-product **3.10a** and imine side-product **3.9a** (from nitrone **3.2a**) are also formed in relatively large quantities, which reaffirms observations made by other groups.

Although the imine **3.9a** appears to be present from the first time point, this is an artifact of the analytical method, not the reaction itself. The acidic buffer for HPLC-MS causes the

nitrone to hydrolyze; hence, the second graph shifts the concentration of imine to zero for a more logical comparison. The imine formation curve's shape is not unlike that of the β-lactam formation. Suspecting that the two processes were linked, more experiments were executed to test this idea. There could be at least two possibilities about the kinetic profile of the imine: it continuously forms from deoxygenation of nitrone **3.2a** in the background, and therefore is only dependent on the concentration of the nitrone, or it is linked to the concentration of another compound.

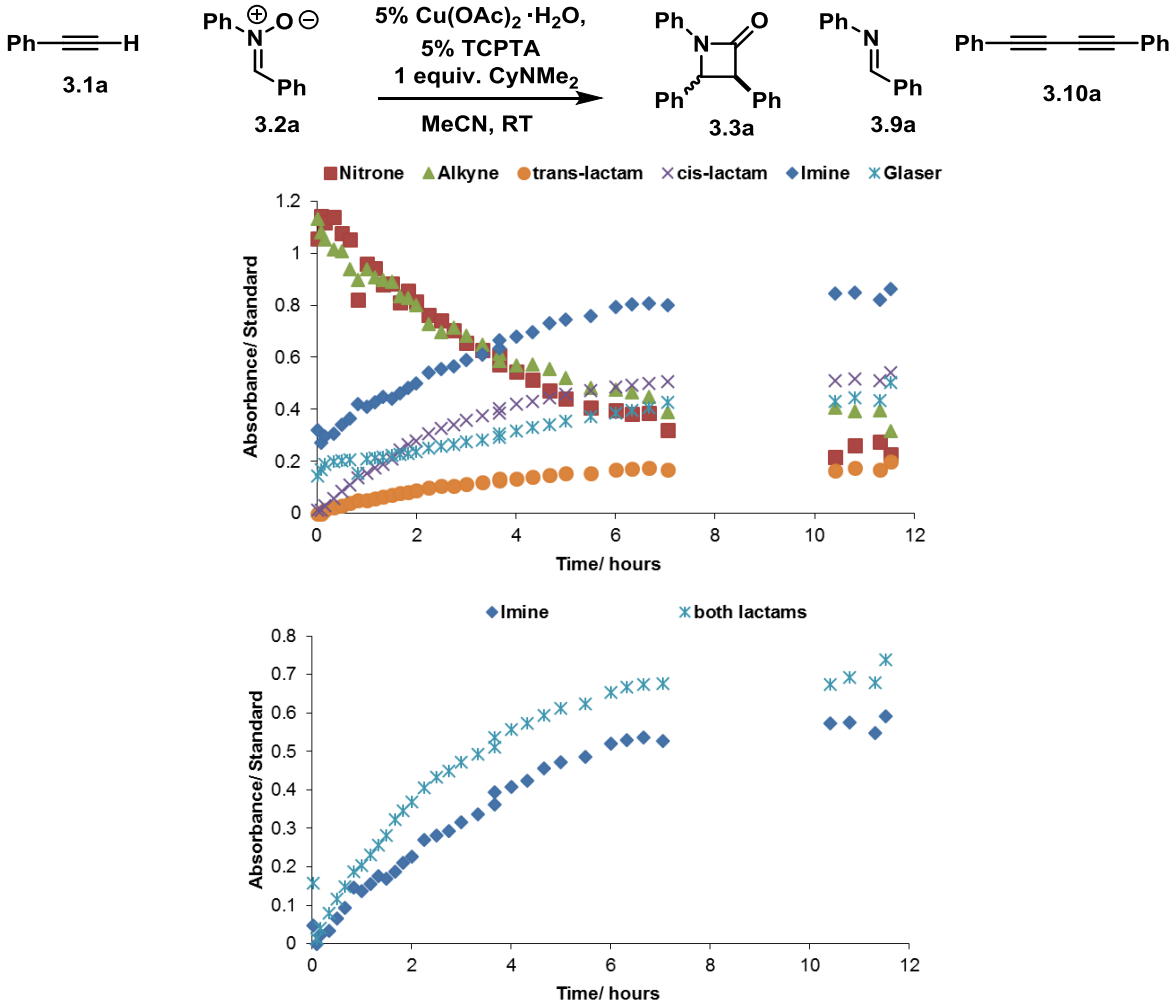

Figure 3.6: Example of reaction monitoring of the Kinugasa reaction by HPLC-MS

An experiment was done where the alkyne was added in small doses, limiting turnover of the catalytic cycle until fresh alkyne is added, if the alkyne concentration has been depleted. This was done to assess whether the nitrone deoxygenation occurred in the background regardless of catalyst turnover, or if it only occurred as β-lactam product was formed. When the alkyne **3.1a** has been depleted, causing lack of turnover to the β-lactam product, it can be seen that deoxygenation of the nitrone **3.2a** is relatively small (Figure 3.7). When fresh alkyne is added, the rate of imine formation **3.9a** increases drastically, mirroring the β-lactam formation. This experiment suggests that imine formation only happens as the catalyst turns over to yield β-lactam, and hardly forms until a certain intermediate in the catalytic cycle is present. This may suggest that both the β-lactam and imine come from a common intermediate.

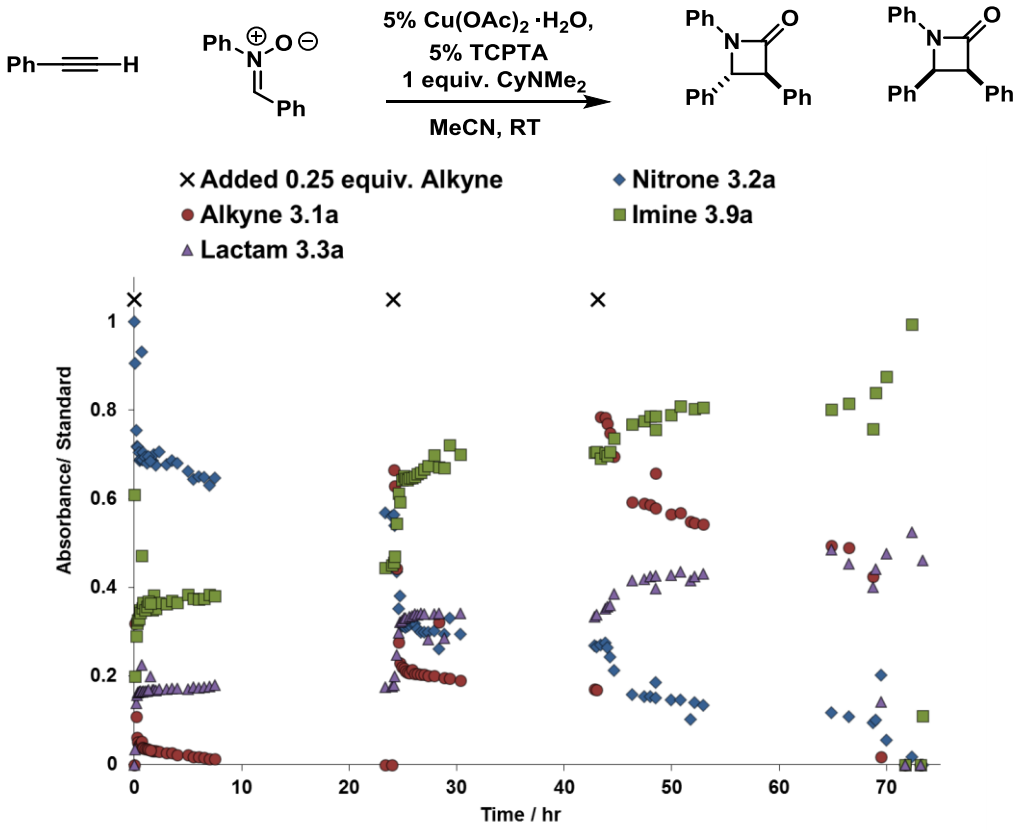

Figure 3.7: Segmented dosing of alkyne into the Kinugasa reaction

With this information in mind, we varied other parameters of the reaction more systematically. The initial concentrations of alkyne, nitrone, and base were varied independently. The set of alkyne and nitrone experiments had already been mentioned above.

To assess the order in base, dimethylcyclohexylamine was chosen as the amine to vary (Figure 3.8). For the first five hours, it appears that the rate of β-lactam formation is slower with increased base (graph a). However, later in the reaction, the yield of the β-lactam increases for more base. While reactions with less base start to equilibrate and stop forming additional β-lactam, reactions with more initial base are still dynamic and forming product. The addition of more base could increase the amount of copper phenylacetylide complexes to form, restricting the amount of available phenylacetylene. Because this process is reversible, the rate of β-lactam formation can be slow but can reach higher concentrations with time.

Notably, across the reactions, the β-lactam product does not equilibrate to the same concentration with time (graph a). More added amine does allow more of the desired product to form. This can be explained by looking at the amount of β-lactam formation relative to imine (graph f). With less base, more imine is formed throughout the course of the reaction, and less β-lactam is formed (graph b). Correspondingly, the ratio of β-lactam : imine increases over time and reaches a higher level for higher amine concentration (graph f).

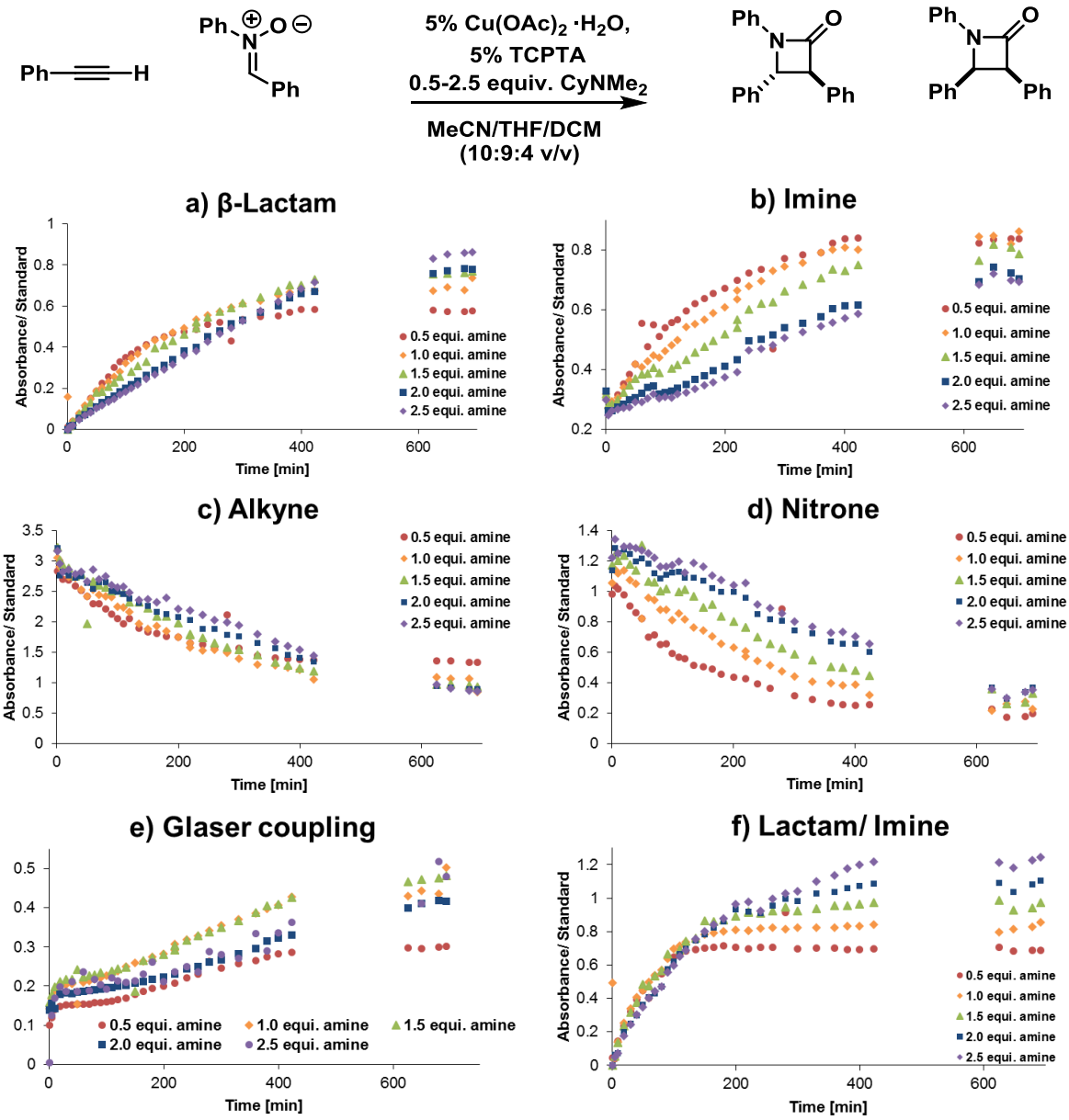

Figure 3.8: Varying amine concentration in the Kinugasa reaction, monitored by HPLC-MS

Complementary to varying the amount of base, acid was added to check if an extraneous proton source was detrimental. Indeed, the addition of trifluoroacetic acid (TFA) at 45 minutes causes a rapid increase in imine formation, stunting the amount of β-lactam (Figure 3.9). Overall, the amount of desired product is depressed by about 30% relative to no added TFA. Conducted

in tandem was an experiment where the nitrone was added late into the reaction, 120 minutes after everything else was added (Figure 3.9). This was done to allow copper acetylide complexes to build up to check if a high concentration of copper phenylacetylide initially was harmful to the reaction. The build-up of copper phenylacetylide seemed to have no bearing on the amount of lactam or imine formed. This suggests that having "too little" or "too much" base, alkyne, or active copper acetylide – which we might think is ready to couple to an electrophile – is not detrimental to the reaction.

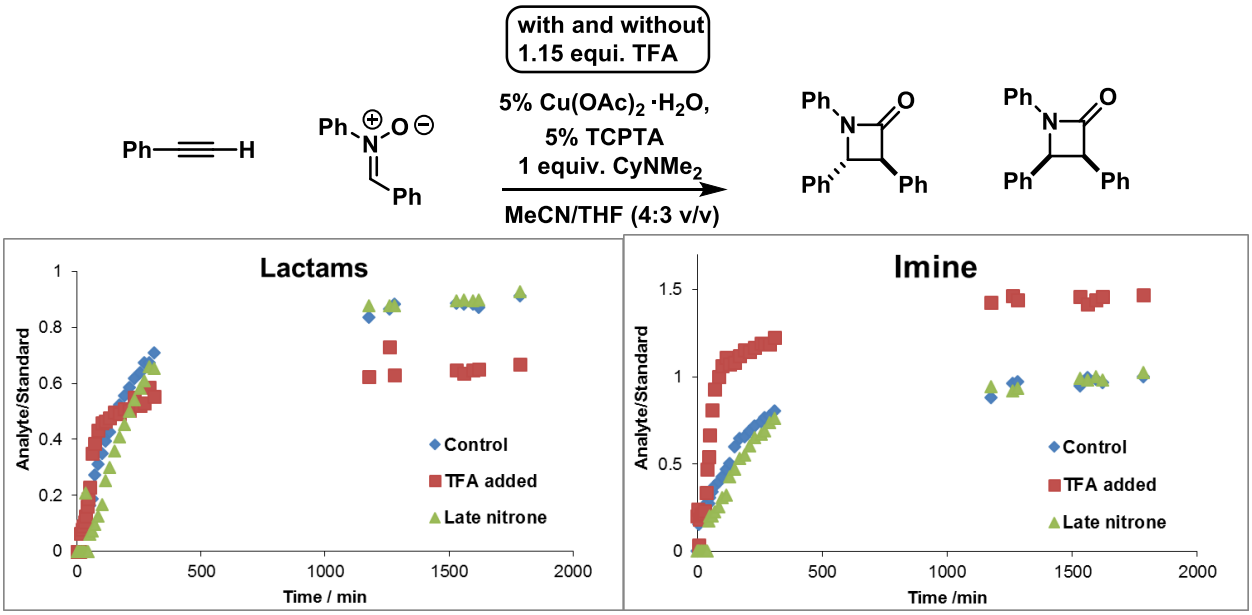

Figure 3.9: The addition of acid to the Kinugasa reaction versus an initial build-up of copper phenylacetylide

Even though the increased presence of alkyne and/or copper phenylacetylide did not seem to be detrimental, an experiment using a gradual addition of alkyne was done (Figure 3.10). The rate of product formation is expectedly slower, and the yield of β-lactam is slightly higher, but not to a large degree. The opposite experiment was also conducted, with a slow addition of the nitrone. It was thought that any nitrone that was not currently participating in the catalytic

cycle could deoxygenate; limiting the amount of free nitrone was thought to decrease the amount of imine formation. However, this only made for a sluggish reaction that eventually yielded even less product. This commonly used trick in process chemistry did not "fix" the reaction.

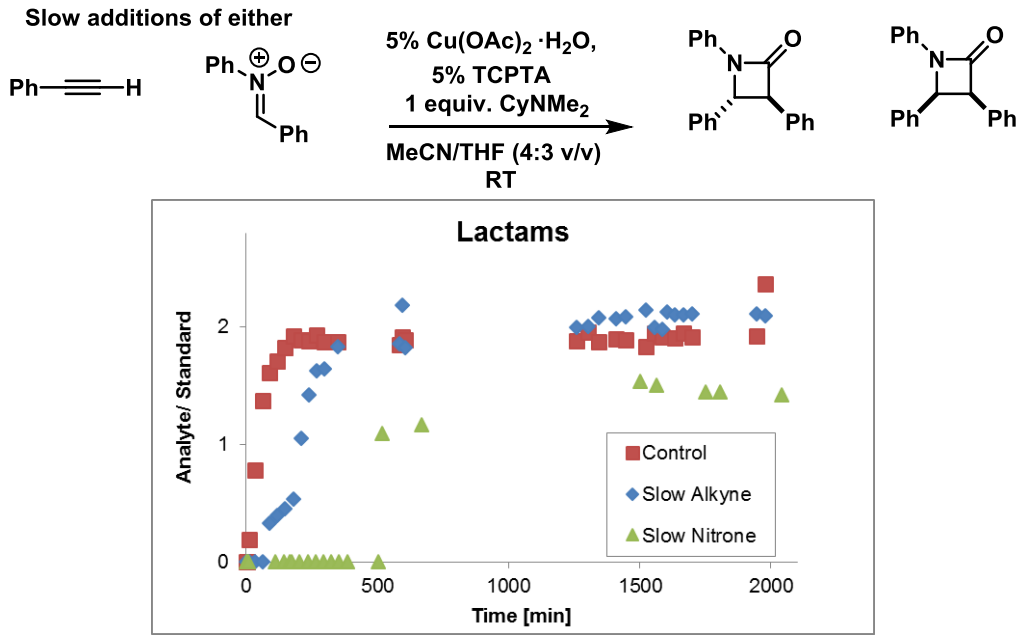

Figure 3.10: Slow additions of nitrone or alkyne into the Kinugasa reaction

It was hoped that combining all the factors that increased the yield of β-lactam into one experiment would improve its yield. However, although the combined excess base (up to four equivalents) and excess alkyne (up to two equivalents) did increase conversion to β-lactam, the yields were still poor to moderate. The only reagent that was seen to have a definitive negative effect was acid, and yet, a large surplus in base did not completely absolve the problem. Imine formation occurred regardless – it merely decreased from being the major side-product to a moderate side-product. Using the same reagents, it seemed that changing the ratios and operational procedure (slow or dosed additions, etc) could positively impact the reaction, but only up to a certain threshold.

3.3 Attempted optimization of the Kinugasa reaction through screening

With the knowledge gleaned from the previous experiments, it was decided to vary more components of the reaction by screening different reagents, one variable at a time. Hence, independent screens varying the copper catalyst, ligand, and solvent were done. While it was understood that changing one parameter could also be effectively a change in a second parameters (e.g., adding more amine base could also be effectively adding more ligand), there would still be more data to work with. In addition, poor or negative results could potentially be informative.

A set of standard conditions for comparisons was chosen based on previous studies, knowing that excess base and excess alkyne were helpful (Scheme 3.12). Reactions were run for two days, at which point they had certainly equilibrated. They were analyzed by HPLC-MS at a few time points until the reaction stopped changing, at which point they were concentrated and stripped of copper catalyst by neutral alumina. The crude mixture was then analyzed by ^{1}H-NMR spectroscopic analysis.

Although analysis based on a single point by NMR in the reaction can lead to incorrect conclusions, it seemed the most efficient method of analysis based on the volume of reactions conducted. The ratios of imine / aldehyde / lactam were calculated, and any leftover nitrone was also noted if the reaction did not go to full conversion of the nitrone. In the chloroform solvent used for NMR analysis, the two β-lactam diastereomers converted into the *cis* isomer. The NMR ratio of the lactam product versus the sum of the imine and aldehyde side products are provided for reactions with complete or high conversion of nitrone. Analysis by a few time points by HPLC-MS allowed some characterization of any unknown compounds, as well as a rough

indicator of any Glaser coupling product, since it did not have distinct proton signals by ^{1}H-NMR. Some of the more important screens are included in this thesis.

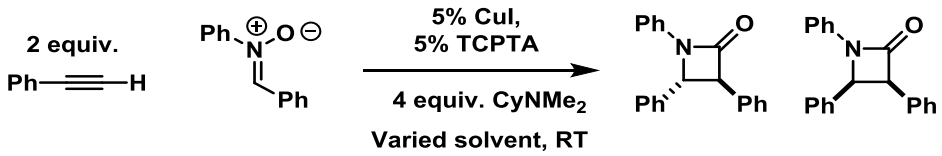

Scheme 3.12: Control reaction for screening experiments

In the tables in the following screening experiments, the NMR ratio of β-lactam to the side products, imine and aldehyde, is provided to give a rough measure of chemoselectivity for the desired product vs side products (excluding the Glaser coupling product). Because the aldehyde comes from the breakdown of the imine, it is grouped with the imine instead of being listed as a separate entity.

3.3.1 Copper(I) salts for the Kinugasa reaction

Different copper salts were premixed with the same TCPTA ligand solution at room temperature (Table 3.2). Although previous literature had suggested that copper(II) salts were observed to be better for the reaction, we did not have the same observation with the formerly used $Cu(OAc)_2$ salt.[79] Under these control conditions, copper(I) salts generally provided better results. Copper(I) bromide (Entry 3) gave the best result, closely followed by copper(I) iodide (Entry 1). Since there did not seem to be a significant difference, most experiments still utilized copper(I) iodide to allow for more direct comparisons with other experiments. Interestingly, increasing the copper and ligand loading to 10% each did not have a positive effect, but gave a decreased yield (Entry 2).

For entry 4 using $CuOAc(PPh_3)_2$, there was no conversion seen at all. Miura and coworkers found that using P-ligands caused the reaction to gravitate toward the propargylic

amine side product **11**, whereas the N-ligands favored the β-lactam product **3**.[84] While our studies did not include quantification of the propargylic amine (as it never seemed to appear), this observation may suggest that it is difficult to find appropriate phosphine ligands that allow the formation of an active copper catalyst. Most published asymmetric studies appear to use *N,N* or *N,O* type ligands.

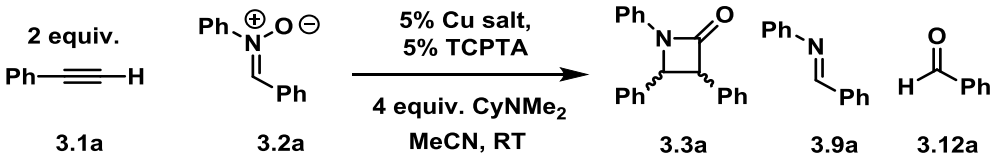

3.1a 3.2a 3.3a 3.9a 3.12a

Entry	Copper catalyst (5 mol %)	Lactam/(Imine + Aldehyde)[a]
1	CuI	0.76
2	10% CuI and ligand	0.50
3	CuBr	0.89
4	$CuOAc(PPh_3)_2$	--
5	$Cu(MeCN)_4\ PF_6$	0.34
6	$Cu(MeCN)_4 BF_4$	0.33
7	5% CuI, 5% $Cu(OAc)_2$, 10% ligand	0.60

[a]calculated by ^{1}H-NMR spectroscopic analysis

Table 3.2: Screen of copper(I) catalysts

3.3.2 Screen of ligands for the Kinugasa reaction

For the copper source of CuI, ligands were varied (Table 3.3). It was questioned whether ligand choice would even have much of an effect, since there was so much excess amine base added that could also potentially act as a ligand. When a control reaction was run with no ligand added, the reaction was radically different: plentiful aggregates of copper phenylacetylides persisted for days and never yielded any β-lactam product (entry 14). Clearly, an added ligand was necessary, and simply adding an amine base was insufficient.

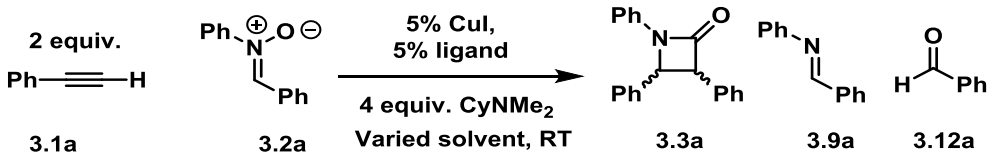

Entry	Ligand (5 mol %)	3.3a/(3.9a + 3.12a)[c]
1	TCPTA	0.68
2	TCPTA (10%)	0.66
3	**TBTA**	1.12[a]
4	1,10-phenanthroline	0.87[a]
5	bipy	1.37[a]
6	4,4′-di-*tert*-butyl-2,2′-dipyridyl	0.78
7	**Imine 1**	1.16[a]
8	**Indabox 1**	0.56
9	*trans*-1,2-diaminocyclohexane	0.42
10	**Imine 2**	-- [b]
11	BINOL (racemic)	0.98
12	BINOL (9%)	0.77
13	6% BINOL (6% CuI, added in two portions)	0.88
14	none	0

[a] used 3.3 equivalents of alkyne instead of 2 equivalents
[b] imine proton peak overlapped with that of the ligand
[c] calculated by ^{1}H-NMR spectroscopic analysis

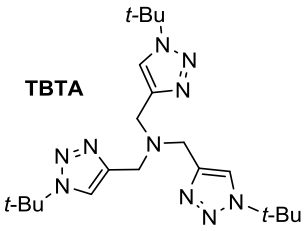

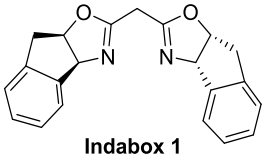

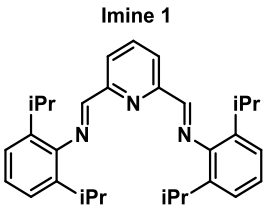

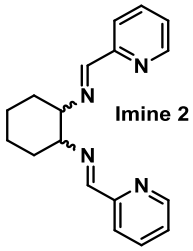

Table 3.3: Ligand screen with CuI catalyst

It is recognized that there are various combinations of copper salt sources (other than CuI) and ligands that could potentially be a magic hit, but such comprehensive cross screens were avoided. The result with our usual polydentate, tris(cyclopentyltriazolyl)amine ligand,

TCPTA, was decided as a baseline, with its lactam/byproduct ratio of 0.68 (Table 3.3, entry 1). Doubling the ligand loading of TCPTA had minimal effect, possibly suggesting that the copper catalyst was already saturated with ligand, or at least that adding excess TCPTA ligand did not suppress byproduct formation or prevent aggregation of copper phenylacetylides (entry 2).

Unfortunately, because some of the experiments utilized more alkyne than others, the comparisons were more difficult to make – all experiments with more alkyne fared better. Of the ligands screened, *trans*-1,2-diaminocyclohexane, with its free amino groups, provided the lowest yield (entry 9). Bidentate, pyrindyl ligands allowed a small increase in selectivity (entries 4, 5, 6). The racemic BINOL ligand, which had been predicted to be too strongly binding, surprisingly gave slightly higher results (entry 11). Interestingly, increasing the amount of the BINOL ligand slightly actually decreased the ratio of desired product to side-products (entry 12). Perhaps the increased amount of BINOL restricted the activity of the copper catalyst, or the acidity of the ligand was detrimental to the reaction overall, as it had been found that added acid suppresses the desirable reaction. No particular ligand or class of ligand was observed to be significantly better or worse than the one used in most of the control reactions, TCPTA. Unfortunately, this set of experiments did not elucidate what type of ligand was best.

3.3.3 Solvent screen for the Kinugasa reaction

It was assumed that the choice of solvents would have a major impact on the reaction, partially because the moderate polarity of the nitrone **3.2a** made it difficult to dissolve in nonpolar solvents. While it is often viewed as counterintuitive to have a solvent that only dissolves a modest amount of a substrate, it was hypothesized that an antisolvent could effectively allow a slow addition of the nitrone into the reaction. This could avoid dissolving the

nitrone in a stock solution which could cause decomposition with time, or trying to optimize a flow rate from a syringe pump. A slow dosing of partially dissolved nitrone into the solution phase could potentially allow for less deoxygenation to occur if the catalytic cycle only occurred in the solution phase. Some solvent conditions included mixtures of solvent and antisolvent for full or partial dissolution of the nitrone, and potentially the catalyst mixture as well. Different solvents could also potentially break up aggregates of phenylacetylide, depress or encourage Glaser coupling, or have a multitude of other unforeseen effects. Because some of these reactions went to low conversion, the ratio of nitrone to lactam is also included in the table.

When dichloromethane was used as solvent for the standard substrates, the Kinugasa reaction was homogenous (Table 3.4). Antisolvent mixtures were used with DCM as the dissolver. If only the ratio of lactam to the byproducts was considered, etheral solvents such as THF and diethyl ether appeared the best (entries 2, 3, 4). However, diethylether gave poor conversion, whereas THF allowed much higher but still incomplete conversion. Hence, conversion was sacrificed for slightly better selectivity, which is in line with Tang et al.'s observations. Solvents that allowed complete conversion of the nitrone – dichloromethane and acetonitrile – gave relatively less of the desired product (entries 1, 5). Aromatic solvents (toluene, xylenes) decreased the yield and also did not allow for high conversion (entries 6, 11). Notably, all of the solvent mixtures gave less than 50% of the β-lactam product relative to the side products, indicating that at least half of the nitrone was deoxygenating during the reaction.

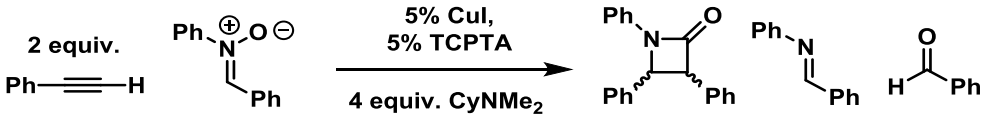

3.1a 3.2a 3.3a 3.9a 3.12a

Entry	Solvent(s)	3.3a/(3.9a + 3.12a)[a]	Leftover 3.2a/ 3.3a[a]
1	DCM	0.75	0
2	4:1 diethylether: DCM	0.99	5.15
3	4:1 THF: DCM	0.96	0.29
4	4:1 MTBE: DCM	0.65	4.04
5	4:1 MeCN: DCM	0.65	0
6	4:1 xylenes: DCM	0.44	1.61
7	4:1 isopropanol : DCM	0.57	
8	4:1 hexanes:DCM; added 10% MeCN by volume later	0.59	
9	1:1 DCM: hexanes	0.50	
10	water, then 1:1 water: DCM	0.29	
11	toluene	0.40	

[a] calculated by ^{1}H-NMR spectroscopic analysis

Table 3.4: Solvent screen

Water was used as a solvent because of previous "on-water" reports that promised good yields.[91,92] Unfortunately, with our choice of substrates, the reaction run in water did not fare well (entry 10). This suggests that the reaction occurs in the homogenous phase, not necessarily at the interface of water and the organic solvent.

3.3.4 Screening the choice of amine base

The choice of amine base was the parameter with the most dramatic effect on the reaction, given the same substrates (Table 3.5). Previously, it had been known that tertiary and secondary amines were most commonly used in the Kinugasa reaction.[82] Primary amines were known to provide low yields, diastereoselectivities, and enantioselectivities when a chiral ligand was used. Secondary amines had been known to give slightly better yields and diastereoselectivities than tertiary amines.[85] There had also been a report that inorganic bases such as potassium carbonate worked well.[84]

Although a few carbonate bases were attempted with our conditions, the conversions were extremely low, likely due to poor solubility (Entries 12, 13). In our lab, weak, aromatic bases such as aniline, pyridine, and 2,6-lutidine (8, 9, 10) were slow and inefficient. Most tertiary amines gave the yields we had come to expect from the substrates, with the exception of *N*-methylmorpholine, which reduced yields in half (entry 7).

Secondary amines had mixed results. Pyrrolidine and morpholine had extremely detrimental results, resulting in rapidly darkening mixtures and no β-lactam formation (Entries 5, 6). In each case, an unidentified byproduct was produced in much higher proportions than any of the familiar byproducts or β-lactam.

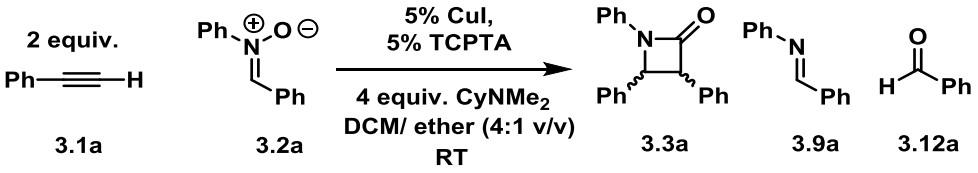

3.1a 3.2a 3.3a 3.9a 3.12a

Entry	Base	3.3a/(3.9a + 3.12a)[c]
1	dimethylhexylamine[a]	0.65, 0.75
2	triethylamine	0.66
3	*N*-methylmorpholine	0.30
4	diisopropylamine[a] (DIPA)	1.05, 0.87
5	pyrrolidine	trace
6	morpholine	trace
7	DBU	--
8	pyridine	0.22
9	2,6-lutidine	0.25
10	aniline	0
11	1,1,3,3-tetramethylguanidine	0.12
12	K_2CO_3[b]	trace
13	Na_2CO_3[b]	trace

[a] attempted twice; [b] conditions used CuBr and bipy instead
[c] calculated by ^{1}H-NMR spectroscopic analysis

Table 3.5: Base screen for the Kinugasa reaction

Another secondary amine, DIPA, seemed to give a relatively high yield of β-lactam and allowed full conversion of the nitrone. Surprisingly, DIPA gave a new byproduct forming in about 20% higher yield than the β-lactam (Entry 4). A new UV active peak (**Unknown 1**) was also observed with a mass of 220 $(M+H)^+$. The NMR spectra showed that remaining DIPA had been removed (possibly from rotary evaporation before NMR), and had been replaced by two doublets at 1.0 ppm and 1.5 ppm, and two quartets at 3.5 ppm and 4.0 ppm (Figure 3.11). It was assumed that DIPA had reacted and formed a new compound that either broke the symmetry of the isopropyl groups, or had hindered rotation in chloroform.

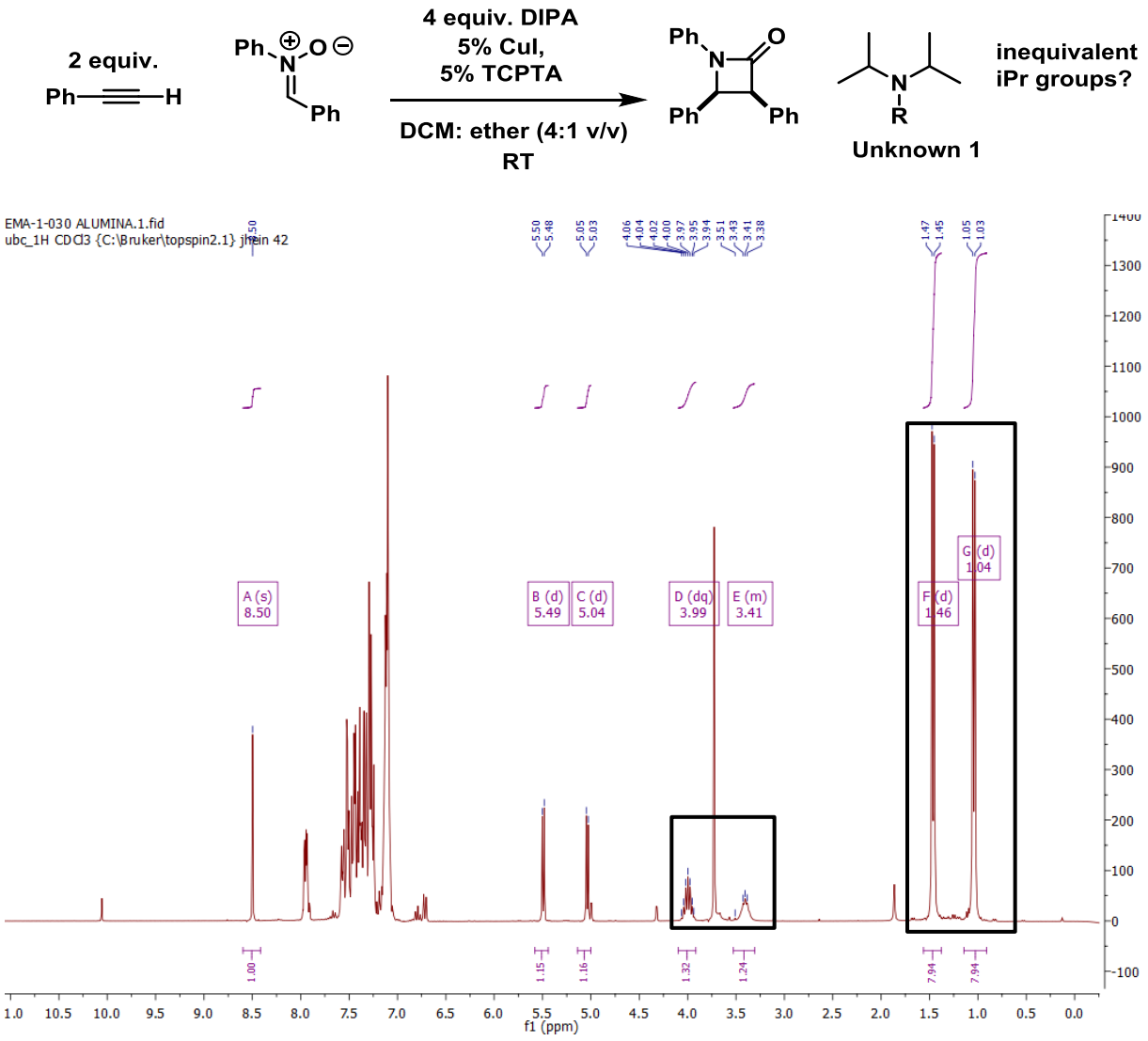

Figure 3.11: Unknown compound detected by ^{1}H-NMR

A short screen was conducted to see if crossing a few ligands in combination with DIPA as the base would once again improve selectivity for the β-lactam (Table 3.6). The highest conversion was with still with the ligand done for most model studies, TCPTA. Unfortunately, the selectivity of 1.56 to 1 for lactam vs the nitrone side-products only gives a conversion of 60.9% of the nitrone to β-lactam. In case a high excess in amine base would improve matters, a

solvent mixture of DIPA and DCM was used in one attempt (entry 2). Such an excess of DIPA caused the selectivity for the lactam to lessen, not increase.

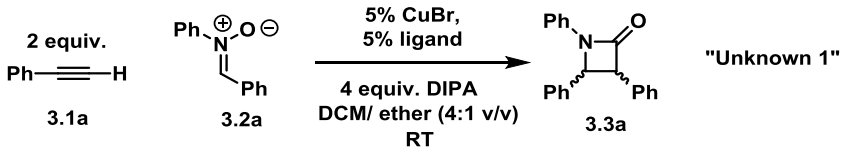

Entry	Ligand	3.3a/(3.9a + 3.12a)[b]	Unknown 1/ 3.3a[b]
1	TCPTA	1.56	1.45
2	TCPTA[a]	1.00	1.12
3	TBTA	1.36	1.28
4	bipyridine	1.26	1.21
5	4,4′-di-tert-butyl-2,2′-dipyridyl	0.88	0.90

[a] 11.5 : 1 v/v DIPA: DCM
[b] calculated by ^{1}H-NMR spectroscopic analysis

Table 3.6: Short ligand screen using DIPA base

3.3.5 Kinetic profiling of the Kinugasa reaction with different amines

Aiming to obtain more detailed information for the effects of each base, we monitored the reaction by manual sampling and subsequent analysis by HPLC-MS, once again using the BCA solution to quench reaction aliquots. The bases $CyNMe_2$ (for comparison), DIPA, and pyrollidine (because it a peculiar result) were chosen to be used in the reactions to be monitored.

In contrast with a reaction utilizing pyrollidine, which yields very little β-lactam, the kinetic profile is drastically different but still informative (Figure 3.12). Some β-lactam product is formed initially, but it is then transformed into something else. The nitrone is depleted almost immediately with a high rate of deoxygenation to become the imine. Surprisingly, it appears that some of the imine is also consumed. To account for their loss, at least three new products increase suddenly. All of this happens within seven hours and little changes afterward; even Glaser coupling stops. The Glaser coupling product is also formed very quickly and in much

higher concentrations than with other bases, but stops after around 400 minutes. Although the catalyst is able to form β-lactam at first in the presence of pyrollidine, after a certain point, the reaction appears to change direction, and the side-product formation takes over. Without identifying the side-products, it is difficult to determine why pyrollidine has such an effect.

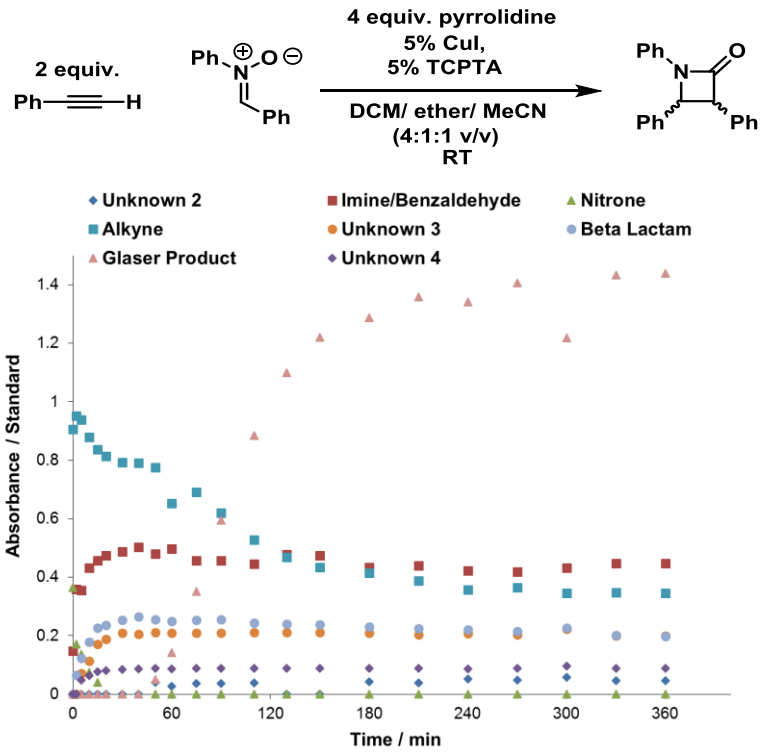

Figure 3.12: Kinetic profiling with pyrrolidine, monitored by HPLC-MS

The reaction run with DIPA can be compared to the reaction with $CyNMe_2$, for which no unidentified major side-product formed. The profiles of the substrates and products are graphed for comparison in Figure 3.13. The reactions with DIPA and $CyNMe_2$ have nearly identical imine formation profiles, showing that imine formation is not suppressed by the formation of **Unknown 1.** The profiles of nitrone consumption and lactam formation are not the same. Rather, it seems that the nitrone is consumed more quickly, going toward forming the desired β-lactam product when DIPA is used as a base. Although the byproduct formation of **Unknown 1** does not

suppress the deoxygenation of the nitrone, it does allow more of the nitrone to be converted into β-lactam.

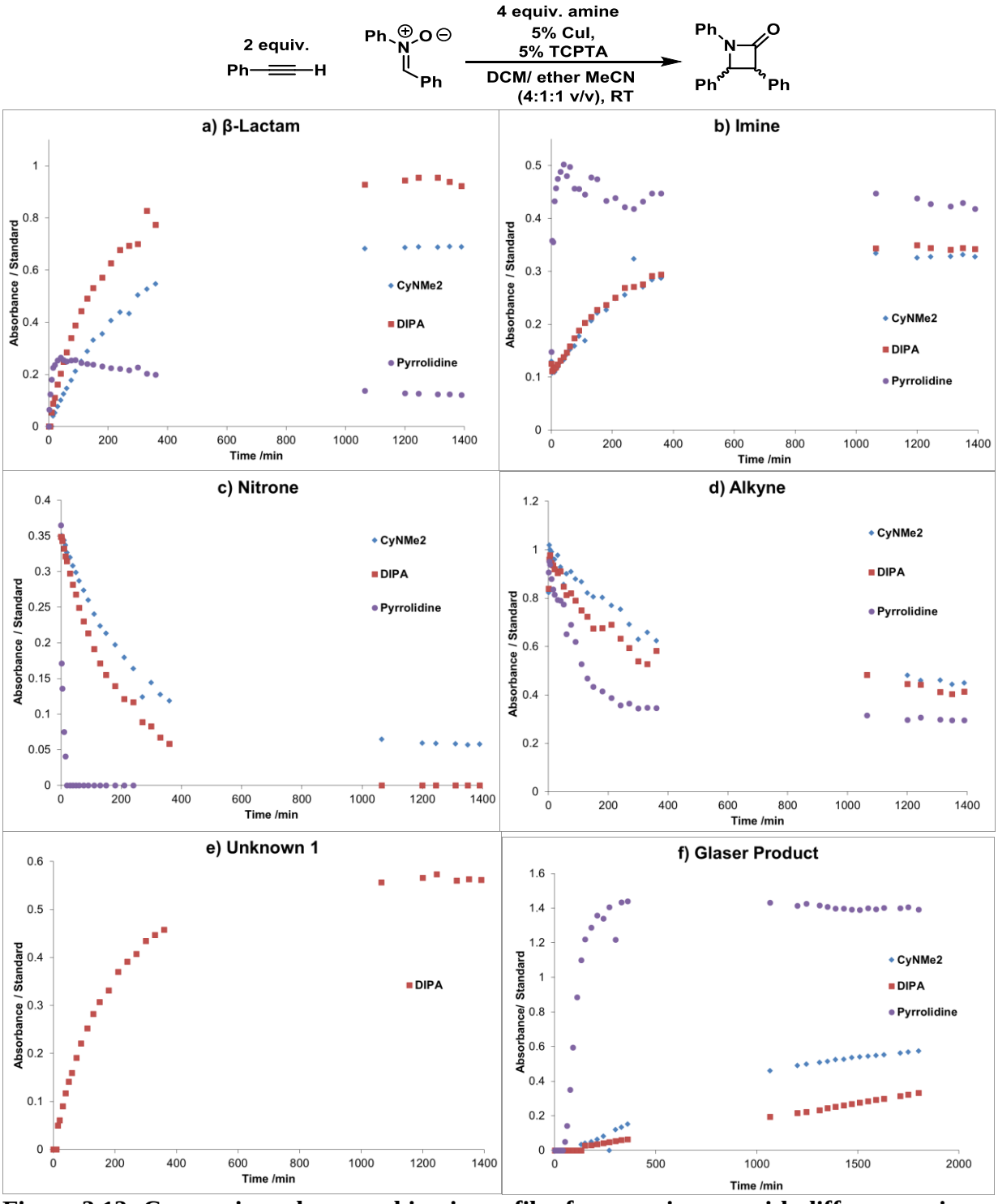

Figure 3.13: Comparisons between kinetic profiles for experiments with different amines

We propose that a common intermediate is formed that leads to either β-lactam or **Unknown 1** in the presence of a suitable nucleophile – which can be DIPA in our previous experiments. If the intermediate is made but cannot rearrange quickly to the β-lactam, it may be possible that it is too unstable, it may be that more imine is formed instead. While this was supported by single-point analysis from the previous screens, the kinetic profiles for imine formation do not support this hypothesis. The imine formation trends appear nearly the same for DIPA and $CyNMe_2$ at first look. However, the nitrone is consumed for reactions that formed **Unknown 1**, whereas for $CyNMe_2$, the nitrone is never fully consumed. Therefore, the ratio of consumed nitrone to side product imine is higher when DIPA is used. Correspondingly, the ratio of β-lactam to imine is also higher when DIPA is used as the base. Hence, when DIPA is used, the selectivity of β-lactam over imine is higher than when $CyNMe_2$ is used.

3.4 Identification of a side product stemming from a common intermediate

After running a Kinugasa reaction on a larger scale, **Unknown 1** was isolated by column chromatography and identified as the amide formed from oxidation of the alkyne and diisopropylamine (**Amide 3.1**, Scheme 3.13).

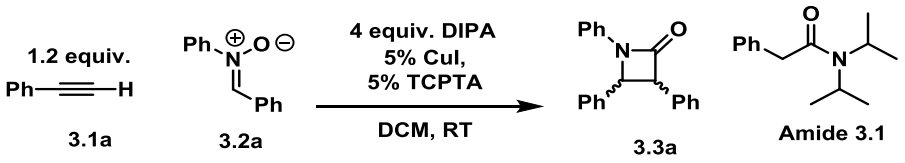

Scheme 3.13 Unknown 1 is identified as Amide 1

The formation of both β-lactam and amide support the hypothesis that a common intermediate formed in the catalytic cycle branches into two products. This common intermediate is probably isoxazole-like **3.5a** and can undergo at least two pathways (Scheme 3.14). As

mentioned before, there is still debate as to which transient intermediates are present to form the β-lactam: either a retrocycloaddition followed by a Staudinger-type pathway involving ketene **3.6a** in Pathway II, or a strained oxaziridinium **3.7a** in Pathway I. Pathway II is thought of as productive allows rearrangement to form the β-lactam **3.3a**. In Pathway II, the initial stereochemistry of β-lactam could be set by the rebinding of the copper-yneoate **3.13** and imine **3.9a**. In Pathway II, the stereochemistry would be set by the initial cycloaddition to form the common isoxazole-like intermediate **3.5a**. From the previous experiments conducted, it appears that there is support for Pathway II due to the formation of **Amide 3.1a** from ketene **3.14**. Nucleophilic attack of ketene **3.14** with a suitable nucleophile (in this case shown, DIPA) leads to **Amide 3.1a**. The formation of **Amide 3.1** and imine **3.9** support the temporary existence of intermediate **3.6**. There has been no evidence for Pathway I.

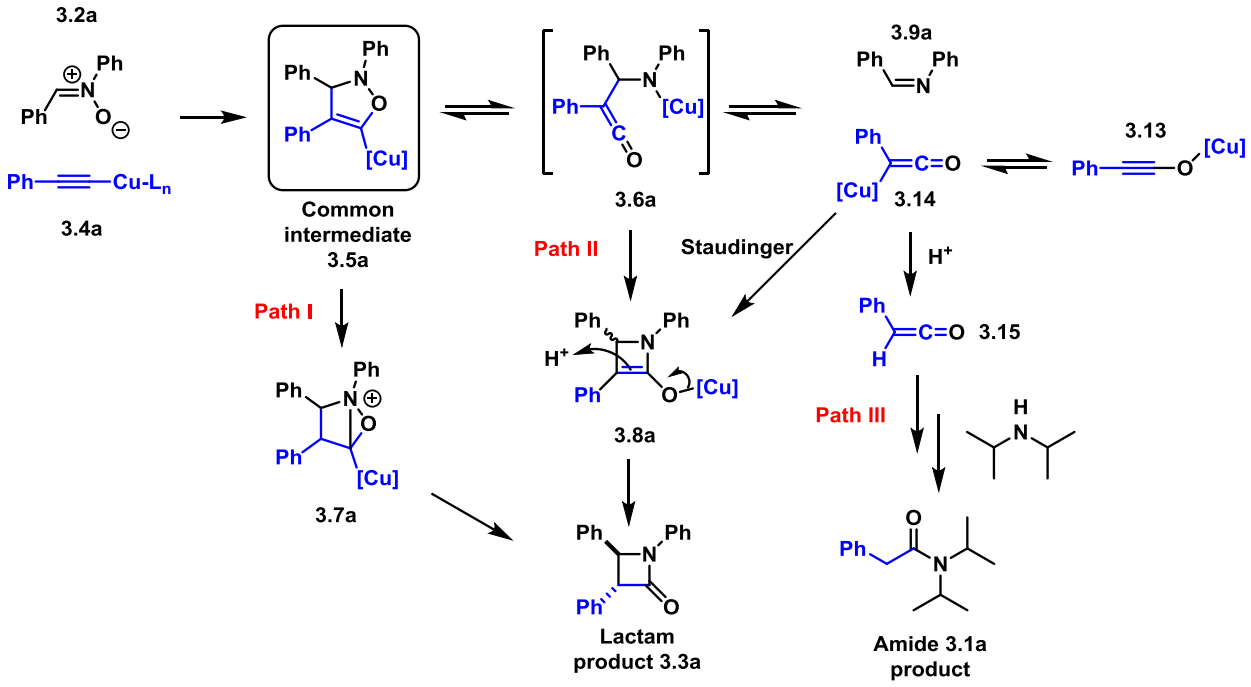

Scheme 3.14: Potential pathways to form multiple products

This amide byproduct from the Kinugasa reactions does not seem to appear more than once in the literature. It is possible that in many cases, conditions do not involve a suitable nucleophile to intercept the ketene to form the amide. Other conditions may drive the reaction toward the β-lactam instead of the amide, or may go through a different intermediate.

The one mention of the side-product in literature occurs with a multicomponent, on-water reaction starting from benzaldehyde, phenylhydroxylamine, and phenylacetylene. The amide byproduct forms from aniline as the nucleophile, generated in situ, presumably from the breakdown of the phenylhydroxylamine. The ratio of lactam to amide is as much as 45:36 in their findings. Since their aim was solely to optimize the yield of the β-lactam, they were disinterested in finding conditions that pushed the reaction toward the amide. For most of their nitrone substrates, the ratios of lactam : amide were actually parity or low, consistent with our findings that show that the amide product can be a major side product.[93]

Interestingly, varying the equivalents of alkyne from one to three did not change the ratio of amide to lactam. Although amide formation could be a competing pathway with the rearrangement to the β-lactam, the amount of alkyne is not a limiting factor. Rather, the conversion of nitrone is affected – increasing alkyne allowed for higher conversion of the nitrone to the β-lactam.

To check that other nucleophiles could lead to the same side product, different amines were added to the reaction using triethylamine as the non-nucleophilic, superfluous base (Table 3.7). Compounds with free hydroxyl groups (Entries 5, 6) yielded neither amide nor lactam products, and the reaction did not progress; it appeared that the copper catalyst had become clumpy, likely because the nucleophiles were too coordinating. A few other nucleophiles that

apparently did not bind to the copper catalyst too tightly did form both presumably amide and β-lactam products, as detected by HPLC-MS. The crude was not analyzed by NMR to give ratios.

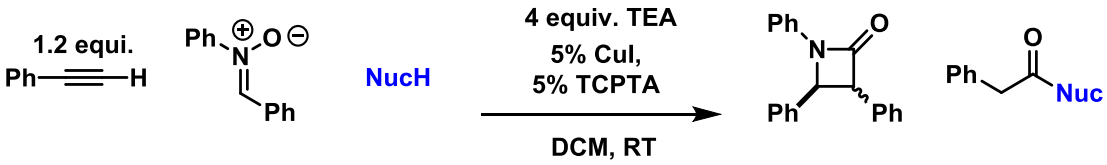

Entry	Nucleophile (Equiv. added)	Amide formation?	β-Lactam formation?
1	DIPA (4)	Yes	Yes
2	DIPEA (4)	Yes	Yes
3	$BnNH_2$ (1)	Yes	Yes
4	BnNH-OBn (1)	Yes	Yes
5	4-hydroxypyridine (1)	No	No
6	MeNHOH (1)	No	No
7	Benzenesulfonamide (1)	n/d	Yes
8	$BnONH_2$ (1)	n/d	No

Table 3.7: Short screen for formation of amide side-products, detected by HPLC-MS

3.5 Kinetic profiling by direct injection into HPLC

Developed as a tool to monitor various types of reactions, a direct injection apparatus was built for in-line analysis of a reaction by HPLC by undergraduate Henry Situ (Scheme 3.15). This apparatus allowed small samples to be automatically withdrawn from the reaction and immediately diluted and routed in-line to the HPLC column for analysis, without need of a vial or quenching solution. The data acquisition is less noisy than quenching individual samples into vials and waiting for offline analysis. In addition to no longer needing a quenching solution, an internal standard in the reaction is also unnecessary because the sample size and dilution factor are consistent. This technique would be useful for the comparison of other future experiments.

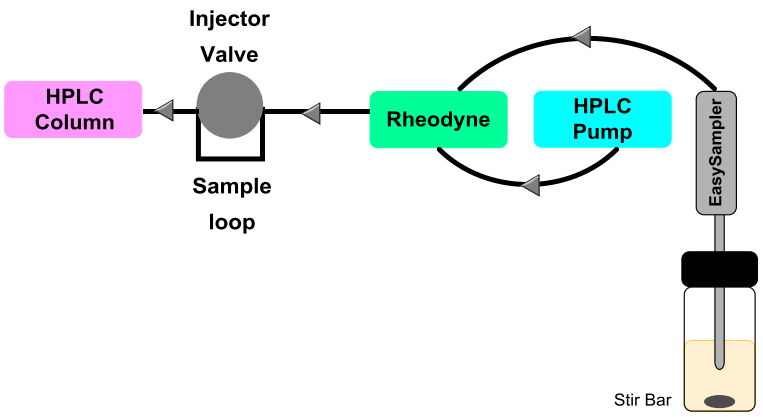

Scheme 3.15: Simplified schematic of direct injection system into the HPLC for reaction monitoring

As a test model, a homogeneous Kinugasa reaction was run (Figure 3.14). This helped validate the results created by manual sampling and quenching with BCA. The Glaser coupling in only DCM is very slow in this reaction and in low concentrations, relative to what has been seen before in mixed solvents. It may be due to a lower concentration of unreacted alkyne in this reaction.

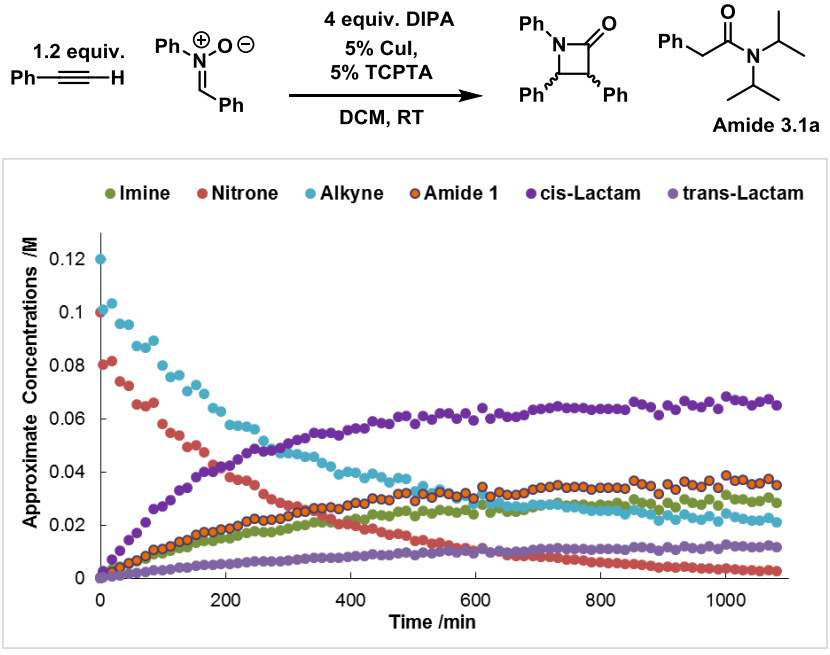

Figure 3.14: Reaction monitoring of the Kinugasa reaction via direct injection into HPLC

Even as an early prototype, it is clear that the data obtained from direct injection into the HPLC is of much higher quality than that obtained from either manual sampling or sampling with the needle of a robotic liquid handler. All the experiments in this chapter before the one in Figure 3.14 utilized manual sampling, quenching, and offline analysis, with the exception of the experiments varying the initial nitrone concentration in Figure 3.2. For the experiments varying initial nitrone concentration, samples were withdrawn by piercing through the reaction vial's septa with a needle from a robotic handler and analyzed offline. Even though this set of experiments was automated, the data quality is still rather scattered, sometimes not any better than sampling by hand (just more convenient). The automated sampling apparatus utilizing PTFE tubing (instead of a needle that repeatedly pierced the septa) and an additional syringe pump from Chapter 2 had not been created at this time.

3.6 Summary and conclusions

For our model substrates, the catalytic Kinugasa reaction was found to have positive orders in nitrone, alkyne, and amine base. Interestingly, reactions with increased base have a reduced reaction rate, but overall yield more of the desired product. Generally, increased amine allowed less imine side-product formation from the nitrone. An experiment with sequential additions of alkyne showed that deoxygenation of the nitrone to form the imine had a very slow background rate. The imine formation was actually likely coupled to the formation of the β-lactam itself. This suggested that a common intermediate is formed that leads to the β-lactam or the imine.

Through screening, there was no particular copper(I) salt and ligand combination that performed superiorly. A solvent screen that included mixed solvents and antisolvents was not particularly useful in determining new solvent choices to improve the conversion to β-lactam. While the previous screens were not as informative as desired, it was found with a base screen that the choice of base was critical in determining whether the reaction proceeded at all, and greatly affected the conversion. Tertiary and secondary amines generally performed well, with the exception of pyrollidine, which caused the reaction to go in several unproductive directions. When diisopropylamine was used as a base, a major side-product was isolated and characterized as the amide formed from the alkyne and amine with an oxygen source, presumably from the nitrone.

The discovery of the amide side-product provided further support that a common isoxazole intermediate is formed, followed by bifurcation to the β-lactam product or the amide byproduct, if there is an appropriate nucleophile available. Otherwise, the common intermediate can lead to increased imine formation.

Nearly all the experiments portrayed in this chapter using HPLC-MS as the analytical method relied on manual sampling, quenching, and subsequent delivery to the HPLC-MS for long method times (7-20 minutes per sample). This was the limited technology available at the time (2012-2013) before the lab acquired a used liquid handler. Had the automated sampling been developed at the time of most of the experiments, it still would not have been possible to monitor kinetics of multiple reactions at the same time, which shows one advantage of manual sampling. Poroshell HPLC columns also became commercially available, enabling methods with higher pressures and shorter run times.

The upgrade from the automated sampling system combined with offline analysis by HPLC-MS from Chapter 2 was upgraded into an automated sampling and injection into the HPLC-MS for online analysis. The latter invention would have made the sequential dosing of alkyne experiment in Figure 3.7 to be done more elegantly, within a reasonable time frame and much less effort. Instead of having long gaps in reaction time where no data is obtained and no new reagent is added, a programmable syringe pump and the direct injection system would have provided higher quality data within hours instead of two days.

3.7 Experimental

3.7.1 General remarks

(E)-*N*-benzylideneaniline oxide was prepared through condensation of aniline and phenylhydroxylamine in dichloromethane. Phenylhydroxylamine was prepared through the previously published procedures.[72] The TCPTA ligand was synthesized from previously published procedures from cyclopentyl azide and tripropargylamine.[94] Cyclopentyl azide was synthesized from the reaction of cyclopentyl bromide and sodium azide in DMSO.

Flash chromatography was carried out using Fisher Chemical silica gel 60 Å (230 x 400 mesh). Analytical thin-layer chromatography (TLC) was performed on Sorbtech glass pre-coated silica gel plates and was visualized with UV light. All other materials were purchased from conventional suppliers and used as received.

^{1}H-NMR spectra were recorded on Bruker or Agilent NMR spectrometers (300, 400, 500 MHz). Data for ^{1}H-NMR spectra are listed as follows: chemical shift (δ, ppm), multiplicity, coupling constant (Hz), integration, and are referenced to the residual solvent peak (7.26 ppm for $CDCl_3$). Abbreviations are as follows: s = singlet, d = doublet, t = triplet, q = quartet, p = pentet,

m = multiplet. ^{13}C-NMR spectra were recorded on Bruker spectrometers (125 MHz), are listed in terms of chemical shift and are referenced to the residual solvent peak (77.16 for $CDCl_3$).

Reaction calorimetry was carried out in an Omnical Insight reaction calorimeter in a glass, septum-cap vial equipped with a magnetic stirring bar. These systems measure the heat released or consumed in a sample vessel compared with that from a reference compartment over the course of the reaction.

3.7.2 Calorimetry experiments, with varying and nitrone and alkyne, separately:

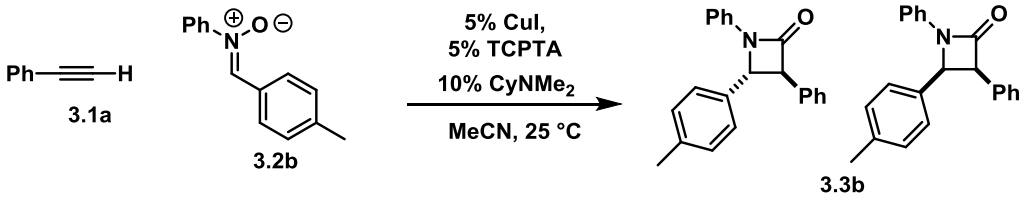

(Information for Figure 3.3 and Figure 3.1) Stock solutions were made for the eight reactions (4 varying nitrone, 4 varying alkyne) to add the appropriate amount of alkyne, nitrone, base, copper catalyst-ligand solution into 16 mL vials with a stir bar each.

A stock solution of phenylacetylene (0.255 g, 2.50 mmol) and *N*,*N*-dimethylcyclohexylamine (0.032 g, 0.251 mmol) was weighed into a 5 mL volumetric flask and diluted with acetonitrile. For reactions with varying nitrone, 1.0 mL of this alkyne-amine stock solution was loaded into a 16 mL reaction vial. For reactions with varying alkyne, a (4-methylbenzylidene)aniline oxide (0.530 g, 2.51 mmol) and *N*,*N*-dimethylcyclohexylamine (0.032 g, 0.251 mmol) stock solution was made in a 5 mL volumetric flask with acetonitrile. For each reaction with varying alkyne, 1.0 mL of this nitrone-amine stock solution was added.

For reactions with varying alkyne, an appropriate amount of phenylacetylene was added to provide 0.072, 0.093, 0.110, and 0.131 M with a constant 0.10 M in nitrone. For reactions with varying nitrone, an appropriate amount of (4-methylbenzylidene)aniline oxide was added to

provide 0.07, 0.09, 0.11, and 0.13 M in nitrone, with a constant 0.10 M in phenylacetylene. These were diluted up to 3.0 mL each and added to the reaction vial for a total of 4.0 mL (from the previous addition of amine/nitrone or amine/alkyne). The reaction vials were then placed into the calorimeter thermostated at 25 °C and allowed to equilibrate for an hour.

A copper-ligand solution was added and diluted. The precatalyst copper(I) iodide (0.0476 g, 0.250 mmol) and TCPTA ligand (0.120 g, 0.258 mmol) was added to a 10 mL volumetric flask and diluted with acetonitrile. 1.0 mL of each catalyst-ligand solution was loaded into 1 mL syringes, placed into the calorimeter without injection, and allowed to equilibrate at 25 °C for an hour. Reactions were initiated by injecting the catalyst/ligand solutions into the reaction vials by the thermally equilibrated syringe (total volume for reaction was 5.0 mL). The reaction was allowed to progress until the heat evolved from the reaction returned to baseline.

3.7.3 Sampling/ quenching procedure for reactions monitored by HPLC

Before reactions were started, a solution of bicinchoninic acid (86.8 mg, 0.252 mmol) and triethylamine (0.07 mL, 0.502 mmol) in 10 mL methanol was prepared. To all LC vials, 15 µL of this quenching solution was added and diluted with 400-1000 µL of methanol. For each time point in a reaction, 10 µL aliquots were taken and diluted in the quench solution in the LC vial. An initial time point ("t=0") was taken after the catalyst was added, before the amine was added for reaction initiation.

3.7.4 HPLC conditions

1) 1260 Infinity HPLC with 6150 Quadrupole MS

Column: Agilent ZORBAX Eclipse XDB C18, 3.5 μm, 3.0 x 100 mm column

Solvent A= H_2O with 0.05% TFA, Solvent B = CH_3CN with 0.05% TFA

Initial B= 30%; 6 min, 52% B; 10.0-13.5 min, 100% B.

Flow rate = 0.400 mL/min

2) 1260 Infinity HPLC with 6150 Quadrupole MS

Column: Agilent ZORBAX Eclipse XDB C18, 3.5 μm, 3.0 x 100 mm column

Solvent A= H_2O with 0.05% TFA, Solvent B = CH_3CN with 0.05% TFA

Initial B= 15%; 14.0-16.0 min, 100% B.

Flow rate = 0.400 mL/min

3) 1260 Infinity HPLC with 6150 Quadrupole MS

Column: Poroshell 120 SB-C18, 2.7 μm, 2.1 x 50 mm

Solvent A= H_2O with 0.05% TFA, Solvent B = CH_3CN with 0.05% TFA

Initial B= 20%; 0.1 min, 30% B; 6.5 min-8.0 min, 100% B.

Flow rate = 0.400 mL/min

4) 1290 Infinity UHPLC with 6150 Quadrupole MS

Column: Poroshell 120 SB-C18, 2.7 μm, 2.1 x 100 mm

Temperature = 30 °C

Solvent A= H_2O with 0.05% TFA, Solvent B = CH_3CN with 0.05% TFA

Initial B= 10%; 0.1 min, 15% B; 3.0 min, 45% B; 5.0-6.0 min, 80% B.

Flow rate = 0.700 mL/min

5) 1290 Infinity UHPLC with 6150 Quadrupole MS

Column: Poroshell 120 SB-C18, 2.7 µm, 2.1 x 30 mm

Temperature = 30 °C

Solvent A= H_2O with 0.05% TFA, Solvent B = CH_3CN with 0.05% TFA

Initial B= 15%; 0.1 min, 20% B; 2.1 min, 44% B; 4.1-5.5 min, 65% B.

Flow rate = 0.650 mL/min

6)

1290 Infinity UHPLC with 6150 Quadrupole MS

Column: Poroshell 120 SB-C18, 2.7 µm, 2.1 x 100 mm

Temperature = 30 °C

Solvent A= H_2O with 0.05% TFA, Solvent B = CH_3CN with 0.05% TFA

Initial B= 15%; 0.1 min, 20% B; 2.1 min, 44% B; 4.1-5.5 min, 65% B.

Flow rate = 0.650 mL/min

7)

1260 Infinity HPLC with 6150 Quadrupole MS

Column: Poroshell 120 EC-C18, 2.7 µm, 2.1 x 30 mm

Temperature = 30 °C

Solvent A= H_2O with 0.05% TFA, Solvent B = CH_3CN with 0.05% TFA

Initial B= 20%; 0.1 min, 27% B; 2.0 min, 40% B; 4.5-6.0 min, 80% B.

Flow rate = 0.625 mL/min

3.7.5 Experiments monitored by HPLC-MS

3.7.5.1 Varying nitrone concentration – analysis by HPLC-MS

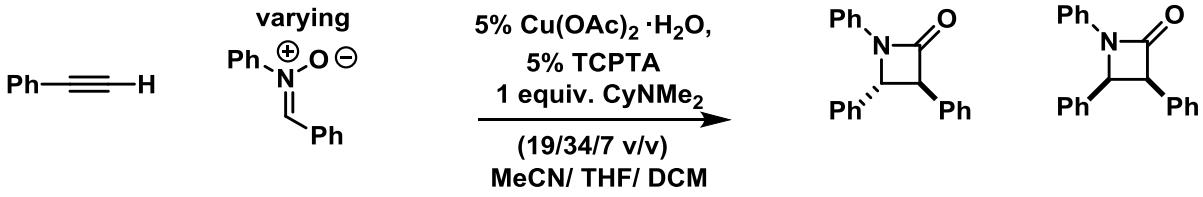

(Information for Figure 3.2) Stock solutions were made for the five reactions to add the appropriate amount of alkyne, nitrone, base, copper catalyst-ligand solution into a 8 mL vial with a stir bar. 0.3 mL of a stock solution of 2-methoxynaphthalene (delivering 0.030 mmol, 4.82 mg) in acetonitrile was added to the vial. To this reaction vial, 0.7 mL of a stock solution of $Cu(OAc)_2 \cdot H_2O$ and TCPTA (9.98 mg catalyst, 23 mg ligand, 0.05 mmol each) in dichloromethane was then added. 0.3 mL of a stock solution of phenylacetylene (to deliver 102.0 mg, 1.00 mmol) in acetonitrile was added. Varying amounts of a stock solution of (E)-*N*-benzylideneaniline oxide (0.80-1.40 mmol) in THF was added. The differences in THF solvent due to varying nitrone solution was added before injection of the amine stock solution. To initiate the reaction, 0.3 mL of a stock solution of $CyNMe_2$ (1.00 mmol, 0.127 g) in acetonitrile was added by syringe. HPLC method #1 was used to analyze the LC vials.

3.7.5.2 Varying alkyne concentration – analysis by HPLC-MS

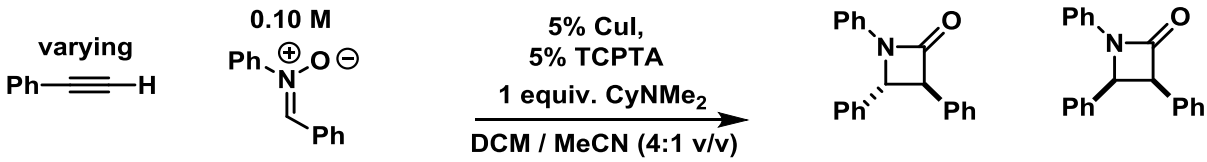

(Information for Figure 3.4) A 0.7 M stock solution of phenylacetylene (0.143 g, 1.40 mmol) was diluted in a 2 mL volumetric flask with dichloromethane. For the following desired reaction concentrations, the following were added into four 8 mL glass reaction vials with stirbars:

[Alkyne in reaction]	Volume of Alkyne stock solution / mL	Volume of DCM added / mL
0.08	0.29	0.21
0.10	0.36	0.14
0.12	0.43	0.07
0.14	0.50	0

Table 3.8: Volumes of solutions used for varying alkyne reactions

A stock solution of (E)-*N*-benzylideneaniline oxide (0.245 g, 1.24 mmol) was prepared with dichloromethane in a 5.00 mL volumetric flask. 1.0 mL of this stock solution was added into the reaction vial. A copper-ligand stock solution of CuI (11.91 mg, 0.063 mmol) and TCPTA (29.05 mg, 0.063 mmol) was diluted with acetonitrile to 2.5 mL. 0.5 mL of this solution was added to each reaction. As a standard for integration, phenanthrene (34.9 mg, 0.20 mmol) was diluted to 2 mL in a volumetric flask with dichlormethane. 0.4 mL of this solution was added to each reaction vial.

A stock solution of *N*,*N*-dimethylcyclohexylamine (0.185 mL, 1.23 mmol) was made with dichloromethane. 0.1 mL of this solution was added to each vial to initate the reactions after a 10 µL aliquot of the reactions were taken. The reactions were sampled by taking 10 µL aliquots and quenching them with the BCA solutions in LC vials. The LC vials were then analyzed by HPLC method #5.

3.7.5.3 Segmented dosing of phenylacetylene

(Information for Figure 3.7) To a 8 mL vial with a stirbar was added (E)-*N*-benzylideneaniline oxide (99.0 mg, 0.50 mmol) in 1 mL THF; $Cu(OAc)_2 \cdot H_2O$ (5.0 mg, 0.025 mmol) and TCPTA (12 mg, 0.025 mmol) in 0.3 mL acetonitrile; and 0.3 mL of a 2-methoxynapthelene stock solution (0.2405 g in 15 mL acetonitrile). After taking a t = zero timepoint, *N*,*N*-dimethylcyclohexylamine (64 mg, 0.50 mmol) in 0.5 mL acetonitrile was added to initiate the reaction. Over the course of the reaction, a 0.5 mL stock solution of phenylacetylene (51.0 mg, 0.50 mmol) was added, 0.1 mL at a time. LC samples were analyzed by HPLC method #2.

3.7.5.4 Varying concentration of amine base

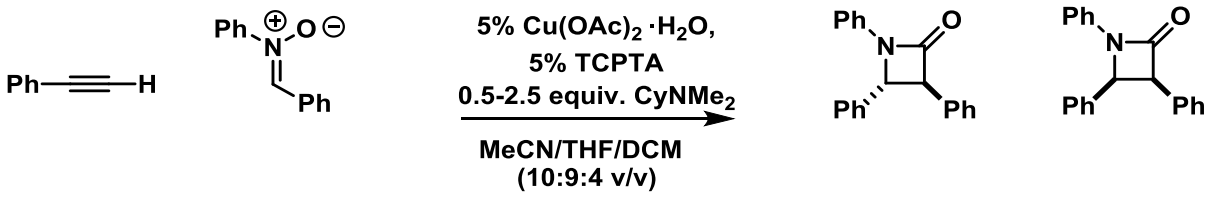

(Information for Figure 3.8) Stock solutions were made for the five reactions to add the appropriate amount of alkyne, nitrone, base, copper catalyst-ligand solution into a 8 mL vial with a stir bar. 0.3 mL of a stock solution of 2-methoxynaphthalene (delivering 0.030 mmol, 4.82 mg) in acetonitrile was added to the vial. To this reaction vial, 0.4 mL of a stock solution of $Cu(OAc)_2 \cdot H_2O$ and TCPTA (5.0 mg catalyst, 12 mg ligand, 0.025 mmol each) in dichloromethane was then added. 0.9 mL of a stock solution of (E)-*N*-benzylideneaniline oxide (99.0 mg, 0.50 mmol) in THF were added. 0.1 mL of a stock solution of phenylacetylene (to deliver 51.0 mg, 0.50 mmol) in acetonitrile was added. To initiate the reaction, 0.1-0.5 mL of a stock solution of $CyNMe_2$ (varying 0.5-2.5 equivalence) in acetonitrile was added by syringe.

The differences in acetonitrile solvent due to varying amine solution was added before injection of the amine stock solution. LC samples were analyzed by HPLC method #2.

3.7.5.5 Addition of TFA and fast copper acetylide formation

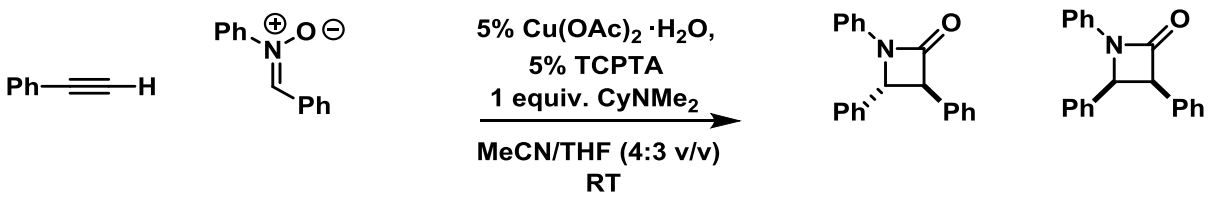

(Information for Figure 3.9) Stock solutions were made for the three reactions to add the appropriate amount of alkyne, nitrone, base, copper catalyst-ligand solution into a 8 mL vial with a stir bar. To the reaction, 0.5 mL of a stock solution of phenylacetylene (to deliver 51.0 mg, 0.50 mmol) in acetonitrile and 1.0 mL of a stock solution of nitrone (99.0 mg, 0.50 mmol) in THF were added. 0.3 mL of a stock solution of $Cu(OAc)_2 \cdot H_2O$ and TCPTA (5.0 mg catalyst, 12 mg ligand, 0.025 mmol each) in acetonitrile was then added. To initiate the reaction, 0.5 mL of a stock solution of $CyNMe_2$ (64 mg, 0.50 mmol) in acetonitrile was added by syringe. As an integration standard, 0.3 mL of a 2-methoxynapthelene stock solution (0.2405 g in 15 mL acetonitrile) was added. LC vials were analyzed with HPLC method #3.

To the reaction to test the effect of added acid, 1.15 equivalents of trifluoroacetic acid (66 mg, 0.575 mmol) was added 45 minutes after the reaction had been initiated.

To the reaction that allowed initial formation of copper(I) phenylacetylide first, the nitrone was not added until 45 minutes later.

3.7.6 Set-up of screening experiments

3.7.6.1 NMR analysis example of crude mixtures from screening experiments

Figure 3.15 shows an example for analysis of a reaction mixture after a reaction has been concentrated, pushed through a pad of neutral alumina, eluted with DCM, and concentrated again. The benzaldehyde peak is at 10 ppm; the imine peak is at 8.5 ppm; leftover nitrone appears at 8.4 ppm; protons representative of the β-lactam are at 5.0 and 5.5 ppm.

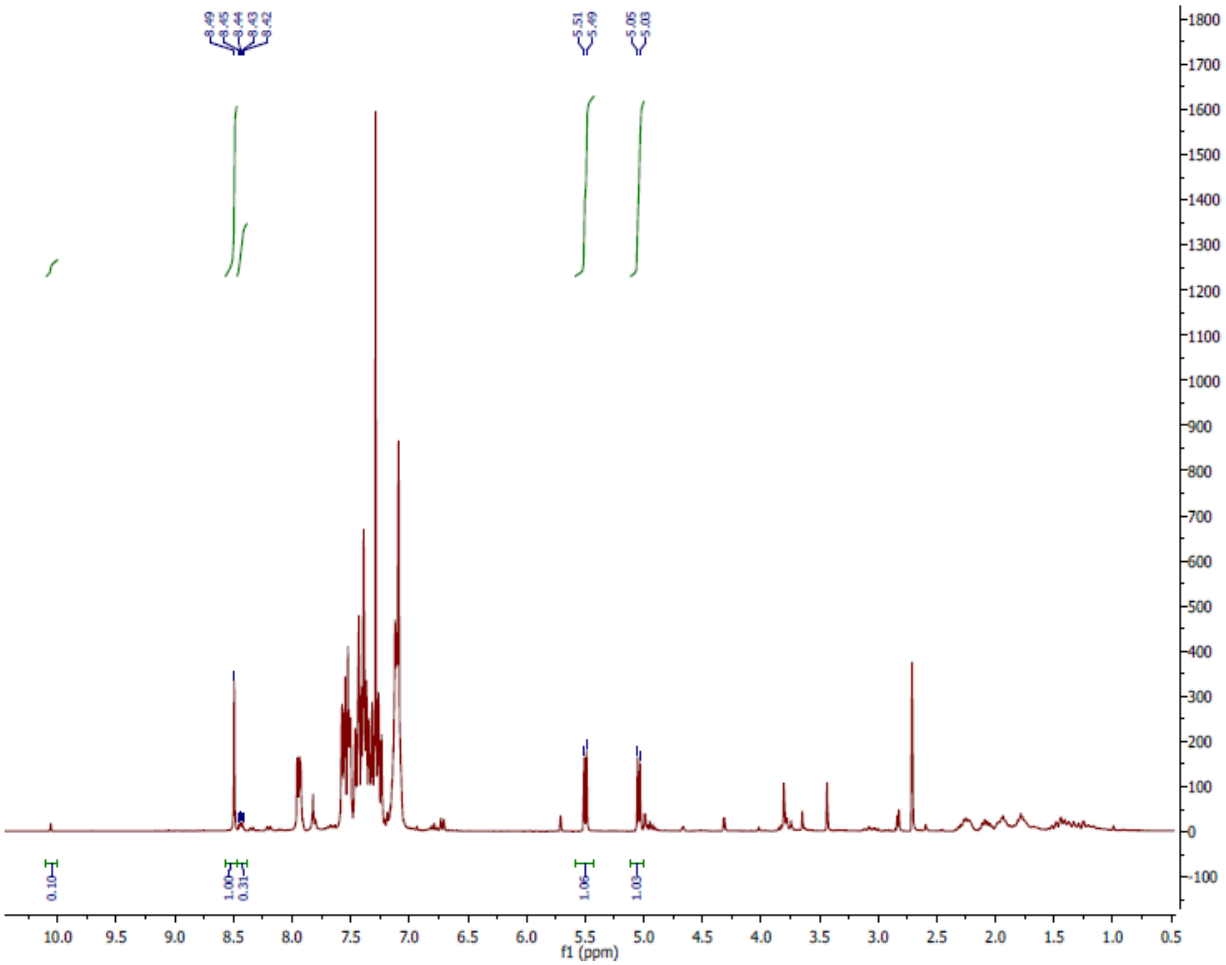

Figure 3.15: ^{1}H-NMR spectrum of crude reaction mixture

3.7.6.2 Ligand screen

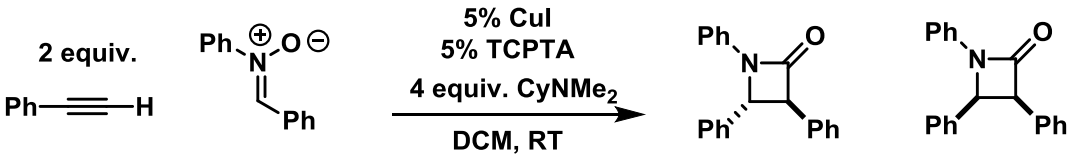

Stock solutions were made for the reactions to add the appropriate amount of alkyne, nitrone, base, copper catalyst-ligand solution into a 8 mL vial with a stir bar. To this reaction vial, 1.0 mL of a nitrone stock solution (to deliver 39.0 mg, 0.20 mmol) in dichloromethane was added. 0.5 mL of a stock solution of phenylacetylene (to deliver 41.0 mg, 0.40 mmol) in dichloromethane was added. 0.5 mL dichloromethane used to dissolve and transfer preweighed CuI and the designated ligand (1.9 mg catalyst, X mg ligand, 0.01 mmol each) into the reaction vial. To initiate the reaction, 0.120 mL of $CyNMe_2$ (0.800 mmol, 0.102 g) was added. A few samples were taken to check conversion by HPLC-MS Method #4. After stirring at room temperature for two days, the reaction was concentrated by blowing down with air. The crude material was then passed through a short pad of neutral alumina, eluted with dichloromethane. This solution was then concentrated by rotory evaporation and analyzed by ^{1}H-NMR in $CDCl_3$ neutralized by K_2CO_3.

3.7.6.3 Varying copper(I) source

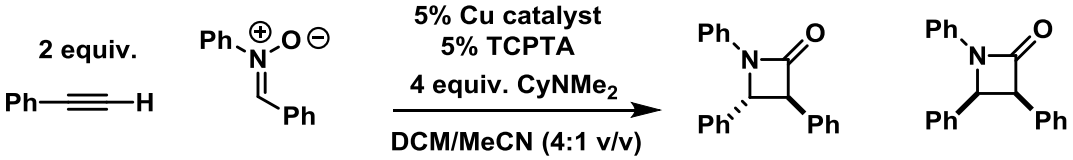

Stock solutions were made for the reactions to add the appropriate amount of alkyne, nitrone, base, copper catalyst-ligand solution into a 8 mL vial with a stir bar. To this reaction vial, the copper catalyst of choice was weighed into the vial (0.01 mmol). 0.5 mL of a stock

solution for the ligand (4.65 mg, 0.01 mmol) in acetonitrile was added. 0.5 mL of a stock solution of phenylacetylene (to deliver 41.0 mg, 0.40 mmol) in dichloromethane was added. 1.0 mL of a nitrone stock solution (to deliver 39.0 mg, 0.20 mmol) in dichloromethane was added. To initiate the reaction, 0.120 mL of $CyNMe_2$ (0.800 mmol, 0.102 g) was added. A few samples were taken to check conversion by HPLC-MS Method #4. After stirring at room temperature for two days, the reaction was concentrated by blowing down with air. The crude material was then passed through a short pad of neutral alumina, eluted with dichloromethane. This solution was then concentrated by rotory evaporation and analyzed by ^{1}H-NMR in $CDCl_3$ neutralized by K_2CO_3.

3.7.6.4 Varying amine base source

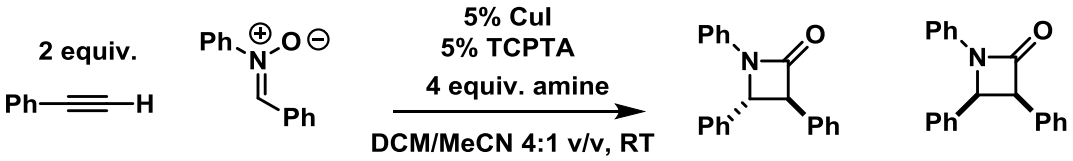

Stock solutions were made for the reactions to add the appropriate amount of alkyne, nitrone, base, copper catalyst-ligand solution into a 8 mL vial with a stir bar. 0.5 mL of a stock solution for the ligand (4.65 mg, 0.01 mmol) and copper(I) iodide (1.91 mg, 0.01 mmol) in acetonitrile was added. 0.5 mL of a stock solution of phenylacetylene (to deliver 41.0 mg, 0.40 mmol) in dichloromethane was added. 1.0 mL of a nitrone stock solution (to deliver 39.0 mg, 0.20 mmol) in dichloromethane was added. To initiate the reaction, the chosen amine base was (0.800 mmol) was added. A few samples were taken to check conversion by HPLC-MS Method #4. After stirring at room temperature for two days, the reaction was concentrated by blowing down with air. The crude material was then passed through a short pad of neutral alumina, eluted

with dichloromethane. This solution was then concentrated by rotory evaporation and analyzed by ^{1}H-NMR in $CDCl_3$ neutralized by K_2CO_3.

3.7.7 Kinetic profiling of amine base screen

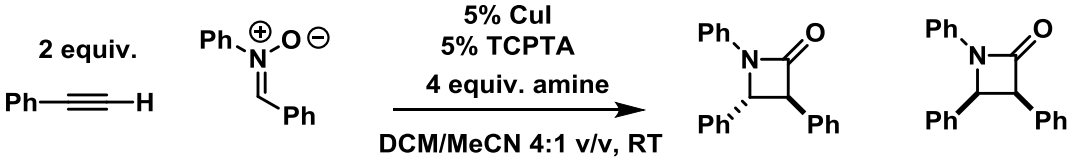

Stock solutions were made for the reactions to add the appropriate amount of alkyne, nitrone, base, copper catalyst-ligand solution into a 8 mL vial with a stir bar. 1.0 mL of a stock solution for the ligand (4.65 mg, 0.01 mmol) and Copper(I) iodide (1.91 mg, 0.01 mmol) in 1:1 acetonitrile/diethylether was added. 0.5 mL of a stock solution of phenylacetylene (to deliver 41.0 mg, 0.40 mmol) in dichloromethane was added. 1.0 mL of a nitrone stock solution (to deliver 39.0 mg, 0.20 mmol) in dichloromethane was added. 0.2 mL of a 1 mL stock solution of phenanthrene (58.85 mg, 0.33 mmol) in acetonitrile was added. To initiate the reaction, the chosen amine base was (0.800 mmol) was added. Samples of 10 µL were taken from the reaction into prepared vials of 600 µL of methanol and 20 µL of the quench solution. The LC samples were analyzed by HPLC Method #6.

3.7.8 Direct injection into the HPLC

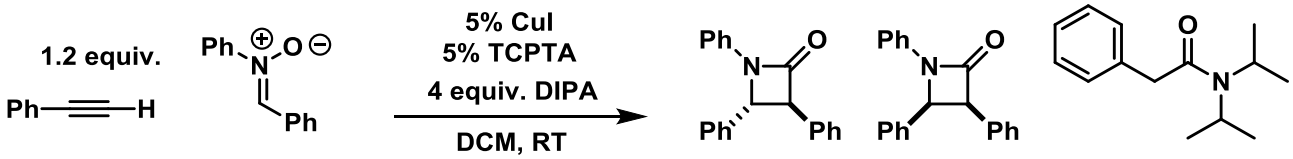

(Information for Figure 3.14) To a 25 mL three-neck flask with stir bar was fitted the EasySampler probe through septa. Dichloromethane (9 mL) was added. To this flask was added *N*-benzylideneaniline oxide (0.178 g, 0.90 mmol) as a solid, and phenylacetylene (0.110 g, 1.08

mmol) by syringe. After full dissolution, CuI (8.57 mg, 0.045 mmol) and TCPTA (21 mg, 0.045 mmol) were addded as solids. A time = 0 sample was taken by the direct injection apparatus. Diisoproylamine (0.505 mL, 3.60 mmol) was added by syringe. Samples were taken every 13 minutes by the EasySampler and appropriately diluted with 675 mL of methanol through a system of pumps and rheodynes until it reached the selection valve for the HPLC. The aliquots were immediately analyzed with HPLC Method #7.

3.7.9 Isolation of the Amide 1 byproduct from the Kinugasa Reaction

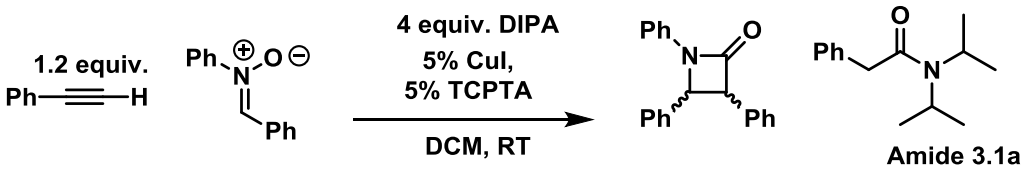

The reaction from direct injection was collected and run through a short column of silica and eluted with petroleum ether and then some ethyl acetate to remove copper salts. This allowed for β-lactam product to precipitate out. The yellow filtrate that contained **Amide 3.1a**, imine, and Glaser product (as analyzed by HPLC) was concentrated. This residue was purified by silica column chromatography with 30:1 petroleum ether/ ethyl acetate. **Amide 3.1a** eluted as the penultimate compound, followed by the *cis*-β-lactam. Fractions with only **Amide 3.1a** were collected and concentrated. The yield was not taken. It was then characterized by ^{1}H-NMR spectroscopy, HSQC, and HMBC. ^{1}H NMR (300 MHz, $CDCl_3$) δ 7.39 – 7.18 (m, 7H), 4.12 – 3.81 (m, 1H), 3.71 (s, 2H), 3.49 – 3.25 (m, 1H), 1.44 (d, J = 6.7 Hz, 6H), 1.03 (d, J = 6.6 Hz, 6H). (The chloroform residual peak overlaps with the compound.) ^{13}C NMR (101 MHz, $CDCl_3$) δ 169.86, 135.93, 128.57, 128.51, 126.53, 135.89, 128.45, 45.76, 43.55, 20.57, 20.53, 20.59. (Peaks taken from HMBC.)

Chapter 4: Automated Reaction Monitoring inside a Microwave Reactor

4.1 Background and previous work

Microwave assisted organic synthesis (MAOS) has become a popular alternative to conventional heating methods for synthetic organic chemistry. Although experiments were originally done in domestic or modified microwaves, the last twenty years has seen an increase in commercially available microwaves better suited for research use. All domestic microwave ovens and microwave reactors for chemical synthesis are made to operate at the single frequency of 2.45 GHz (which is 12.24 cm or 0.082 cm^{-1}), which is too low energy to break chemical bonds or even for promoting electronic or vibrational excitations.[95,96] Aside from shortening reaction times, microwave heating has oftentimes allowed for milder reaction conditions, higher yields, and less catalyst decomposition relative to its counterpart, conventional heating (using a hotplate with an oil bath, sand bath, aluminum block, etc).[97] The results have been observed as so spectacular and widespread that "microwave effects" were attributed to MAOS.

Microwave effects are now split into two categories: thermal and non-thermal microwave effects. Most accelerative or other remarkable effects have been attributed to thermal microwave effects. Thermal effects include the creation of hot spots and selective heating, and presently there is relatively little argument to their importance in accelerating and altering organic reactions. Thermal microwave effects refer to conditions (temperature, pressure, or heating rates) that are difficult to duplicate by conventional heating, if at all. In contrast, non-thermal effects refer to acceleration in rate or changes in chemoselectivity that cannot be attributed to rapid heating. Usually these non-thermal effects are attributed to the polarizing microwave field or effects concerning molecular mobility and diffusion. Currently, the existence of these non-thermal effects is hotly contested, with several individuals insisting that they are really thermal

effects that have been poorly measured. It seems that for whichever side one chooses, there are studies whose results are interpreted to support them.

4.1.1 Thermal effects

4.1.1.1 Differences in heating modes

Thermal effects can result from microwave radiation doing work on the medium, causing the reaction medium to generate heat. Whereas energy transmission in conventional heating is caused by convection and conduction, energy transmission in a microwave is caused by dielectric losses. The dielectric properties of the molecules themselves affect the extent to which they can transform electromagnetic energy into heat.[97] In conventional heating, the heat must travel from the surface touching the heat source toward the inside, and often requires the external heating source to be set at a higher temperature for the reaction vessel to reach the indicated temperature. In contrast, microwave heating allows irradiation of the entire sample from the inside-out.

4.1.1.2 Superheating and boiling

Superheating has also been observed in microwaving polar solvents, allowing them to reach temperatures 13-26 °C above their boiling point even when flasks are outfitted with a reflux condenser (to allow for ambient pressure), and temperatures are measured with a fiber optic probe. Instead of superheating, Mingas and coworkers suggest calling the elevated boiling point at which the system is at equilibrium a nucleation limited boiling point. His explanation is that bubbles form differently due to the inside-out heating mechanism that can occur in microwaved reactions.[98] The ability to heat above a solvent's standard boiling point may aide in

accelerating reactions beyond their conventional heating counterpart. This can allow chemists to work with less conventional combinations of concentration, temperature, pressure.

Dudley and Stiegman report with new experiments that with enough stirring and/or the addition of stirring chips, these nucleation-limited "superboiling" events disappear. Instead, the boiling point of the solvent will be very close to those at atmospheric pressure (Figure 4.1).[99]

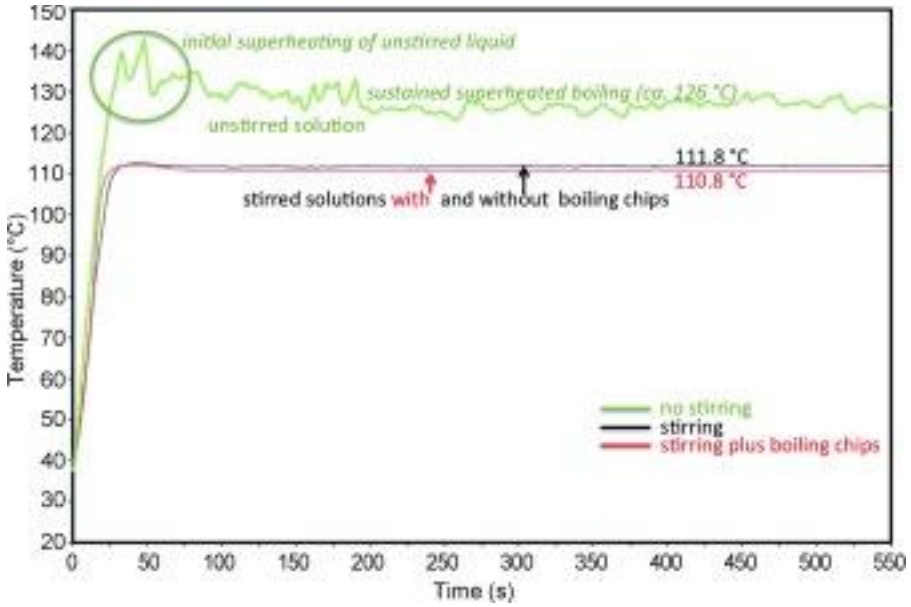

Figure 4.1: The effects of stirring and boiling chips on a superheated liquid[99]

4.1.1.3 Hotspots and selective heating

The inhomogeneity of the applied microwave field can cause "hot spots" to form in the reaction, causing localized higher temperatures than can be measured in the bulk medium. This can also lead to higher conversions for reactions that are done at the same bulk temperature as with conventional heating.

Polar substances are more susceptible to absorbing microwave radiation and can heat up more quickly than nonpolar substances. This characteristic, combined with inhomogeneity of the

microwave field within the reaction sample itself, can allow for selective heating of polar compounds that is inaccessible to conventional heating (even in homogeneous solutions). This can sometimes be carefully exploited to change reactions. For example, a biphasic Hoffman elimination was conducted in a microwave using water and chloroform. The water temperature rose to 110 °C while the chloroform's temperature only reached 50 °C. The transfer of the product into the chloroform layer allowed it to not decompose.[100] This selective heating has also been applied to catalysts in heterogeneous reactions, which will not be discussed here. In the case where nonpolar solvents are used, the substrates must be polar enough to act as molecular radiators, transferring heat to the bulk solvent.

Today, most scientists agree that the accelerating effects observed in microwave reactors are purely thermal effects due to how quickly polar materials can be irradiated in a microwave field.[101] Indeed, most would agree that if two reactions are truly run at the same internal temperature inside a microwave and in an oil bath, it should not be surprising if the rates are the same. The changes in chemoselectivity with time due to differences in heating modes, however, are less well-studied.

4.1.2 Non-thermal effects

In contrast, the existence of non-thermal effects in the microwave is still debated, referring to physical interactions between the molecules in the reaction media and the electromagnetic field. Such non-thermal effects could change bond-breaking and/or bond-making, contributing to any differences in reaction progress or selectivity. In cases where microwave irradiation provided faster reaction rates than conventional heating at the same temperature, often non-thermal effects are suggested.

Unfortunately, many such cases involve experiments that utilized an external IR sensor for temperature measurements of the reaction vessel, not the internal temperature of the reaction itself. This IR sensor is still common in many commercially available microwaves for use in research (Anton Parr, Biotage) .This caused many misinterpretations of data, as the internal temperatures inside the microwave were reported as significantly lower than they actually were.[102] With better internal temperature sensing with a fiber optic probe, it was often found that such rate accelerations at the same temperature were nonexistent. This caused some to change proposals of non-thermal effects.[103,104] Unfortunately, many groups still report rate-accelerations without accurately measuring temperature. This lack of certainty makes it difficult for some claims in microwave chemistry to be believable, especially pertaining to non-thermal effects.

4.1.3 Methods of rate-acceleration through non-thermal effects – correct or not?

Currently, it is believed to be unlikely that any non-thermal effects arise from molecular resonance processes, since the frequency of the microwave reactor is far too low. It is important to note that our collaborators do not champion for their existence, either.[105] Any effects must still originate from relaxation processes that result in heat, dispersed into translational and vibrational degrees of freedom. While rotational and vibrational activation can occur, it would be through dissipated heat, not through targeted absorption of microwave radiation.[96]

Others suggest that rate changes can occur by changing the value of the activation energy or the pre-exponential term of the Arrhenius equation for the reaction in question. That is, the activation energy can be decreased if the dipole moment of a transition state couples with the oscillating electric field.[106] It is already known that microwave radiation can couple to permanent molecular dipole moments, so it would be feasible for it to couple with more transient species.

While it is unlikely that the microwave's electromagnetic field to couple to a transition state because of the short life time of transition states, the field could potentially couple with longer-lived intermediates.[96]

Despite the controversy surrounding non-thermal effects, it is still worthwhile to find ways to exploit microwave heating in organic synthesis. Microwaves heat through a fundamentally different mechanism than conventional methods, and it is possible that thermal microwave-specific effects can be realized under appropriate conditions. Stiegman writes that these effects are likely to come from selective heating of molecules, as mentioned earlier.[105]

Such extraordinary effects are difficult to measure due to having few tools for measuring reaction conversion and product distribution inside microwave reactions. Leadbeater and coworkers have previously monitored progress of a microwave reaction with in situ Raman and then in situ FTIR.[107, 19] Since then, in situ methods of microwave reaction monitoring have been absent from the literature. As recently as 2016, the technique of stopping microwave heating of a reaction at a specified time and then subjecting new reaction mixtures for different time points is still used.[108]

4.1.4 Previous work

The Dudley group has identified reaction parameters where non-thermal effects are most likely to play an important role, leading to acceleration in reaction rate. Criteria included a polar, highly-absorbent substrate in an aromatic, non-absorbing solvent. The first example was a Friedel-Crafts benzylation of toluene using an ionic benzyl transfer reagent, 2-benzyloxy-1-methylpyridinium tetrakis[3,5-bis(trifluoromethyl)phenyl]borate (Scheme 4.1). It was found that under microwave heating, there was a rate enhancement as compared to heating in an oil bath.

However, this rate enhancement was most pronounced in an open quartz vessel, not a closed vessel. Furthermore, the effects were most prominent under more dilute, less synthetically relevant conditions.[109]

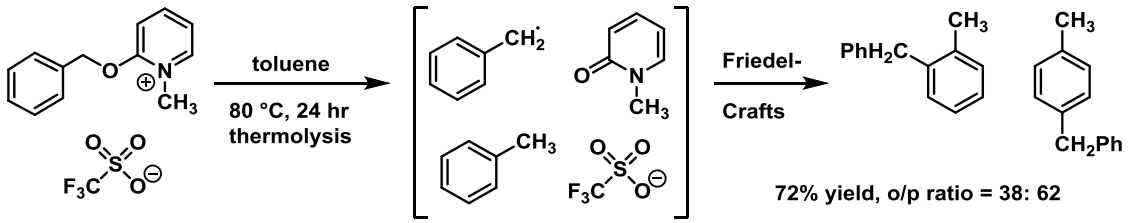

Scheme 4.1: Friedel-Crafts benzylation of toluene under microwave conditions

The second reaction investigated was the aryl Claisen rearrangement of allyl *p*-nitrophenyl ether (**4.1**) in *p*-xylene. This substrate with a nitro group was chosen because it has a high microwave cross section and large dipole moment relative to allyl phenylether. These reactions were also done open-vessel at ambient temperatures in melted naphthalene because the substrate was found to have the highest microwave cross section in this solvent. When reactions were run at the same internal temperature between the microwave and conventional heating in an oil bath, there were no meaningful differences in rate. However, it was found that for constant power experiments, there was a small rate increase calculated as expected from the bulk temperature profile. This rate difference was much more pronounced (5 and 9 fold) for pulsed experiments where the reaction was allowed to cool between cycles (Figure 4.2).[110]

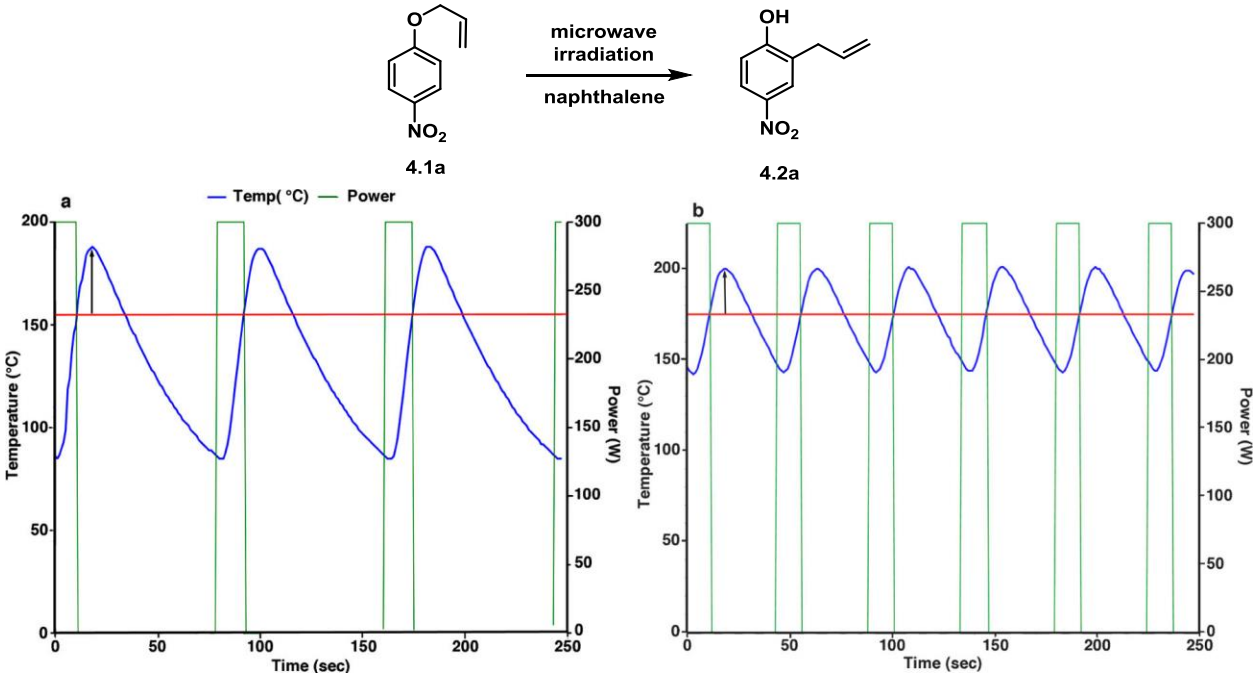

Figure 4.2: Claisen rearrangement of allyl *p*-nitrophenyl ether under pulsed microwave settings[110]

The work in this thesis follows specifically on the previous work exploring non-thermal effects of the aryl Claisen rearrangement of **4.1** by Dudley and Stiegman, et al. We sought to gain more data and insight into the controversial previous results. As a means to create a more informative, reliable, and less labor intensive method of acquiring data, we aimed to develop a high throughput offline method of monitoring for microwave reactions. Since then, we have created a new automated sampling apparatus adaptable to a CEM microwave reactor that allows us to broaden the scope of kinetic experiments that are possible within a microwave reactor by tracking conversion rates of multiple substrates. In the process, we also designed experiments to look for any non-thermal effects in the Claisen rearrangement of **4.1**.

4.2 Creation of an automated sampling set-up for a microwave reactor

Due to the difficulties in making direct comparisons between microwave and convectional heating methods, finding and replicating evidence for or against non-thermal microwave effects has been a slow and tedious process. Traditional techniques of quantifying reaction progress entail manually taking a sample and analyzing it by HPLC-MS, GCMS, or NMR. Traditional kinetic experiments with conventional heating often utilize an internal standard to offset differences in sample size, and a suitable compound must act as an innocent bystander for which to integrate against. For microwave reactions, the use of an added standard is undesirable for our studies, as its presence could alter the effective heating of the solute molecules or the bulk temperature. This would be called adding a susceptor, which can absorb energy and transfer its energy to the surroundings, even if it does not react.[97] Such an additive could have an observable effect in the microwave that would not be reflected in the parallel reaction under conventional heating. In order to make the reaction conditions between conventional and microwave heating identical in all parameters aside from heating, no additives were used in either setting.

Data collected from Dudley's original work was done by stopping reactions and taking samples by hand, followed by offline analysis by GC-MS. Stopping the reaction and allowing it to cool was necessary for consistent and reproducible data collection, due to the unusual reaction solvent, naphthalene. Since naphthalene is solid below 80 °C, we switched to a synthetically more relevant solvent, *p*-xylene, which would cause less problems in the fluidics of our sampling apparatus. *p*-Xylene is still a nearly-microwave transparent solvent due to its low dipole moment.[109]

The previous automated sampling system that was used in the study of the Aza-Piancatelli Rearrangement (Chapter 2) under conventional heating methods was modified for this work on microwave reactions. We sought to extend this sampling system to the microwave reactor, with some changes to the reaction vessel.

We envisioned many challenges needed to be addressed in our attempts to directly sample the Claisen rearrangement in *p*-xylene. Because the rearrangement is extremely slow below 165 °C, the reaction had to be conducted in a sealed vial to allow the bulk temperature to rise significantly above the boiling point of the solvent (138.4 °C). Hence, our sampling apparatus had to take aliquots out of a closed system while under pressure without introducing leaks. All samples taken would have to be representative of the whole chemical system. Furthermore, the act of withdrawing aliquots had to not perturb the reaction progress. An automated sampling rig that allowed for consistent sample sizes taken at pre-programmed times was also desirable to allow higher reproducibility and ease of experimentation.

Studies were conducted with a microwave appropriate for both sealed and open-flask reactions, the CEM Discover. We envisioned a reactor top that could be easily fitted onto the reaction to allow temperature sensing and sampling. We designed and fabricated a custom reactor head, which was only a slight modification from the commercially available CEM design (Figure 4.3). This reactor head had one port for a fiber optic probe encased in a sapphire thermowell typical of the original CEM Discover, which is microwave transparent. The second port was used for sampling with a quartz capillary tube connected to Teflon and PEEK tubing. The quartz capillary was chosen due to quartz' transparency to microwave irradiation, as most other materials would absorb irradiation. Commercially available fittings were used to keep the system pressure-tight and free of leaks.

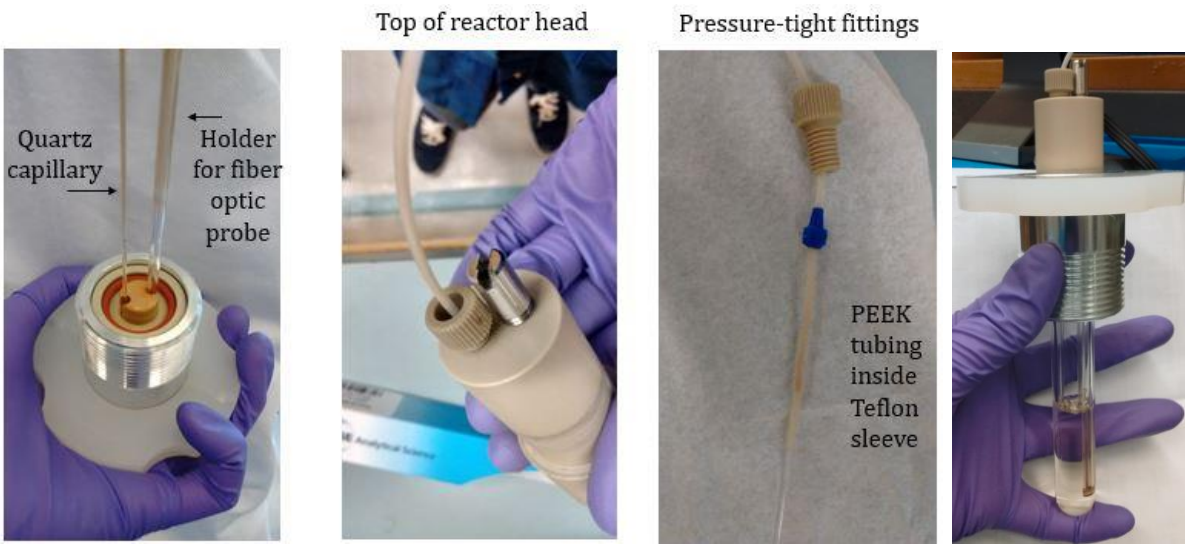

Figure 4.3: Modifications to microwave reactor head

Samples were withdrawn by a programmable syringe pump from the reaction vial through the tubing connected to a Gilson 815 rheodyne valve. The timing was configured such that the withdrawal of the syringe pump triggered the actuation of the rheodyne, which is coupled to a Gilson 215 automated liquid handling robot. Triggering of the liquid handler by the rheodyne allows for dilution with methanol of the reaction aliquot into waiting LC vials. Offline analysis was conducted from these LC vials after completion of the sampling period (Figure 4.4).

Experiments were conducted under three settings: constant temperature mode (as monitored by a fiber optic probe), constant power mode (allowing temperature to vary) and pulsed settings (a prefixed power set on or off for fixed intervals). Both power output, temperature, and conversion from starting material to product by HPLC were monitored for all experiments. All reactions, unless otherwise stated, were run in nonabsorbent quartz vials so that any microwave effects resulting from the reaction mixture would not be an effect of an absorbent borosilicate vial. Borosilicate glass (Pyrex) vials are not transparent to microwave irradiation, and therefore the vial material itself would contribute to heat build-up.

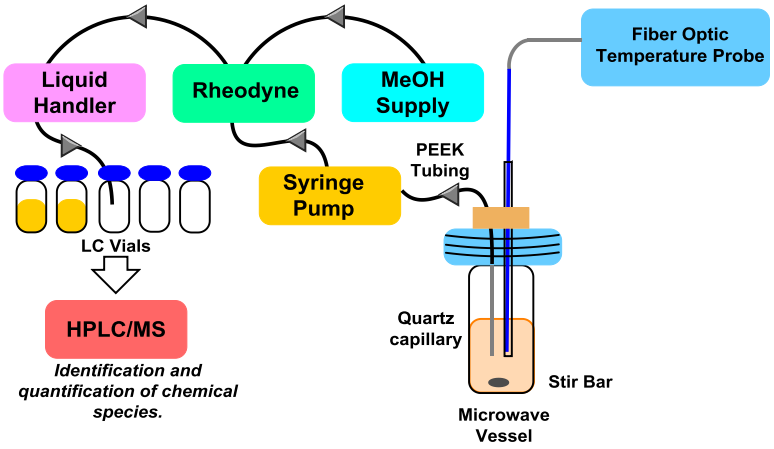

Figure 4.4: Schematic for automated sampling out of a microwave reactor

An example of a reaction progress plot for the Claisen rearrangement molecule **4.1a** is shown in Figure 4.5 for 23% conversion. Concentrations are calculated by their relative extinction coefficients to *p*-xylene. Due to the tendency of the reaction to become darkly colored due to decomposition, reactions were not run to full conversion to avoid discoloration of the quartz vials, which would make them increasingly more absorbent. The reaction times were also limited to avoid side product formation.

While the product formation curve appears to be clean, it was observed that with many experiments, the substrate **4.1a** gave somewhat scattered data when it was the sole substrate. Several similar substrates, as will be shown later, showed much less scattered data. Their presence in the same vial (for the purpose of a competition experiment) allowed cleaner profiles of substrate **4.1a**. It is unclear why substrate **4.1a** in particular appears as scattered, but it is possible that it is difficult to collect samples that are perfectly representative of the solution for that particular substrate. This may be the case if **4.1a** forms aggregates, as will be discussed later.

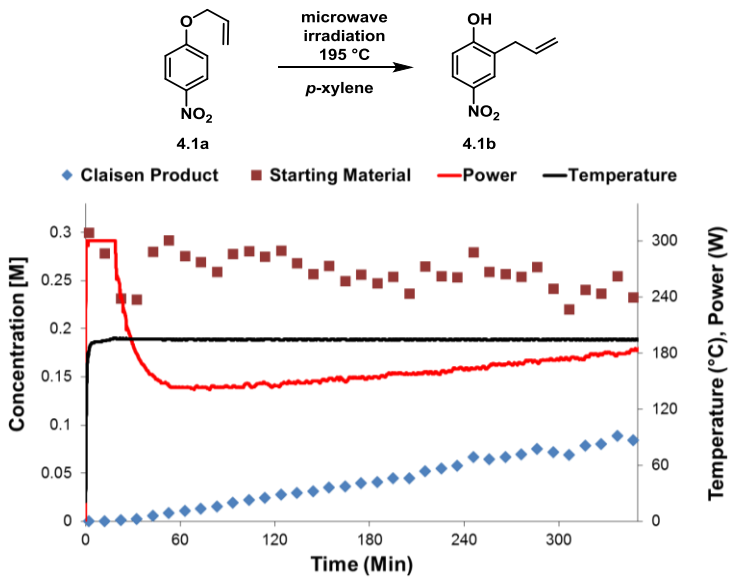

Figure 4.5: Example of reaction progress from a microwave using automated sampling

One concern is that withdrawing aliquots from the superheated reaction could potentially perturb the reaction progress due to variations in pressure or solution volume. To address this point, two experiments were conducted at the same temperature with different sampling frequencies – one with a very low sampling frequency, and one with a high sampling frequency (Figure 4.6). Reaction progress was the same, so it appeared that at a constant temperature setting, the reaction was not affected by the small volume changes resulting from sampling.

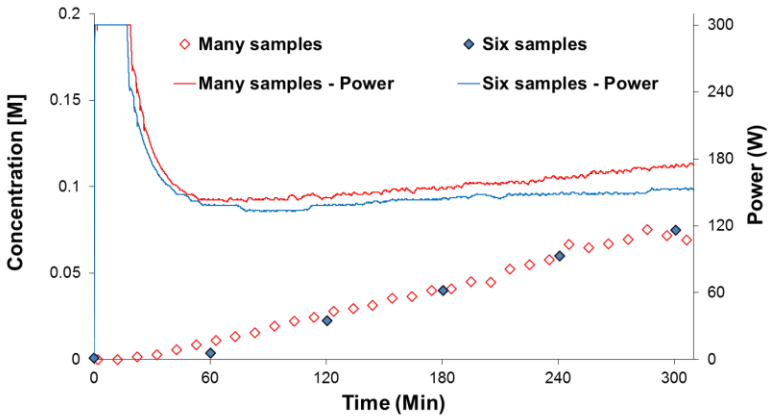

Figure 4.6: Frequent vs infrequent sampling from the microwave reactor

Up to 30% conversion for substrate **4.1a**, there were very few side products observed by HPLC-MS. They appeared to be extremely low concentration, such that they were not observed when the samples were withdrawn for analysis by ^{1}H-NMR. Consequently, these side products were not isolated. Two examples of side products that have been observed in literature with a different substrate under different conditions are seen in Scheme 4.2.[111] It is hoped that even if the analogous side products are formed, their seemingly trace concentrations do not significantly affect our interpretation of the results by acting as suspectors.

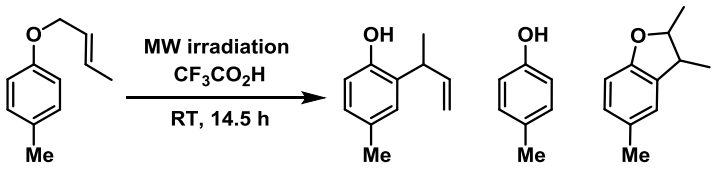

Scheme 4.2: Side products from the aryl Claisen rearrangement observed from literature[111]

4.3 One-to-one comparisons with a conventional thermal heating

One key advantage in our method of analysis is the consistency of all analytical equipment between the microwave and thermal heating sources. Everything between the microwave and the thermal set-up was kept the same except for the heating source. (See Experimental section for picture) The microwave reactor set-up was designed to be completely transferrable to a heated sand bath for direct comparisons between the two heating methods. The microwave reactor vial, head, and vial holder was lifted out of microwave and immersed into a large, preheated sand bath at an elevated temperature to allow quick equilibration to the desired temperature. While there was an external thermocouple to sense the heat of the sand bath, the same software and fiber optic probe was used internally to achieve the same temperatures as in the microwave. As demonstrated by previous research groups, it is imperative that such measurements are taken carefully so that reactions are run with the same internal temperature, as

much as possible. Our reaction set-ups allow for exact comparisons to be made, since nothing has been changed except the method of heating.

Reactions with **4.1a** were run at 180-203 °C in both the microwave and sand bath (Figure 4.7). The Arrhenius plot below compares both sets of reactions. It is clear that reacting **4.1a** under these conditions does not result in any significant variation in reaction behavior between microwave and thermal heating. This is consistent with most observations done with manual sampling where the microwave is used under constant temperature setting, compared to thermal experiments. This is unsurprising for reactions run at the same internal temperature, and has also been observed by more traditional, infrequent sampling.[108]

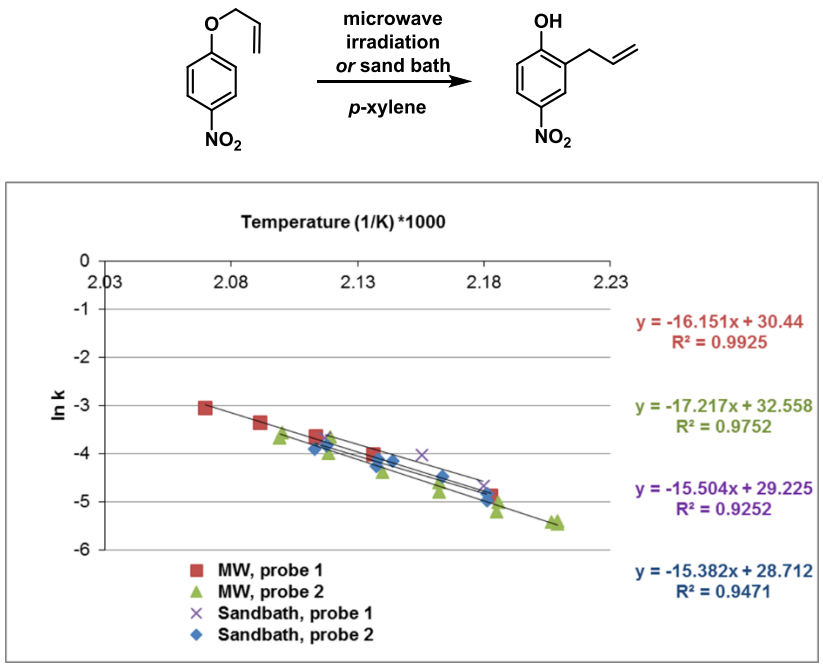

Figure 4.7: Arrhenius plot for thermal and microwave-assisted Claisen rearrangement

The rearrangement was also run at different initial concentrations from 0.2-0.5 M at the same constant temperature of 186 °C in the microwave and in a sand bath (Figure 4.8). The results are nearly the same. Although there appears to be a slight increase in rate for the

experiments done in a sand bath, this can likely be accounted for by slight variances in the temperature, as the sand bath's temperature was manipulated manually, whereas the microwave temperature is controlled automatically by the software.

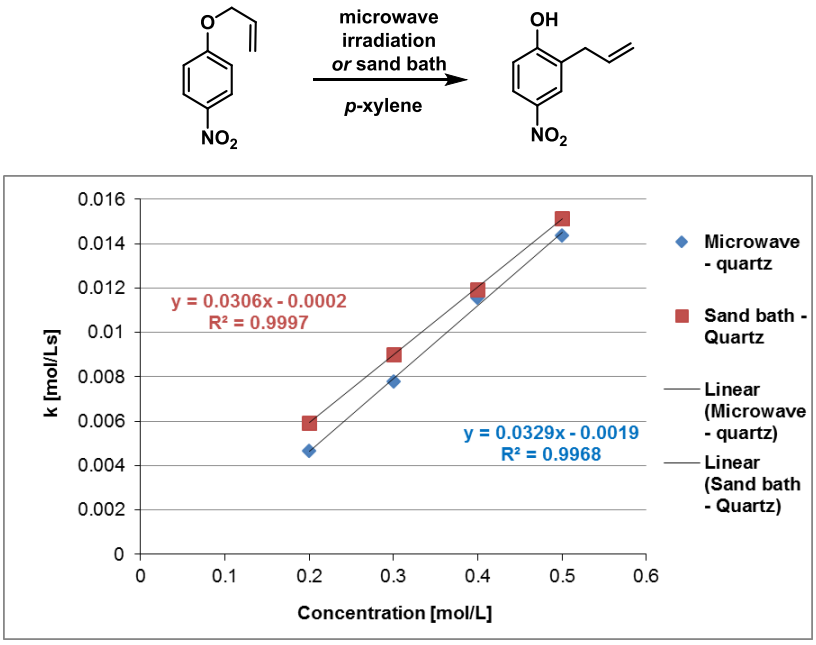

Figure 4.8: Varying initial concentrations at a constant temperature

4.4 Constant power settings do not always provide reproducible results

Reactions run under constant power settings are in no way comparable to those run under constant temperature settings. As more microwave power is absorbed with time, there is a greater probability for accumulating excess thermal energy. A low average of applied power can lessen any thermal effects that would be observed with a high average of applied power.[105] Indeed, it has been argued that reactions run with the same power settings should not be compared even between two instruments of the same model.[112] The microwave cavity, as well as the age and temperature of the magnetron, can affect the power output despite the supposed applied power.

Intrigued, we used our sampling apparatus to give a measure of the inconsistencies of constant power experiments.

A reaction was run at a constant power setting of 190 W three times (Figure 4.9). The temperature profiles graphed for experiments run at the same power are not quite the same. These small changes in the measured bulk temperature are reflected in the product formation. Although the constant power setting does not have an analogue in conventional heating in a sand or oil bath, those using constant power settings for synthetic purposes should be aware that it might not provide the same conditions every time, especially as most commercial microwaves for benchtop synthesis come with an external IR temperature probe.

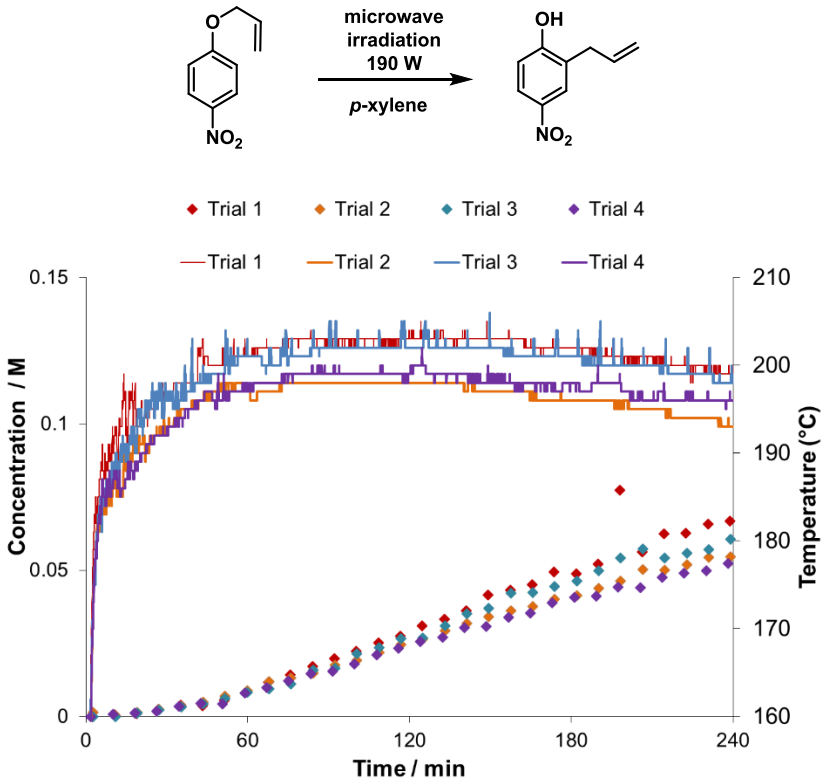

Figure 4.9: Claisen rearrangement at constant 190 W setting in the microwave

Duplicates of reactions were run at constant power setting at a range of settings from 150-210 W in 10 W increments. Higher constant microwave power levels did not always

reproducibly cause higher reaction rates, nor even the same reaction rates for duplicates run at the same power. (See reactions run at 210 and 190 W then between 170 and 180 W). One could propose that the sampling rig simply does not hold up to variable temperatures caused by the constant power mode. However, if this were true, it is likely that individual experiments would have more scattered data than those shown in Figure 4.10.

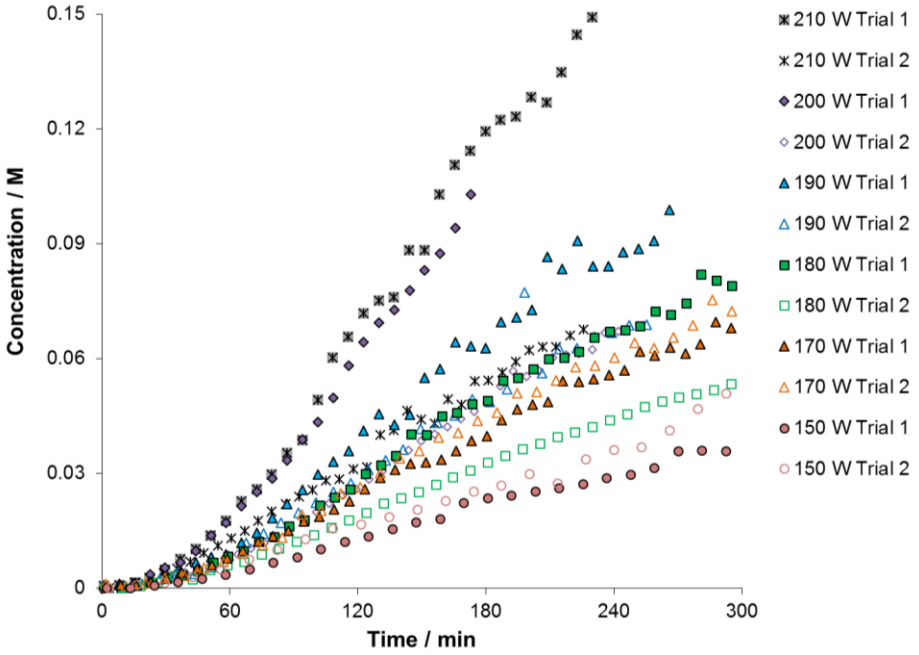

Figure 4.10: Claisen product formation with varying microwave power

Reactions with varying initial concentrations of substrate **4.1a** were also run with an applied constant 200 W (Figure 4.11). As expected, increasing the concentration of **4.1a** under constant power settings increases the reaction rate, as can be seen between the experiments with 0.2 and 0.3 M concentrations. However, it is still not predictable or consistent: a change as small as 0.05 M is not reliable, as the constant power setting itself is not necessarily consistent. See 0.30 M and 0.35 M as an example.

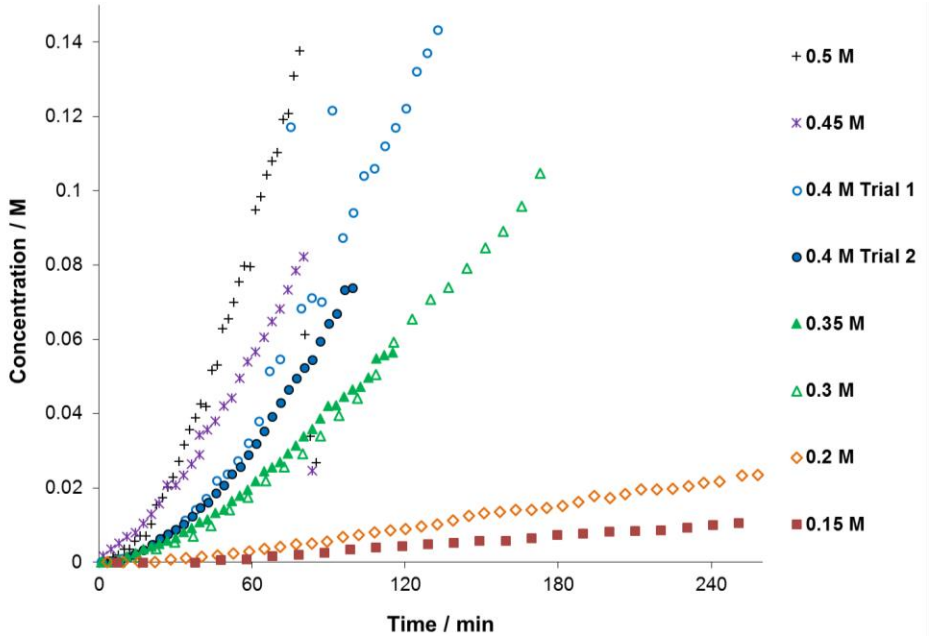

Figure 4.11: Varying initial concentration of substrate at constant 200 W

To check that the inconsistencies were not merely artifacts of the sampling rig, the substrate **4.1a** was heated at a constant 190 W with only stirring, no sampling, and in triplicate (Figure 4.12). Indeed, the bulk temperature profiles are not identical, showing differences such as 198-206 °C. While the differences are not extremely large, they are likely large enough to show inconsistencies between conversions of reactions at constant power. This reaffirms that it is difficult to compare small differences for reactions run at constant power setting (versus constant temperature setting).

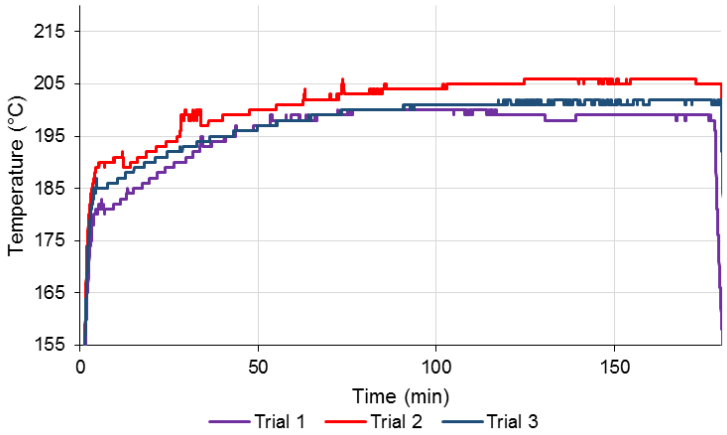

Figure 4.12: Temperature profiles of heating substrate 4.1a at 190 W with no sampling

4.5 Kinetics between pulsed power settings and constant temperature settings

Previous work in the Dudley lab found that the greatest rate enhancement was observed under pulsed microwave conditions, when compared to the predicted progress by conventional heating. 300 W pulses were conducted to cycle the temperature of the bulk reaction from 145-175 °C, turning the microwave power off when the temperature was 175 °C, and then back on when the reaction was cooled down to 145 °C. A twofold rate enhancement was measured for this pulse program. A more prominent, nine-fold rate enhancement occurred when the pulse program was set for 85-155 °C cycles instead.[110]

Our particular model of microwave did not have the same mode for dynamic cycling in a temperature range. However, the microwave did allow cycling between different powers. Hence, the following experiments are not replicates of the previous work, but should allow analogous comparisons to be drawn.

The same pulsed power settings were applied to solutions of 0.2, 0.3, and 0.45 M **4.1a** n *p*-xylene. The microwave was turned on at a constant 200 W for twelve minutes, off for two

minutes, and this cycle was repeated ten times while samples were automatically taken. The reaction progress, temperature profile, and power cycling is shown in Figure 4.13 for the reaction of 0.3 M **4.1a**.

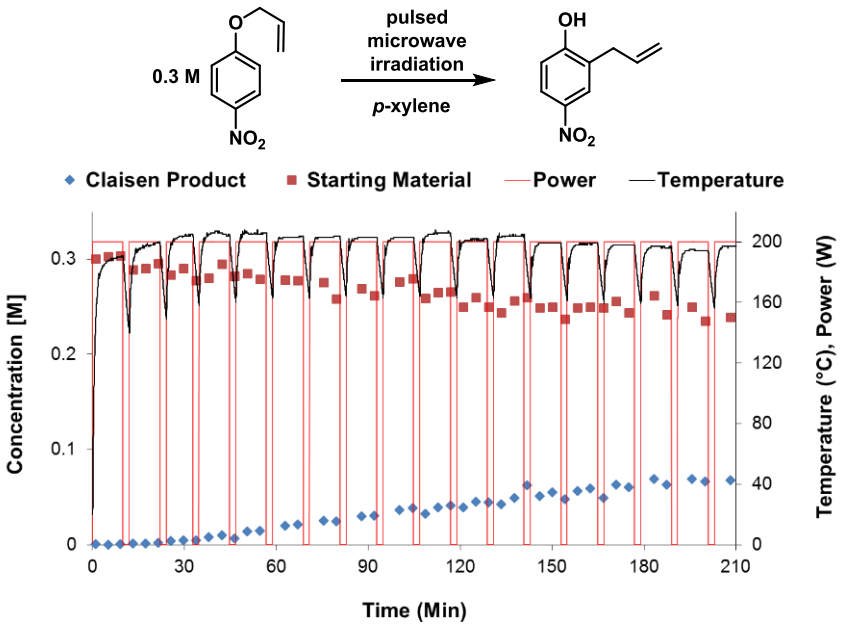

Figure 4.13: Reaction progress for a pulsed power experiment for 0.3 M initial concentration of substrate

The average temperature of the reaction at 0.3 M was calculated for only when the microwave power was on (196 °C). The average temperature of the reaction at 0.3 M was also calculated for the entire reaction, including when the power was off (193 °C). Subsequently, control reactions were conducted under standard microwave heating at constant temperatures equal to the average temperature observed during the pulsed experiments (193, 196 °C). These reactions utilized varying but continuous microwave power. The reaction progress of the product from both the pulsed and continuous, varying power reactions are shown in Figure 4.14

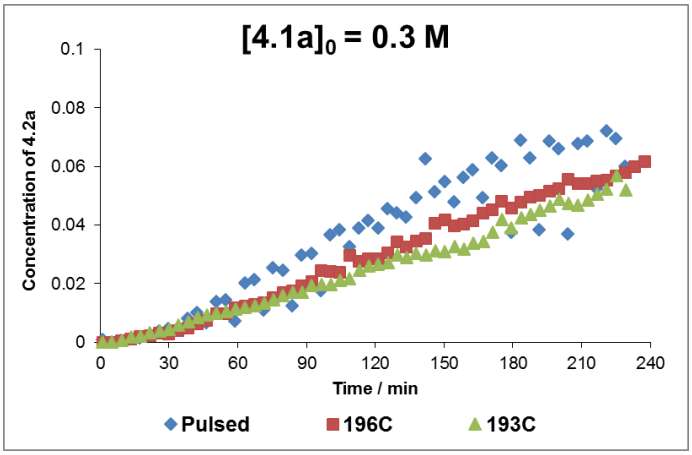

Figure 4.14: Reaction progress compared between pulsed power and continuous power experiments with a temperature

A similar set of experiments was at the initial concentrations of 0.2 and 0.45 M as well. Pulsed power experiments (200 W for twelve minutes, 0 W for two minutes, and repeated) were conducted. The average temperature was calculated for only when the microwave was on. Subsequently, an experiment was run with that temperature, using sustained but varying microwave power (no pulsing) (Figure 4.15). It was observed that for the lower initial concentrations 0.2 and 0.3 M of **4.1a**, the reactions conducted with pulsed power reached about 20-30% higher conversion, especially for the 0.2 M solution. At 0.45 M, there is little difference between the two heating modes. This is consistent with observations that there is less of an accelerating effect for more concentrated solutions. It is more likely for energy to be transferred by the absorbent substrate to the surrounding solvent molecules at higher concentrations; therefore, the measured temperature of the bulk solution is closer to the effective temperature of small aggregations of the solute when the solute is more concentrated.

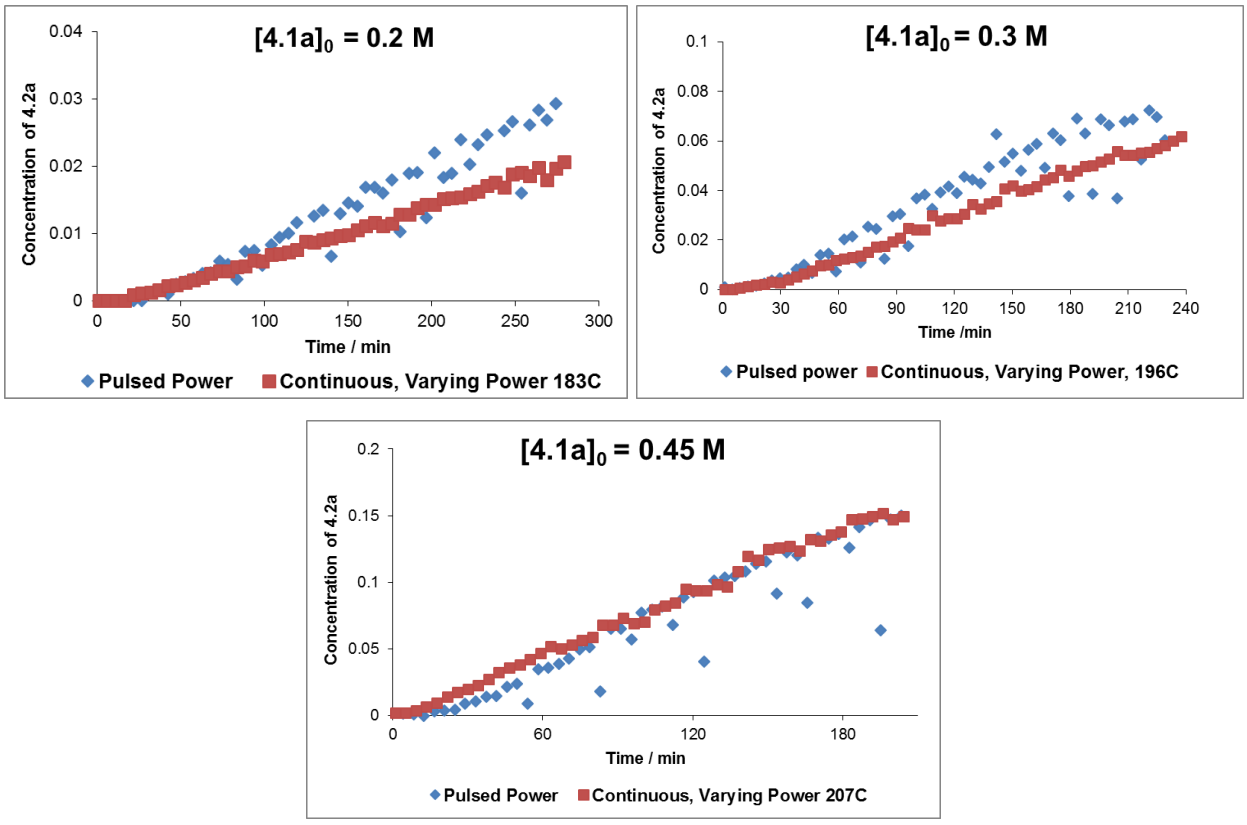

Figure 4.15: Comparisons between product formation for pulsed power and varying, continuous power

An immediate observation can be made that the product formation curves look much more scattered for these pulsed experiments. These presumably uneven samples are taken when the internal temperature changes dramatically. This is illustrated in Figure 4.16 where the same data is coded by the on/ off pattern of the pulse sequence. When the microwave temperature has become steady after the microwave is turned on again, the samples taken describe a believable curve. When the reaction has only been heated for a couple seconds or when the microwave power has been turned off, the samples are suddenly of poor quality.

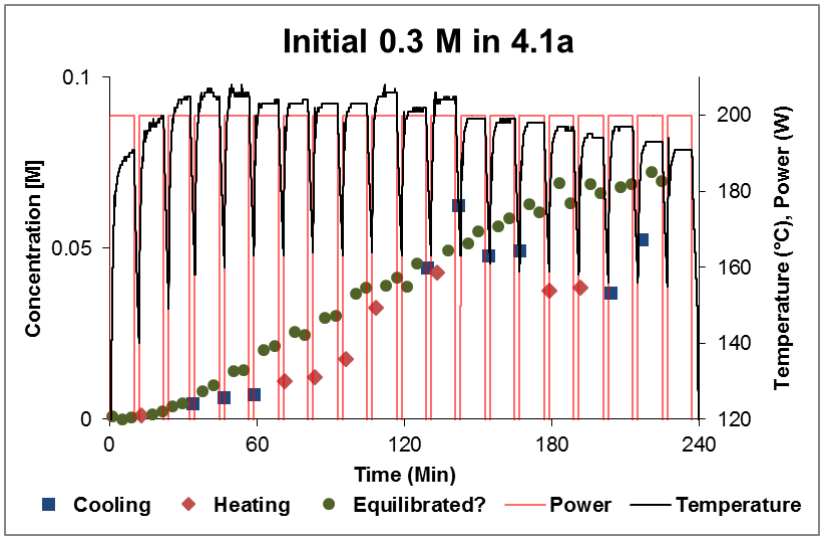

Figure 4.16: Coding samples for different microwave heating regimes

4.6 Good vs poor molecular heaters

We were curious about using other compounds as good or poor molecular heaters. As an example of a very poor molecular heater, we heated solutions of molecule 4.1b, which should have a very low dipole moment (Figure 4.17). If heated in a borosilicate vial, which is most commonly used for synthetic microwave chemistry, the bulk temperature of the solution takes about an hour to equilibrate and is hot enough for the Claisen rearrangement to proceed. In contrast, if the vial is composed of a nonabsorbent material such as quartz, the solution never heats up enough for the rearrangement to actually occur. For conventional use of the microwave, one would not see this effect since borosilicate glass vials are usually cheap and sufficient for synthesis. The inability to effectively heat compound **4.1b** in a quartz vial results in no productive Claisen rearrangement, and is a phenomenon unique to the microwave reactor, This example serves to illustrate the major contributions played by an appropriately chosen solvate, as well as the likelihood that borosilicate reaction vessel will provide sufficient absorptive properties when no other option is available. In either case, the rate of heating for substrate **4.1b**

is significantly slower than strongly microwave absorbing **4.1a**, illustrating the negligible contribution of vessel effects.

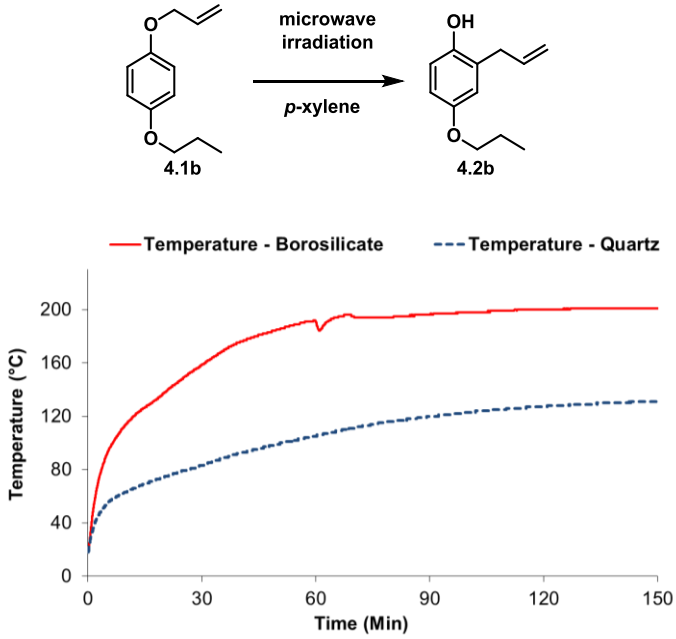

Figure 4.17: Heating in quartz vs borosilicate vials for a poor molecular heater

In contrast for **4.1a**, a good molecular heater, it can be seen that the conversion to product is essentially identical between quartz and borosilicate vials, and that the temperature profiles are fairly similar (Figure 4.18).

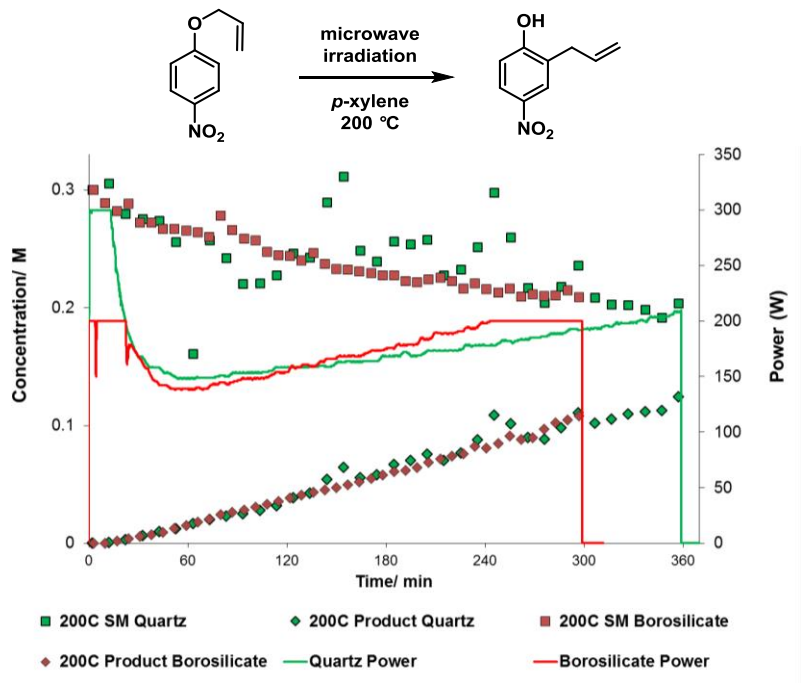

Figure 4.18: Heating in quartz vs borosilicate vials for a good molecular heater

When equimolar amounts of molecules **4.1a** and **4.1b** were heated in the same quartz vial, it was thought that the rate of Claisen rearrangement of **4.1a** would be faster than that of molecule **4.1b**, since molecule **4.1b** was shown to be a poor molecular heater. Surprisingly, the rate of product formation from molecule **4.1b** greatly exceeded **4.1a**'s rearrangement (Figure 4.19). This is consistent with previous experiments conducted neat with electron-donating groups.[111] As long as sufficient energy can be obtained by having a molecular heater such as **4.1a** present, the electronic effects can control the rates of rearrangement of *para*-substituted allylphenyl ethers. It is important to note that the rate of product formation from **4.1a** is the same whether run in a competition experiment or independently: its conversion to product did not slow down in the presence of another substrate, and there is no competition for a catalyst.

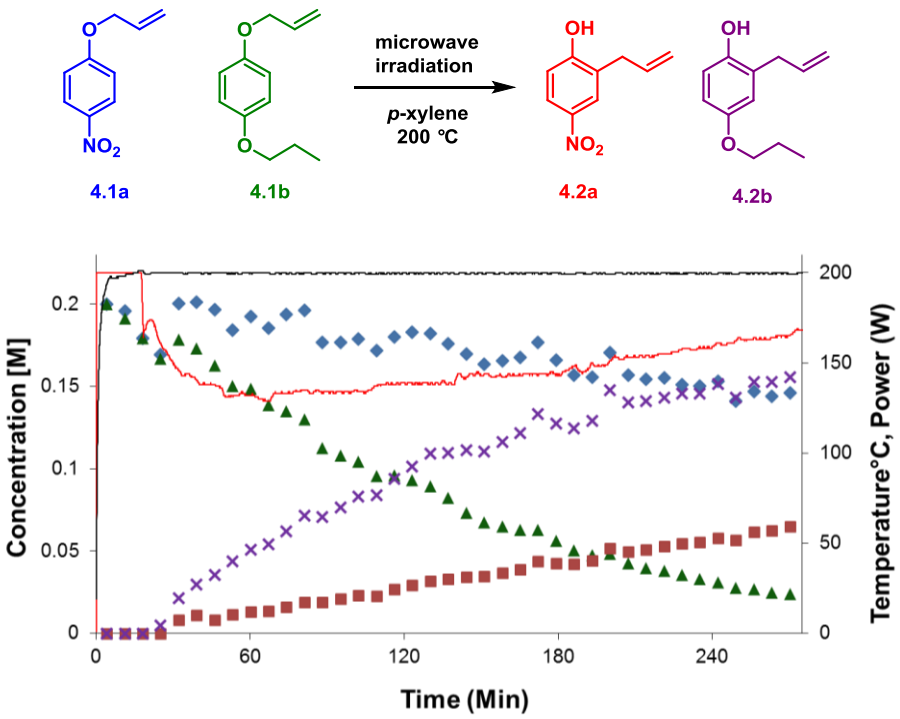

Figure 4.19: Competition experiment between a poor and good molecular heater

4.7 Linear free energy relationships for the Claisen rearrangement

Other *para*-substituted allylphenyl ethers were heated to measure their reaction rates. It was soon apparent that like molecule **4.1b**, in quartz vials, all the substrates could not be effectively heated enough to react in *p*-xylene. Hence, an equimolar amount of **4.1a** was added. In effect, a Hammett-like plot was made (Figure 4.20). When traditional LFER analysis of reaction rates for a Hammett plot were applied by graphing relative rates to X=H against the sigma parameter, the results did not have the typical linear or even V-shape.

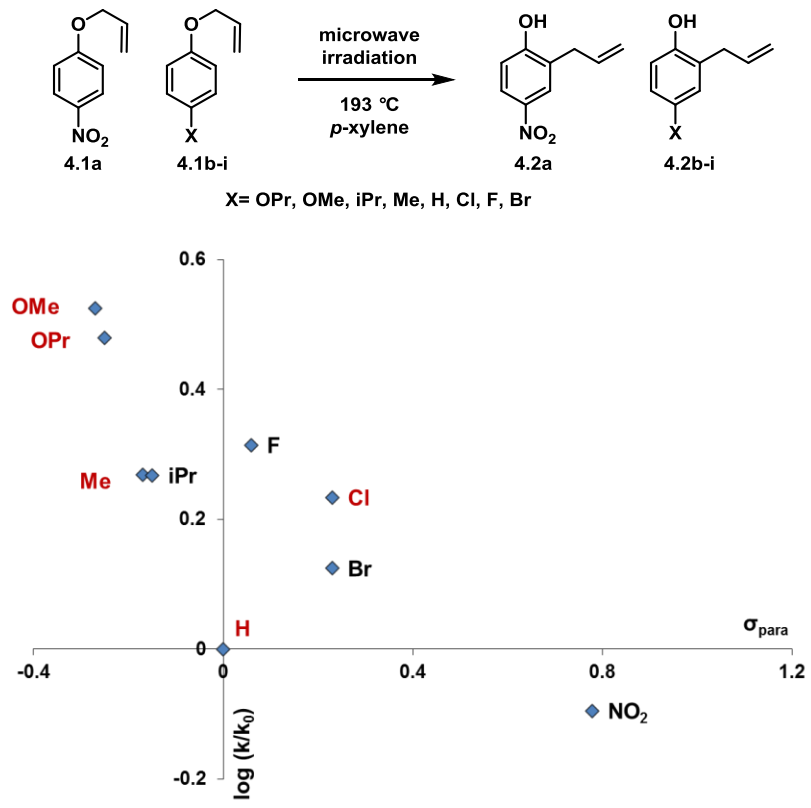

Figure 4.20: Linear free energy relationships for 4-substituted allylphenyl ethers – traditional Hammett plot

With the understanding that perhaps the sigma parameter was not the optimal parameter to find a meaningful relationship, the two components (resonance and the inductive effect) were varied until the best fit was found by inspection. By including the full resonance effect but only taking 15% of the inductive effect, a decent fit of 0.94 R^2 was found (Figure 4.21). However, this correlation may be arbitrary, not having any real physical meaning. Instead of having a good correlation stemming solely from electronic effects, it may be possible that interactions between *p*-xylene and the type of substrate affect the reaction rates. Solute aggregation specific to the solvent and substrates could result in selective localized heating. This may create small domains where the effective temperature is higher than the measured bulk temperature, causing rate

enhancement. Experimentally, the results show that substrates with similar X groups are clustered together. The O-alkyl substrates (OPr, OMe) are clustered together, as are the alkyl (Me, iPr), and the halogens (F, Cl, Br) are also somewhat close to each other.

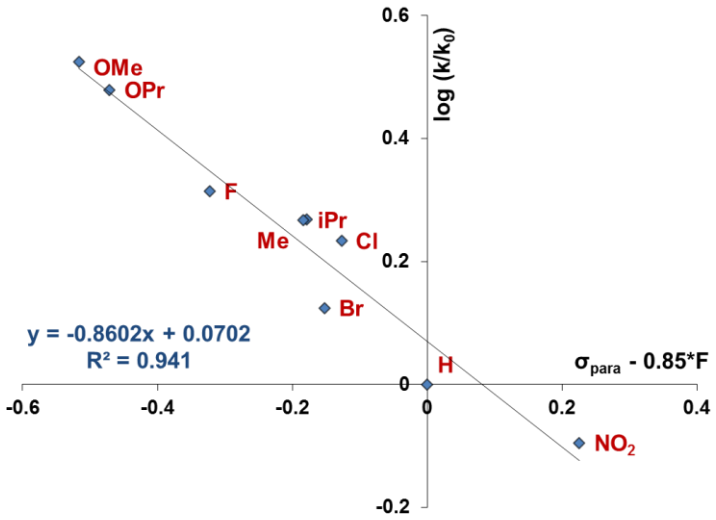

Figure 4.21: Linear free energy relationships for 4-substituted allylphenyl ethers vs a different parameter

The same experiments were rerun in the sand bath for a thermal comparison (Figure 4.22). Unfortunately, the fit is not as good, possibly because the temperature of the sandbath is manually controlled instead of automated. Although the overlay is not excellent, the qualitative results are the same.

It could be argued that the unusual data arises from the addition of **4.1a**. The presence of **4.1a** could potentially change the reaction rates of the other substrate, or vice versa. To address this point, graphing the product formation **4.2a** from all the experiments shows that the rates are nearly identical, within statistical variations (Figure 4.23). Hence, the two substrates and products do not seem to affect each other.

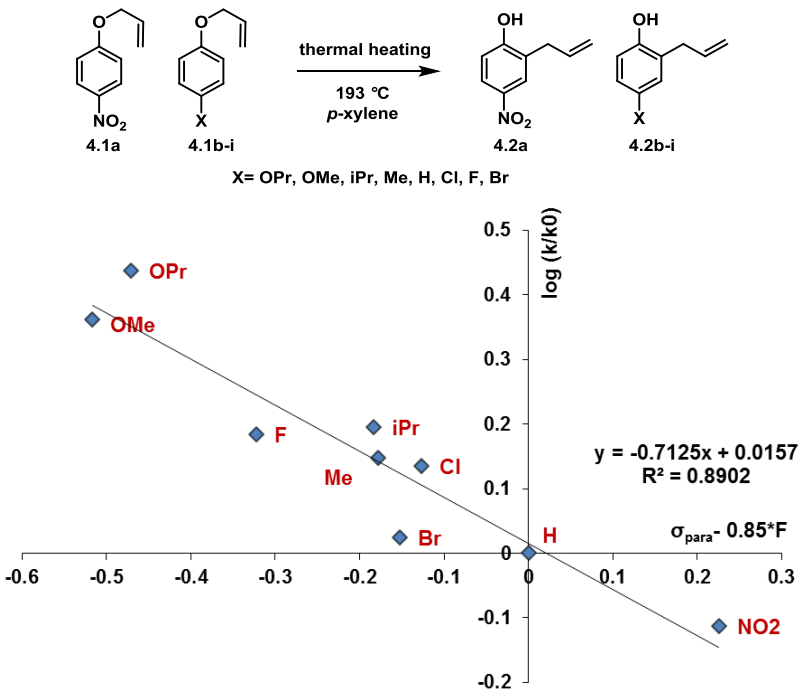

Figure 4.22: Linear free energy relationships for 4-substituted allylphenyl ethers – thermal experiments

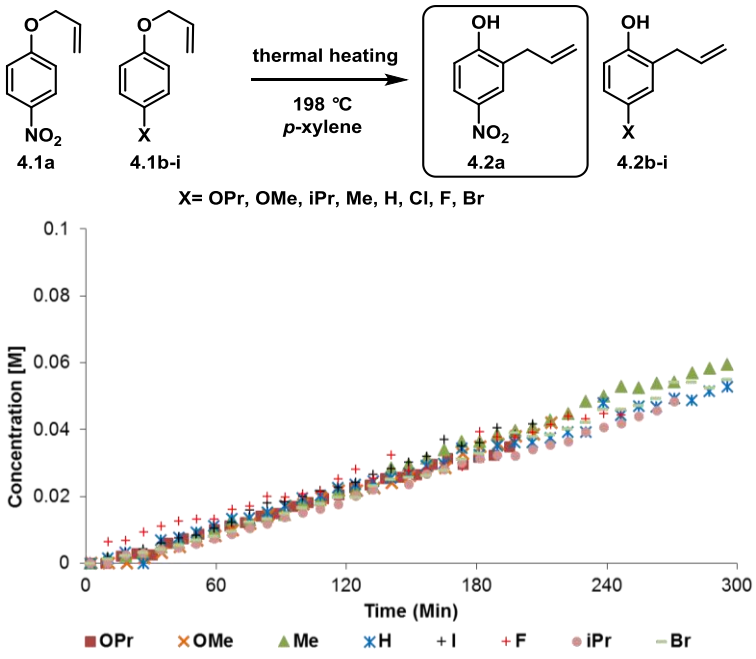

Figure 4.23: Product 4.2a only in dual substrate experiments

4.8 Summary and conclusions

Our automated sampling apparatus allowed us to take thousands of data points from a microwave with a robot with hardly any more work than simply setting up a normal reaction. This is in great contrast to the traditional method of manually taking hundreds of samples and setting up new reactions to avoid discrepancies due to cooling and reheating, which is potentially more susceptible to scatter. The ability to obtain information from the reaction with minimal perturbation has arguably been met by automated sampling, despite the high heat and pressure inside the microwave reactor. Arguably, spectroscopic techniques such as ReactIR would be even less of a disturbance, but the microwave field can potentially damage the probe.

We have concluded from our findings that experiments under constant power mode are difficult to reproduce to a high degree of precision. Even simply heating the same reagents with the same constant power does not provide the same temperature profile. By extension, experiments with the same power setting will not necessarily produce identical temperature profiles, therefore altering reaction conversions. While these results are not surprising, they can be a useful contribution to the microwave chemistry literature, which seems to be viewed with a relatively low degree of trust from the scientific community.

The set of experiments measuring the kinetics of the microwave-assisted vs the thermal Claisen rearrangement of allyl phenyl ethers is possibly the most direct one-to-one comparison between microwave and conventional heating, as the heating vessel, pressure-tight reactor head, fittings, and method of conducting measurements were identical. When LFER experiments were conducted on the Claisen rearrangement in *p*-xylene, the nonlinear results were unexpected. They could potentially be explained by modifying the parameter on which they were used for comparison by excluding most of the inductive effects and including all of the resonance effects.

4.9 Experimental

4.9.1 General procedures

Allyl *p*-nitrophenyl ether was made by a previously published synthetic procedure, except that instead of a cold recrystallization, the product was purified by a pad of silica, eluted with petroleum ether.[113] Allyl *p*-hydroxyphenyl ether was made by a previously published procedure.[114] Allyl *p*-propoxyphenyl ether was made from allyl *p*-hydroxyphenyl ether by a previously published procedure.[115] Other 4-substituted allyl phenyl ethers and their corresponding Claisen rearrangement products were isolated and purified for calibration curves using standard procedures.[116]

Flash chromatography was carried out using Fisher Chemical silica gel 60 Å (230 x 400 mesh). Analytical thin-layer chromatography (TLC) was performed on Sorbtech glass pre-coated silica gel plates and was visualized with UV light. All other materials were purchased from conventional suppliers and used as received.

^{1}H-NMR spectra were recorded on Agilent or Bruker NMR spectrometers (300, 400, 500 MHz). Data for ^{1}H-NMR spectra are listed as follows: chemical shift (δ, ppm), multiplicity, coupling constant (Hz), integration, and are referenced to the residual solvent peak (7.26 ppm for $CDCl_3$). Abbreviations are as follows: s = singlet, d = doublet, t = triplet, q = quartet, p = pentet, m = multiplet. ^{13}C-NMR spectra were recorded on Bruker spectrometers (125 MHz), are listed in terms of chemical shift and are referenced to the residual solvent peak (77.16 for $CDCl_3$).

Microwave experiments were done with a CEM Discover series microwave system in 10 mL quartz vials, unless otherwise noted. A Discover fiber optic probe was used for internal temperature measurements.

4.9.2 Synthetic procedures for allyl phenyl ethers and Claisen products

4.9.2.1 Synthesis of allyl 4-nitrophenyl ether, 4.1a

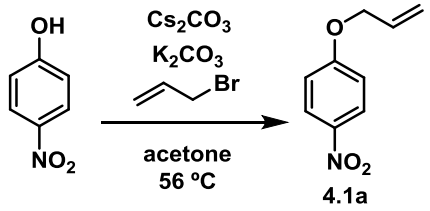

4.1a

4-nitrophenol (8.04 g, 57.8 mmol) was diluted with acetone (263 mL) in a round bottom flask with a stirbar. Potassium carbonate (11.98 g, 87 mmol) and cesium carbonate (38 mg, 0.12 mmol) were added. Allyl bromide (9.0 mL, 104 mmol) was then added. The reaction was heated to reflux overnight. After cooling to room temperature, the reaction mixture was filtered to remove solids. The resulting filtrate was concentrated by rotary evaporation and diluted with brine. The aqueous layer was washed with DCM (3 x 75 mL). The combined organic layers were washed with 0.25% sodium hydroxide solution (3 x 50 mL) and then with water (2 x 50 mL). The organic layer was then dried with Na_2SO_4, filtered, and concentrated by rotary evaporation to a yellow-orange oil. The residue was purified by silica column chromatography with 50:1 Hex:EtOAc and concentrated to provide a yellow oil (9.96 g, 96% yield). ^{1}H NMR (300 MHz, Chloroform-d) δ 8.09 (dd, J = 6.6, 2.8 Hz, 2H), 6.91 (d, J = 9.6 Hz, 1H), 6.20 – 5.93 (m, 1H), 5.73 (s, 1H), 5.39 – 5.25 (m, 1H), 3.50 (d, J = 6.4 Hz, 2H).

4.9.2.2 Synthesis of allyl 4-propoxyphenyl ether, 4.1b

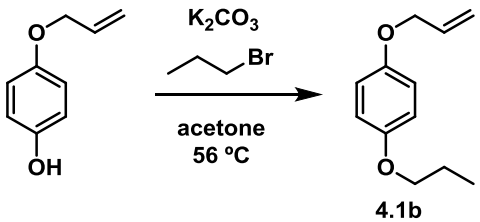

4.1b

4-(allyloxy)phenol (3.27 g, 21.8 mmol) was diluted with acetone (218 mL) in a round bottom flask with a stirbar. Potassium carbonate (6.02 g, 43.6 mmol) was added. 1-bromopropane (65.0 mL, 715 mmol) was then added in three portions. The reaction was heated to reflux for five days. After cooling to room temperature, the reaction mixture was filtered to remove solids. The resulting filtrate was concentrated by rotary evaporation and was combined with the crude product from a previous reaction. The residue was diluted with brine. The aqueous layer was washed with DCM (3 x 40 mL). The organic layer was then dried with Na_2SO_4, filtered, and concentrated by rotary evaporation. The residue was recrystallized with methanol to form white platelets (combined yield of two experiments: 4.65 g, 48.6%).

4.9.2.3 Synthesis of allyl phenyl ether, 4.1c

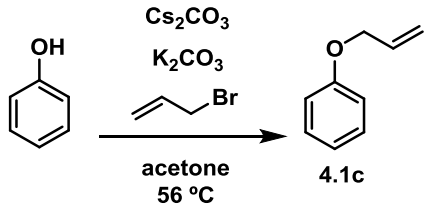

Phenol (6.34 g, 67.4 mmol) was diluted with acetone (306 mL) in a round bottom flask with a stirbar. Potassium carbonate (14.0 g, 101 mmol) and cesium carbonate (44 mg, 0.14 mmol) were added. Allyl bromide (10.5 mL, 121 mmol) was then added. The reaction was heated to reflux overnight. Another dose of cesium carbonate was added (150 mg, 0.48 mmol) was added, and the reaction was heated for an additional two days. After cooling to room temperature, the reaction mixture was filtered to remove solids. The resulting filtrate was concentrated by rotary evaporation and diluted with brine. The aqueous layer was washed with DCM (3 x 50 mL). The combined organic layers were washed with 0.25% sodium hydroxide

solution (3 x 40 mL) and then with water (2 x 40 mL). The organic layer was then dried with Na_2SO_4, filtered, and concentrated by rotary evaporation. The residue was purified by silica column chromatography with 50:1 Hex:EtOAc and concentrated to provide a clear oil, of which the yield was not taken. ^{1}H NMR (400 MHz, Chloroform-*d*) δ 7.43 – 7.19 (m, 2H), 7.01 – 6.82 (m, 3H), 6.25 – 5.87 (m, 1H), 5.42 (dd, J = 17.3, 1.6 Hz, 1H), 5.29 (dd, J = 10.5, 1.4 Hz, 1H), 4.54 (dt, J = 5.3, 1.5 Hz, 2H).

4.9.2.4 Synthesis of allyl 4-chlorophenyl ether, 4.1d

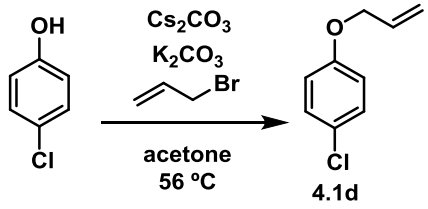

4-chlorophenol (6.25 g, 48.6 mmol) was diluted with acetone (221 mL) in a round bottom flask with a stirbar. Potassium carbonate (12.09 g, 87 mmol) and cesium carbonate (80 mg, 0.24 mmol) were added. Allyl bromide (7.6 mL, 88 mmol) was then added. The reaction was heated to reflux overnight. After cooling to room temperature, the reaction mixture was filtered to remove solids. The resulting filtrate was concentrated by rotary evaporation and diluted with brine. The aqueous layer was washed with DCM (3 x 50 mL). The combined organic layers were washed with 0.25% sodium hydroxide solution (3 x 40 mL) and then with water (2 x 40 mL). The organic layer was then dried with Na_2SO_4, filtered, and concentrated by rotary evaporation. The residue was purified by silica column chromatography with 50:1 Hex:EtOAc and concentrated to provide a clear oil (7.31 g, 89% yield).

4.9.2.5 Synthesis of allyl 4-bromophenyl ether, 4.1e

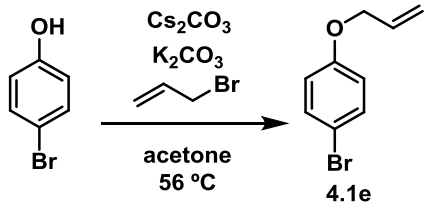

4-bromophenol (4.7 g, 27.2 mmol) was diluted with acetone (123 mL) in a round bottom flask with a stirbar. Potassium carbonate (6.76 g, 48.9 mmol) and cesium carbonate (18 mg, 0.05 mmol) were added. Allyl bromide (4.2 mL, 48.9 mmol) was then added. The reaction was heated to reflux overnight. After cooling to room temperature, the reaction mixture was filtered to remove solids. The resulting filtrate was concentrated by rotary evaporation and diluted with brine. The aqueous layer was washed with DCM (3 x 40 mL). The combined organic layers were washed with 0.25% sodium hydroxide solution (3 x 30 mL) and then with water (2 x 30 mL). The organic layer was then dried with Na_2SO_4, filtered, and concentrated by rotary evaporation. The residue was purified by silica column chromatography with 50:1 Hex:EtOAc and concentrated to provide a clear oil (4.80 g, 83% yield). ^{1}H NMR (300 MHz, Chloroform-*d*) δ 7.44 – 7.30 (m, 2H), 6.89 – 6.69 (m, 2H), 6.19 – 5.89 (m, 1H), 5.53 – 5.18 (m, 2H), 4.51 (dt, J = 5.2, 1.3 Hz, 2H).

4.9.2.6 Synthesis of allyl 4-fluorophenyl ether, 4.1f

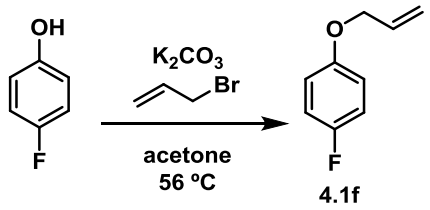

4-fluorophenol (7.5 g, 66.9 mmol) was diluted with acetone 304 mL) in a round bottom flask with a stirbar. Potassium carbonate (16.6 g, 120 mmol) was added. Allyl bromide (11 mL, 127 mmol) was then added. The reaction was heated to reflux overnight. After cooling to room temperature, the reaction mixture was filtered to remove solids. The resulting filtrate was concentrated by rotary evaporation and diluted with brine. The aqueous layer was washed with DCM (3 x 50 mL). The combined organic layers were washed with 0.25% sodium hydroxide solution (3 x 40 mL) and then with water (2 x 30 mL). The organic layer was then dried with Na_2SO_4, filtered, and concentrated by rotary evaporation. The residue was purified by silica column chromatography with 50:1 Hex:EtOAc and concentrated to provide a nearly colorless oil (5.04 g, 50% yield). ^{1}H NMR (300 MHz, Chloroform-*d*) δ 7.14 – 6.67 (m, 4H), 6.23 – 5.90 (m, 1H), 5.41 (dd, J = 17.3, 1.5 Hz, 1H), 5.35 – 5.14 (m, 1H), 4.50 (d, J = 5.3 Hz, 2H).

4.9.2.7 Synthesis of allyl 4-methylphenyl ether, 4.1g

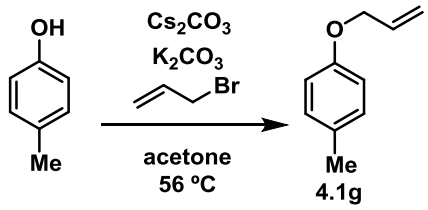

4-methylphenol (6.59 g, 60.9 mmol) was diluted with acetone (277 mL) in a round bottom flask with a stirbar. Potassium carbonate (15.2 g, 110 mmol) and cesium carbonate (40 mg, 0.12 mmol) were added. Allyl bromide (9.5 mL, 110 mmol) was then added. The reaction was heated to reflux overnight. Another dose of allyl bromide was added (4.0 mL, 46.3 mmol) was added the next day, and the reaction continued to be heated for another day. After cooling to room temperature, the reaction mixture was filtered to remove solids. The resulting filtrate was

concentrated by rotary evaporation and diluted with brine. The aqueous layer was washed with DCM (3 x 60 mL). The combined organic layers were washed with 0.25% sodium hydroxide solution (3 x 50 mL) and then with water (2 x 50 mL). The organic layer was then dried with Na_2SO_4, filtered, and concentrated by rotary evaporation. The residue was purified by silica column chromatography with 50:1 Hex:EtOAc and concentrated to provide a pale yellow oil (7.69 g, 85% yield). ^{1}H NMR (400 MHz, Chloroform-*d*) δ 7.08 (d, J = 8.4 Hz, 2H), 6.94 – 6.66 (m, 2H), 6.22 – 5.88 (m, 1H), 5.40 (dq, J = 17.3, 1.5 Hz, 1H), 5.27 (dq, J = 10.5, 1.3 Hz, 1H), 4.51 (dt, J = 5.3, 1.5 Hz, 2H), 2.28 (s, 3H).

4.9.2.8 Synthesis of allyl 4-isopropylphenyl ether, 4.1h

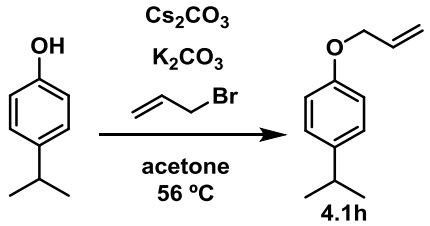

4-isopropylphenol (7.00 g, 51.4 mmol) was diluted with acetone (234 mL) in a round bottom flask with a stirbar. Potassium carbonate (12.8 g, 93 mmol) and cesium carbonate (16 mg, 0.05 mmol) were added. Allyl bromide (8.0 mL, 93 mmol) was then added. The reaction was heated to reflux for two days. After cooling to room temperature, the reaction mixture was filtered to remove solids. The resulting filtrate was concentrated by rotary evaporation and diluted with brine. The aqueous layer was washed with DCM (3 x 60 mL). The combined organic layers were washed with 0.25% sodium hydroxide solution (3 x 50 mL) and then with water (2 x 50 mL). The organic layer was then dried with Na_2SO_4, filtered, and concentrated by rotary evaporation. The residue was purified by silica column chromatography with 50:1 Hex:EtOAc and concentrated to provide a pale yellow oil (8.30 g, 92% yield). ^{1}H NMR (300

MHz, Chloroform-*d*) δ 7.14 (d, J = 8.6 Hz, 2H), 6.86 (d, J = 8.6 Hz, 2H), 6.07 (ddd, J = 22.5, 10.5, 5.3 Hz, 1H), 5.41 (dd, J = 17.3, 1.5 Hz, 1H), 5.35 – 5.16 (m, 1H), 4.70 – 4.35 (m, 2H), 2.86 (p, J = 6.9 Hz, 1H), 1.23 (d, J = 6.9 Hz, 6H).

4.9.2.9 Synthesis of 2-allyl-4-nitrophenol, 4.2a

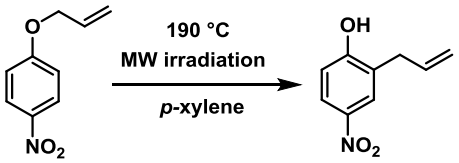

4.1a 4.2a

This purification was done on many combined microwave reactions. The reaction solution was reduced in volume by a stream of air and by rotary evaporation. The residue was purified by silica column chromatography with 100% hexanes to 8:1 Hex:EtOAc and concentrated to provide a yellow-orange solid. ^{1}H NMR (300 MHz, Chloroform-d) δ 8.09 (dd, J = 6.6, 2.8 Hz, 2H), 6.91 (d, J = 9.6 Hz, 1H), 6.20 – 5.93 (m, 1H), 5.73 (s, 1H), 5.39 – 5.25 (m, 1H), 3.50 (d, J = 6.4 Hz, 2H).

4.9.2.10 Synthesis of 2-allyl-4-propoxyphenol, 4.2b

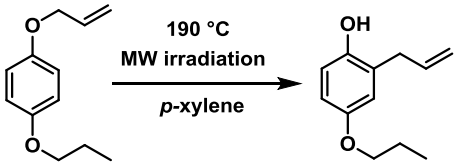

4.1b 4.2b

This purification was done on many combined microwave reactions. The reaction solution was reduced in volume by a stream of air and by rotary evaporation. The residue was purified by silica column chromatography with 100% hexanes to 40:1 Hex:EtOAc and

concentrated to provide a light yellow solid. ^{1}H NMR (400 MHz, Chloroform-d) δ 6.81 – 6.57 (m, 2H), 6.00 (dd, J = 17.6, 9.7 Hz, 1H), 5.25 – 5.02 (m, 2H), 4.57 (s, 1H), 3.86 (t, J = 6.6 Hz, 2H), 3.37 (d, J = 6.3 Hz, 2H), 1.77 (q, J = 6.8 Hz, 2H), 1.02 (d, J = 14.8 Hz, 2H). ^{13}C NMR (101 MHz, $CDCl_3$) δ 153.32, 147.83, 136.18, 126.31, 116.69, 116.53, 116.44, 113.33, 109.99, 77.31, 76.99, 76.68, 70.09, 35.35, 22.69, 10.53.

4.9.2.11 Synthesis of 2-allyl-phenol, 4.2c

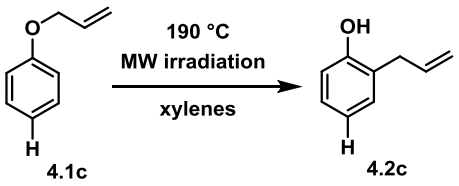

Allyl phenyl ether (0.61 g, 4.51 mmol) was diluted with xylenes (2.5 mL) in a borosilicate Biotage microwave vial with a stirbar. It was heated at a constant 200 °C for ten hours in a Biotage microwave reactor. The reaction solution was then reduced in volume by a stream of air. The residue was purified by silica column chromatography with 100% pet ether to 20:1 pet ether:EtOAc and concentrated to provide a pale yellow-orange oil (0.10 g, 16.3% yield). ^{1}H NMR (300 MHz, Chloroform-d) δ 7.22 – 7.01 (m, 2H), 7.01 – 6.71 (m, 2H), 5.98 (s, 1H), 5.33 – 5.04 (m, 2H), 4.91 (s, 1H), 3.42 (d, J = 6.3 Hz, 2H).

4.9.2.12 Synthesis of 2-allyl-4-chlorophenol, 4.2d

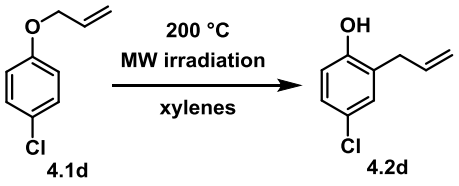

Allyl 4-chlorophenyl ether (0.40 g, 2.34 mmol) was diluted with xylenes (3.0 mL) in a borosilicate Biotage microwave vial with a stirbar. It was heated at a constant 200 °C for eight hours in a Biotage microwave reactor. The reaction solution was then reduced in volume by a stream of air. The residue was purified by silica column chromatography with pet ether to 35:1 pet ether:EtOAc and concentrated to provide a pale yellow oil (0.14 g, 35.2% yield). ^{1}H NMR (300 MHz, Chloroform-d) δ 7.08 (dd, J = 6.3, 2.6 Hz, 2H), 6.86 – 6.61 (m, 1H), 6.16 – 5.78 (m, 1H), 5.38 – 5.04 (m, 2H), 4.91 (s, 1H), 3.37 (d, J = 6.3 Hz, 2H).

4.9.2.13 Synthesis of 2-allyl-4-bromophenol, 4.2e

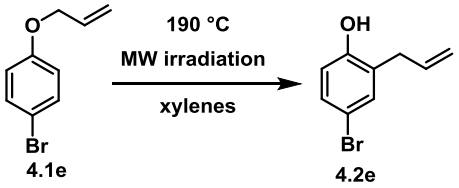

Allyl 4-bromophenyl ether (0.48 g, 2.3 mmol) was diluted with xylenes (3.0 mL) in a borosilicate Biotage microwave vial with a stirbar. It was heated at a constant 190 °C for eight hours in a Biotage microwave reactor. The reaction solution was then reduced in volume by a stream of air. The residue was purified by silica column chromatography with 40:1 pet ether :EtOAc and concentrated to provide a pale orange oil (0.26 g, 53.9% yield). ^{1}H NMR (300 MHz, Chloroform-d) δ 7.26 (dd, J = 7.7, 5.2 Hz, 3H), 6.84 – 6.63 (m, 1H), 6.14 – 5.86 (m, 1H), 5.30 – 5.09 (m, 2H), 4.93 (s, 1H), 3.40 (d, J = 6.3 Hz, 2H).

4.9.2.14 Synthesis of 2-allyl-4-fluorophenol, 4.2f

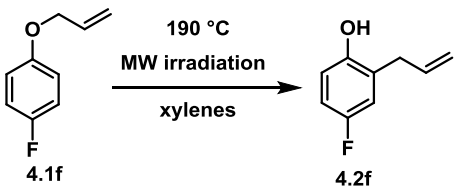

Allyl 4-fluorophenyl ether (0.48 g, 3.1 mmol) was diluted with xylenes (3.0 mL) in a borosilicate Biotage microwave vial with a stirbar. It was heated at a constant 190 °C for eight hours in a Biotage microwave reactor. The reaction solution was then reduced in volume by a stream of air. The residue was purified by silica column chromatography with 40:1 to 35:1 pet ether :EtOAc and concentrated to provide a volatile pale yellow oil (0.31 g, 66% yield). ^{1}H NMR (300 MHz, Chloroform-*d*) δ 6.93 – 6.59 (m, 3H), 6.15 – 5.82 (m, 1H), 5.29 – 5.05 (m, 2H), 4.72 (s, 1H), 3.38 (d, J = 6.3 Hz, 2H).

4.9.2.15 Synthesis of 2-allyl-4-methylphenol, 4.2g

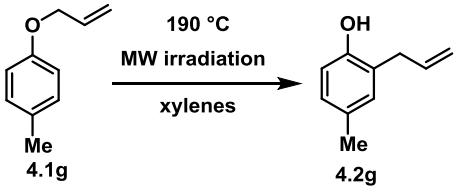

Allyl 4-methylphenyl ether (0.49 g, 3.3 mmol) was diluted with xylenes (2.5 mL) in a borosilicate Biotage microwave vial with a stirbar. It was heated at a constant 190 °C for ten hours in a Biotage microwave reactor. The residue was purified by silica column chromatography with 40:1 to 8:1 pet ether: EtOAc and concentrated to provide a pale yellow oil (0.31 g, 63.7% yield). ^{1}H NMR (300 MHz, Chloroform-d) δ 6.93 (d, J = 7.4 Hz, 2H), 6.71 (d, J = 8.0 Hz, 1H), 6.20 – 5.85 (m, 1H), 5.18 (dt, J = 4.8, 1.6 Hz, 1H), 5.13 (t, J = 1.5 Hz, 1H), 4.74 (s, 1H), 3.38 (d, J = 6.3 Hz, 2H), 2.26 (s, 3H).

4.9.2.16 Synthesis of 2-allyl-4-isopropylphenol, 4.2h

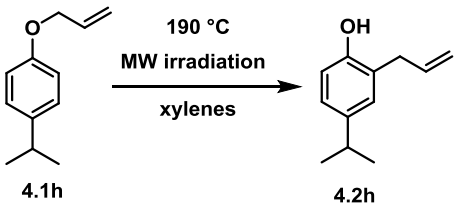

Allyl 4-isoproylphenyl ether (0.44 g, 2.5 mmol) was diluted with xylenes (3.5 mL) in a borosilicate Biotage microwave vial with a stirbar. It was heated at a constant 190 °C for eight hours in a Biotage microwave reactor. The solution was concentrated by a stream of air. The residue was purified by silica column chromatography with 50:1 pet ether: EtOAc and concentrated to provide a light beige oil (0.10 g, 21.9% yield). ^{1}H NMR (300 MHz, Chloroform-d) δ 7.10 – 6.89 (m, 2H), 6.75 (d, J = 8.1 Hz, 1H), 6.03 (dd, J = 16.9, 10.3 Hz, 1H), 5.30 – 5.08 (m, 2H), 4.77 (s, 1H), 3.40 (d, J = 6.4 Hz, 2H), 2.95 – 2.71 (m, 1H), 1.22 (d, J = 6.9 Hz, 6H).

4.9.2.17 Synthesis of 2-allyl-4-methoxyphenol, 4.2i

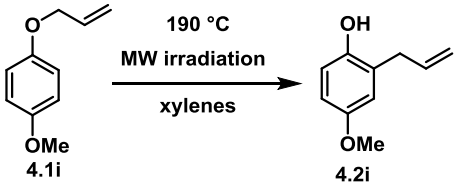

Allyl 4-methoxyphenyl ether (0.51 g, 3.1 mmol) was diluted with xylenes (2.5 mL) in a borosilicate Biotage microwave vial with a stirbar. It was heated at a constant 190 °C for ten hours in a Biotage microwave reactor. The reaction solution was then reduced in volume by a stream of air. The residue was purified by silica column chromatography with 100% pet ether to 30:1 pet ether:EtOAc and concentrated to provide a pale yellow oil (0.34 g, 66% yield). ^{1}H NMR (300 MHz, Chloroform-d) δ 6.72 (ddd, J = 20.4, 6.1, 3.5 Hz, 3H), 6.13 – 5.89 (m, 1H), 5.16 (ddd, J = 13.7, 3.7, 1.8 Hz, 2H), 4.58 (s, 1H), 3.76 (s, 3H), 3.38 (d, J = 6.3 Hz, 2H).

4.9.3 Automated reaction monitoring from the microwave reactor or sand bath

A programmable syringe pump was used to withdraw samples from the reaction and into a sample loop on a Gilson Injection Valve Actuator 819 (rheodyne), which is triggered by the syringe pump. This sample is then diluted with methanol through the sample loop into an empty

LC vial by the Gilson 215 Liquid Handler. The internal temperature of the reaction was monitored by a Discover fiber optic probe and recorded by the CEM Microwave software. The microwave reactor head and plates can be lifted from the microwave and placed into a sand bath for the corresponding conventional heating experiment.

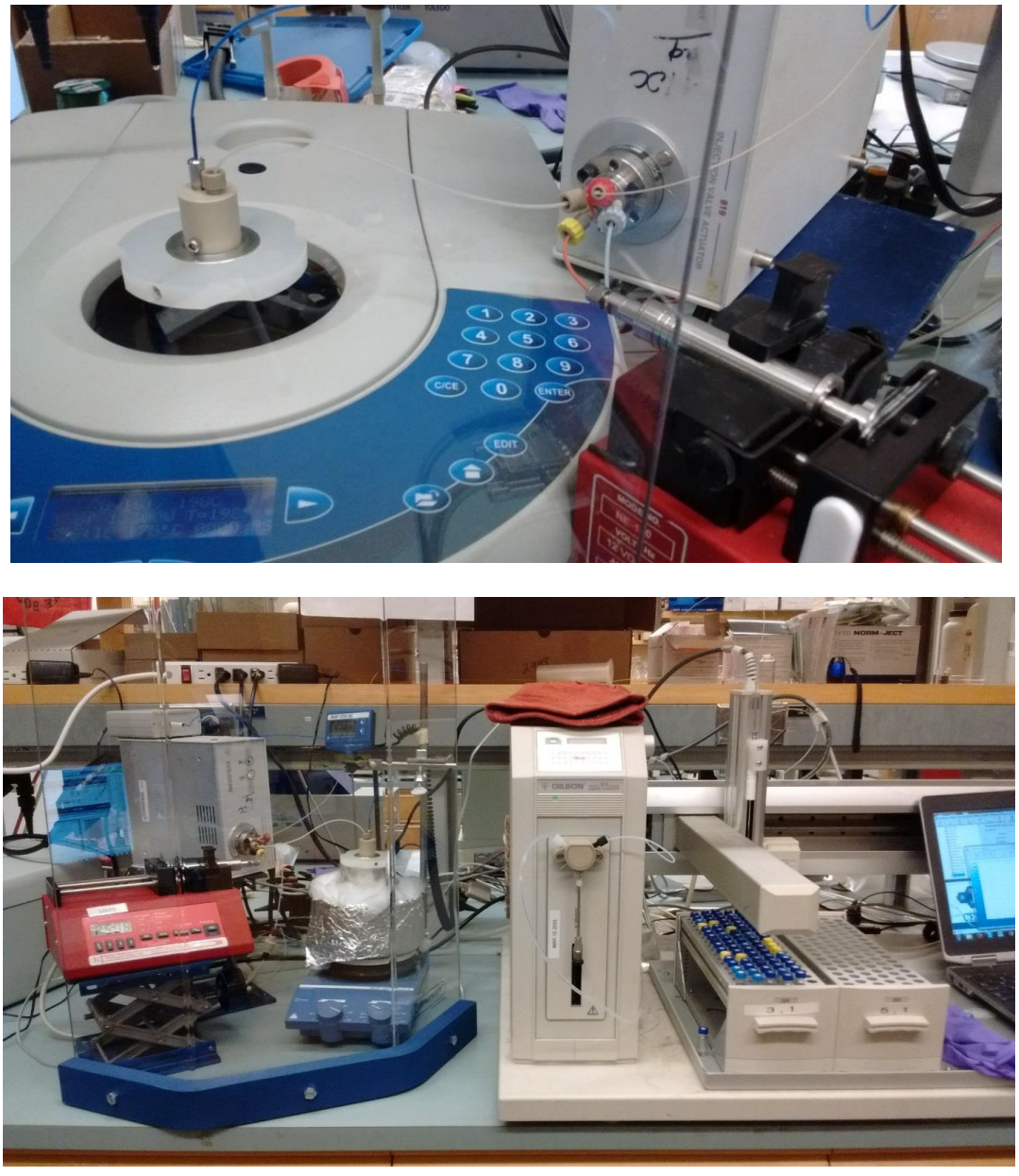

Figure 4.24: Set up for automated reaction monitoring from a microwave reactor

Figure 4.25: Set up for automated reaction monitoring from a sand bath

4.9.3.1 General procedure for kinetic profiling from a microwave reactor

To a 10 mL quartz tube with a flea stirbar, a 0.5 M stock solution of allyl *p*-nitrophenyl ether **4.1a** was diluted until it reached the desired concentration such that the total volume was 4.4 mL. The reactor head is screwed into the vial after the vial is placed into the microwave cavity. The fiber optic temperature probe is inserted into the thermowell screwed into the reactor head. The sampling tubing from the modified microwave head is connected to the rheodyne. The appropriate tubing is connected between the reactor head, rheodyne, and programmable syringe pump. The rheodyne is also connected to a programmable liquid handler, the Gilson 215. The microwave is programmed with a specific experiment (constant power, constant temperature, or cycles of power phases) that is started. The automated sampling apparatus is started after the

internal temperature reaches at least 165 °C. Samples of a predetermined frequency were taken, diluted with 450 µL methanol by the liquid handler, and collected for offline analysis by HPLC during or after the experiment was finished. 20 µL samples were withdrawn at a rate of 200 mL/min by the syringe pump.

4.9.3.2 General procedure for kinetic profiling from a sand bath

The same procedure for sampling from the microwave reactor was used, except for the following changes: A large sand bath was preheated to a much higher temperature with the hotplate's thermocouple. The same microwave head and screw plates were taken out of the microwave reactor and used for the same quartz vial. When the sand bath was hot enough, the pre-screwed vial was submersed into the sand with the fiber optic temperature probe inside the vial. The temperature of the externally sand bath was controlled manually to adjust for changes in the internal temperature reading throughout the reaction.

4.9.4 Pulsed power experiments

The pulsed power experiments had the following phases on the CEM microwave:

12 min: 200 W
2 min: 0 W
12 min: 200 W
2 min: 0 W

This cycle was repeated ten times. The first sample was taken at 1 minute, and 55 samples were taken.

The average temperature was computed for a) the entire experiment and b) only when the microwave was on. Another experiment with the microwave power always on and an average temperature of b) was run afterward with the same sampling frequency.

4.9.5 LFER experiments

The appropriate 4-substituted allyl phenylether was weighed into a 1 mL volumetric flask, which was then transferred quantitatively into the reaction vial and diluted into 2.2 mL of *p*-xylene. The allyl *p*-nitrophenyl ether was added via a stock solution to make a 4.4 mL solution, 0.2 M in each allyl phenylether. Reactions were run at 193 °C.

4.9.6 Calibration curves and HPLC Methods

For conditions utilizing HPLC, the instrument was an Agilent Infinity series 1260. For conditions utilizing UHPLC, the instrument was an Agilent Infinity series 1290. For all methods:
Solvent A= water + 0.05% TFA, Solvent B = acetonitrile with 0.05% TFA
Temperature: 30 °C
X= NO_2
HPLC
Column: Poroshell EC-C18, 2.1 x 30 mm, 2.7 µm
Method: Initial B=20%; 0.1 min, 40% B; 2.5 min, 55% B; 3.4-4.0 min, 100% B.
Flow rate: 0.625 mL/min

Calibration curves for competition experiments analyzed by HPLC were created by using individual stock solutions of known amounts of both starting materials and their corresponding isolated products (X= NO_2 and X= other substituent) and p xylene. Varying amounts of each stock solution were allocated into LC vials and diluted with known amounts of methanol. These LC vials were analyzed by the HPLC method corresponding to the mixture. The extinction coefficients relative to p-xylene were then used to assess the concentrations of each starting material and product during a reaction.

The remaining HPLC methods were made for the purpose of separating mixtures of *p*-xylene, substrates and products for both the Claisen rearrangement of the compound of interest and for X=NO_2.

X= Me

HPLC

Column: Poroshell SB-C18, 2.1 x 30 mm, 2.7 µm

Method: Initial B=20%; 0.1-0.5 min, 33% B; 1.0 min, 34% B; 3.8 min, 39% B; 4.6-6.0 min, 75% B.

Flow rate: 0.625 mL/min

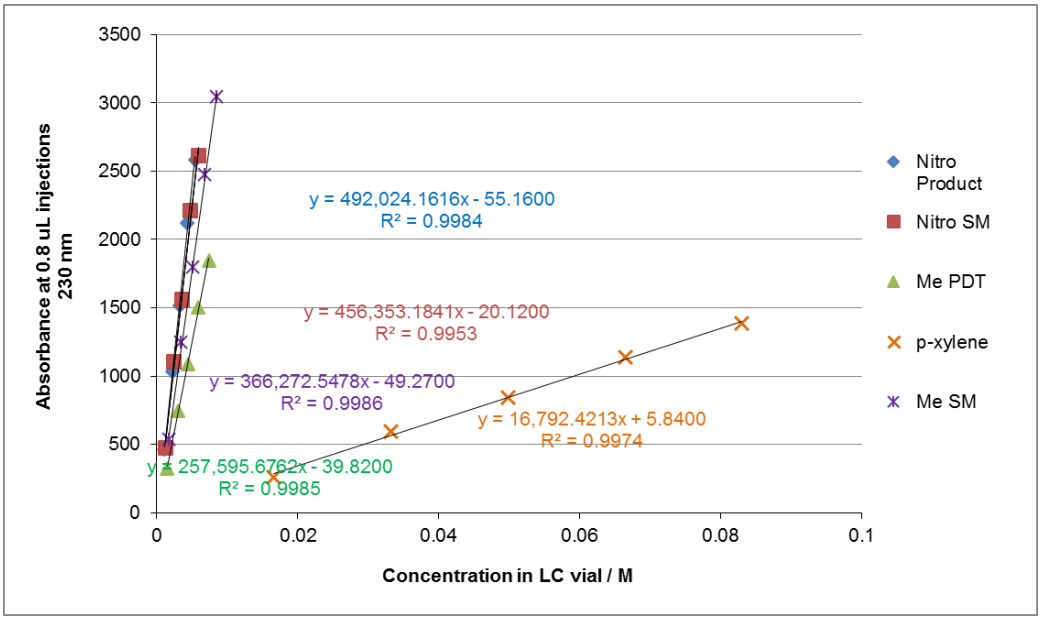

Figure 4.26: Calibration curve for X=Me and X=NO_2

X= OMe,

HPLC

Column: Poroshell EC-C18, 2.1 x 30 mm, 2.7 µm

Initial B=20%; 0.1-0.5 min, 33% B; 1.0 min, 34% B; 3.8 min, 39% B; 4.6-5.8 min, 75% B.

Flow rate: 0.625 mL/min

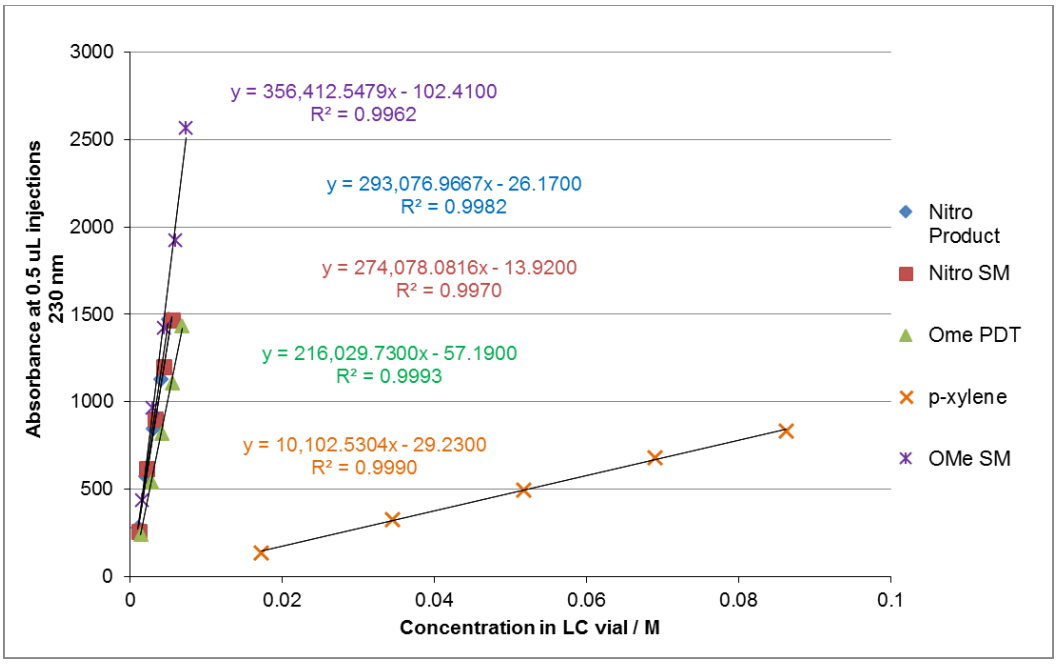

Figure 4.27: Calibration curve for X=OMe and X=NO_2

X= OPr

HPLC

Column: Poroshell EC-C18, 2.1 x 30 mm, 2.7 µm

Method: Initial B=20%; 0.1-0.5 min, 33% B; 1.0 min, 34% B; 3.8 min, 39% B; 4.6-6.60 min, 75% B.

Flow rate: 0.625 mL/min

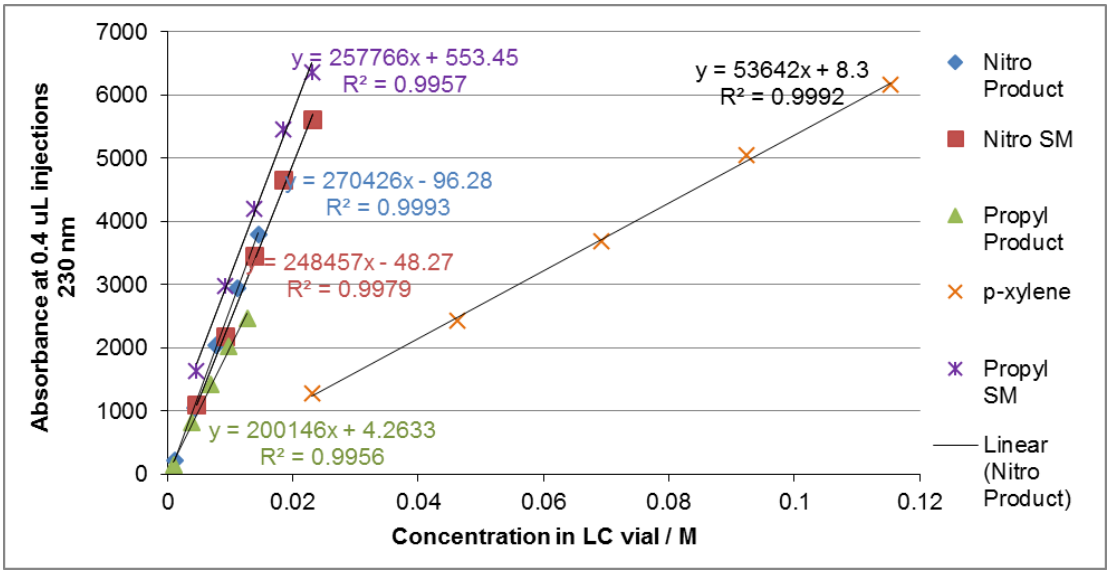

Figure 4.28: Calibration curve for X=OPr and X=NO_2

X= Br

HPLC

Column: Poroshell EC-C18, 2.1 x 30 mm, 2.7 µm

Method: Initial B=20%; 0.1 min, 30% B; 4.0-5.5 min, 53% B.

Flow rate: 0.650 mL/min

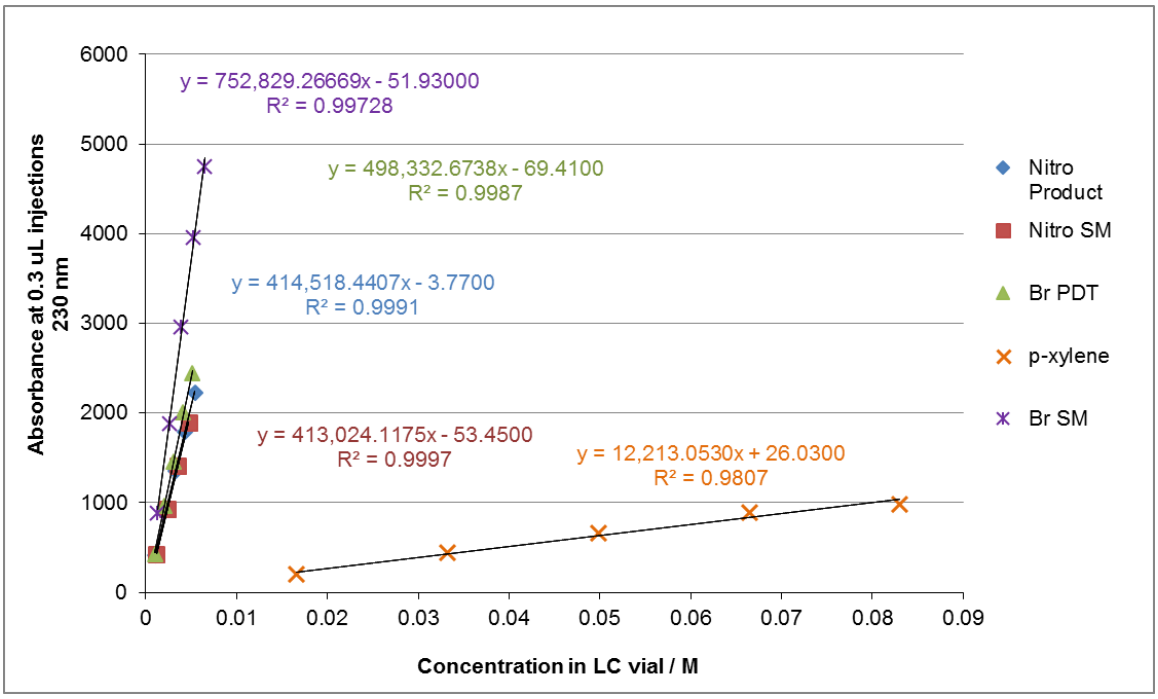

Figure 4.29: Calibration curve for X=Br and X=NO_2

X=iPr

HPLC

Column: Poroshell EC-C18, 2.1 x 30 mm, 2.7 µm

Method: Initial B=20%; 2.7 min, 43% B; 3.5 min, 43% B; 5.3 min, 46% B; 7.0-9.0 min, 95%.

Flow rate: 0.625 mL/min

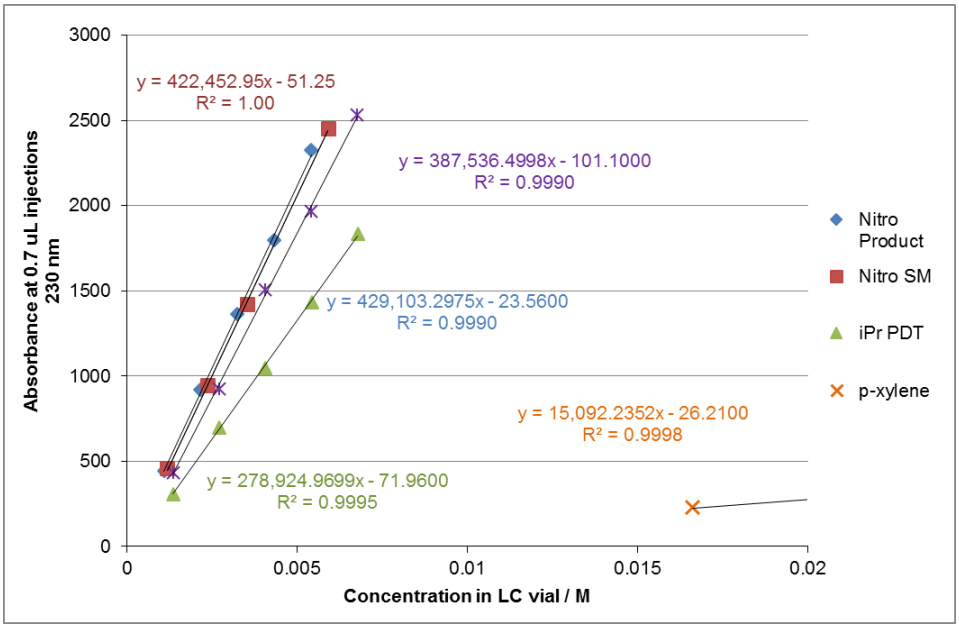

Figure 4.30: Calibration curve for X=iPr and X=NO_2

H Method 1

X= H

HPLC

Column: Poroshell SB-C18, 2.1 x 30 mm, 2.7 µm

Method: Initial B=10%; 0.1 min, 24% B; 5.0 min, 32% B; 5.5-7.5 min, 50% B.

Flow rate: 0.650 mL/min

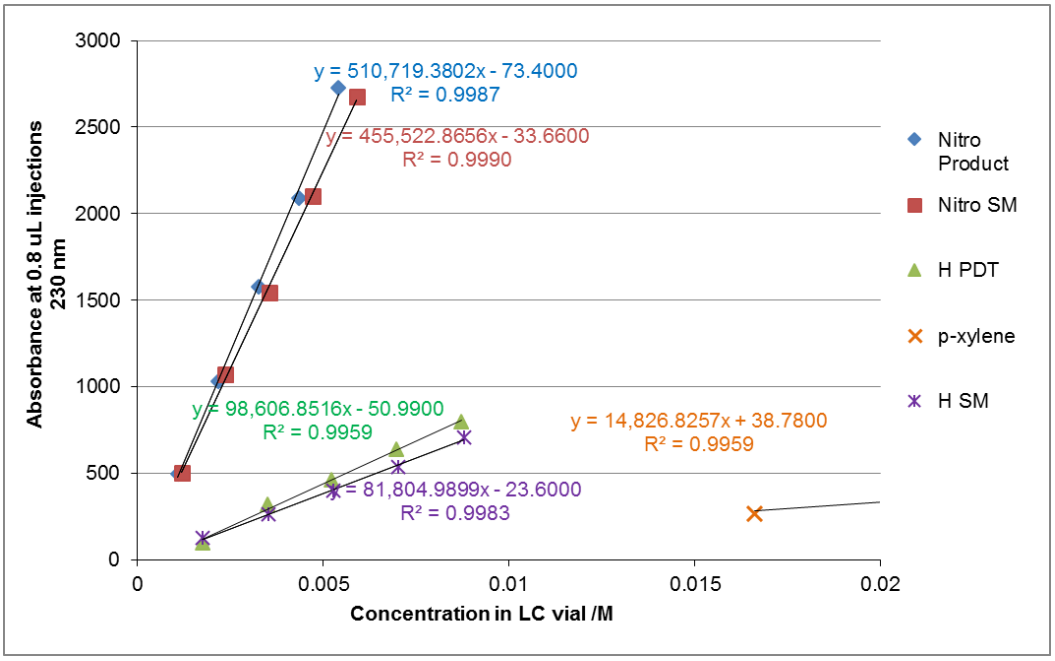

Figure 4.31: Calibration curve for X=H and X=NO_2 for method 1

Or H Method 2

UHPLC

Column: Poroshell SB-C18, 2.1 x 30 mm, 2.7 µm

Method: Initial B=10%; 0.1 min, 24% B; 5.1 min, 29% B; 5.5 min, 30% B; 6.0-7.0 min, 50% B.

Flow rate: 0.700 mL/min

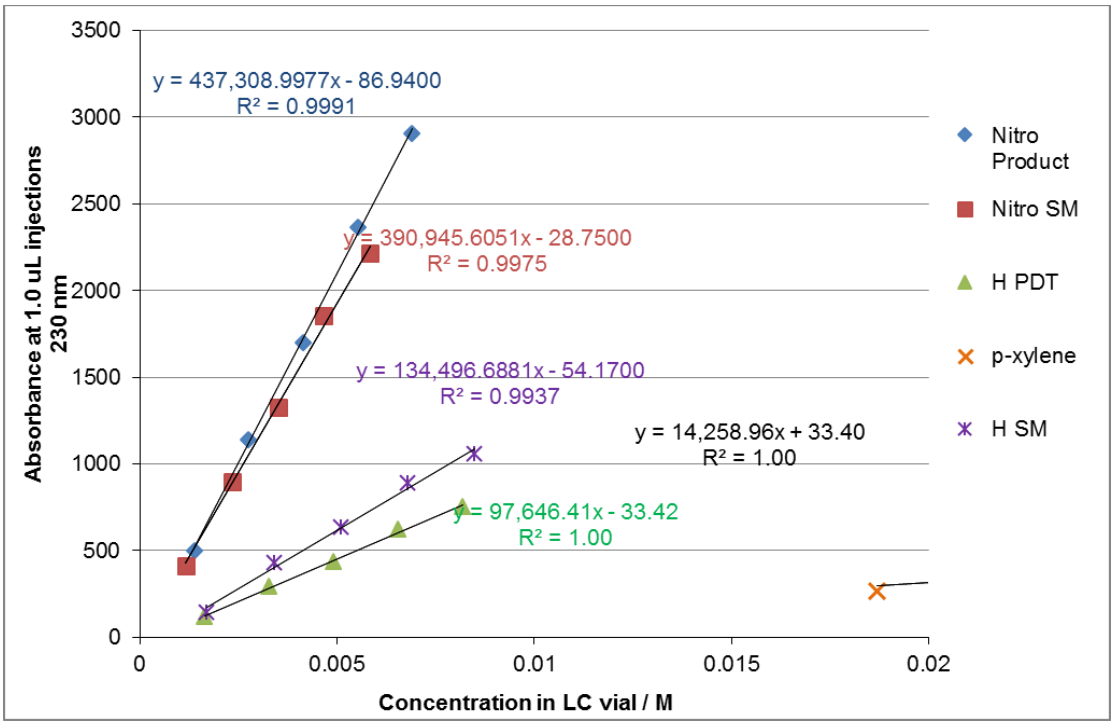

Figure 4.32: Calibration curve for X=H and X=NO_2 for method 2

X= Cl

UHPLC

Column: Poroshell EC-C18, 2.1 x 30 mm, 2.7 µm

Method: Initial B=27%; 0.0-3.8 min, 27% B; 5.0 min, 33% B; 6.0-6.7 min, 65% B.

Flow rate: 0.700 mL/min

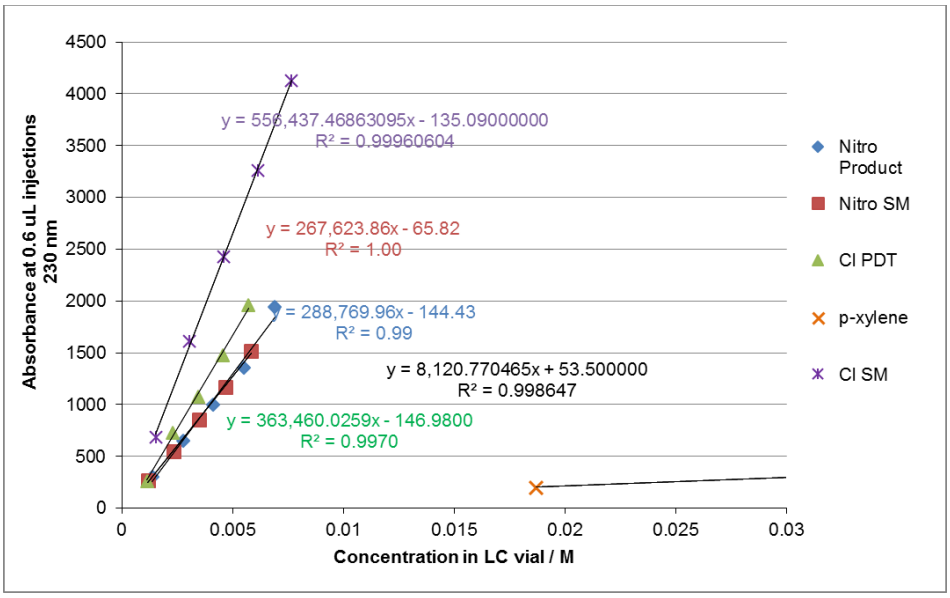

Figure 4.33: Calibration curve for X=Cl and X=NO_2

X= F

UHPLC

Column: Poroshell SB-C18, 2.1 x 30 mm, 2.7 µm

Method: Initial B=15%; 0.1 min, 20% B; 2.7-4.4 min, 28% B; 4.9 min, 35% B; 5.2 min, 40% B; 6.0-6.1 min, 55% B.

Flow rate: 0.800 mL/min

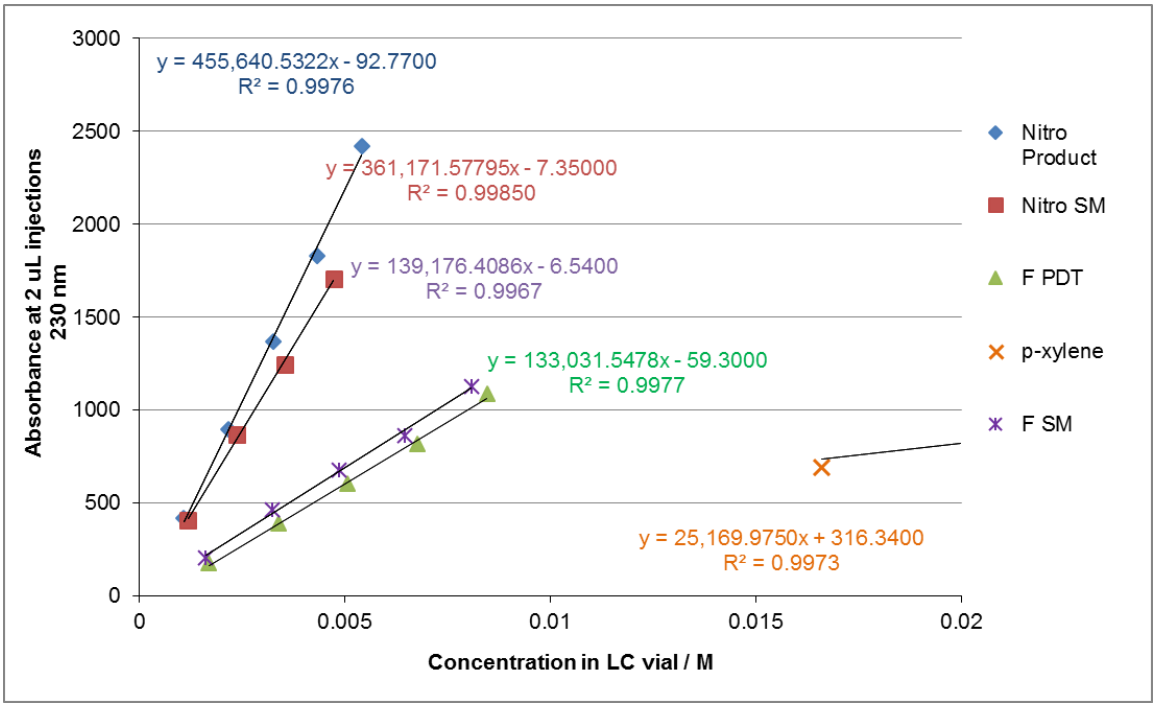

Figure 4.34: Calibration curve for X=F and X=NO_2

Chapter 5: Future Work

5.1 Further studies on the Aza-Piancatelli rearrangement

Although the studies on how using NaBARF as a co-catalyst were cut short, the room temperature Aza-Piancatelli rearrangement potentially opens up many new avenues. Expansion to substrates that still do not work well (external alcohols, alkylamines, unprotected hydroxylamines) may be possible with the new catalyst/co-catalyst system. The lower temperature required for the reaction could potentially aid in the efforts to create an asymmetric rearrangement, as it has not been confirmed whether the higher reaction temperatures made high enantioselectivities difficult to achieve.

The previous efforts in expanding the utility of the Aza-Piancatelli rearrangement based on the addition of NaBARF could include mechanistic studies. The identity of the active metal catalyst may have changed, therefore potentially changing the selectivity and reactivity. Flame atomic absorption spectroscopy (FAAS) could be used to analyze of the remaining precipitate from the reaction to see if it can provide any clues about the reaction between $Dy(OTf)_3$ and NaBARF.

While the Aza-Piancatelli rearrangement at 60 °C did not provide a meaningful profile in heat-flow calorimetry, the room temperature, the NaBARF-cocatalyzed reaction could be potentially evaluated by heat-flow calorimetry. Even if the heat produced does not correspond to product formation, it may correlate with precipitation or dissolution. An unrelated heterogenous reaction conducted with a scandium catalyst and NaBARF cocatalyst system has been successfully studied on the heat-flow calorimeter in our lab, with heat flow corresponding to the rate of product formation. Another reaction monitoring technique can be used to track concentrations of penitent species in tandem, such as ReactIR or sampling with HPLC-MS.

Future directions on the Aza-Piancatelli rearrangement currently focus on a collaboration on a medicinal chemistry project with Pfizer. Aminocarbinol **5.1** currently requires a 10-15 step synthesis to provide the desired stereochemistry and arrangement of functional groups. When the Aza-Piancatelli rearrangement was introduced to them, it was suggested that conversion of cyclopentenone **5.2** could be a much more direct path to forming aminocarbinol **5.1** (Scheme 5.1). Hence, instead of aryl-substituted furans, the reaction will start with a methyl-substituted furan. The appropriate nitrogen nucleophile needs to be optimized to allow both 1) rearrangement to the cyclopentenone and 2) facile deprotection to provide the free amine, as some N-nucleophiles have been surprisingly difficult to reduce and cleave.[63]

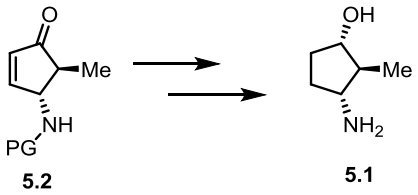

5.2 **5.1**

Scheme 5.1: Aza-Piancatelli product can be used as a scaffold for an aminocarbinol

5.2 Further studies on the Kinugasa reaction

Future work will continuing monitoring the Kinugasa reaction through direct-injection into the HPLC-MS to give more information on how chemoselectivity between the β-lactam and amide products changes for different conditions and substrates. While my studies were limited to the phenyl, phenyl substituted nitrone, graduate student Tom Malig will expand mechanistic studies to a variety of nitrones, including cyclic nitrones (Scheme 5.2). The mechanistic studies need to be expanded to different substrates to see if our general conclusions still hold true.

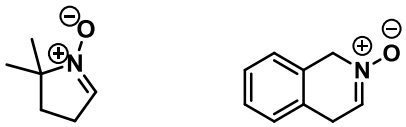

Scheme 5.2: Examples of cyclic nitrones for future experiments

In particular, the finding that room-temperature, catalytic conditions provided the amide is an unusual find. While there are many methods of forming amides, most start from the amine and a carbonyl, whether it be a carboxylic acid or an acyl chloride. Reactions starting with an alkyne and amide to make the amide are relatively scarce. Often, the alkyne must first be oxidized to the carboxylic acid (via a hypervalent iodine agent). The coupling of an alkyne with an amine to make an amide has been previously accomplished with heating with molecular oxygen or with coated solid supports.[117,118]

Presumably, in our findings, the oxygen atom in the amide originates from the nitrone. The finding that under Kinugasa reaction conditions, an alkyne can be oxidized and couple to the amine, means that the same transformation can occur under extremely mild and catalytic conditions, using an oxygen source that isn't molecular oxygen. Of course, the use of a nitrone as an oxygen source has poor atom economy. Hence, we envision that similar transformations would occur with a lower molecular weight oxygen transfer reagent. If we are able to drive the reaction away from the lactam product, and use a cheap, low molecular weight oxygen source, then we could invent a room temperature coupling that requires no handling of oxygen or carbon monoxide. It would be of interest to explore how tolerant the reaction is to different kinds of nitrogen nucleophiles, or if varying conditions could alter the selectivity for different nucleophiles.

Nearly all the kinetic experiments from this chapter were monitored by manual sampling, which allowed for data with moderate to large amounts of scattering. The new apparatus

allowing direct injection into the HPLC will allow future reaction monitoring to be done with much less effort for higher-quality, more resolved data. Unfortunately, the current apparatus only allows one reaction to be monitored at a time, whereas manually sampling from multiple reactions is only limited by the user. Using a robotic liquid handler to automatically sample out of multiple reactions would be a compromise: multiple reactions can be monitored simultaneously, but direct injection of multiple reactions into the HPLC is not yet possible.

In addition, it would be worthwhile to monitor the enantioselectivity of an asymmetric Kinugasa reaction with time. As Fu reported, the enantioselectivity of the product seems to decrease with higher yield.[88] It is unclear whether the selectivity of the catalyst system is eroded with time, or if the stereochemistry of the product is changing with time (which is possible for de but unlikely with ee), or if the enantioselectivity is locked in after the initial cycloaddition.

5.3 Kinetic studies of different reactions in the microwave reactor

A variety of thermally-promoted homogeneous reactions could be studied in the microwave reactor using the automated sampling system. While studying the kinetics and mechanisms of reactions run in the microwave and comparing them to conventionally heated reactions may be worthwhile, the experimenter must be prepared for the very likely possibility that there is little to no difference between the heating methods when the internal temperatures are truly kept the same. Rather, it could be more interesting to ascertain whether the chemoselectivity of reactions forming multiple products remains the same between the two heating modes. For example, if the power output is varied throughout the reaction with a reprogramed profile, but the average temperature is kept the same as measured in a conventionally heated reaction, are the conversion and chemoselectivity always the same? In

particular, if the microwave power output can be cycled on and off, this could avoid the formation of potential undesirable side products. Such repeated cooling and reheating could be more difficult to reproduce using conventional heating.

An example of a reaction that shows surprising acceleration of product formation and similar selectivity is the Heck reaction shown in Scheme 5.3. It seems inconceivable that the microwave can provide the same yield in only three minutes when conventional heating requires twenty hours.[119] Modifying the conditions in order to get more reaction progress (for a slower reaction than three minutes) may help explain such a large thermal microwave effect.

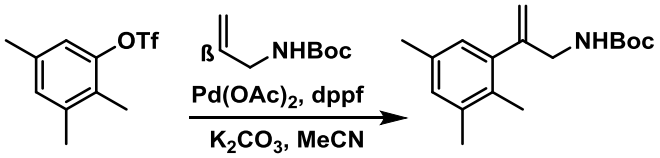

Heating method, conditions	Yield %	Selectivity β/γ of product
Thermal: 20 h, 80 °C	68	99.5 / 0.5
Microwave: 3 min, 20 W	68	98 / 2

Scheme 5.3: Heck reaction with an accelerating microwave effect

It would also be interesting to monitor enantioselectivity. A reaction that may show interesting results is showing the racemization of *atropo*-enantiomers of the biaryl lactones shown in Scheme 5.4. Only the enantiomer shown can react under the provided reducing conditions, whereas microwave irradiation can cause the enantioenriched lactone to racemize.[120]

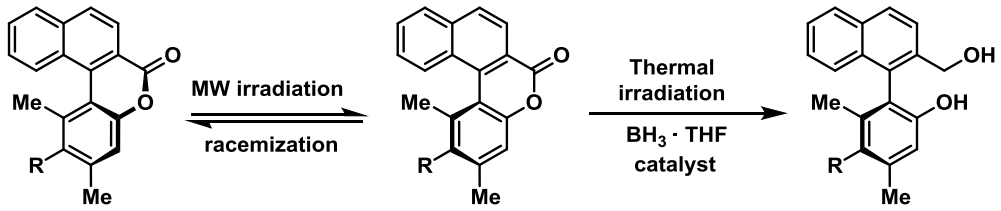

Scheme 5.4: Ring-opening and racemization of biaryl lactones

Our lab has since bought an adaptation of the microwave head to allow reactions to be done in flow for the Discover microwave system. This would be useful for looking at reactions with the ReactIR flow cell or other FTIR instruments that can be fitted with a flow attachment.

References

(1) Susanne, F.; Smith, D. S.; Codina, A. *Org. Process Res. Dev.* **2012**, *16* (1), 61–64.

(2) Smallcombe, S. H.; Patt, S. L.; Keifer, P. a. *J. Magn. Reson. Ser. A* **1995**, *117* (2), 295–303.

(3) Gonzalez, J. A.; Ogba, O. M.; Morehouse, G. F.; Rosson, N.; Houk, K. N.; Leach, A. G.; Cheong, P. H.-Y.; Burke, M. D.; Lloyd-Jones, G. C. *Nat. Chem.* **2016**, *8*, 1067–1075.

(4) Beach, N. J.; Knapp, S. M. M.; Landis, C. R. *Rev. Sci. Instrum.* **2015**, *86* (10).

(5) Foley, D. A.; Dunn, L.; Zell, M. T. *Magn. Reson. Chem.* **2016**, *54*, 451–456.

(6) Archambault, C. M.; Leadbeater, N. E. *RSC Adv.* **2016**, *6* (103), 101171–101177.

(7) Ferretti, A. C.; Mathew, J. S.; Blackmond, D. G. *Ind. Eng. Chem. Res.* **2007**, *46* (25), 8584–8589.

(8) Burés, J. *Angew. Chem. Int. Ed.* **2016**, *55* (6), 2028–2031.

(9) Blackmond, D. G.; Rosner, T.; Pfaltz, A. *Org. Process Res. Dev.* **1999**, *3* (4), 275–280.

(10) Thibblin, A. *J. Phys. Org. Chem.* **2002**, *15* (4), 233–241.

(11) Cruz, S. C.; Aarnoutse, P. J.; Rothenberg, G.; Westerhuis, J. a.; Smilde, A. K.; Bliek, A. *Phys. Chem. Chem. Phys.* **2003**, *5* (20), 4455.

(12) Carter, C. F.; Lange, H.; Ley, S. V; Baxendale, I. R.; Wittkamp, B.; Goode, J. G.; Gaunt, N. L. *Org. Process Res. Dev.* **2010**, *14* (2), 393–404.

(13) O-Brien, A. G.; Maruyama, A.; Inokuma, Y.; Fujita, M.; Baran, P. S.; Blackmond, D. G. *Angew. Chem. Int. Ed.* **2014**, *53* (44), 11868–11871.

(14) Brodmann, T.; Koos, P.; Metzger, A.; Knochel, P.; Ley, S. V. *Org. Process Res. Dev.* **2012**, *16* (5), 1102–1113.

(15) Mettler-Toledo AutoChem, I. Columbia, MD, USA October 2014.

(16) Steinfeldt, N.; Bentrup, U.; Jähnisch, K. *Ind. Eng. Chem. Res.* **2010**, *49* (1), 72–80.

(17) Baxter, R. D.; Sale, D.; Engle, K. M.; Yu, J. Q.; Blackmond, D. G. *J. Am. Chem. Soc.* **2012**, *134* (10), 4600–4606.

(18) Nett, A. J.; Zhao, W.; Zimmerman, P. M.; Montgomery, J. *J. Am. Chem. Soc.* **2015**, *137* (24), 7636–7639.

(19) Schmink, J. R.; Holcomb, J. L.; Leadbeater, N. E. *Chem. Eur. J.* **2008**, *14* (32), 9943–9950.

(20) Hart, R. J.; Pedge, N. I.; Steven, A. R.; Sutcli, K. *Org. Process Res. Dev.* **2014**, *19*, 195–202.

(21) Schafer, W. A.; Hobbs, S.; Rehm, J.; Rakestraw, D. A.; Orella, C.; McLaughlin, M.; Ge, Z.; Welch, C. J. *Org. Process Res. Dev.* **2007**, *11* (5), 870–876.

(22) Welch, C. J.; Gong, X.; Cuff, J.; Dolman, S.; Nyrop, J.; Lin, F.; Rogers, H. *Org. Process Res. Dev.* **2009**, *13* (5), 1022–1025.

(23) Chisolm, C. N.; Evans, C. R.; Jennings, C.; Black, W. A.; Antosz, F. J.; Qiang, Y.; Diaz, A. R.; Kennedy, R. T. *J. Chromatogr. A* **2010**, *1217* (48), 7471–7477.

(24) Obradors, C.; Martinez, R. M.; Shenvi, R. A. *J. Am. Chem. Soc.* **2016**, *138* (14), 4962–4971.

(25) Vikse, K. L.; Ahmadi, Z.; McIndoe, S. J. *Coord. Chem. Rev.* **2014**, *279*, 96–114.

(26) Browne, D. L.; Wright, S.; Deadman, B. J.; Dunnage, S.; Baxendale, I. R.; Turner, R. M.; Ley, S. V. *Rapid Commun. Mass Spectrom.* **2012**, *26* (17), 1999–2010.

(27) Schroder, D. *Acc. Chem. Res.* **2012**, *45* (9), 1521–1532.

(28) Yunker, L. P. E.; Stoddard, R. L.; McIndoe, J. S. *J. Mass Spectrom.* **2014**, *49* (1), 1–8.

(29) Theron, R.; Wu, Y.; Yunker, L. P. E.; Hesketh, A. V.; Pernik, I.; Weller, A. S.; McIndoe, J. S. *ACS Catal.* **2016**, *6*, 6911−6917.

(30) Dell'Orco, P.; Brum, J.; Matsuoka, R.; Badlani, M.; Muske, K. *Anal. Chem.* **1999**, *71* (22), 5165–5170.

(31) Bordawekar, S.; Chanda, A.; Daly, A. M.; Garrett, A. W.; Higgins, J. P.; LaPack, M. A.; Maloney, T. D.; Morgado, J.; Mukherjee, S.; Orr, J. D.; Reid, G. L.; Yang, B. S.; Ward, H. W. *Org. Process Res. Dev.* **2015**, *19* (9), 1174–1185.

(32) Foley, D. A.; Wang, J.; Maranzano, B.; Zell, M. T.; Marquez, B. L.; Xiang, Y.; Reid, G. L. *Anal. Chem.* **2013**, *85* (19), 8928–8932.

(33) Drexler, M. T.; Foley, D. A.; Ward, H. W.; Clarke, H. J. *Org. Process Res. Dev.* **2015**, *19* (9), 1119–1127.

(34) Foley, D. A.; Doecke, C. W.; Buser, J. Y.; Merritt, J. M.; Murphy, L.; Kissane, M.; Collins, S. G.; Maguire, A. R.; Kaerner, A. *J. Org. Chem.* **2011**, *76* (23), 9630–9640.

(35) Anslyn, E. V.; Dougherty, D. A. *Modern Physical Organic Chemistry*; 2005.

(36) Blackmond, D. G. *Angew. Chem. Int. Ed.* **2005**, *44* (28), 4302–4320.

(37) Blackmond, D. G. *J. Am. Chem. Soc.* **2015**, *137* (34), 10852–10866.

(38) Hansch, C.; Leo, A.; Taft, R. W. *Chem. Rev.* **1991**, *91* (2), 165–195.

(39) Santiago, C. B.; Milo, A.; Sigman, M. S. *J. Am. Chem. Soc.* **2016**, *138*, 13424–13430.

(40) Schreck, J. O. *J. Chem. Educ.* **1971**, *48* (2), 103.

(41) Santerre, G. M.; Hansrote Jr, C. J.; Crowell, T. I. *J. Am. Chem. Soc.* **1958**, *80*, 12–15.

(42) Fuchs, Richard; Nisbet, A. *J. Am. Chem. Soc.* **1959**, *81* (10), 2371–2373.

(43) Lewis, C. A.; Gustafson, J. L.; Chiu, A.; Balsells, J.; Murry, J.; Reamer, R. A.; Hansen, K. B.; Miller, S. J.; Pollard, D. *J. Am. Chem. Soc.* **2008**, *130*, 16358–16365.

(44) Sigman, M. S.; Harper, K. C.; Bess, E. N.; Milo, A. *Acc. Chem. Res.* **2016**, *49* (6), 1292–1301.

(45) Charton, M. *J. Am. Chem. Soc.* **1974**, *96*, 1552–1556.

(46) Piou, T.; Romanov-Michailidis, F.; Romanova-Michaelides, M.; Jackson, K. E.; Semakul, N.; Taggart, T. D.; Newell, B. S.; Rithner, C. D.; Paton, R. S.; Rovis, T. *J. Am. Chem. Soc.* **2017**, *139*, 1296–1310.

(47) Piancatelli, G.; Scettri, A.; Barbadoro, S. *Tetrahedron Lett.* **1976**, *17* (39), 3555–3558.

(48) Henschke, J. P.; Liu, Y.; Huang, X.; Chen, Y.; Meng, D.; Xia, L.; Wei, X.; Xie, A.; Li, D.; Huang, Q.; Sun, T.; Wang, J.; Gu, X.; Huang, X.; Wang, L.; Xiao, J.; Qiu, S. *Org. Process Res. Dev.* **2012**, *16* (12), 1905–1916.

(49) Kumaraguru, T.; Babita, P.; Sheelu, G.; Lavanya, K.; Fadnavis, N. W. *Org. Process Res. Dev.* **2013**, *17* (12), 1526–1530.

(50) Li, S.-W.; Batey, R. A. *Chem. Commun.* **2007**, *8* (36), 3759–3761.

(51) Veits, G. K.; Wenz, D. R.; Read De Alaniz, J. *Angew. Chem. Int. Ed.* **2010**, *49*, 9484–9487.

(52) Palmer, L. I.; Read De Alaniz, J. *Angew. Chem. Int. Ed.* **2011**, *50* (31), 7167–7170.

(53) Wabnitz, T. C.; Yu, J.-Q.; Spencer, J. B. *Chemistry* **2004**, *10*, 484.

(54) Fisher, D.; Palmer, L. I.; Cook, J. E.; Davis, J. E.; Read De Alaniz, J. *Tetrahedron* **2014**, *70* (27–28), 4105–4110.

(55) Veits, G. K.; Read De Alaniz, J. *Tetrahedron* **2012**, *68* (8), 2015–2026.

(56) Moschetta, E. G.; Gans, K. M.; Rioux, R. M. *J. Catal.* **2013**, *302*, 1–9.

(57) Persson, I.; D'Angelo, P.; De Panfilis, S.; Sandstrom, M.; Eriksson, L. *Chem. Eur. J.* **2008**, *14* (10), 3056–3066.

(58) Smith, D. W. *J. Chem. Educ.* **1977**, *54* (9), 540.

(59) Fortuna, C. G.; Musumarra, G.; Nardi, M.; Procopio, A.; Sindona, G.; Scire, S. *J. Chemom.* **2006**, *20*, 418–424.

(60) Allred, A. L. *J. Inorg. Nucl. Chem.* **1961**, *17* (3–4), 215–221.

(61) Yadav, J. S.; Reddy, B. V. S.; Jain, R.; Reddy, C. S. *Tetrahedron Lett.* **2007**, *48* (18), 3295–3298.

(62) Xie, W.; Bloomfield, K. M.; Jin, Y.; Dolney, N. Y.; Wang, P. G. *Synlett* **1999**, *4*, 498–500.

(63) Wenz, D. R. The Development of an aza-Piancatelli Rearrangement. Ph.D. Dissertation., University of California, Santa Barbara, 2014.

(64) Veits, G. K.; Wenz, D. R.; Palmer, L. I.; St. Amant, A. H.; Hein, J. E.; Read de Alaniz, J. *Org. Biomol. Chem.* **2015**, *13* (31), 8465–8469.

(65) Bissot, T. C.; Parry, R. W.; Campbell, D. H. *J. Am. Chem. Soc.* **1957**, *79* (4), 796–800.

(66) Palmer, L. I.; De Alaniz, J. R. *Org. Lett.* **2013**, *15* (3), 476–479.

(67) Ball-Jones, N. R.; Badillo, J. J.; Tran, N. T.; Franz, A. K. *Angew. Chem. Int. Ed.* **2014**, *53* (36), 9462–9465.

(68) Macdonald, J. P.; Shupe, B. H.; Schreiber, J. D.; Franz, A. K. *Chem. Commun.* **2014**, *50*, 5242–5244.

(69) Diaz-Torres, R.; Alvarez, S. *Dalt. Trans.* **2011**, *40*, 10742.

(70) Csákÿ, A.; Mba, M.; Plumet, J. *Synlett* **2003**, *13*, 2092.

(71) Yakelis, N. A.; Bergman, R. G. *Organometallics* **2005**, *24* (14), 3579–3581.

(72) Kamm, O. *Org. Synth.* **1941**, *1*, 445–447.

(73) Yu, D.; Thai, V. T.; Palmer, L. I.; Veits, G. K.; Cook, J. E.; Read De Alaniz, J.; Hein, J. E. *J. Org. Chem.* **2013**, *78* (24), 12784–12789.

(74) Tidwell, T. T. *Angew. Chem. Int. Ed.* **2008**, *47* (6), 1016–1020.

(75) Stecko, S.; Furman, B.; Chmielewski, M. *Tetrahedron* **2014**, *70* (43), 7817–7844.

(76) Willcox, D.; Chappell, B. G. N.; Hogg, K. F.; Calleja, J.; Smalley, A. P.; Gaunt, M. J. *Science (80-.).* **2016**, *354* (6314), 851–857.

(77) Staudinger, H. *Liegbis Ann. Chem.* **1907**, *356*, 51–123.

(78) Ding, L. K.; Irwin, W. J. *J. Chem. Soc. Perkin Trans. 1* **1976**, 2382–2386.

(79) Ye, M. C.; Zhou, J.; Tang, Y. *J. Org. Chem.* **2006**, *71* (9), 3576–3582.

(80) Mames, A.; Stecko, S.; Mikołajczyk, P.; Soluch, M.; Furman, B.; Chmielewski, M. *J. Org. Chem.* **2010**, *75* (22), 7580–7587.

(81) Sakakura, A.; Hori, M.; Fushimi, M.; Ishihara, K. *J. Am. Chem. Soc.* **2010**, *132* (44), 15550–15552.

(82) Saito, T.; Kikuchi, T.; Tanabe, H.; Yahiro, J.; Otani, T. *Tetrahedron Lett.* **2009**, *50* (35), 4969–4972.

(83) Singh, S. K.; Srinivasa Reddy, M.; Mangle, M.; Ravi Ganesh, K. *Tetrahedron* **2007**, *63* (1), 126–130.

(84) Miura, M.; Enna, M.; Okuro, K.; Nomura, M. *J. Org. Chem.* **1995**, *60* (16), 4999–5004.

(85) Ye, M.-C.; Zhou, J.; Huang, Z.-Z.; Tang, Y. *Chem. Commun.* **2003**, 2554–2555.

(86) Kabala, K.; Grzeszczyk, B.; Stecko, S.; Furman, B.; Chmielewski, M. *J. Org. Chem.* **2015**, *80* (24), 12038–12046.

(87) Kowalski, M. K.; Mlostoń, G.; Obijalska, E.; Linden, A.; Heimgartner, H. *Tetrahedron* **2016**, *72* (35), 5305–5313.

(88) Lo, M. M. C.; Fu, G. C. *J. Am. Chem. Soc.* **2002**, *124* (17), 4572–4573.

(89) Marco-Contelles, J. *Angew. Chem. Int. Ed.* **2004**, *43* (17), 2198–2200.

(90) Walker, J. M. *The Bicinchoninic Acid (BCA) Assay for Protein Quantitation*, 1st ed.; Walker, J. M., Ed.; Humana Press, 1994.

(91) Chen, Z.; Lin, L.; Wang, M.; Liu, X.; Feng, X. *Chem. Eur. J.* **2013**, *19* (23), 7561–7567.

(92) Chigrinova, M.; MacKenzie, D. A.; Sherratt, A. R.; Cheung, L. L. W.; Pezacki, P. *Molecules* **2015**, *20* (4), 6959–6969.

(93) McKay, C. S.; Kennedy, D. C.; Pezacki, J. P. *Tetrahedron Lett.* **2009**, *50* (17), 1893–1896.

(94) Hein, J. E.; Krasnova, L. B.; Iwasaki, M.; Fokin, V. V. *Org. Synth.* **2011**, *88*, 238.

(95) Gabriel, C.; Gabriel, S.; Grant, E. H.; Halstead, B. S. J.; Mingos, D. M. P. *Chem. Soc. Rev.* **1998**, *27*, 213–223.

(96) Dudley, G. B.; Richert, R.; Stiegman, A. E. *Chem. Sci.* **2015**, *6*, 2144–2152.

(97) Hoz, A. de la; Diaz-Ortiz, A.; Moreno, A. *Chem. Soc. Rev.* **2005**, *34*, 164–178.

(98) Baghurst, D. R.; Mingos, D. M. P. *J. Chem. Soc. Chem. Commun.* **1992**, No. 9, 674.

(99) Ferrari, A.; Hunt, J.; Stiegman, A.; Dudley, G. B.; Radoiu, M.; Vanden Eynde, J. J.; Mayence, A. *Molecules* **2015**, *20* (12), 21672–21680.

(100) Raner, K. D.; Strauss, C. R.; Trainor, R. W.; Thorn, J. S. *J. Org. Chem.* **1995**, *60* (8), 2456–2460.

(101) Kappe, C. O. *Angew. Chem. Int. Ed.* **2004**, *43*, 6250–6284.

(102) Kappe, C. O. *Chem. Soc. Rev.* **2013**, *42* (42), 4977–4990.

(103) Jahngen, E. G. E.; Lentz, R. .; Pesheck, P. S.; Sackett, P. H. *J. Org. Chem.* **1990**, *55* (10), 3406–3409.

(104) Laurent, R.; Laporterie, A.; Dubac, J.; Berlan, J.; Lefeuvre, J. S.; Audhuys, M. *J. Org. Chem.* **1992**, *57* (26), 7099–7102.

(105) Dudley, G. B.; Stiegman, A. E.; Rosana, M. R. *Angew. Chem. Int. Ed.* **2013**, *52* (31),

7918–7923.

(106) Perreux, L.; Loupy, A. *Tetrahedron* **2001**, *57* (45), 9199–9223.

(107) Leadbeater, N. E. *Chem. Commun.* **2010**, *46* (36), 6693–6695.

(108) Horikoshi, S.; Watanabe, T.; Kamata, M.; Suzuki, Y.; Serpone, N. *RSC Adv.* **2015**, *5* (110), 90272–90280.

(109) Rosana, M. R.; Hunt, J.; Ferrari, A.; Southworth, T. A.; Tao, Y.; Stiegman, A. E.; Dudley, G. B. *J. Org. Chem.* **2014**, *79* (16), 7437–7450.

(110) Chen, P. K.; Rosana, M. R.; Dudley, G. B.; Stiegman, A. E. *J. Org. Chem.* **2014**, *79* (16), 7425–7436.

(111) Castro, A. M. M. *Chem. Rev.* **2004**, *104* (6), 2939–3002.

(112) Kappe, C. O. *Angew. Chem. Int. Ed.* **2013**, *52* (31), 7924–7928.

(113) Chen, P.; Rosana, M. R.; Dudley, G. B.; Stiegman, A. E. *J. Org. Chem.* **2014**, *79*, 7425–7436.

(114) Guo, J.; Mayers, P. C.; Breault, G. A.; Hunter, C. A. *Nat Chem* **2010**, *2* (3), 218–222.

(115) Plettner, E.; Isman, M. B. Methods and Compositions for Control of Cabbage Looper, Trichoplusia NI. US 2010/0160451 Al, 2010.

(116) Sanford, E. M.; Lis, C. C.; McPherson, N. R. *J. Chem. Educ.* **2009**, *86* (12), 1422–1423.

(117) Jin, X.; Yamaguchi, K.; Mizuno, N. *Chem. Lett.* **2012**, *41* (9), 866–867.

(118) Kim, J.; Stahl, S. S. *J. Org. Chem.* **2015**, *80* (4), 2448–2454.

(119) Olofsson, K.; Sahlin, H.; Larhed, M.; Hallberg, A. *J. Org. Chem.* **2001**, *66* (2), 544–549.

(120) Tashima, S.; Nushiro, K.; Saito, K.; Yamada, T. *Bull. Chem. Soc. Jpn.* **2016**, *89*, 833–835.

Appendices

Appendix A Compounds from the Aza-Piancatelli rearrangement

A.1 Characterization of 4-(Benzyl(benzyloxy)amino)-5-phenylcyclopent-2-en-1-one (2.6)

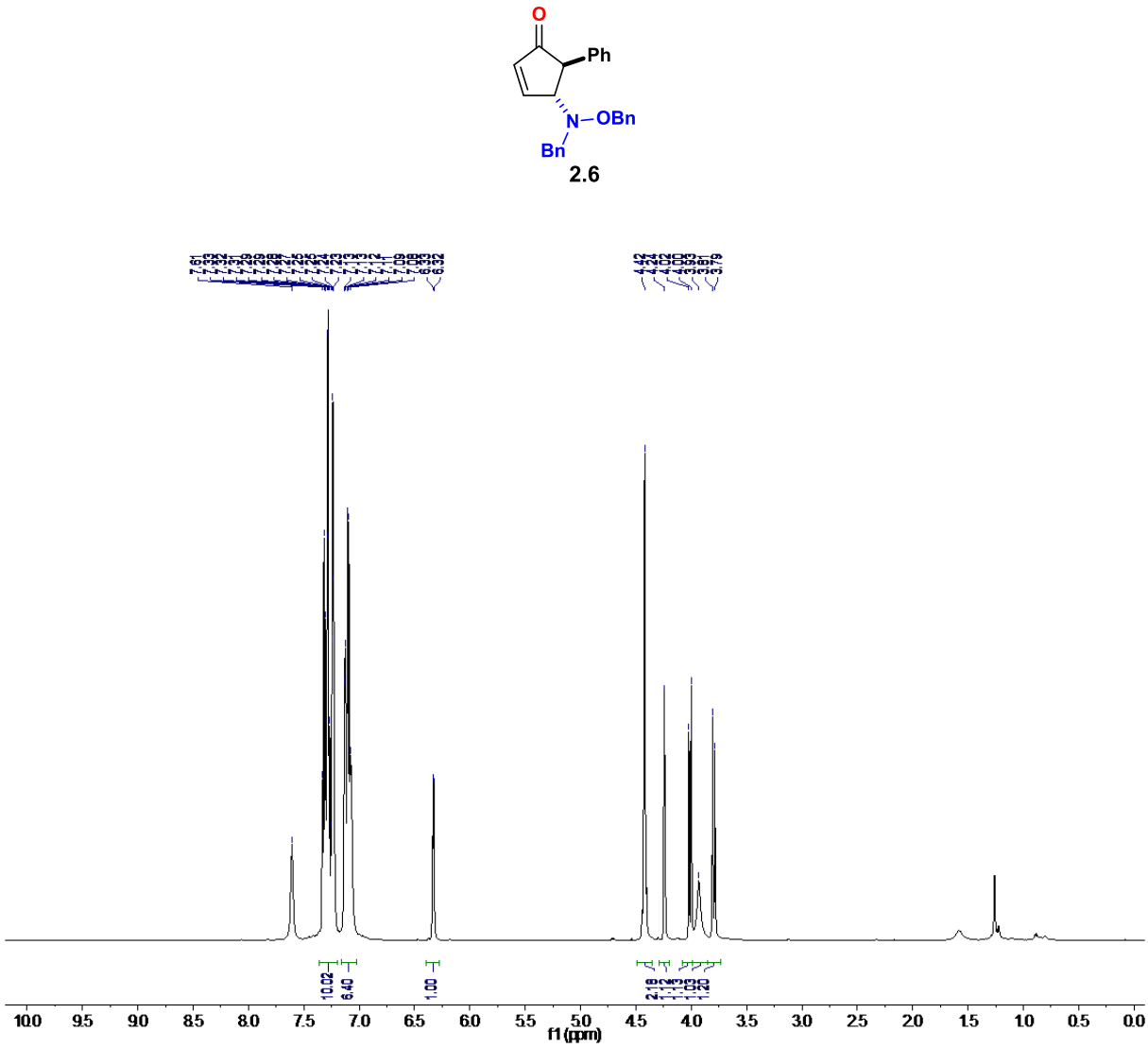

Figure A 1: ^{1}H-NMR spectra of Compound 2.6

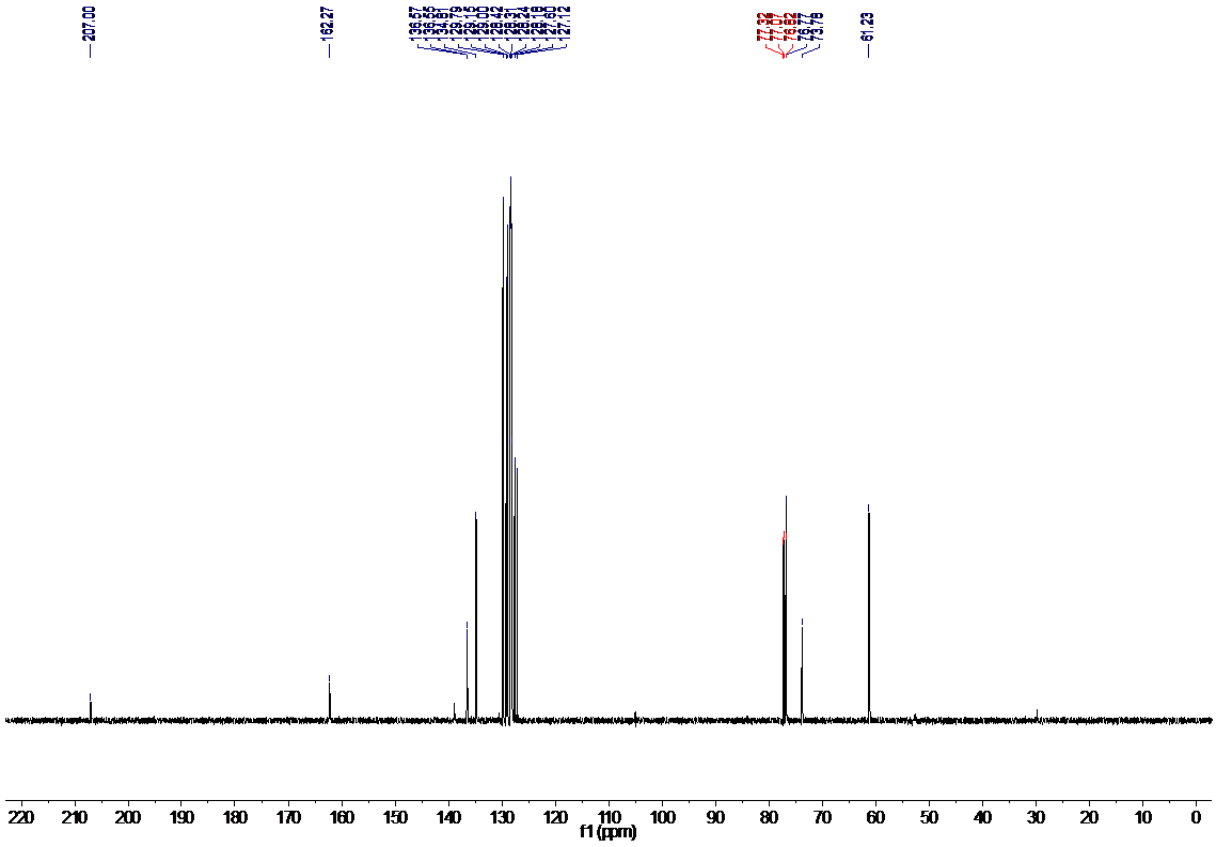

Figure A 2: ^{13}C-NMR spectra of Compound 2.6

A.2 Characterization of N,O-dibenzyl-N-(furan-2-yl(phenyl)methyl)hydroxylamine (2.7)

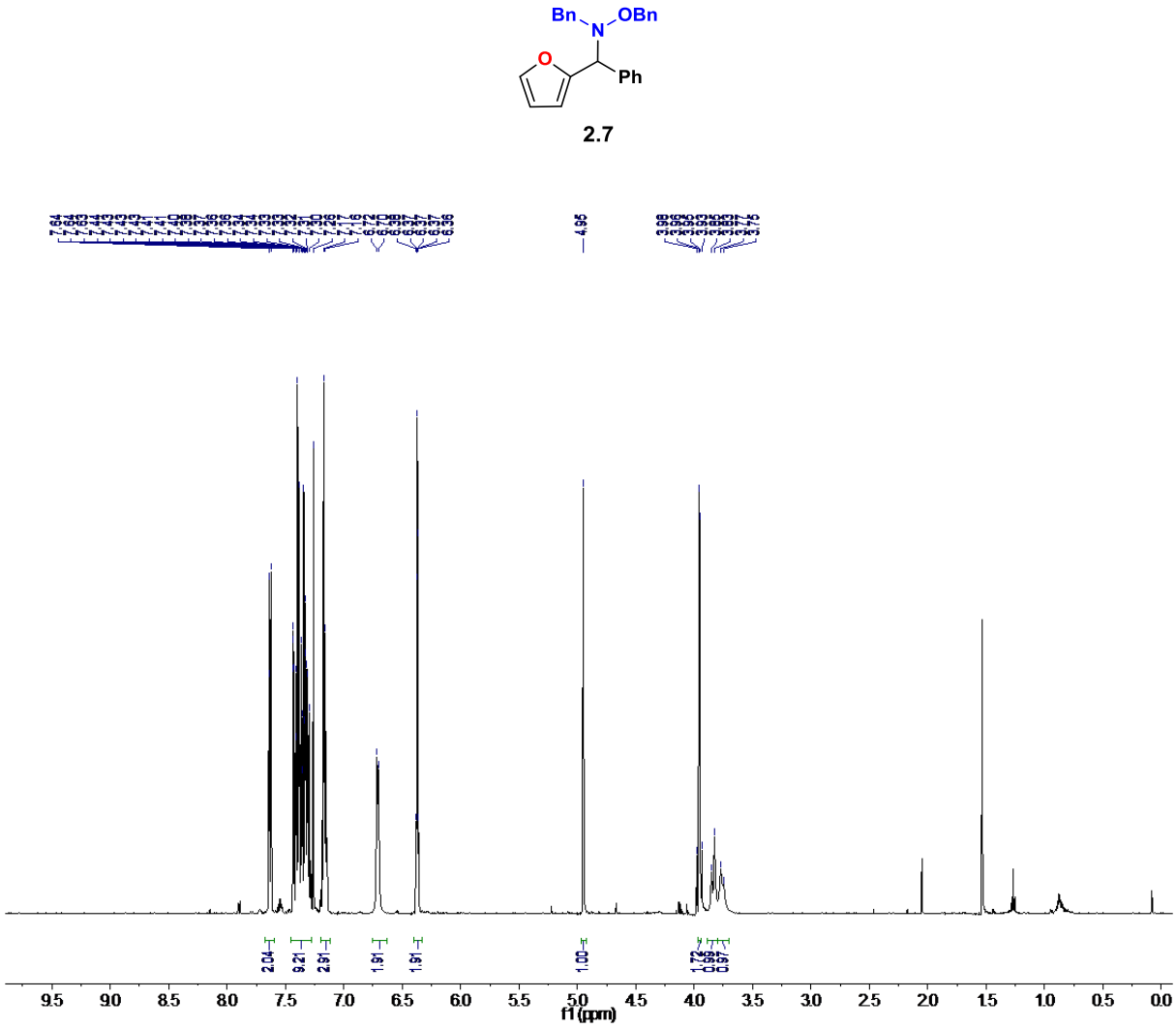

Figure A 3: ^{1}H-NMR spectra of Compound 2.7

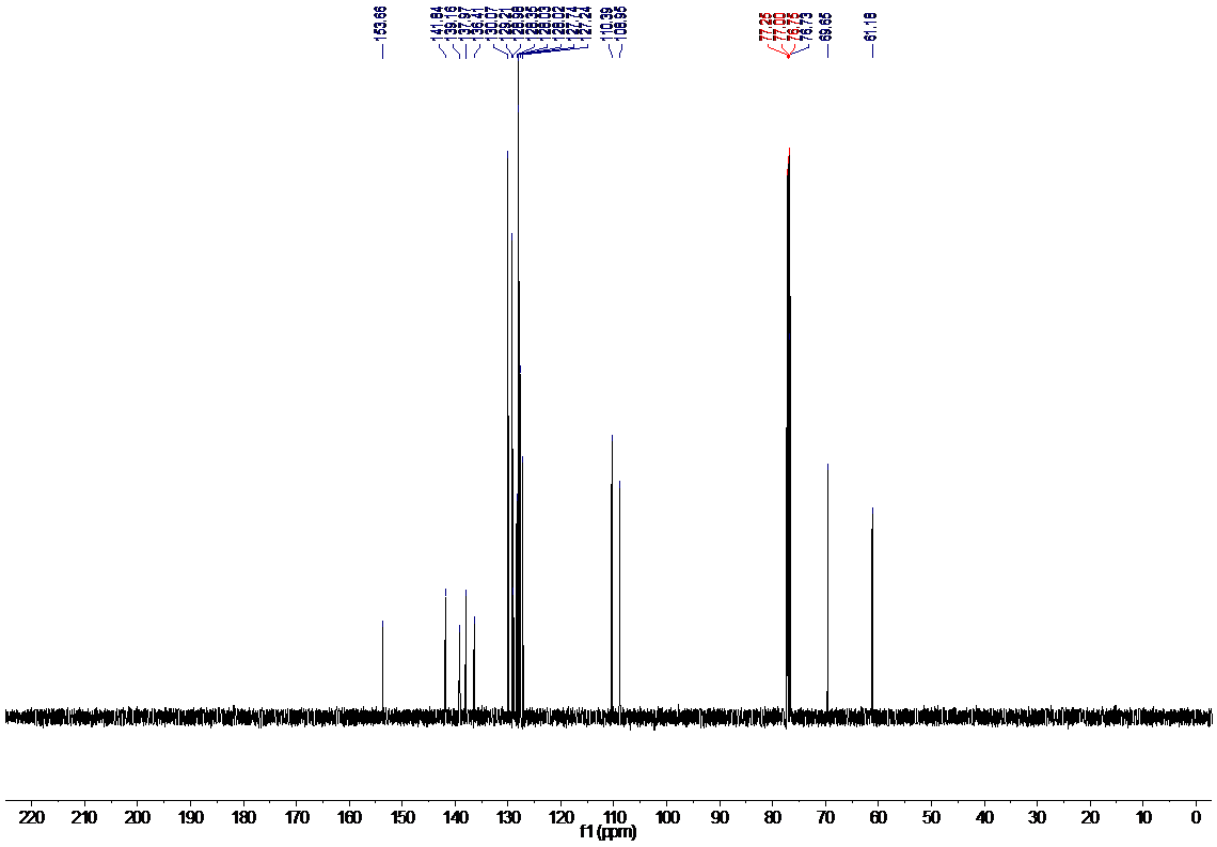

Figure A 4: ^{13}C-NMR spectra of Compound 2.7

Appendix B Side-product isolated from the Kinugasa reaction

B.1 Characterization of isolated amide side product

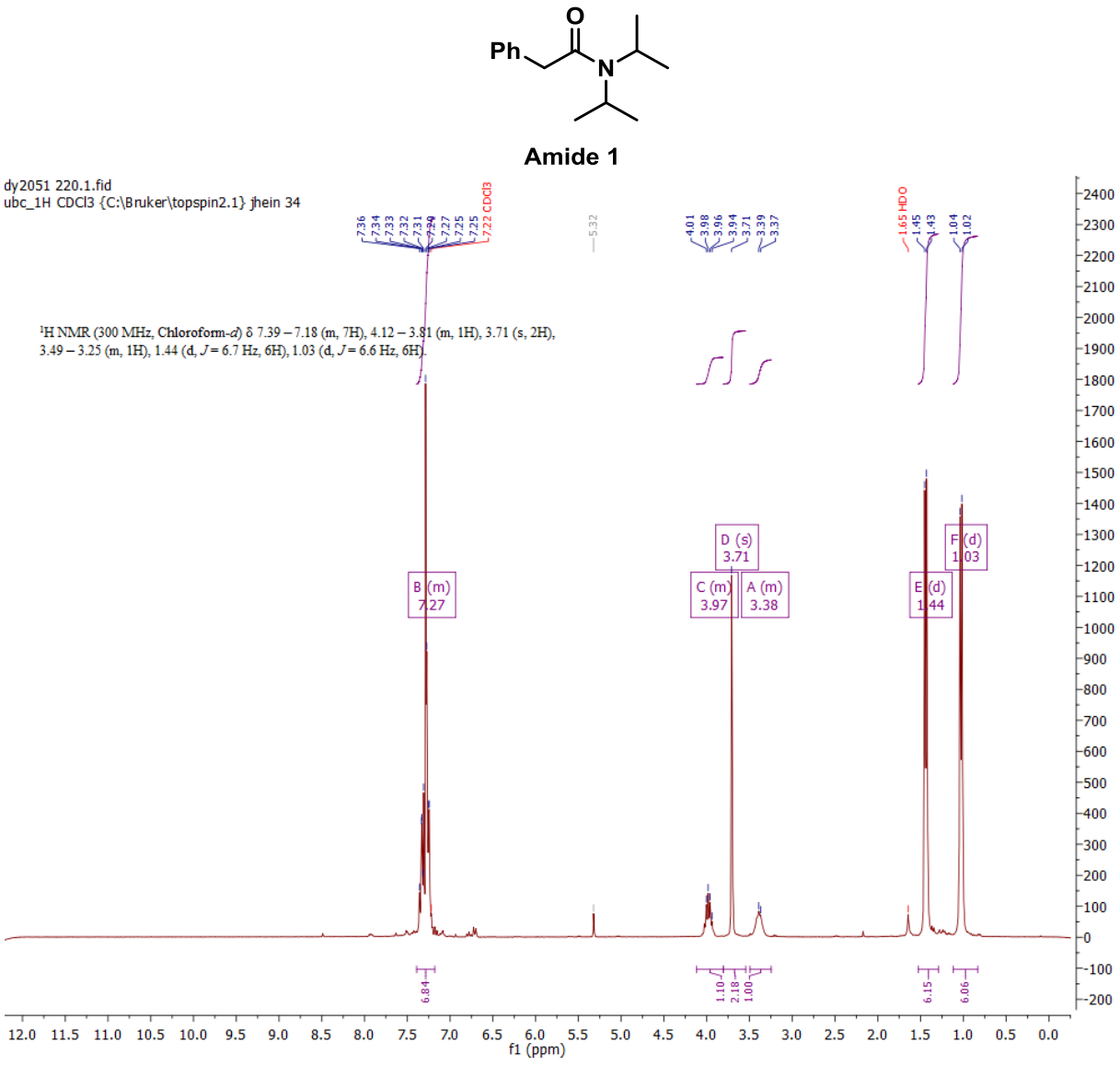

Figure B 1: ^{1}H-NMR of Amide 1, *N*,*N*-diisopropyl-2-phenylacetamide

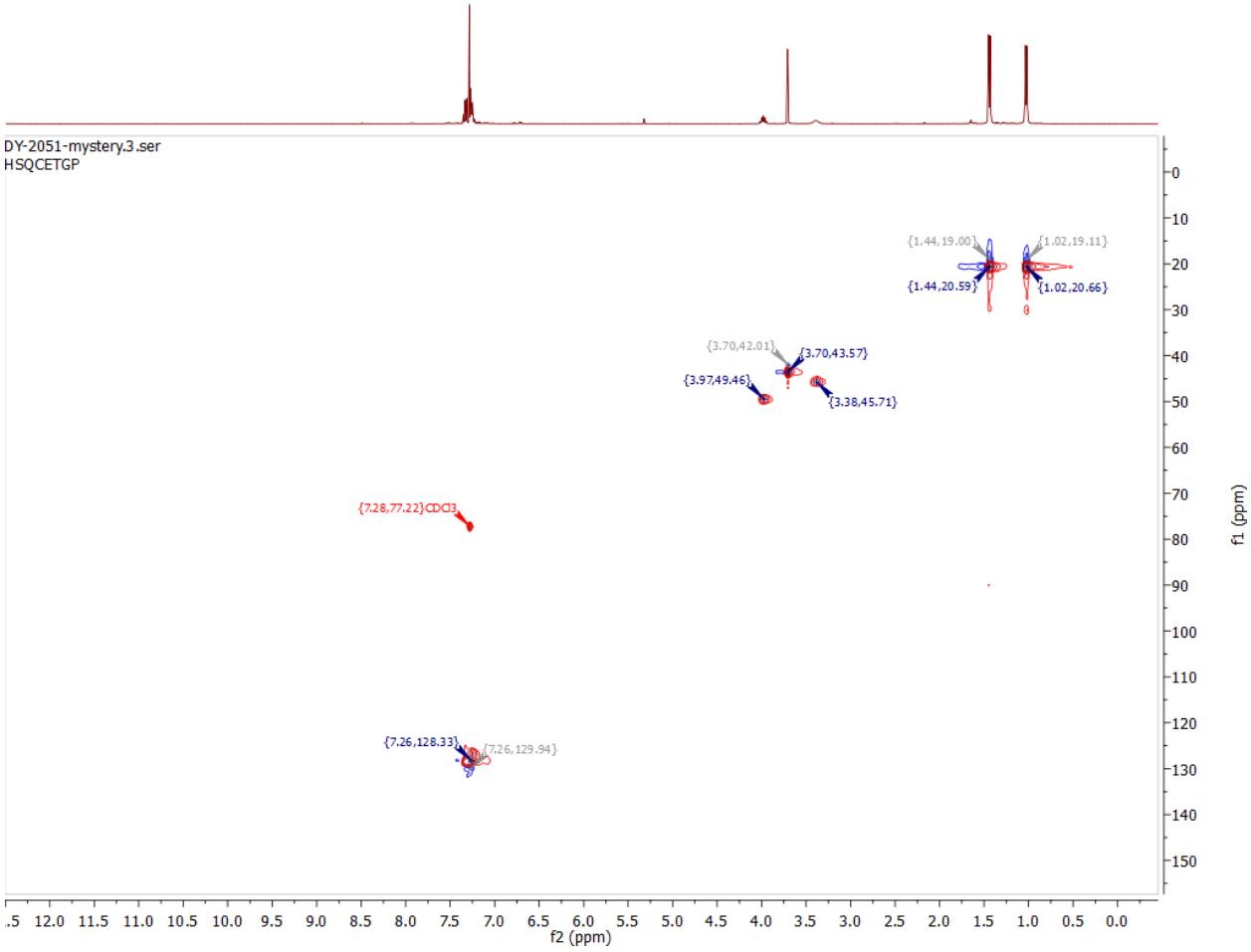

Figure B 2: HSQC of Amide 1, *N,N*-diisopropyl-2-phenylacetamide

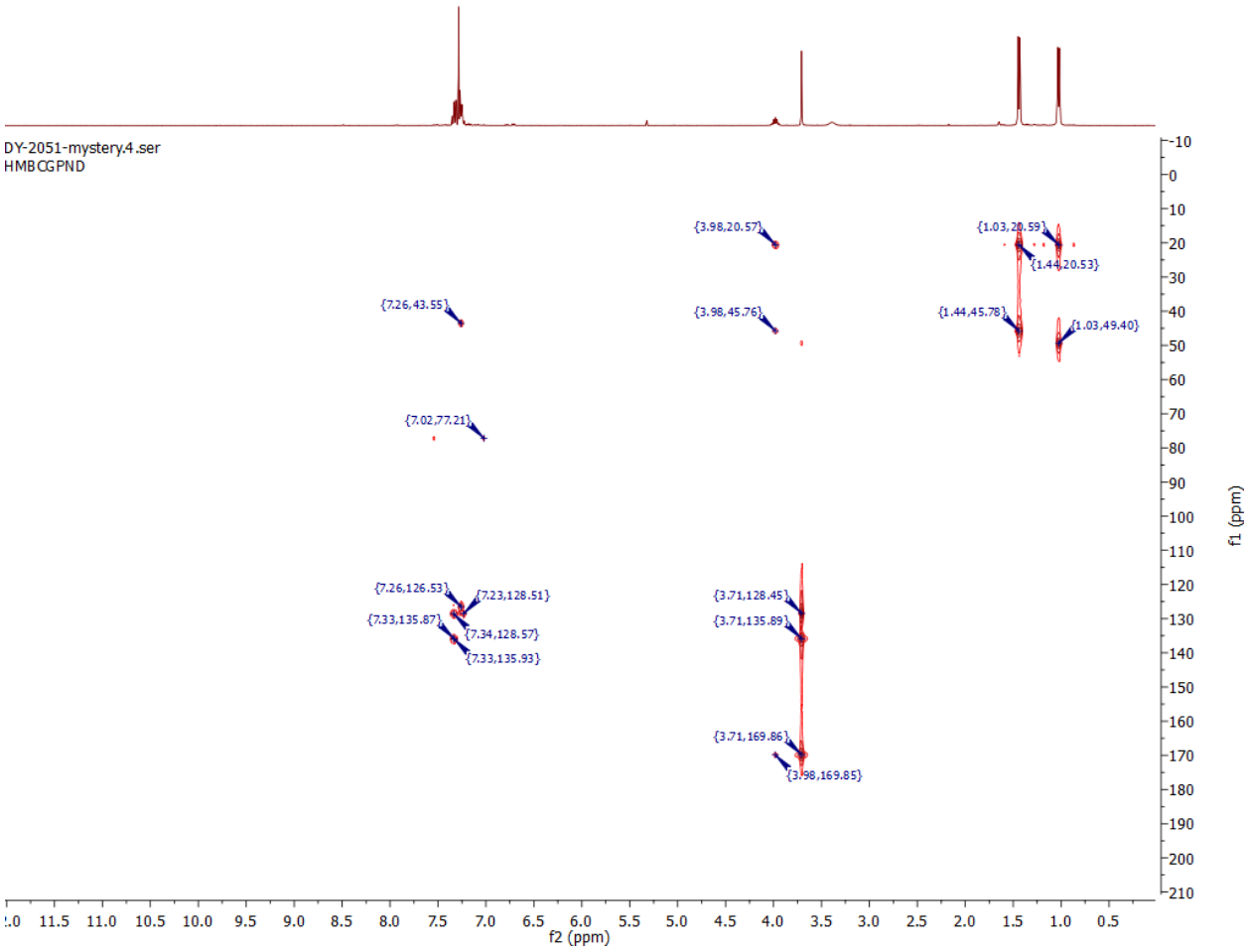

Figure B 3: HMBC of Amide 1, *N,N*-diisopropyl-2-phenylacetamide

Appendix C Characterization of β-lactam 3.3a

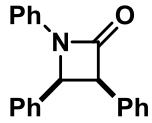

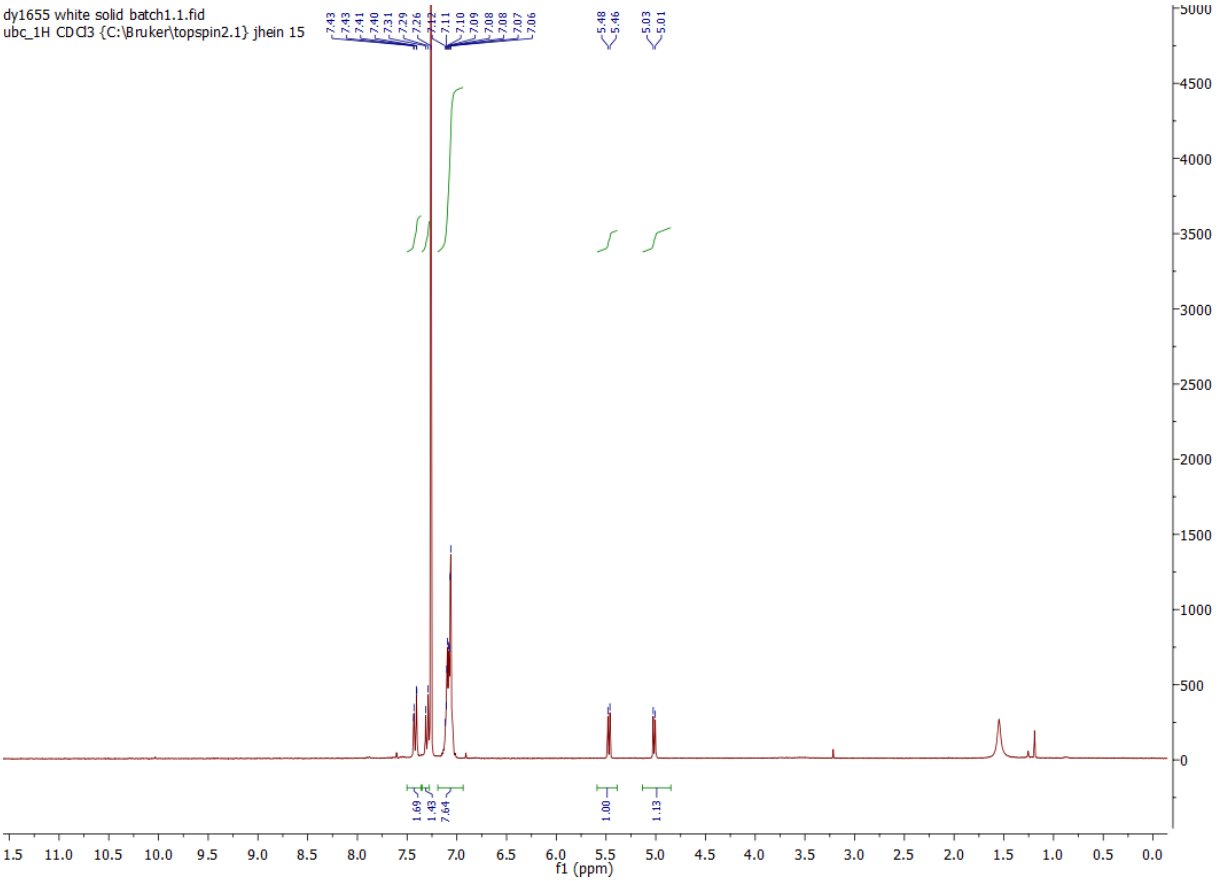

Figure C 1: ^{1}H-NMR spectrum of product 3.3a

Appendix D Characterization of allyl phenyl ethers and their corresponding Claisen products

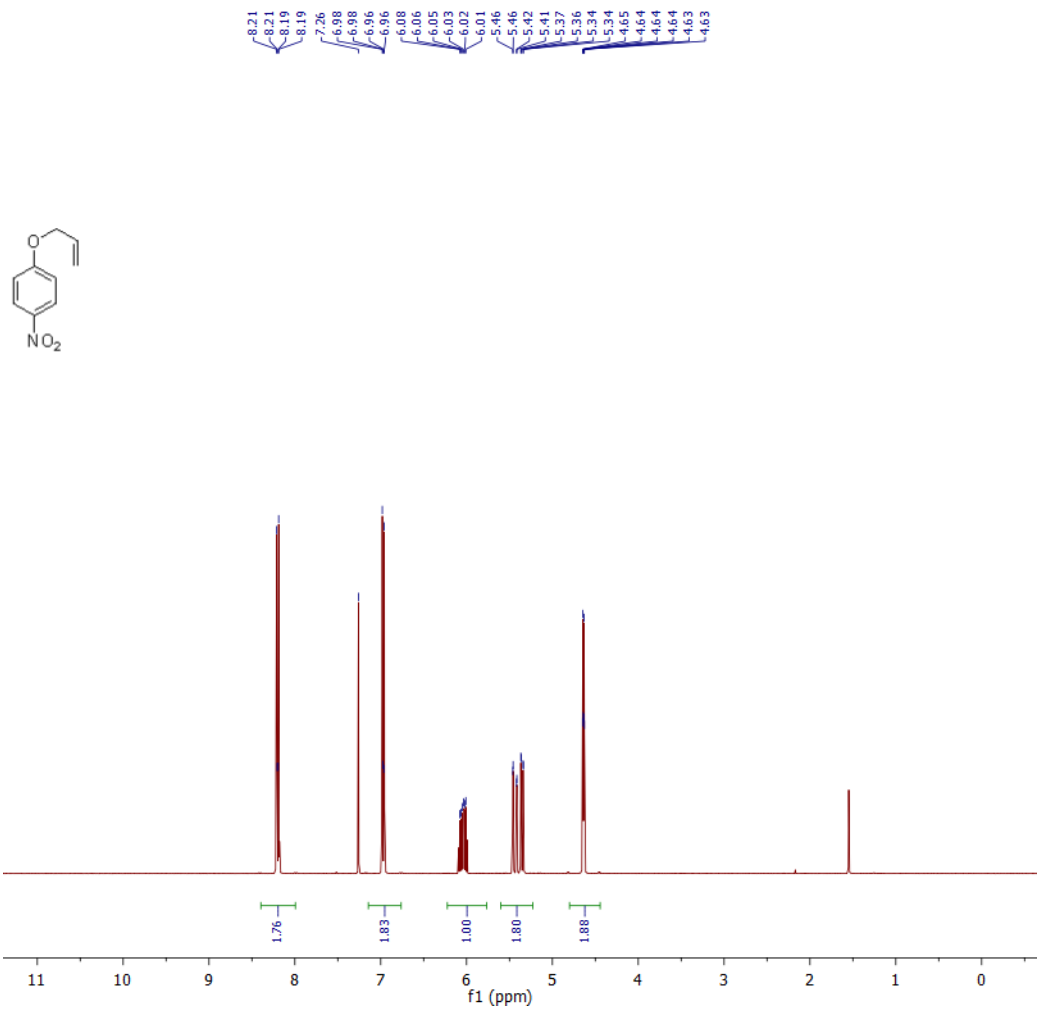

Figure D 1: ^{1}H-NMR spectrum of compound 4.1a

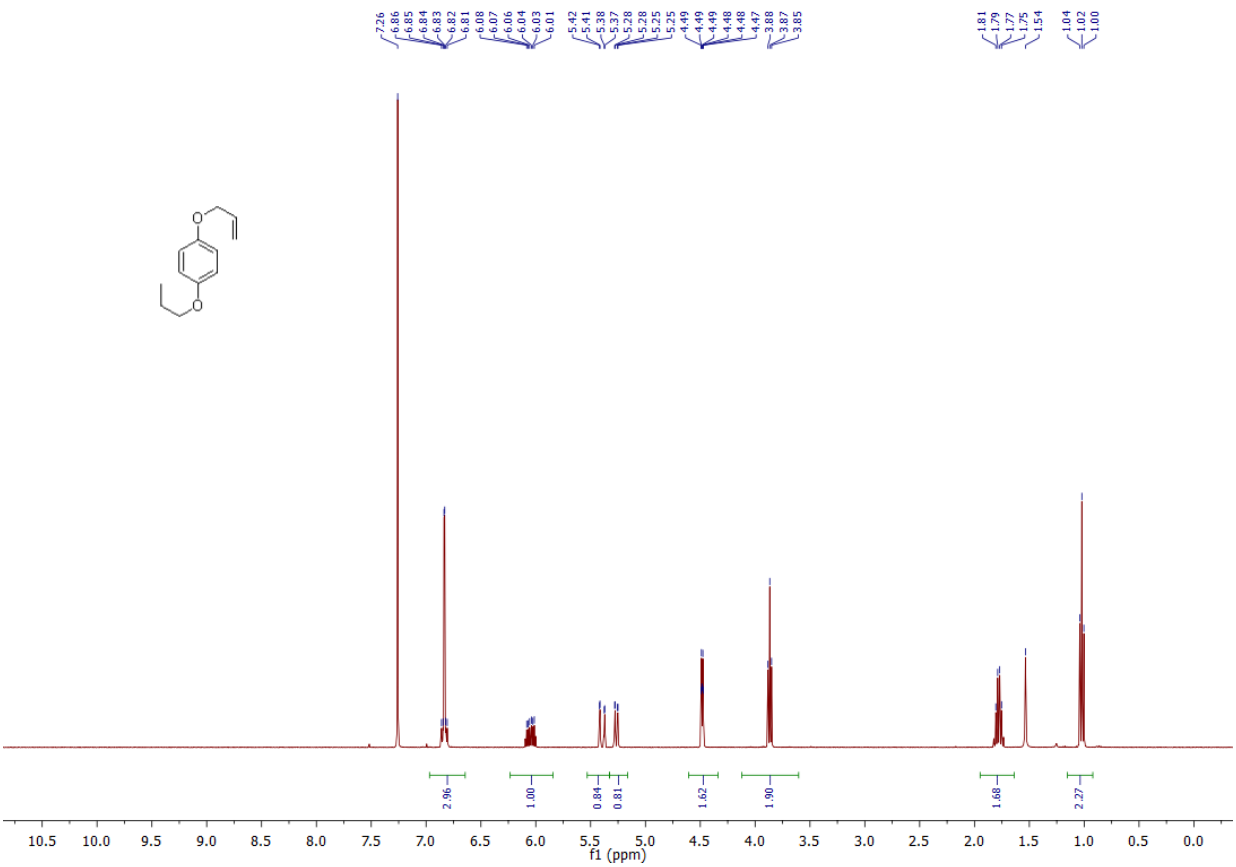

Figure D 2: ^{1}H-NMR spectrum of compound 4.1b

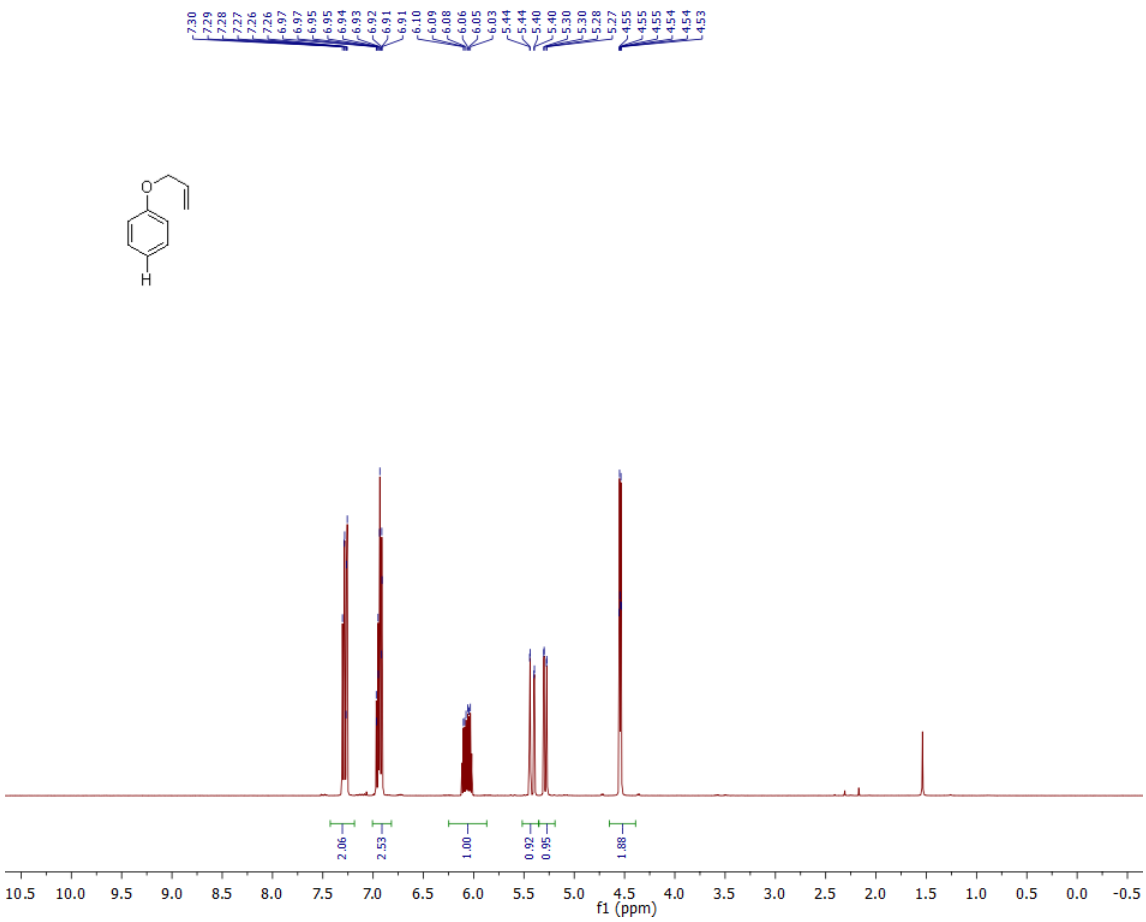

Figure D 3: ^{1}H-NMR spectrum of compound 4.1c

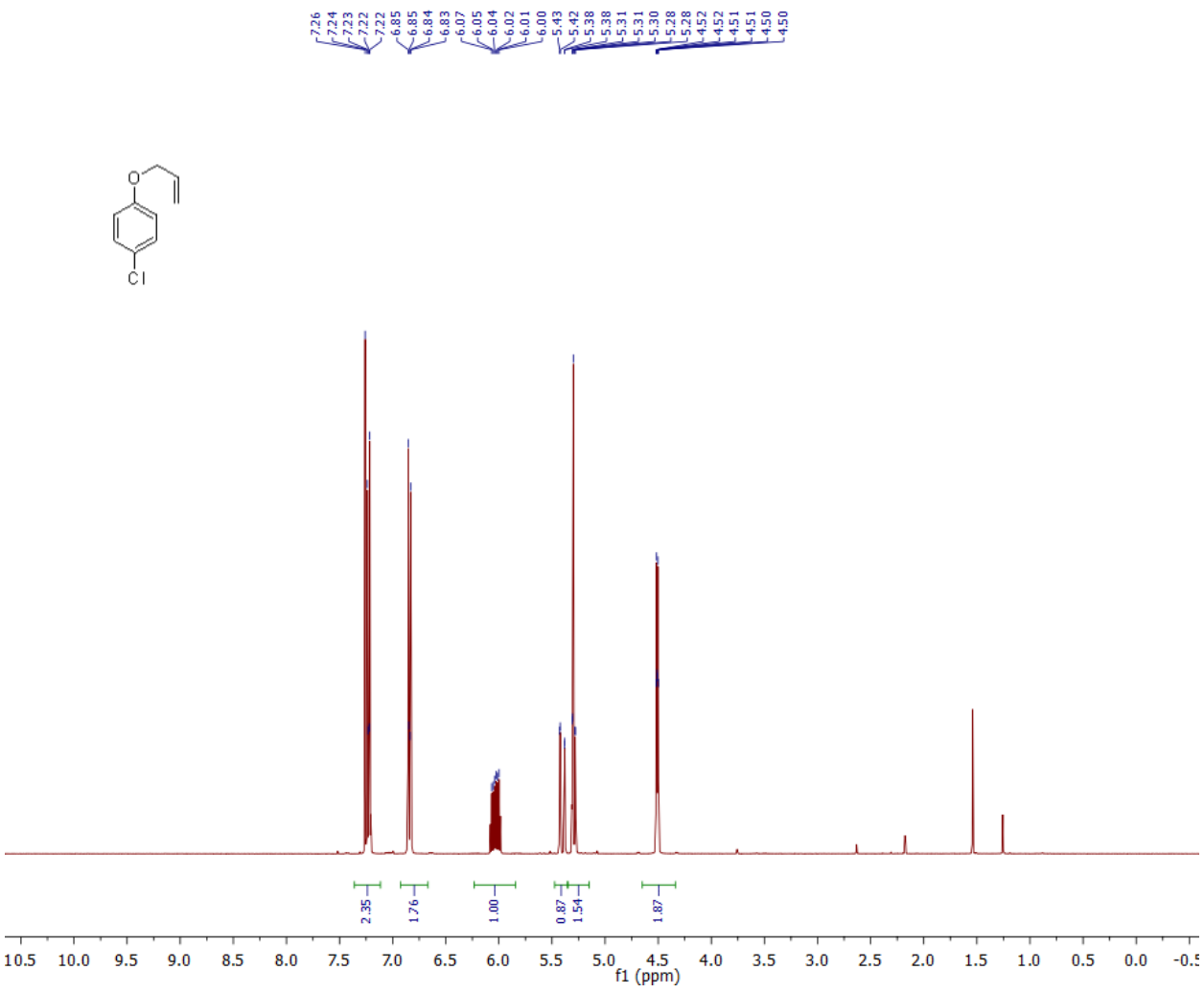

Figure D 4: ^{1}H-NMR spectrum of compound 4.1d

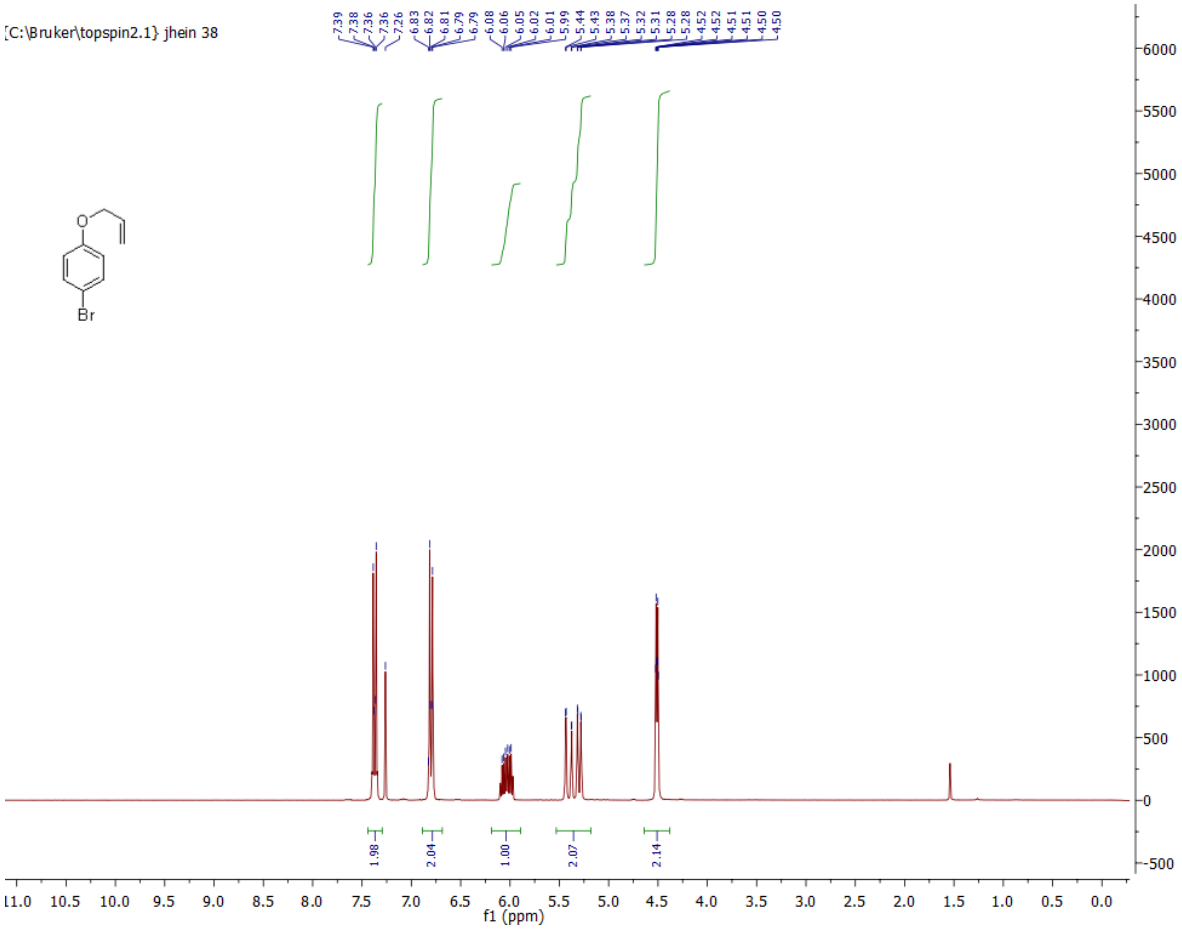

Figure D 5: ^{1}H-NMR spectrum of compound 4.1e

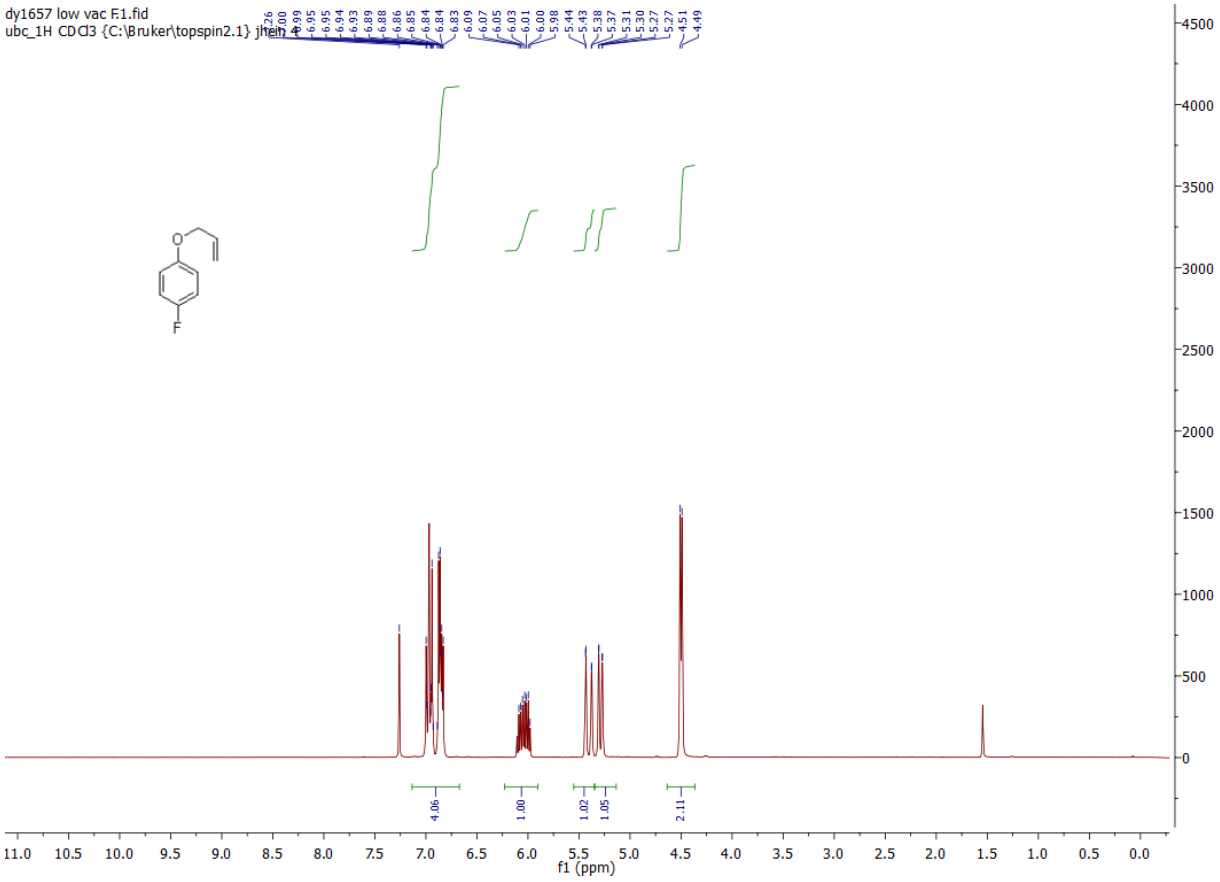

Figure D 6: ^{1}H-NMR spectrum of compound 4.1f

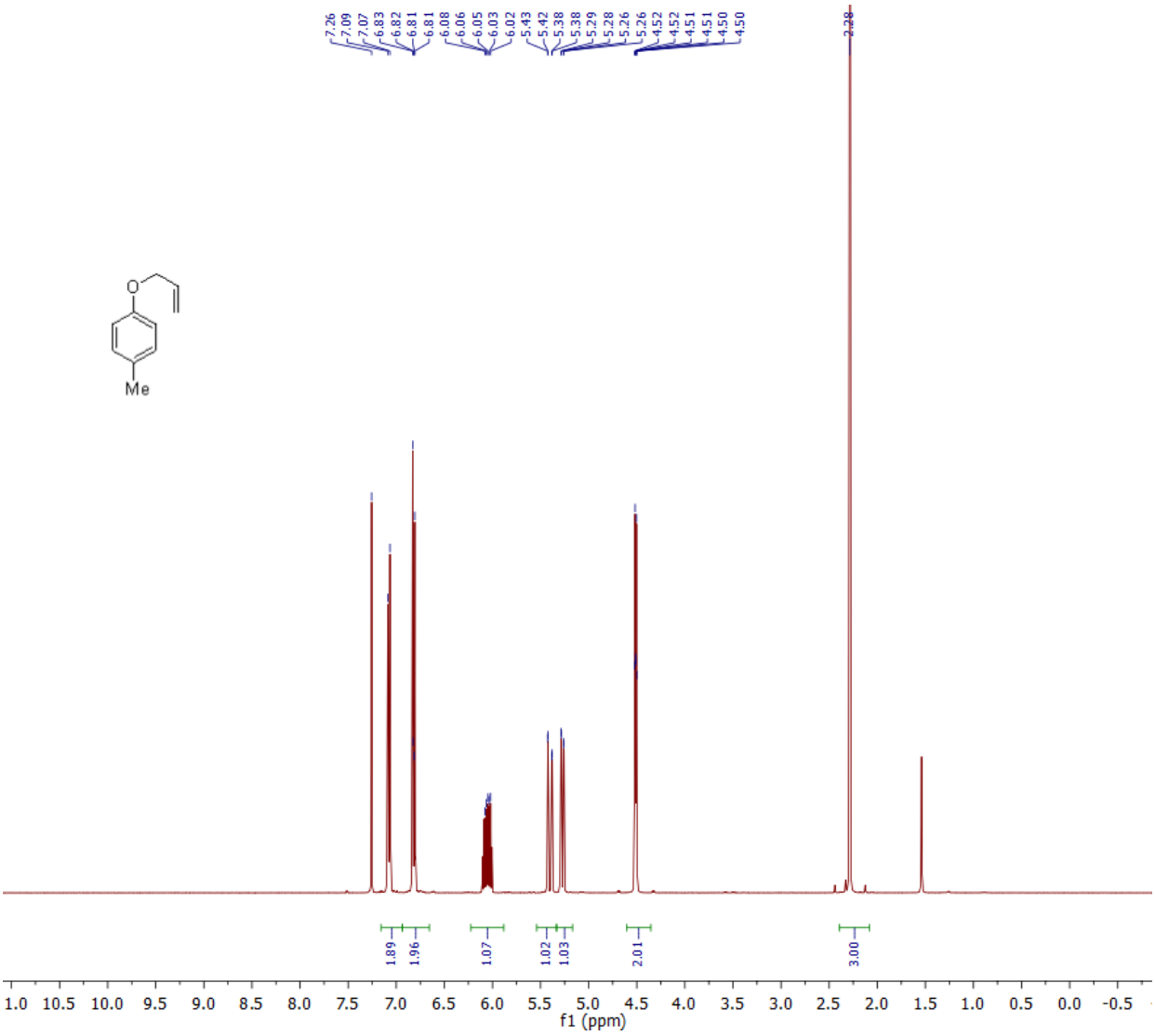

Figure D 7: ^{1}H-NMR spectrum of compound 4.1g

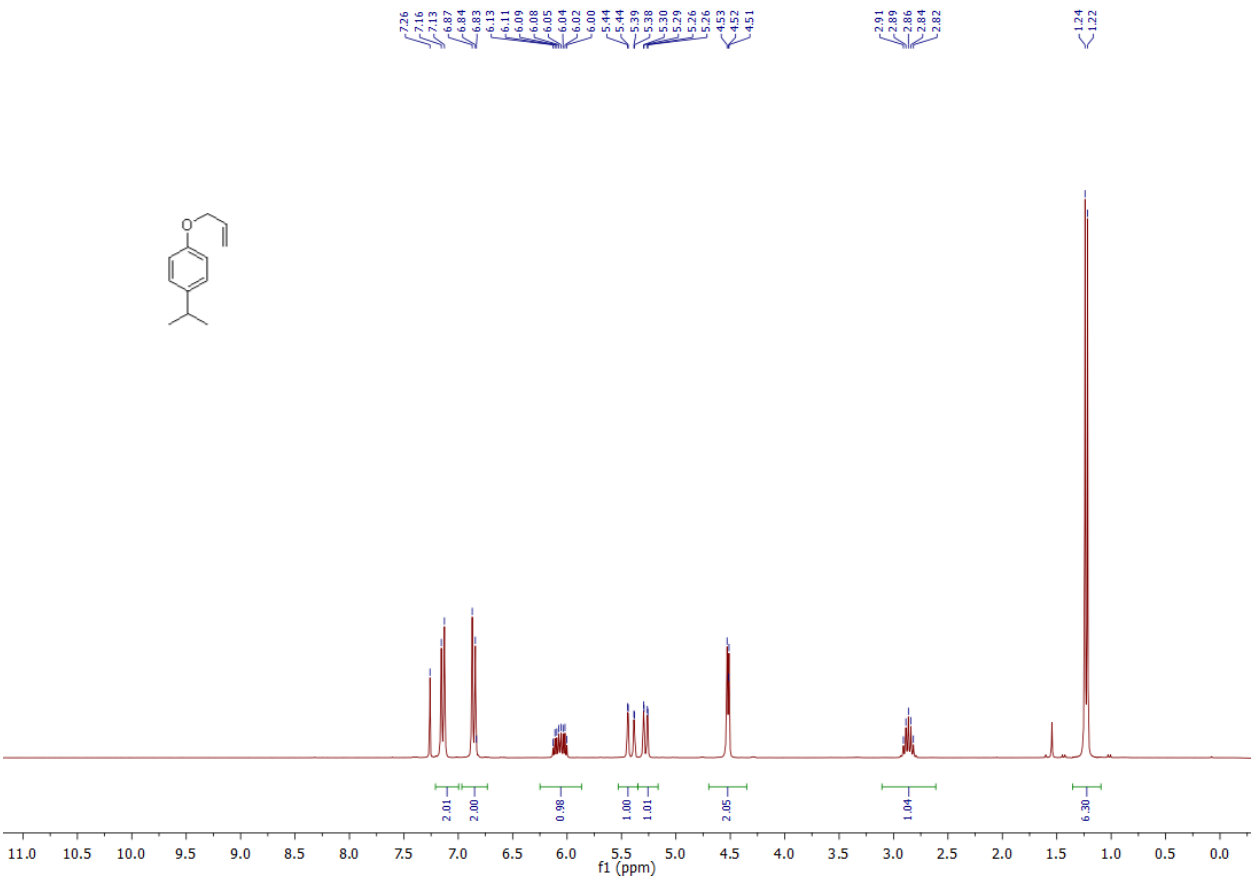

Figure D 8: ^{1}H-NMR spectrum of compound 4.1h

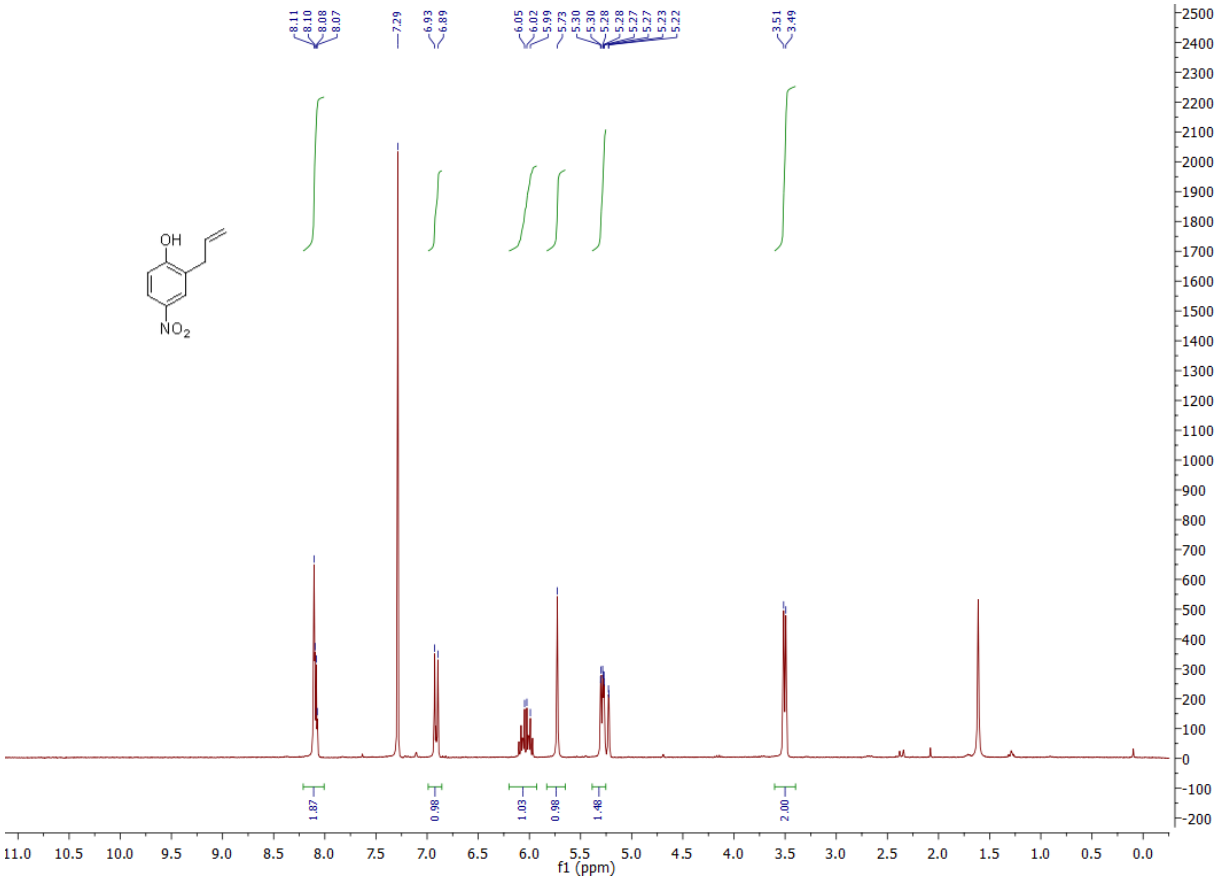

Figure D 9: ^{1}H-NMR spectrum of compound 4.2a

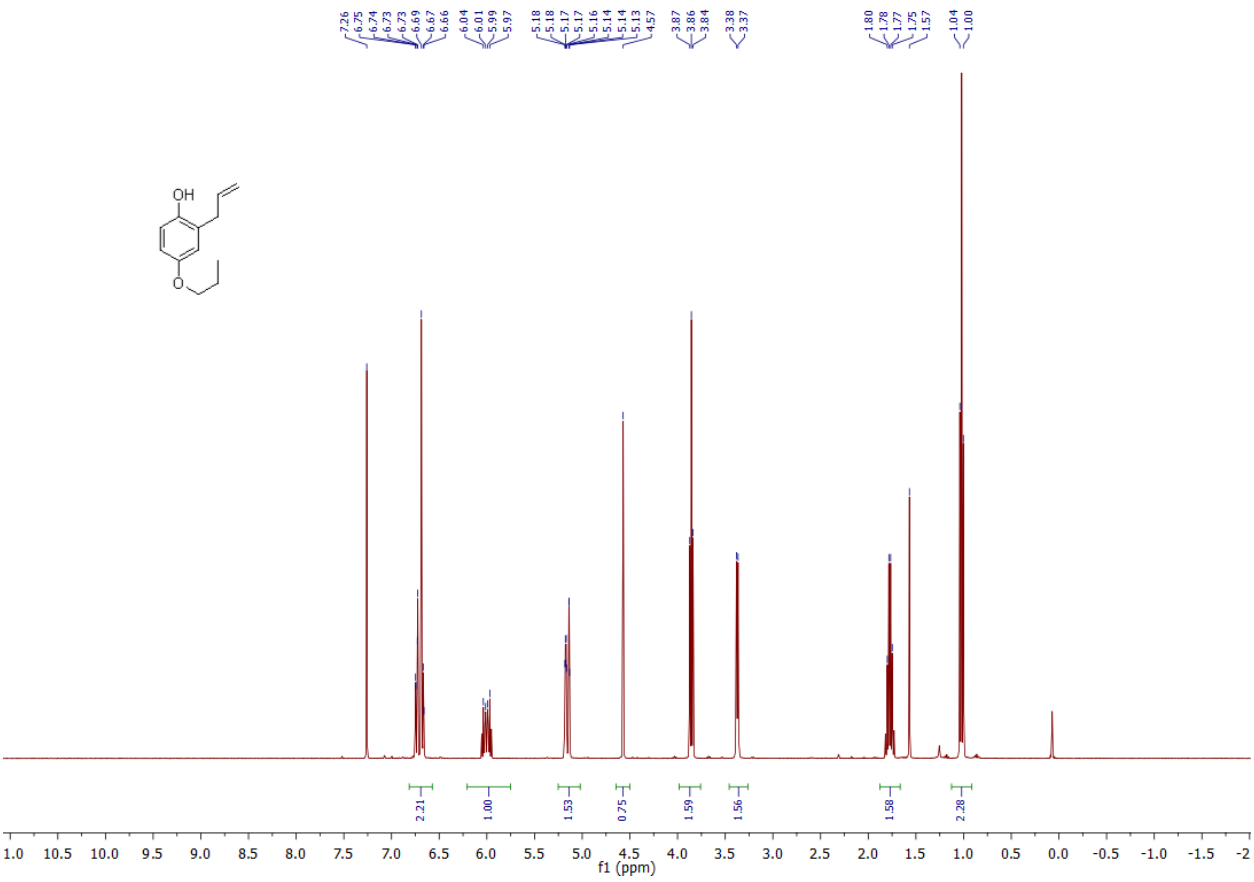

Figure D 10: ^{1}H-NMR spectrum of compound 4.2b

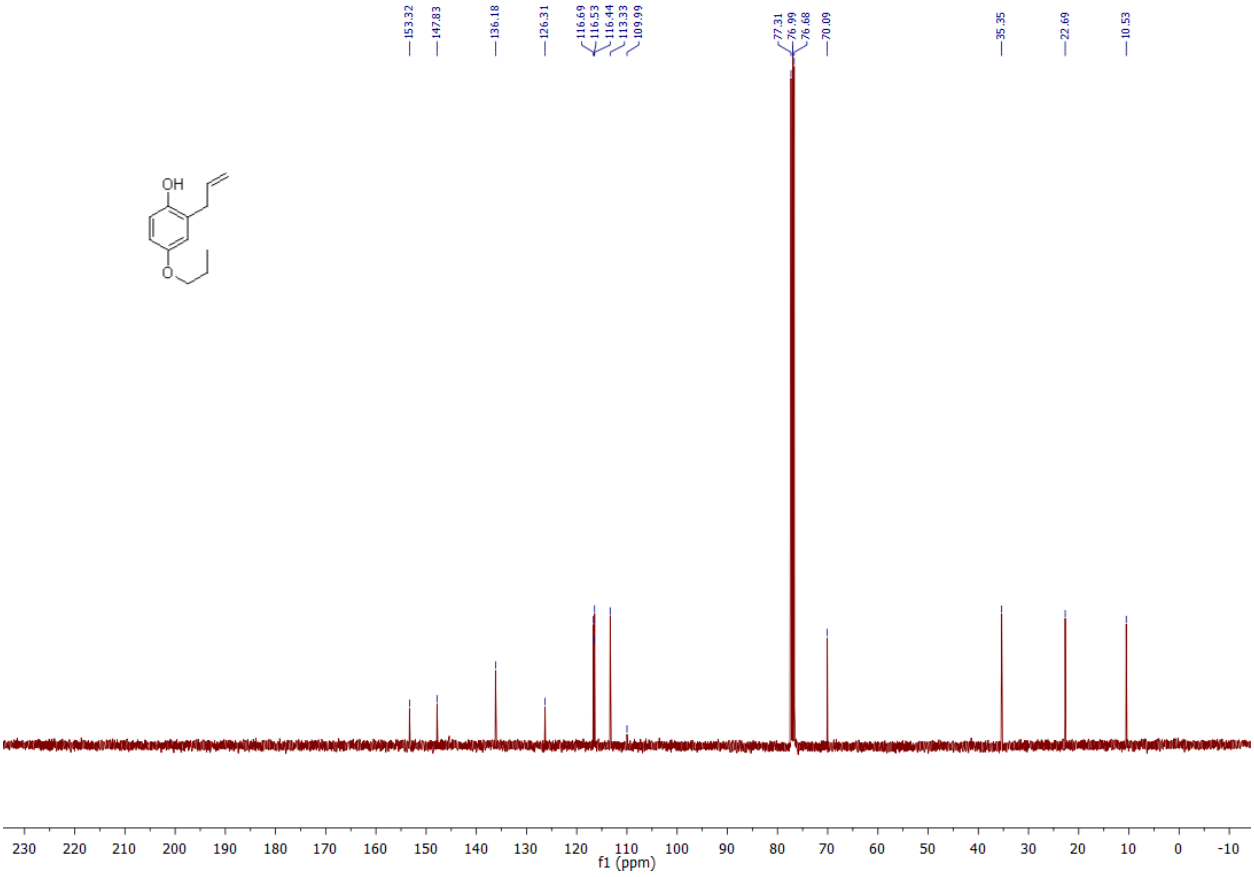

Figure D 11: ^{13}C-NMR spectrum of compound 4.2b

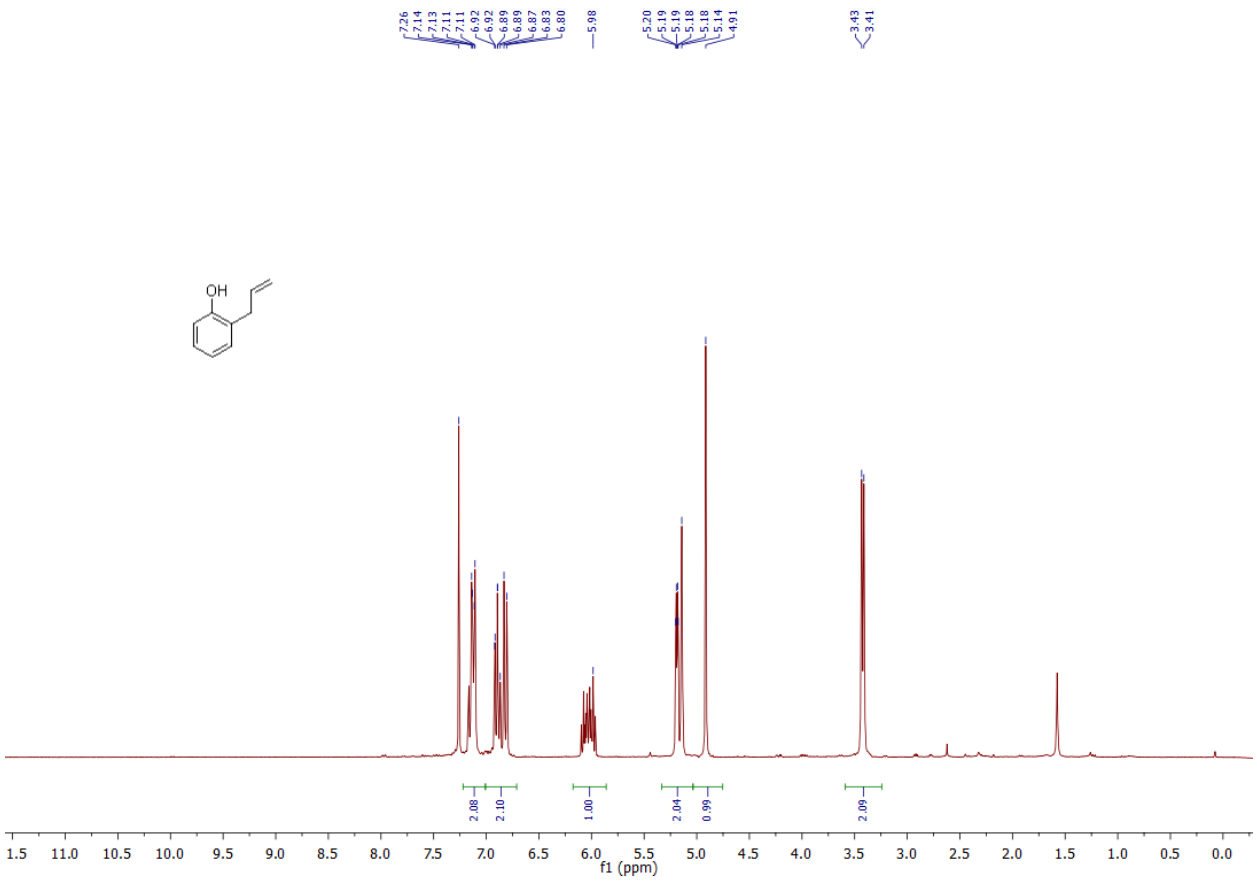

Figure D 12: ^{1}H-NMR spectrum of compound 4.2c

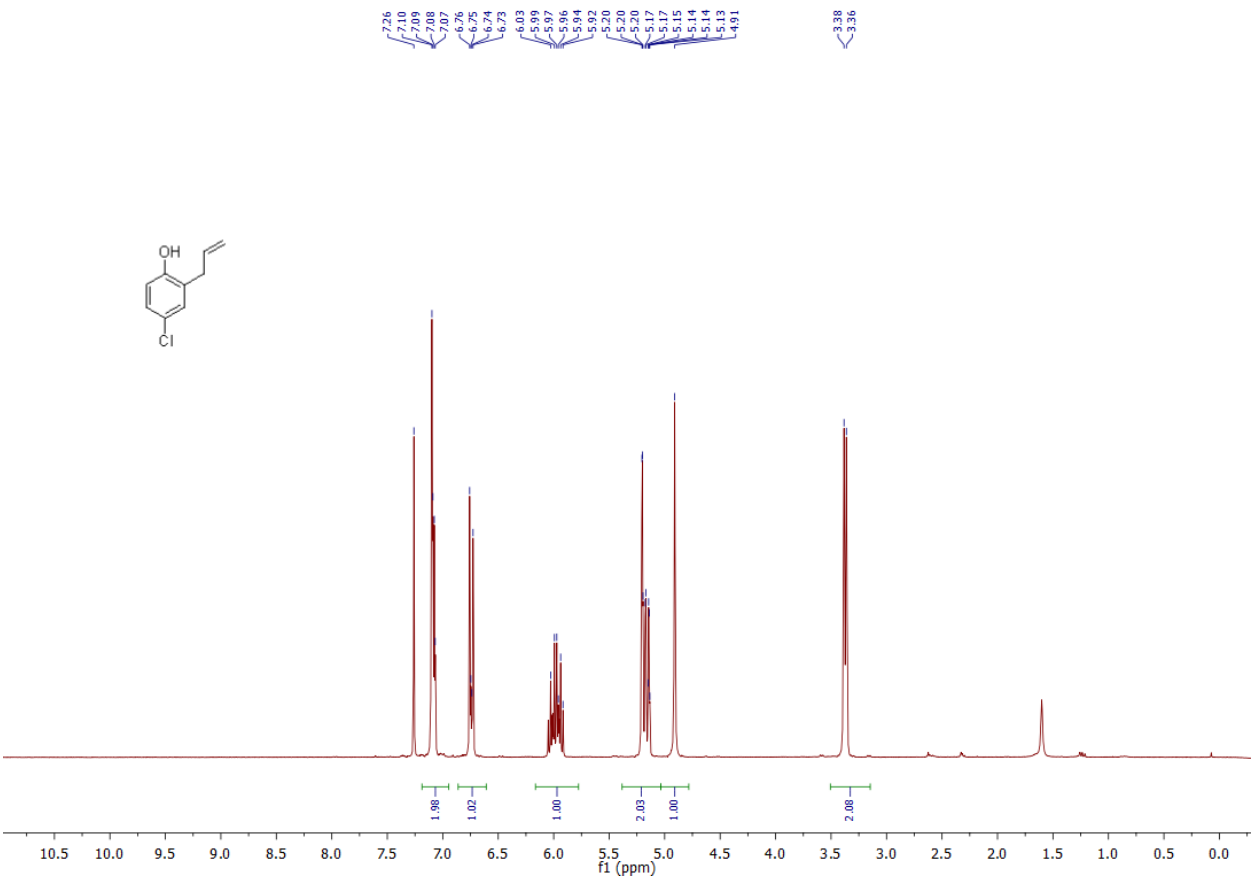

Figure D 13: ^{1}H-NMR spectrum of compound 4.2d

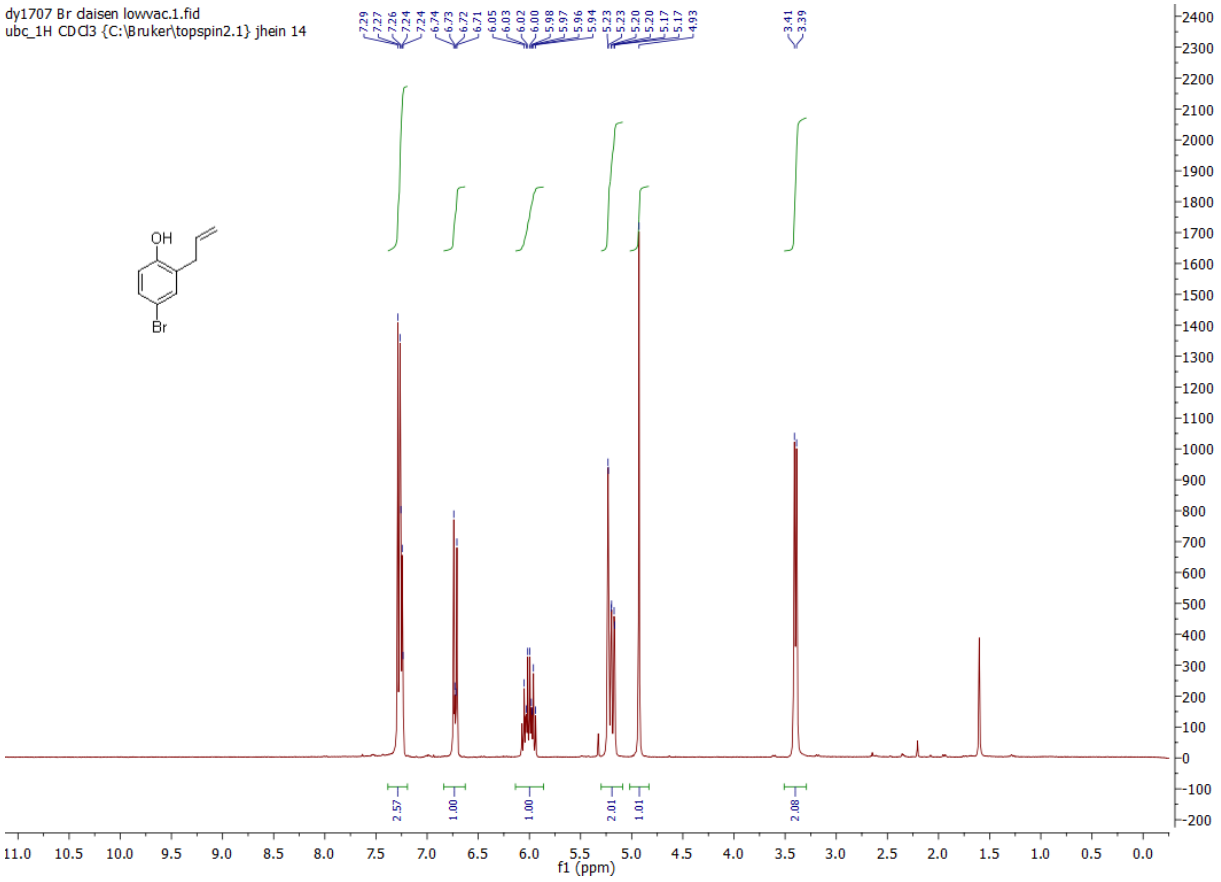

Figure D 14: ^{1}H-NMR spectrum of compound 4.2e

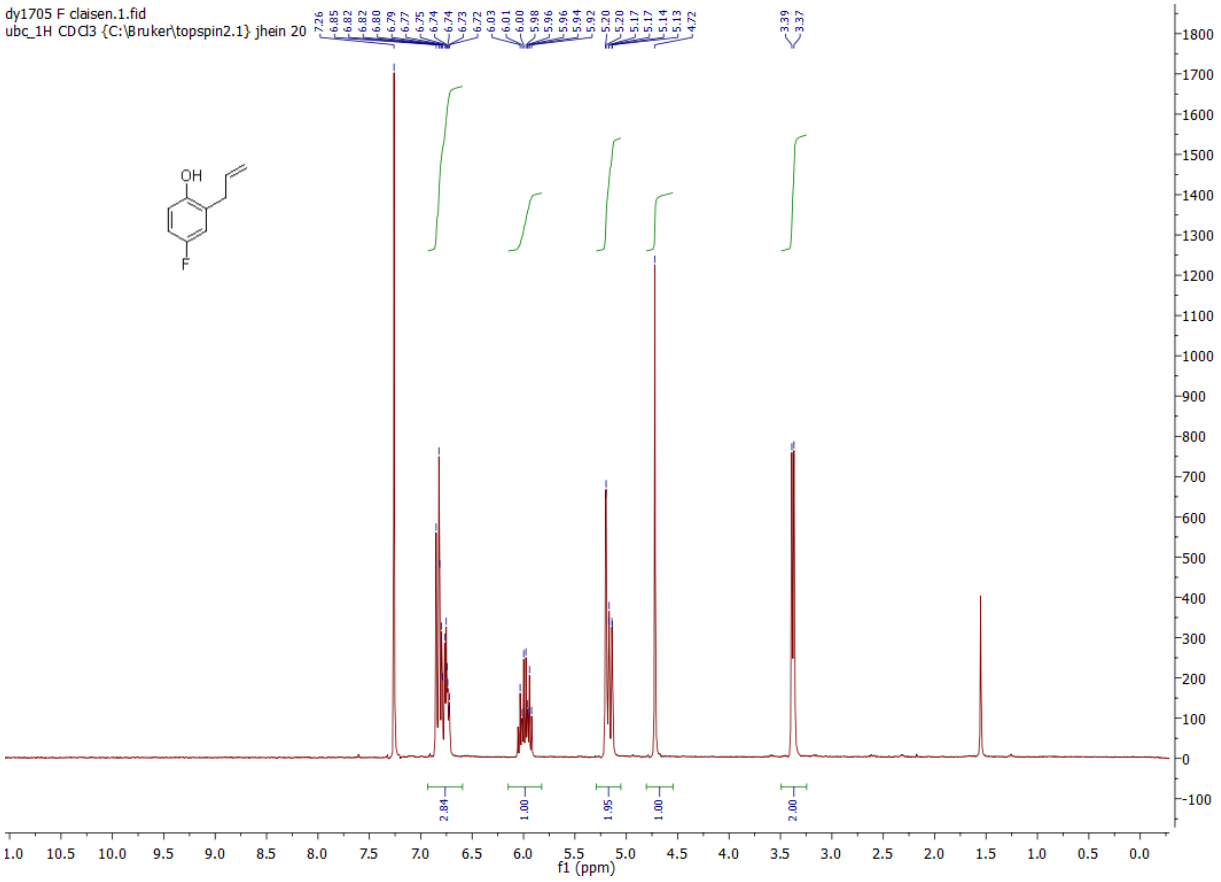

Figure D 15: ^{1}H-NMR spectrum of compound 4.2f

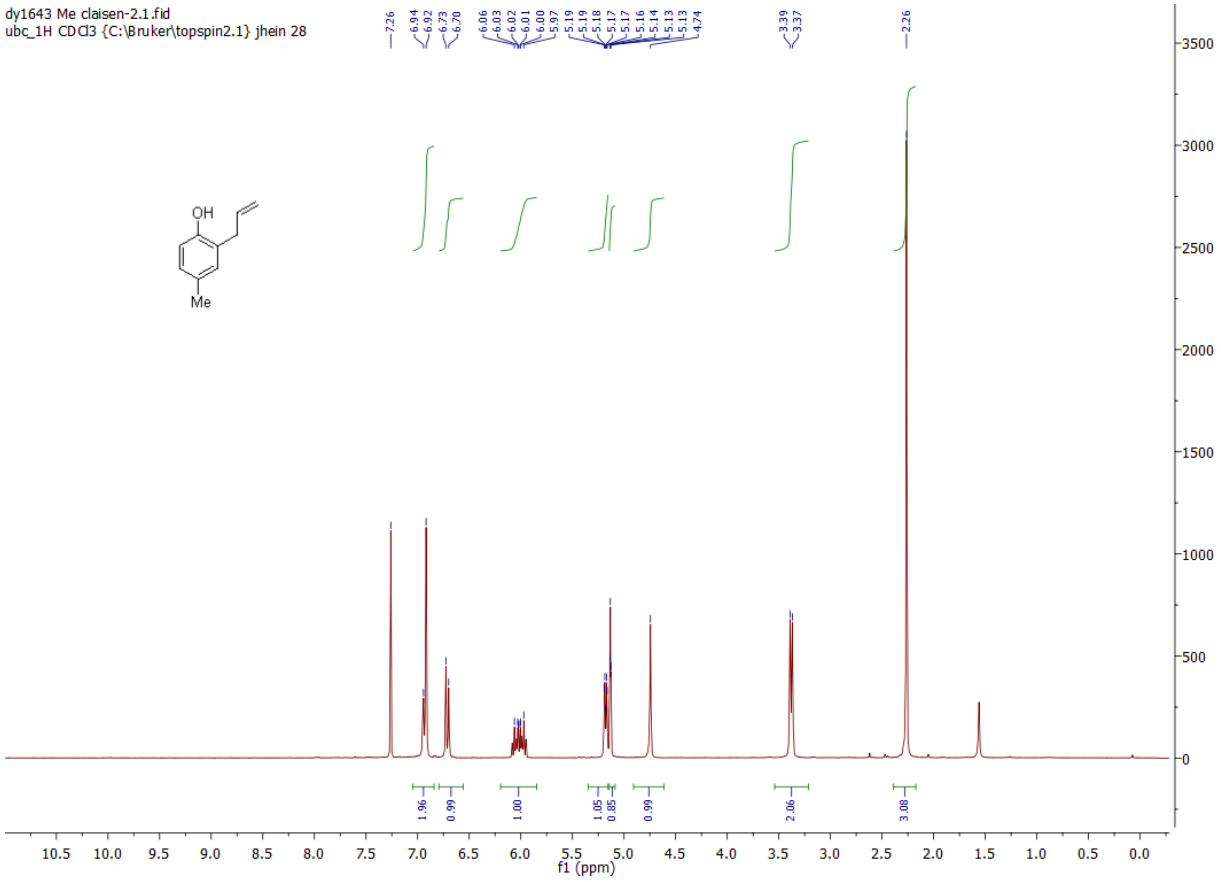

Figure D 16: ^{1}H-NMR spectrum of compound 4.2g

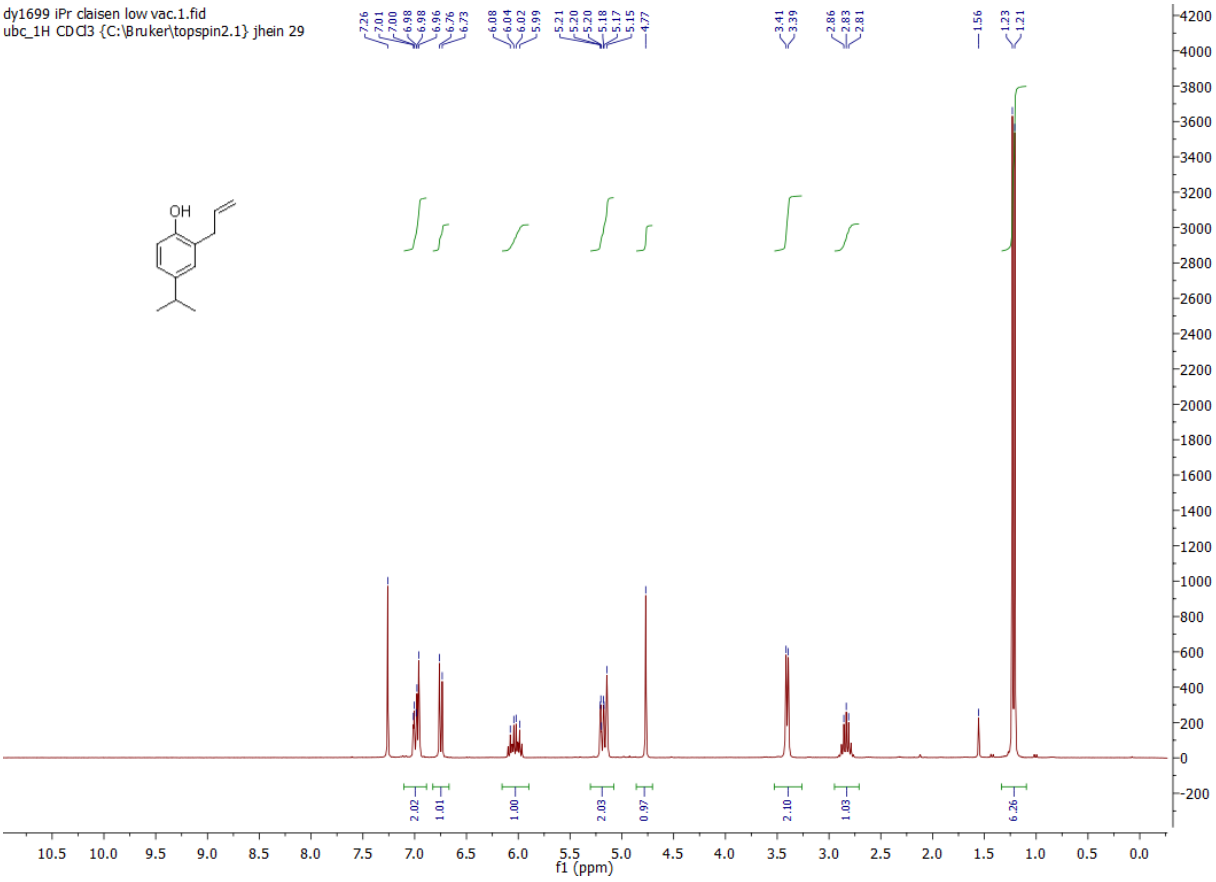

Figure D 17: ^{1}H-NMR spectrum of compound 4.2h

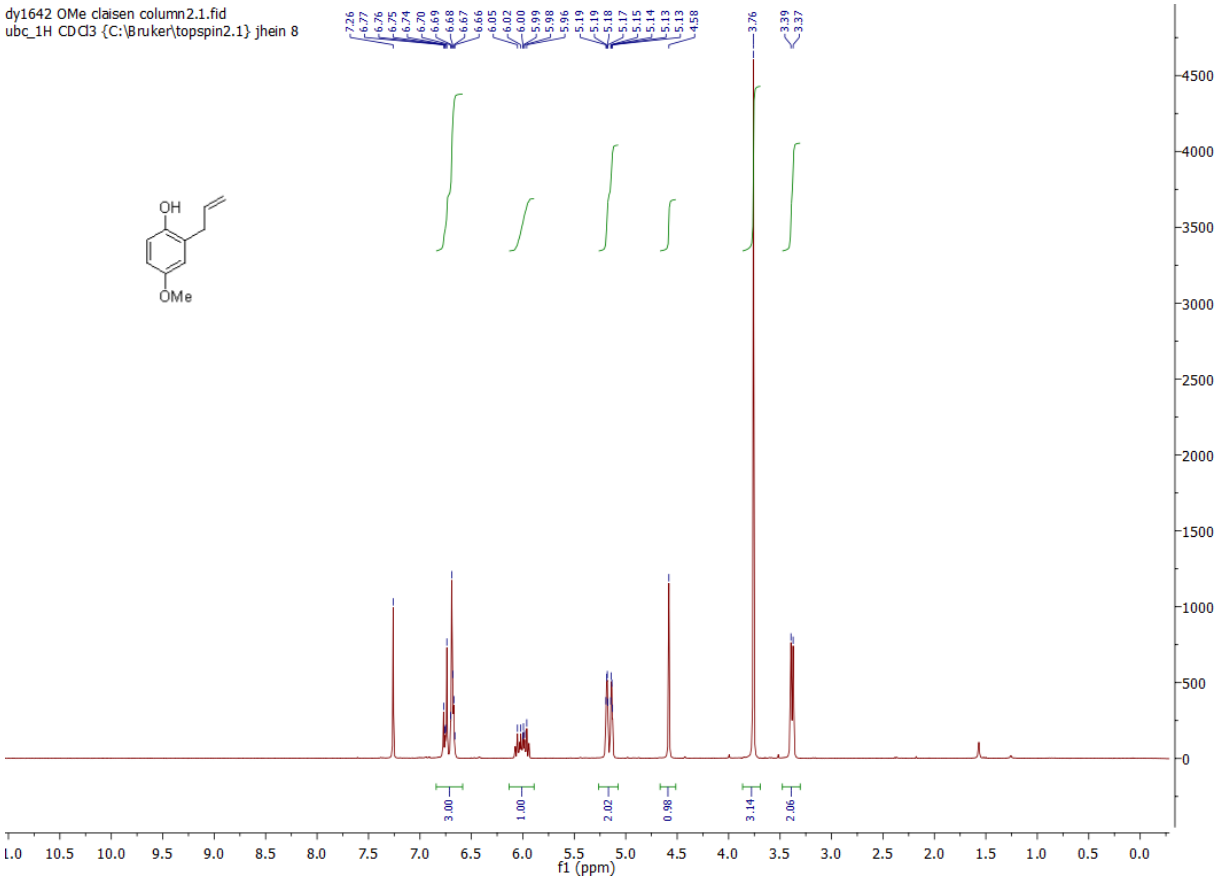

Figure D 18: ^{1}H-NMR spectrum of compound 4.2i